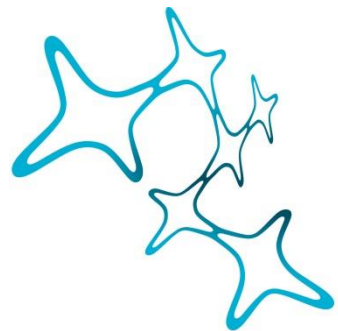# THE COMPLEMENT SYSTEM IN THE RETINA

MÜLLER CELLS AS TARGETS FOR COMPLEMENT MODULATING GENE ADDITION THERAPY

Josef Biber

Graduate School of Systemic Neurosciences

LMU Munich

Dissertation at the
Graduate School of Systemic Neurosciences
Ludwig-Maximilians-Universität München

31st of August, 2023

Supervisor
Prof. Dr. rer. nat. Antje Grosche
Ludwig-Maximilians-Universität München
Department of Physiological Genomics

First Reviewer: Prof. Dr. Antje Grosche
Second Reviewer: Prof. Dr. Olaf Strauß

Date of Submission: 29.08.2023
Date of Defense: 18.12.2023

"If I have seen further, it is by standing on the shoulders of giants."

Isaac Newton

Inhalt

Summary

The complement system is a component of the innate immune response in that recognizes and eliminates pathogens and damaged cells. In addition to its role in the systemic immune system, the complement system also operates within the retina where it plays a crucial role in maintaining retinal homeostasis, regulating synaptic function, and facilitating tissue repair and regeneration.

One distinguishing feature of the retina is its immune-privileged nature. It allows the retina to preserve its intricate structure and visual function while minimizing immune-mediated damage. Several factors facilitate the immune privilege of the retina, including a physical blockade of systemic proteins called blood-retinal barrier and an immunosuppressive microenvironment. These mechanisms help to prevent excessive activation of the complement system and subsequent inflammatory responses, which could be detrimental to the highly organized and tightly regulated retinal tissue.

While a lot of research has been done on the local complement in the retina, it is still lacking a complete picture of which complement factors are expressed, which cell types express complement, what parts of the complement cascade are active for homeostasis and what changes in a disease state. With this knowledge it would be possible to make a rational approach to developing complement modulating therapies that counteract excessive, inappropriate and degeneration inducing complement activation.

Consequently, we mapped cell type-specific complement expression by single cell RNA seq, qPCR and in situ hybridization for murine and human healthy and diseased retinal tissue. We detected complement proteins by mass spectrometry and western blot in purified retinal cell fractions and localized them with immunohistochemical staining. Retinal and choroidal tissue from healthy donors, as well as patients with different states of age-related macular degeneration (AMD) was analyzed. We characterized albino $Abca4^{-/-}$ mice, a model organism that mimics the accumulation of toxic lipofuscin pigments in Stargardt disease, with regards to its complement expression during aging. Additionally, we looked at the complement system in the sodium iodate mouse model that recapitulates the degeneration of retinal pigment epithelium as observed in AMD patients to examine changes during an acute event of retinal degeneration. Lastly, the knowledge gathered on the complement system was used to develop means of complement modulation in the form of truncated versions of complement factor H (CFH) to counteract unnecessary complement mediated neuronal degeneration.

While we found key complement components that can execute pivotal complement functions, several complement factors were absent in retinal tissue. Formation of the C1 complex for instance was feasible with local expression of all necessary molecules in the human retina. On the other hand, several terminal pathway components like C8 and C9 were not detected even in disease states. Analysis of the complement of human donor retinas revealed that the cellular reaction to early AMD was more pronounced in the choroid with a shift to stronger effects in the retina of late-stage AMD patients. Classical pathway initiators seem to play a particularly important role at this stage with high protein and transcript levels in the central retinal tissue. Distinct patterns of complement

expression changes were also found in response to acute retinal degeneration which could be alleviated by our CFH-based treatment.

In conclusion, my PhD studies provide valuable insights into the diverse responses of different cell types in terms of complement expression in healthy and AMD-affected human eyes as well as different mouse models of retinal degeneration. We also propose an efficient and save complement modulating gene addition therapy that could be applied for the treatment of a wide variety of retinal diseases with underlying complement dysregulation.

Background

Anatomy of the vertebrate retina

In the vertebrate retina, a wide variety of cell types are organized in a layered structure (Stenkamp 2015). Five major neuronal cell classes connected in circuits that are diverse in both morphology and function work together to produce the complex visual signal that constitutes trichromatic photopic vision in humans (Stenkamp 2015).

Retinal organization is conserved across all vertebrate species and generally structured in an outer nuclear layer containing cell bodies of photoreceptors, an inner nuclear layer with the bipolar, horizontal, amacrine and Müller cell bodies and the innermost ganglion cell layer contrived of ganglion cells, displaced amacrine cells and astrocytes (Fig. 1) (Masland 2012). Photoreceptors synapse with bipolar cells and horizontal cells in the outer plexiform layer while the vertical information propagation via bipolar cells onto ganglion cells is mediated in the inner plexiform layer (IPL) (Fig. 1) (Masland 2012). Further bipolar signal modification through amacrine cells is conducted in the IPL (Masland 2001; Kolb 1995). Humans and nonhuman primates also have a central cone rich area called macula (Kolb 1995). It covers only about 4% of the human retina but is functionally responsible for high resolution color vision in good light conditions (Gehrs et al. 2006). In its center, the macula has a small depression called fovea responsible for central vision where the acuity is highest (Masland 2012).
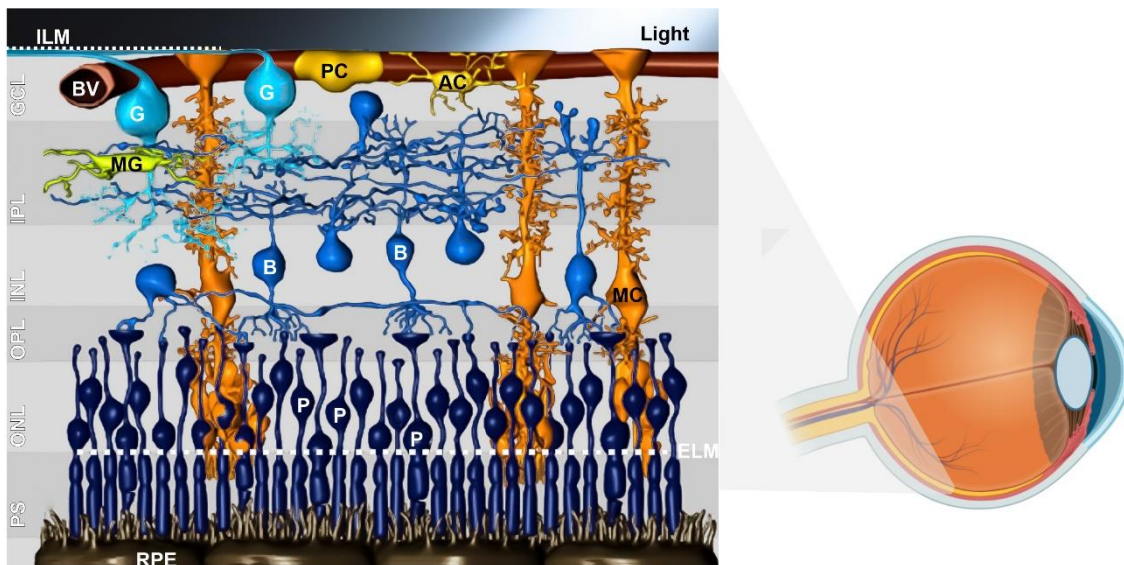
Figure 1: Sagittal schematic of the human retina. AC: Astrocyte, B: bipolar cells, BV: blood vessel, ELM: external limiting membrane. G: ganglion cell, ILM: Inner limiting membrane, MC: Müller cell, MG: Micro glia, P: photoreceptor, PC: pericyte. Retinal layers: GCL: ganglion cell layer, IPL: inner plexiform layer, INL: inner nuclear layer, OPL: outer plexiform layer, ONL: outer nuclear layer, PS: photoreceptor segments, RPE: retinal pigment epithelium.
Image source: Effigos AG Leipzig; Biorender

The photoreceptor outer segments closely interact with the retinal pigment epithelium (RPE), a cell monolayer which absorbs scattered light, phagocytizes outer segment

discs, and performs critical homeostatic secretive functions like recycling all-trans retinal to its active form (Fig. 1) (Masland 2001). RPE cells create a barrier through their tight junctions, regulating the passage of substances between the retina and the choroid (Campbell and Humphries 2012). This forms the outer part of the blood-retinal barrier (BRB), effectively controlling the movement of potentially harmful or disruptive substances from the circulation and thus protecting the neural tissue of the retina (Campbell and Humphries 2012). The outer layers of the retina are nutritionally supported by a blood vessel-rich choroid. It contains pericytes/smooth muscle cells, fibroblasts, melanocytes, neurons, and immune cells (Hoon et al. 2014). The choroid is separated from the RPE by Bruch's membrane, a 0.3 µm thick collagen and elastin rich extracellular matrix. It functions as diffusion barrier to the choriocapillaris that allows the transport of nutrients, oxygen, biomolecules and metabolites between the choroid and the RPE (Maddox and Brenner 1977). Supply of oxygen and essential nutrients to the inner retinal layers is facilitated by intraretinal blood vessels. It consists of the central retinal artery which enters the retina close to the optic nerve and branches into retinal capillaries (Dartt and Besharse 2010). Tight junction connections of endothelial cells that line the intraretinal blood vessel form the inner part of the BRB, which is regulated by various surrounding cells, especially neuronal cells and glial cells (Campbell and Humphries 2012).

The largest macroglia of the vertebrate retina, Müller cells, play an important part in this mechanism. They also act as light guides similar to fiber optic cables (Agte et al. 2011; Labin and Ribak 2010; Franze et al. 2007). The latter is advantageous because light must travel through the inner retinal layers to reach the photoreceptors where the coding of visual information starts. Additionally, they maintain structural integrity of the retina and play essential roles in retina homeostasis further elaborated below (Reichenbach and Bringmann 2013; Tout et al. 1993). Retinal integrity is also maintained by a second type of retinal macroglia, astrocytes, which are present in the nerve fiber- and, to a lesser extent, ganglion cell layer of the retina. They are also associated with the BRB formation and perform supporting functions in metabolism neurotrophy and (Fernández-Sánchez et al. 2015; Rashid et al. 2019).

The continuous surveillance of the retina for the detection of noxious stimuli is mainly performed by microglia cells, the resident tissue macrophages which confer neuroprotection against transient pathophysiological insults (Rashid et al. 2019). However, under sustained pathological stimuli, microglial inflammatory responses can become dysregulated, often worsening disease pathology (Rashid et al. 2019).

The retina as light sensor

When light eventually reaches the outer retina, a change in photoreceptor membrane potential leads to a stop in neurotransmitter release and the beginning of the phototransduction cascade. The outer segment discs of the rod and cone photoreceptors are lined with opsin complexes that contain 11-cis-retinal which changes its

confirmation to all-trans-retinal when hit by photons (Dale Purves et al. 2001). This causes the opsin to change its conformation to a state where it can activate the G-protein Transducin. Transducin dissociates from guanosine diphosphate (GDP) and binds guanosine triphosphate (GTP) (Dale Purves et al. 2001). This is followed by a dissociation of an alpha subunit – GTP complex from the beta and gamma subunit (Dale Purves et al. 2001). The alpha subunit of transducing activates the phosphodiesterase (PDE) on the outer segment disc membrane of rod photoreceptors by binding a regulatory subunit of PDE. PDE reduces cyclic GMP to GMP and the drop in cGMP levels causes cGMP-dependent sodium channels on the photoreceptor membranes to close, reducing sodium influx that leads to hyperpolarization and a halt in glutamate release from photoreceptor synaptic terminals (Dale Purves et al. 2001). Lack of glutamate causes both, enhanced depolarization of ON center bipolar cells and hyperpolarization in OFF bipolar cells, which pass the neural impulse to ganglion cells via glutamate release (Dale Purves et al. 2001). Photoreceptor signals are refined by horizontal cells that are hyperpolarized by signal from depolarizing photoreceptors and giving negative feedback to neighboring photoreceptors (Stenkamp 2015; Masland 2012). This is hypothesized to increase contrast by lateral inhibition of surrounding photoreceptors and keeping photoreceptor responses in a physiological optimal range (Dale Purves et al. 2001). Another type of interneurons of the retina, the amacrine cells, contribute to intraretinal information processing. They connect with ganglion and bipolar cell and coordinate the switch from scotopic (rod-driven) to photopic (cone-driven) vision or the perception of movement (Kolb 1995; Dale Purves et al. 2001; Purves et al. 2001). They are also discussed to contribute to the regulation of the circadian rhythm, highlighting the extent of the diverse signal processes taking place in the retina (Zhang et al. 2005). Finally, ganglion cell axons from each eye partially cross at the optic chiasm, located just below the brain's hypothalamus (Purves et al. 2001). As a result of this partial crossing, each hemisphere of the brain receives visual information from both eyes. This crossover is the reason why the left visual field is processed by the right hemisphere and the right visual field by the left hemisphere (Purves et al. 2001). After the partial crossover at the optic chiasm, the nerve fibers continue as optic tracts. The optic tracts extend posteriorly toward the thalamus, hypothalamus, and midbrain, where they relay visual information to various regions in the brain. The optic tracts make synapses with neurons in the lateral geniculate nucleus, a structure located in the thalamus (Purves et al. 2001). The Lateral Geniculate Nucleus acts as a relay station, processing and relaying visual information to the primary visual cortex in the occipital lobe of the brain. The destination of the optic pathway is the primary visual cortex (also known as V1 or Brodmann area 17) (Dale Purves et al. 2001). It is located at the back of the brain's occipital lobe. The primary visual cortex is responsible for processing and analyzing visual information, such as shape, color, motion, and depth perception. From the primary visual cortex, visual information is further processed and integrated in various visual association areas located in different parts of the brain (Purves et al. 2001). These areas help in recognizing objects, interpreting complex visual scenes, and forming higher-order visual perceptions.

Role of Müller cells in retinal health and disease

Müller cells are a type of macroglia and integral for retinal structure, nutrient transport, ionic and volume regulation, neurotransmitter recycling, clearance of metabolic waste, reactive gliosis, and potassium regulation (Newman and Reichenbach 1996). They span the retina from the inner limiting membrane to the outer limiting membrane with their somata lying in the inner plexiform layer (Reichenbach et al. 1989; Uga and Smelser 1973; Agte et al. 2011; Reichenbach and Bringmann 2013). Müller Cell processes are in close contact with neuronal processes, neuronal stomata, microglia, the retinal resident tissue macrophages and blood vessels which they can manipulate by releasing vasodilators like K+ ions (Liepe et al. 1994; Newman and Reichenbach 1996; Paulson and Newman 1987). They take up nutrients like lactate/pyruvate and oxygen from the blood and distribute them to neurons. Müller cells also remove metabolites and balance the extracellular milieu in the retina, the subretinal space and the vitreous with regards of pH, water and ion composition (Reichenbach and Bringmann 2013).

Müller cells become reactive as response to injury or inflammatory stimuli in a process called gliosis. In this state, they release neuroprotective factors and antioxidants (Schütte and Werner 1998; Maria Frasson et al. 1999; Oku et al. 2002; Bringmann et al. 2006). While initially neuroprotective, gliosis can also have detrimental effects like promoting vascular leakage by vascular endothelial growth factor (VEGF) release, nitrogen oxide accumulation due to nitric oxide synthase expression and general dedifferentiation of the Müller cells accompanied by loss of functions (Yasuhara et al. 2004; Abu El-Asrar et al. 2001; Koeberle and Ball 1999; Bringmann et al. 2000; Bringmann et al. 2006). Like astrocytes, Müller cells in reactive gliosis can enter the cell cycle and proliferate. They start producing extracellular matrix proteins like fibronectin and laminin, recruit immune cells and finally fill spaces left by dead neurons (Kang et al. 2020; Geoffrey P. Lewis and Steven K. Fisher 2000). While the scar provides a fast framework for tissue repair and maintaining tissue stability, it also creates an environment that poses challenges for regeneration and axonal regrowth (Wang et al. 2018). A hallmark of Müller cell gliosis is the expression of glial fibrillary acidic protein (GFAP), an intermediate filament protein that contributes to the mechanical strength of the cells (Cullen et al. 2007). In response to inflammatory signals, such as tumor necrosis factor alpha (TNFA) released by activated microglia, Müller cells undergo gliotic changes, including increased expression of intermediate filaments such as glial fibrillary acidic protein (GFAP).

Interactions between Müller cells and Microglia represent a crosstalk integral to the retinal immune response as well as in healthy states. The translocator protein (TSPO) is an important player in these mechanisms, as it Müller cells release diazepam binding inhibitor (DBI), an endogenous TSPO ligand which suppresses microglia activation during pathological events (Wang et al. 2014). Elevated Müller cell DBI secretion led to lower TNFA expression and less proliferation and production of oxygen species in Microglia (Wang et al. 2014). These changes amplify the neuroinflammatory response,

affecting neuronal survival and retinal function. Moreover, the crosstalk between microglia and Müller cells involves the release of various neurotrophic factors by Microglia like BDNF and CNTF that had neuroprotective functions by inducing or inhibiting release of secondary factors by Müller cells (Wang et al. 2011a; Harada et al. 2000). Factors which mediate photoreceptor survival and apoptosis like Glial cell line-derived neurotrophic factor, leukemia inhibitory factor and basic fibroblast growth factor were found to have altered secretion in Müller cells Müller cells dependent on Microglia input (Harada et al. 2002; Harada et al. 2000; Wang et al. 2011a).

Disruption of the immune homeostasis in retinal diseases

The delicate cellular interplay in the retina is disrupted by a wide range of inherited, acute, and age-related diseases that often lead to a loss of visual acuity, dyschromatopsia or blindness depending on which cell type is primarily affected. Among the most prevalent retinal diseases is AMD - the major cause of vision loss worldwide with 200 million people currently affected (Wong et al. 2014; Vyawahare and Shinde 2022). In Europe's aging population, by 2040, up to 21.5 million people are expected to be affected by early and 3.9 million by late AMD (Wong et al. 2014; Colijn et al. 2017). Many retinal diseases entail an inflammatory response to intrinsic or extrinsic antigens. Inflammation can occur in slowly progressing diseases like AMD, diabetic retinopathy, retinitis pigmentosa, uveitis and glaucoma or as a response to an acute incident like ischemic injury or retinal detachment following a blunt trauma (Kaur and Singh 2021; Chen et al. 2022; Eastlake et al. 2016; Wang et al. 2011b).Understanding the inflammatory involvement in disease progression would bring great benefits for the development of drugs that could protect retinal tissue from degeneration by limiting the inflammatory response to a necessary minimum and stop para-inflammatory processes that are part of a degenerative spiral (Chen and Xu 2015; Wang et al. 2011b). In AMD, a part of the innate immune system, the complement system, was discovered to play a large part in pathophysiology (Anderson et al. 2010; Ricklin et al. 2010; Merle et al. 2015b). Genetic risk variants of several complement factors were shown to greatly increase the chances to develop AMD (Giannakis et al. 2003; Anderson et al. 2010). The complement system was also shown to be activated in glaucoma, DR, ischemic injury and uveoretinitis (Tezel et al. 2010; Shahulhameed et al. 2020; Yang et al. 2017; Inafuku et al. 2018). Consequently, complement-based therapies are currently under development. Since the blood retina barrier makes the retina an immune privileged tissue, complement factors involved in immune responses during early disease stages (while the barrier is still intact) are all produced by retinal cells. Leakiness of the BRB is often a disruption of the tight functions cause by degeneration of cells that are involved in the formation of the barrier like pericytes, endothelial cells or RPE (Vinores 2010). It can occur because of inflammation, vascular disorders, age-related changes, hypertension and ischemia and lead to influx of systemic complement components (Vinores 2010).

The local complement environment makes it important to understand how the complement system works in the retina and how it adapts to disease states. In my PhD work, I conducted multiple studies on complement homeostasis and activation in health, disease models and diseased donor tissue to close this knowledge gap. This work, thus, contributes to a better understanding of the local, retinal complement biogenesis and underlines the idea that complement regulatory intervention could shift diseases prognosis.

The complement system

As an important part of the innate immune system, the complement system is involved in the recognition and clearance of pathogens and other foreign matter (Merle et al. 2015a; Ricklin et al. 2010). Besides its surveillance and immune response coordination duties, it has additional physiological roles in maintaining the immune homeostasis and synaptic pruning (Merle et al. 2015a; Ricklin et al. 2010; Wakselman et al. 2008; Coffey et al. 2007).
While lots of cell types produce and release complement factors, the gross of the soluble complement proteins in the plasma is secreted by the liver and found in the blood circulation (Merle et al. 2015a; Ricklin et al. 2010).

The complement system consists of a cascade of subsequently activated serine proteases that is initiated by recognition molecules becoming active upon conformational changes that occur after interactions with recognition sites (Ricklin et al. 2010; Merle et al. 2015a). In their active state, the proteases of the complement system can cleave downstream molecules thus turning them into their active state. Three pathways of initiation are generally distinguished: The classical, the lectin and the alternative pathway. All lead to the formation of a C3 convertase that cleaves the central complement component C3 (Fig. 2) (Ricklin et al. 2010). Generally, the pathways differ in their initiation mechanisms. The classical pathways triggered by antibody-antigen complexes, the lectin pathway is activated by specific sugar molecules on pathogens, and the alternative pathway is spontaneously activated through the hydrolysis of complement proteins. Of special interest to this work is the alternative pathway since it contains means of tuning the complement response. The amplification loop of the alternative pathway can greatly enhance complement responses if not inhibited (Merle et al. 2015a). Inhibition of the alternative pathway is the central idea behind the gene addition therapy proposed here.
The recognition molecule of the classical pathways C1q (Fig. 2). It binds to immunoglobulin/antigen complexes (IgM and IgG), phosphatidylserine, double stranded DNA, bacterial prions, C-reactive protein (CRP), pentraxin, lipopolysaccharides and synaptosomes (Reid 2018; Györffy et al. 2018; Ricklin et al. 2010). Upon binding a recognition molecule, C1q recruits C1s and C1r to form the C1 complex (Reid 2018) (Fig. 2). This complex has serine protease capabilities and cleaves

C2 and C4, thus creating C2a, C2b, C4a and C4b. Of these, the C3 convertase C4b2a is created (Fig. 2).

In the lectin pathway, recognition of pathogens is facilitated by collectin 11 (CL-K1), and ficolins (Ficolin-1, Ficolin-2, and Ficolin-3) and mannose binding lectin (Merle et al. 2015a; Ricklin et al. 2010). The latter can bin to pathogen surface oligosaccharides with sugars that have 3-4 terminal OH groups like mannose or glucose (Ricklin et al. 2010; Merle et al. 2015a). Ficolins and collectin bind acetylated residues. Downstream activation of the complement cascade is, like in the classical pathway, also the formation of C3 convertase C4b2a by cleavage of C2 and C4 (Fig. 2).

The alternative pathway is not activated by the binding of recognition proteins to specific targets but is characterized by the direct deposition of C3b to cell surfaces (Fig. 2). The initial C3 cleavage and subsequent formation of the alternative pathway C3 convertase C3bBb is hypothesized to be spontaneous hydrolysis (Fearon et al. 1973; Fromell et al. 2020). This hypothesis is supported by an uncontrolled alternative pathway activation when its tight regulatory machine is disabled (Bexborn et al. 2008; Fromell et al. 2020). If not degraded or inhibited by regulators, the alternative pathway C3 convertase is assembled by binding of factor B to hydrolyzed $C3b(H_2O)$ in the presence of Mg^{2+} (Merle et al. 2015a). The C3bBb complex is then formed by factor D facilitated cleavage of factor B into Ba and Bb. This proteatically active molecule can then cleave additional circulating C3 molecules to generate more C3b, forming a positive feedback reaction called the alternative pathway amplification loop.

In the AP, the C3 convertase is stabilized by properdin which can bind on microbe or damaged host cell surfaces after C3 deposition (Harboe et al. 2017).
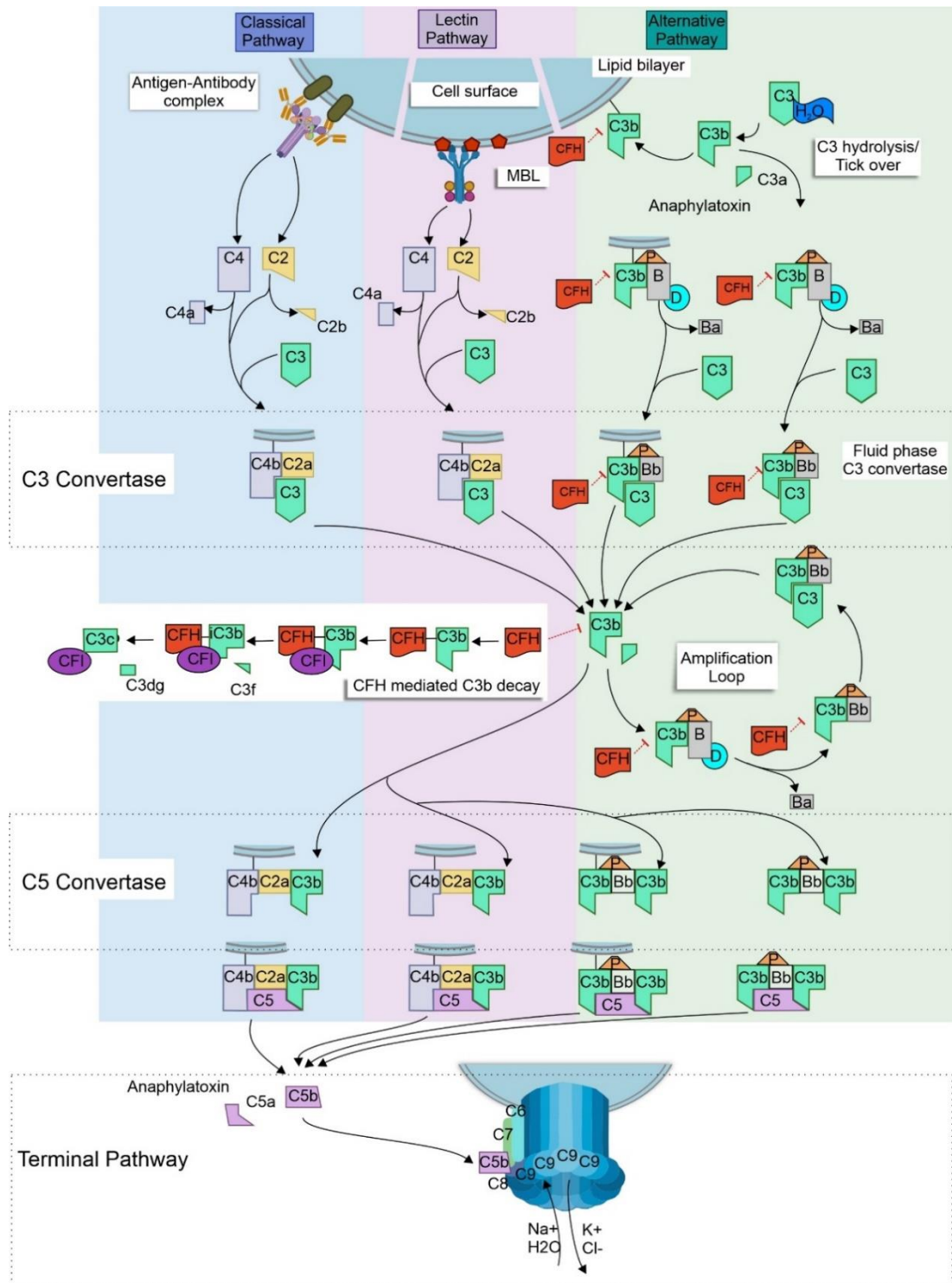
Figure 2. Schematics of the complement system. MBL: Mannose binding lectin, C2-9: Complement component 2-9, CFH: Complement Factor H; CFI: Complement Factor I, MAC: Membrane Attack Complex, D: Complement Component D; P: Properdin, B: Complement component B

Image partially created with Biorender

Complement effectors and terminal pathway

Complement activation's effector mechanisms include recruiting leukocytes and directing their immunological response by boosting their chemotaxis, migration, and phagocytosis. Innate immune cells like macrophages and microglia are capable of identifying, consuming, and eliminating apoptotic cells by recognizing complement factors on target surfaces and damaged neuronal synapses (Taylor et al. 2000; Merle et al. 2015a). This tagging for phagocytosis is called opsonization and is facilitated by recognition of complement molecules by complement receptors (CRs) expressed by the phagocytes. Besides the C3 convertase, lysis of C3 leads to pro-inflammatory mediators like the anaphylatoxic C3a or opsonins iC3b, C3dg and C3d (Bajic et al. 2013; Merle et al. 2015a). C3a stimulates endothelial cells to produce P-selectin, which has a CCP (complement control protein repeats) domain that binds C3b, thus promoting further formation of C3 convertases and the generation of more C3a (Merle et al. 2015a). C3b on its own is also a potent opsonization agent which, after binding to a cell surface, marks them to be phagocytosed.

During the development of the retina and the brain, "weak" or inactive synapses are removed by complement-mediated microglial phagocytosis in a process called synaptic pruning (Vizi et al. 2010; Anderson et al. 2010). This mechanism appears to be regulated through signaling pathways involving C3a/CR3 and C5a/C5aR interactions, which mark damaged or excessive synapses for opsonization by phagocytic cells (van der Laan et al. 1996; Vizi et al. 2010). C3a and C5a have also been shown to stimulate neutrophils and endothelial cells for the release of complement stabilizing factors like properdin and p-selectin respectively (Merle et al. 2015a).

All complement activation pathways share the terminal pathway which produces more anaphylactic molecules and can shift the complement cascade from opsonization to a direct lysis of pathogens (Merle et al. 2015a). The C3 convertases C4b2a and C3bBb can recruit another C3b to change affinity from C3 to C5 to form an enzymatic complex that converts C5 into its active fragments C5a and C5b (C3bBb can also cleave C5 but with much lower affinity (Rawal et al. 2008). C5b associates with C6, C7, C8 and C9 that form the membrane-attack-complex (MAC). The MAC resembles a ring shaped porous that spans from the target surface to the cytosol, leading to Ca^+ efflux and lysis (Fig. 2).

Alternative pathway amplification loop and positive regulation of complement

A special mechanism that tunes the complement response is the amplification loop. As mentioned above, once a C3 convertase is formed it cleaves more C3 into C3a and C3b,

which leads to more C3 convertase. As C3b is constantly being broken down by CFI, the amplification loop is sometimes viewed as the balance between C3 breakdown and C3 feedback cycle (Lachmann 2009).

C3 convertases can form on target surfaces or in fluid phase. In the alternative pathway activation, $C3(H_2O)Bb$ is a fluid phase convertase that produces C3b molecules with short half-life of their thioester bonds ($60\mu s$) (Fromell et al. 2020). This leads to the formation of a nascent form of C3b that quickly reacts with water to form a fluid phase C3b which is incapable of binding cell surfaces (Fromell et al. 2020; Merle et al. 2015a). The fluid phase C3bBb is tightly regulated by factor H to prohibit unwanted complement activation (Zipfel and Skerka 2009; Merle et al. 2015a; Zewde et al. 2016). The nascent C3b however, can covalently bind to host surfaces or pathogens and with recruitment of CFB (cleaved by CFD) form a short lived C3 convertase (~90 seconds) that gets stabilized by neutrophil released properdin to last about 15 minutes (Zewde et al. 2016). Properdin can also bind the cell surface first, recruiting C3b and leading to an even more stable and potent version of C3bBbP (Merle et al. 2015a). This highlights properdin not only as a stabilizer, but also as a positive regulator of the AP. It facilitates surface binding of C3b which initiates the formation of stable C3 convertase amplification loop. Blocking of this function has diminished AP activation (Pauly et al. 2014).

An inadequate complement response magnitude or activation on healthy host cells can have dire results, calling for a tight regulation of the system. Several inhibitors have overlapping and redundant effects which displays the evolutionary necessity for a controlled complement system. A central role in complement regulation is occupied by the serine protease CFI. Fluid phase or surface bound cofactors form a complex with C3b and recruit CFI to subsequently degrade it to an inactive form called iC3b and further to C3c and C3dg. While cofactors decay acceleration factor (DAF), complement receptor 1 and membrane cofactor protein (MCP) and C4b-binding protein are located on host cell membranes, while CFH is a soluble regulator of the C3 convertase.

Complement factor H

CFH is a soluble protein with 20 complement regulatory domains. It has C3b and glycosaminoglycans (GAG) as the primary ligands and can inhibit C3 convertase formation by competitively binding the factor B binding site with its CCP modules 1-2 (Merle et al. 2015a). With the GAG binding, it actively protects host cell surfaces and also acts on fluid phase $C3(H_2O)Bb$ and C3b but not C3. Taking into account that the complement positive regulator properdin is also binding heparin, GAG expression has a high impact on complement modulation (Perkins et al. 2014; Yu et al. 2005).

As opposed to C3, C3b has an exposed "complement C1r/C1s, UEGF, BMP1" domain and thioester-containing domains (TED) which CFH binds to with its CCP 19-20 and CCP 1-4 (Merle et al. 2015a). Domains 20 and 7 have an affinity to heparan sulfate moieties (although not the same) and therefore facilitate host cell surface recognition (Perkins et al. 2014). The most common CFH polymorphism (Y402H) associated with

AMD is also located in CCP 7 (Hageman et al. 2005; Haines et al. 2005). This domain has been shown to, in addition to GAGs, also bind malondialdehyde, an oxidized lipid commonly found in the RPE of AMD patients (Merle et al. 2015b).

CFH functions are also tuned by different means. Complement factor H-related proteins (CFHR1-5) are located on cell surfaces and can recruit CFH and enhance the complement inhibition (CFHR1, 2 and 5) or competitively block binding sites (Hannan et al. 2016; Skerka et al. 2013). CCPs 6-8 of CFH facilitate binding to CRP, which recruits CFH to sites of tissue damage, effectively downregulating inflammatory activity (Mihlan et al. 2009; Molins et al. 2016). While the interactions are not quite understood, CRP1 is hypothesized to enhance CFH mediated inhibition on apoptotic cells to block complement terminal pathway activation and inflammatory activation (Zipfel and Skerka 2009). However, this mechanism is theorized to suppress necrosis and promote an inflammation free opsonization of apoptotic cells (Zipfel and Skerka 2009).

Complement system in the retina

The complexity and diverse functions of the complement system in the retina an exciting topic for the studies presented here. The involvement of complement in several retinal diseases with the premise that all factors involved in the disease stem from local sources made repair or regulation of the defective system a viable goal (Anderson et al. 2010; Bora et al. 1993). Before intervening with complement caused disease progression, a profound understanding of how the local retinal complement system works had to be established.

The possibility that immune cells and complement factors circulating in the bloodstream could influence the retinal microenvironment is still debated (Armento et al. 2021). However, in recent years, as the understanding of the complexity of the blood-retinal barrier and the local immune environment in the retina grew, it became clear that, while systemic complement factors might have some influence, the local production and regulation of complement within the retina itself played a more significant role in retinal health and disease (Luo et al. 2011; Schäfer et al. 2017; Anderson et al. 2010). The connection between complement activation in the retina and in the blood circulation observed in early research is still subject of research and some conclusions describe retinal diseases as local manifestations of systemic diseases (Scholl et al. 2008). While the retinal complement system is largely independent of the systemic one, risk factors and genetic prevalence for complement disease in the retina are still also present in other parts of the body and can lead to complement activation there. (Scholl et al. 2008; Armento et al. 2021)

Expression and presence of complement components in the retina has previously been shown in a healthy and diseased retinal state. *Mannose-binding-lectin* (*MBL*), *C1qb*, *C1r*, *C2*, *C3*, *C4* and *C5* transcripts have previously been identified in retinal and RPE/Chroroid human tissue (Xu and Chen 2016; Anderson et al. 2010; Luo et al. 2011).

Presence of complement regulators CFH, Membrane Cofactor Protein (MCP), Decay Accelerating Factor (DAF) and CR1 have also been previously reported by immunohistochemistry in healthy human eyes and in eyes with early onset AMD (Fett et al. 2012). Transcript levels of *CFH* were shown to be downregulated in vitro in RPE cells exposed to oxidative stress (Chen et al. 2007).

Through clearance of immune complexes and apoptotic cells, complement has been shown to play a critical role in several processes that maintain retinal integrity. In a study on various mouse lines that were deficient for *C1q*, *Mbl a/c*, *Fb*, *C3 or C5* Mukai et. al observed a decrease in ERG amplitudes and a thinning of the INL in each of the respective mouse lines (Mukai et al. 2018). Especially C1q and C3 knockouts have led to abnormal retinal development in this context further discussed below.

In contrast, Schweigard et. al found that retinal detachment in *Cfb* or *C3* knockout mice led to less apoptotic cells following the injury (Sweigard et al. 2014). In alternative pathway deficient (*Fb$^{-/-}$*), the same group found an increase of neovascularization following an oxygen-induced retinopathy (Sweigard et al. 2014). They concluded an involvement of the AP on pathological angiogenesis that affects mainly neovascularization and not existing vessels through *Cd55* downregulation (Sweigard et al. 2014).

Presence of the C3a and C5a pathways for mediating anaphylatoxicitity has also been found in the retina. Immunohistochemical analysis of healthy human retinas also revealed anaphylatoxin receptors C3aR and C5aR presence in Müller cells and other structures of the retina (Vogt et al. 2006). This was also an interesting discovery since C3a signaling has been shown to induce retina regeneration in chicken embryos by activating STAT3 that causes IL-6, IL-8 and TNFA activation (Haynes et al. 2013).

Mediators and modulation of the complement system in the retina

A common thread through all the work presented here is the hypothesis of a local complement homeostasis that is controlled by the cells of the retina itself. Several studies have shown that complement expression in the retina is modulated by inflammatory cytokines and chemokines. Microglia, astrocytes and Müller glia have been identified to orchestrate inflammation-mediated tissue damage through complement (Markiewski and Lambris 2007; Chen and Xu 2015). For instance, these cells release cytokines like TNFA, interferon gamma (IFN-g) and IL-27, which have been reported to regulate expression of complement. The anti-inflammatory cytokine IL27 was shown to increase CFH expression in human RPE and mouse retinal cells through the STAT1 pathway (Amadi-Obi et al. 2012). Luo et al. also discovered that supernatants of activated macrophages massively (10-30 fold) increased CFB and C3 expression in mouse RPE cells (Luo et al. 2013). Schmalen et al. showed a distinct reactivity of the Müller cell complement secretion to certain cytokines of MIO-M1 immortalized Müller cells and primary porcine RMGs (Schmalen et al. 2021). C1q levels for instance dropped after TNFA treatment but increased by IFN-g. INF-g also increased C4 expression while

TNFA lead to higher levels of the central complement component C3 (Schmalen et al. 2021).

Complement regulatory protein expression in the cell membrane of RPE cells is well characterized ex vivo in mice and humans as mentioned above (Yang et al. 2009). Following inflammatory stimulation by tumor necrosis factor alpha (TNF-a) and interleukin 1b (IL1b) and hydroquinone, all membrane regulators were upregulated, highlighting complement responsiveness to cytokines (Yang et al. 2009).

Complement in AMD

AMD is a slowly progressing degeneration of the central region of the retina with the highest photoreceptor density. While asymptomatic in early stages, gradual photoreceptor atrophy in the parafoveal region causes reduced contrast sensitivity and stinted dark adaption (Sunness et al. 1997; Jager et al. 2008). Patients often retain high visual acuity (20/40 or better) but often are unable to recognize larger shapes like faces or headline letters due to degeneration near the fovea (Sunness et al. 1997; Jager et al. 2008). Over years, the irregularly shaped patches of retinal cell death termed geographic atrophy (GA) will affect the fovea. Advanced stages are marked by severe vision with absolute scotomas (blind spots) associated with patches of GA (Sunness et al. 1997; Jager et al. 2008).

10-15% of AMD cases are accompanied by neo-vascularization, adding to the risk of severe vision loss with potential subretinal hemorrhage (Fig. 3) (Jager et al. 2008). The bleeding can lead to legal blindness within days and overall, neovascular AMD is responsible for over 80% of cases of legal blindness caused by AMD (Jager et al. 2008).
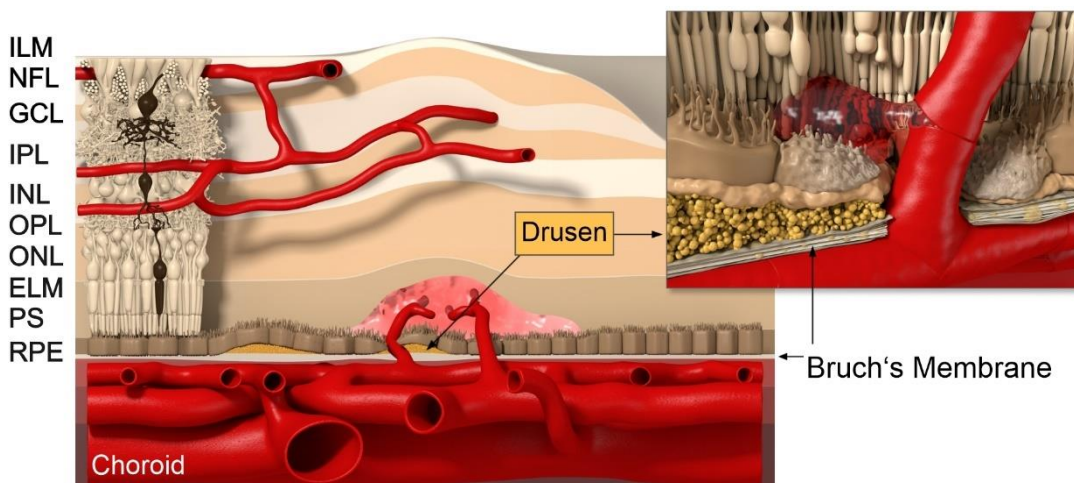
Figure 3. Schematic of the retina with macular neovascularization type 2 in AMD. Growth of vessels from the choroid through the RPE, presence of drusen and vascular leakage are depicted as well as disruption of RPE cells and Bruch's membrane.

ILM: inner limiting membrane, NFL: nerve fiber layer, GCL: ganglion cell layer, IPL: inner plexiform layer, INL: inner nuclear layer, OPL: outer plexiform layer, ONL: outer nuclear layer, ELM: external

limiting membrane, PS: photoreceptor segments, RPE: retinal pigment epithelium.
Image source: Effigos AG Leipzig

Deposits of acellular polymorphous debris called drusen are commonly found in people that are over 50 years old (Fig. 3) (Jager et al. 2008). Drusen are categorized into hard and soft and small to large in size and are located between the RPE and Bruch's membrane (Jager et al. 2008). As a sign of increased risk, drusen are often used to classify AMD. Presence of excessive numbers and sizes of drusen is used to determine disease stages, e.g. early stage AMD is characterized by the presence of less than 20 drusen that are 63 to 124 µm in size (Crabb et al. 2002; Abdelsalam et al. 1999; Jager et al. 2008). These yellowish extracellular deposits have been shown to contain oxidized remnants of outer segment contents (Crabb et al. 2002). Mass spectrometry studies revealed over 129 different proteins, including C3, C5, C6, C5, C8, C9, C5b-9 (MAC) and CFH (Wang et al. 2010; Crabb et al. 2002). The presence of complement factors in drusen led to the development of an inflammation model of AMD pathogenesis. In this theory, local chronic inflammation along with complement activation at Bruch's membrane causes a bystander effect that ultimately leads to photoreceptor degeneration (Anderson et al. 2010). Drusen are a byproduct in this model that accumulates the remnants of the lysed cells trapped between RPE and Bruch's membrane with the complement factors that contributed to the lysis (Anderson et al. 2010).

Several complement component variants and polymorphisms have been found to be risk factors for AMD. While some components (e.g. in CFHR1 and CFHR3) were found to be protective of AMD (Hannan et al. 2016; Skerka et al. 2013), several have been shown to be disadvantageous. Besides the already mentioned CFH Y402H, a disease association was found for CFI, C2, C3, C9, CFB and vitronectin variants (Fagerness et al. 2009; Fritsche et al. 2016; Maller et al. 2007) .

While anti-VEGF agents are successfully used to treat neovascular AMD, atrophic AMD drugs tend to focus on complement inhibition. Recent studies on an CFD- (lampalizumab) and a C5 inhibitor (eculizumab) however failed in clinical trials which highlights the need for further investigation into the mechanics of the local complement system in the retina.

Thesis aim

The involvement of the complement system in AMD and other retinal diseases makes it a prominent field of study with more than 100 studies being published yearly since 2014 (PubMed 2023). This thesis encompasses five of these studies that are part of an endeavor fueled by a passion for unraveling the intricacies of ocular immunity and vision preservation. The complement system, once thought to be primarily involved in immune defense, has revealed its multifaceted role in maintaining retinal homeostasis. Exploring the interplay between complement components and retinal cells ignites excitement as it uncovers potential insights into retinal diseases like AMD. With each discovery, a piece

of the puzzle that connects inflammation, neural connections, and visual function falls into place. This pursuit was driven by the desire to not only comprehend the complex interactions within the retina but also to pave the way for innovative therapies that could one day protect and restore the gift of sight. Consequently, the work on this thesis included the mapping of RNA and protein presence of complement components in the murine and human retina. Mechanisms of the complement system during acute injury events in the form of sodium iodate induced degeneration were investigated as well as during different stages of AMD. Finally, a gene addition therapy based on these finding was developed that preserves homeostatic complement functions while suppressing degeneration caused by excessive complement activity.

First Author Publications and Manuscripts

This thesis consists of four peer-reviewed studies that were accepted for publication in scientific journals and one unpublished manuscript. The papers/manuscripts are presented here, with contributions of the author of this thesis stated in the manuscripts and in detail at the end of this thesis.

Publication 1 – (Zauhar, Biber, Jabri, et. al., 2022)

As in Real Estate, Location Matters: Cellular Expression of Complement Varies Between Macular and Peripheral Regions of the Retina and Supporting Tissues

Randy Zauhar*, **Josef Biber***, Yassin Jabri*, Mijin Kim, Jian Hu, Lew Kaplan, Anna M. Pfaller, Nicole Schäfer, Volker Enzmann, Ursula Schlötzer-Schrehardt, Tobias Straub, Stefanie M. Hauck, Paul D. Gamlin, Michael B. McFerrin, Jeffrey Messinger, Christianne E. Strang, Christine A. Curcio, Nicholas Dana, Diana Pauly, Antje Grosche, Mingyao Li and Dwight Stambolian

*: Shared first authorship

Conceptualization: D.P., A.G., M.L., D.S. Methodology: R.Z., J.B., D.S., Y.J., M.K., J.H., L.K., A.P., N.S., V.E., U.S.-S., T.S., S.H., P.G., M.M., J.M., C.S. Investigation: R.Z., J.B., Y.J., D.S., M.K., L.K., A.P. Visualization: R.Z., J.B., Y.J., M.K., L.K., A.P. Supervision: D.P., A.G., M.L., D.S.. Writing—original draft: R.Z., J.B., Y.J., D.P., A.G., M.L., D.S. Writing—review & editing: R.Z., J.B., Y.J., L.K., S.H., C.C., D.P., A.G., M.L., D.S. All authors contributed to the article and approved the submitted version

Check for updates

As in Real Estate, Location Matters: Cellular Expression of Complement Varies Between Macular and Peripheral Regions of the Retina and Supporting Tissues

Randy Zauhar[1†], Josef Biber[2†], Yassin Jabri[3†], Mijin Kim[4], Jian Hu[5], Lew Kaplan[2], Anna M. Pfaller[2], Nicole Schäfer[3,6], Volker Enzmann[7,8], Ursula Schlötzer-Schrehardt[9], Tobias Straub[10], Stefanie M. Hauck[11], Paul D. Gamlin[12], Michael B. McFerrin[13], Jeffrey Messinger[12], Christianne E. Strang[13], Christine A. Curcio[12], Nicholas Dana[4], Diana Pauly[3,14‡], Antje Grosche[2‡], Mingyao Li[5‡] and Dwight Stambolian[4*‡]

[1] Department of Chemistry and Biochemistry, The University of the Sciences in Philadelphia, Philadelphia, PA, United States, [2] Department of Physiological Genomics, Ludwig-Maximilians-Universität München, Planegg-Martinsried, Germany, [3] Department of Ophthalmology, University Hospital Regensburg, Regensburg, Germany, [4] Department of Ophthalmology, Perelman School of Medicine, University of Pennsylvania, Philadelphia, PA, United States, [5] Department of Biostatistics, Epidemiology and Informatics, University of Pennsylvania Perelman School of Medicine, Philadelphia, PA, United States, [6] Department of Orthopaedic Surgery, Experimental Orthopaedics, Centre for Medical Biotechnology (ZMB), University of Regensburg, Regensburg, Germany, [7] Department of Ophthalmology, Inselspital, Bern University Hospital, University of Bern, Bern, Switzerland, [8] Department of BioMedical Research, University of Bern, Bern, Switzerland, [9] Department of Ophthalmology, Friedrich-Alexander-Universität Erlangen-Nürnberg, Erlangen, Germany, [10] Bioinformatics Unit, Biomedical Center, Ludwig-Maximilians-University Munich, Planegg-Martinsried, Germany, [11] Metabolomics and Proteomics Core and Research Unit Protein Science, Helmholtz-Zentrum München, Neuherberg, Germany, [12] Department of Ophthalmology and Visual Sciences, University of Alabama at Birmingham, Birmingham, AL, United States, [13] Department of Psychology, University of Alabama at Birmingham, Birmingham, AL, United States, [14] Experimental Ophthalmology, University of Marburg, Marburg, Germany

The cellular events that dictate the initiation of the complement pathway in ocular degeneration, such as age-related macular degeneration (AMD), is poorly understood. Using gene expression analysis (single cell and bulk), mass spectrometry, and immunohistochemistry, we dissected the role of multiple retinal and choroidal cell types in determining the complement homeostasis. Our scRNA-seq data show that the cellular response to early AMD is more robust in the choroid, particularly in fibroblasts, pericytes and endothelial cells. In late AMD, complement changes were more prominent in the retina especially with the expression of the classical pathway initiators. Notably, we found a spatial preference for these differences. Overall, this study provides insights into the heterogeneity of cellular responses for complement expression and the cooperation of neighboring cells to complete the pathway in healthy and AMD eyes. Further, our findings provide new cellular targets for therapies directed at complement.

Keywords: single cell, complement, age-related macular degeneration, retina, RPE/choroid

23

INTRODUCTION

Complement, a part of innate immunity serves as the first line of defense against foreign pathogens and altered cells. Depending on context, it is initiated by three distinct pathways: classical (CP), lectin (LP) and alternative pathway (AP). There are 40 - 60 complement proteins with various functions such as chemoattraction of immune cells, activation of leukocytes, opsonization of invading pathogens, lysis of susceptible pathogens, and synaptic pruning (1–4). The effector functions of the complement system are controlled through proteolytic generation of activation fragments that either bind to cell receptors or covalently attach to cell surfaces adjacent to sites of complement activation. It is the job of membrane bound regulatory molecules to modulate complement pathway activation proportionally to limit damage to host tissues (5, 6). The primary site of biosynthesis for the majority of the fluid-phase complement proteins is the hepatocyte and more than 90% of plasma complement is derived from the liver. Extrahepatic cells such as macrophages, endothelial cells and neurons can also produce complement constitutively and when induced (7).

CP activation is dependent on the binding of the recognition molecule C1q to patterns like IgM and IgG immune complexes, RNA, DNA, phosphatidylserine, CRP and others while the LP is activated when mannose binding lectin (MBL) or ficolins (FCN) bind to carbohydrate structures. Following activation, the CP and LP lead to successive cleavage of C4 and C2 and formation of the C3 convertase [C4bC2bC3b]. The AP is activated by spontaneous hydrolysis of C3 to $C3(H_2O)$ that subsequently binds complement factor B (FB). Cleavage of FB to Bb and Ba by complement factor D (FD) leads to formation of the AP C3 convertase $[C3b(H_2O)Bb]$. Of note, the AP includes an amplification loop for the CP and LP through the action of C3 $(H_2O)Bb$ on C3 to generate C3b which forms C3bBb and additional cleaving of C3. Finally, generation of C3b by any of the three pathways will lead to the generation of the C5 convertase and the common terminal pathway (1–4).

Structures such as the brain and eye have their own local complement expression due to the inability of bloodborne complement proteins to pass through the blood-brain and blood-retinal barriers (8–12). The retina is a specialized light-sensitive multilayered tissue composed of neurons, glia, and vasculature. The retinal pigment epithelium (RPE) is a monolayer of pigmented cells that metabolically supports outer retina and participates in the renewal of photoreceptor outer segments (13, 14). The underlying choroid is a specialized component of the systemic circulation, with pericytes/smooth muscle cells, fibroblasts, melanocytes, neurons, and immune cells (15). Understandably, it is important to determine the complement expression of the distinct cell types in the human retina, RPE and choroid. The idea of a local complement biosynthesis in the retina, RPE and choroid has been supported by earlier studies (16, 17). Importantly, several eye diseases such as glaucoma, diabetic retinopathy, autoimmune uveitis and age-related macular degeneration (AMD), have reported genetic associations with complement (18–20). A large effort of AMD research has been complement based due to strong evidence for complement

dysregulation and the identification of complement protein in extracellular deposits called drusen (21, 22). C3, complement receptor 1 (CR1), and terminal complement proteins C5b-9 (membrane attack complex, MAC) have been identified within drusen (23–25). In addition, genome wide association studies (GWAS) have reported significant associations of *complement factor H (CFH)*, *C3*, *complement factor I (CFI)*, *complement factor 9 (C9)*, and *complement factor B (CFB)* with AMD, further evidence that complement is involved in AMD (26).

AMD is a major cause of visual impairment in patients over the age of 65 (27). Currently it affects about 200 million worldwide and is predicted to increase to 300 million by 2040 (28). For reasons still being learned, AMD primarily affects the macula region (29), a specialized region in the retina of humans and non-human primates. In its advanced stages, there are two forms of AMD, geographic atrophy (GA; dry AMD) and choroidal neovascularization (CNV; wet AMD) (30). Both forms are associated with degeneration of photoreceptors, RPE and choroid. Although the current treatment for the wet form of AMD are intraocular injections of antibodies directed at vascular endothelial growth factor (VEGF) many of these treated patients go on to develop atrophy and further vision loss (31–33). Currently, there is no effective treatment for dry AMD. Biochemical, histological, and genetic studies have implicated several pathways involved in AMD, including oxidative damage, chronic inflammation, complement system malfunction and dysregulation of lipids as well as extracellular matrix (34, 35).

Recent clinical trials have utilized drugs to delay AMD progression through alteration of the complement pathway (reviewed in [36–38]). C3 inhibitors have received the most attention due to the dominant role of C3 as a control point for all three complement pathways. POT-4, a compstatin derivative and C3 inhibitor was used in clinical trials but had to be terminated due to lack of efficacy (39, 40). A second derivative of POT-4, APL-2 (Pegcetacoplan), recently completed phase 3 trials and showed a decrease in GA growth by 25% but was complicated by new onset choroidal neovascularization (CNV) (41). Clinical trials aiming to inhibit C5 have been met with modest success. Avacincaptad Pegol, a C5 inhibitor, was effective at reducing geographic atrophy (GA) growth by 28% but also suffered from a higher onset of CNV in the treated group (41, 42). Monoclonal antibodies directed at C5, Eculizumab and LFG316, have been used to treat GA but were unsuccessful in reducing GA progression (43). Other clinical trials directed at complement factors FD, properdin and FB did not show clinical efficacy (43, 44). Recent reports have raised concerns about treating GA with complement inhibitors (44). Reasons for these failures or modest successes with complications might include route of administration, inappropriate target cells for modulation, failure to select patients most likely to benefit, insensitive trial endpoints, and limited understanding of both complement expression in healthy retina, RPE and choroid and the role of complement in AMD pathophysiology.

This urgent need to assess the complement gene expression in single cells, resolve cell types, characterize the signature of complement expression across cells, and identify differences in

health and disease can now be met implementing recent technological breakthroughs in single cell RNA-sequencing (scRNA-seq) (45–47). To the best of our knowledge, this is the first comprehensive study that describes the single cell RNA and protein expression of complement in the human retina, RPE and choroid. Protein expression was determined for many of the complement expressing genes either by mass spectrometry or western blotting. We also compared our human complement expression to our previously published mouse complement single cell retina data to report differences that should be considered before testing drugs targeted for humans in preclinical mouse studies (48). Finally, we identified local complement expression changes in retina and choroid from post-mortem eyes affected with early AMD. Our results underscore the power of single cell technologies to gain deeper insight into complement homeostasis and assist in our understanding of the complement dysregulation occurring in AMD. Our results increase the knowledge base that exists for ocular complement and will provide investigators with essential additional information to design novel therapies.

RESULTS

Atlas of Complement Expression in the Human Retina, RPE and Choroid Identified by scRNA-seq

Aiming to better understand the contribution of locally produced complement components to immune homeostasis in the posterior part of the human eye, we generated complement expression profiles for all cell types of the human retina, RPE and choroid *via* scRNA-seq (**Table S1**). Cell clusters were annotated using known gene markers for retina and choroidal cell types and clusters sharing the same markers were combined into 11 cell types for the retina and 10 cell types for the choroid (49–51). To analyze the RPE for complement expression we re-processed the scRNA-seq data from Voigt et al (51).

Only a few complement activators were expressed in the retina and included *C1QA-C, C1R, C1RL, C1S, CFB, CFD, C3* and *C7* (**Figure 1A**). Activators for the LP, *FCN1/3* and *MASP1/3*, had minimal expression. By *in situ* hybridization, *CFD* and *C3* transcripts were confirmed in microglia (**Figure 2A**). Moreover, the *C7* expression that surprisingly was confined to horizontal cells was verified as well (**Figure 2A**). Of the cells expressing secreted complement components, microglia had the highest transcription especially for *C1QA-C*. Surprisingly, the RPE had negligible expression of complement activators (**Figure 1B**), while all the activators for the CP were expressed in the choroid, albeit not in every cell type (**Figure 1C**). In the choroid, macrophages had the highest expression of *C1QA-C* while fibroblasts demonstrated robust expression signals for *C1R, C1RL* and *C1S*. Of note, *C3* the central component of the complement pathway was robustly transcribed in fibroblasts (**Figure 1C**).

The soluble complement regulators *component 1q subcomponent binding protein* (*C1QBP*) and *clusterin* (*CLU*)
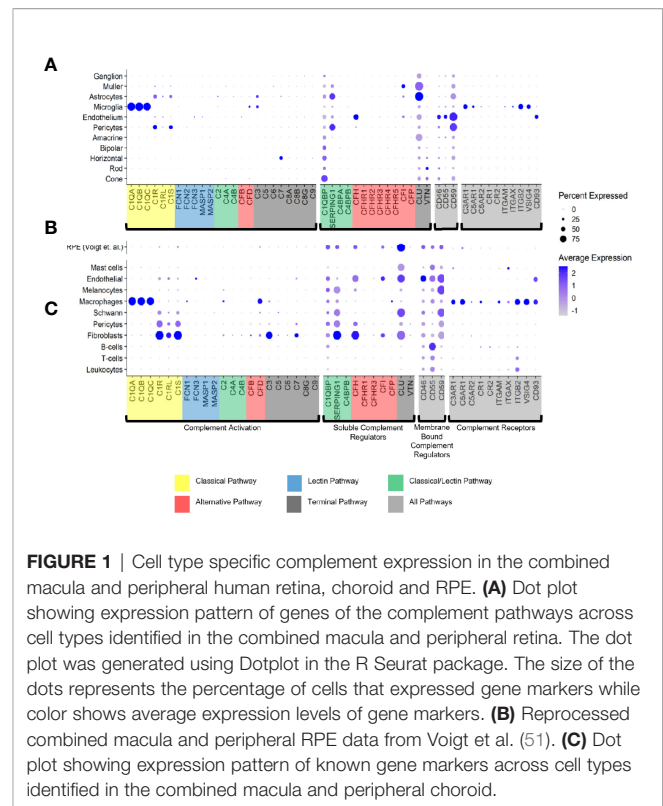

FIGURE 1 | Cell type specific complement expression in the combined macula and peripheral human retina, choroid and RPE. **(A)** Dot plot showing expression pattern of genes of the complement pathways across cell types identified in the combined macula and peripheral retina. The dot plot was generated using Dotplot in the R Seurat package. The size of the dots represents the percentage of cells that expressed gene markers while color shows average expression levels of gene markers. **(B)** Reprocessed combined macula and peripheral RPE data from Voigt et al. (51). **(C)** Dot plot showing expression pattern of known gene markers across cell types identified in the combined macula and peripheral choroid.

were transcribed by all the retinal cell types, while *CFH* transcription was mostly confined to the endothelium (**Figures 1A**, **2B**). A modest *CFI* expression signal was present in Müller glia and endothelium (**Figures 1A**, **2B**). SERPING1, a regulator dissociating the C1 complex by binding C1r and C1s, showed robust expression in both pericytes and astrocytes. In the RPE, we found moderate expression of regulators *C1QBP, SERPING1, CFH, CFI* and robust expression of *CLU* (**Figure 1B**). Finally, most of the regulators were expressed in various cell types of the choroid (**Figure 1C**). Choroidal fibroblasts had robust signals for *SERPING1, CFH* and *CLU*. It should be noted that *CFHR2* and *CFHR5* had no detectable expression in the retina and RPE/choroid. *CFHR1, CFHR3* and *CFHR4* expression was weak and limited to specific cell types in the retina and RPE/choroid.

The membrane bound complement regulators *CD46, CD55* and *CD59*, demonstrated robust expression in retinal vascular endothelium (**Figure 1A**). Surprisingly, *CD55* transcripts were also found by *in situ* hybridization to co-localize with the microglia marker *AIF1* (**Figure 2B**). CD59, which blocks membrane perforation of C5b-9, is expressed on all retinal cell types to varying degrees. Positive expression of *CD59* across all retinal cell types would make the retina resistant to MAC damage unless the regulators became overwhelmed. A similar conclusion would apply for the RPE and choroid due to moderate to robust expression of all three membrane bound regulators in most cell types. Noteworthy is the absence of *CD59* from choroidal B and T cells.
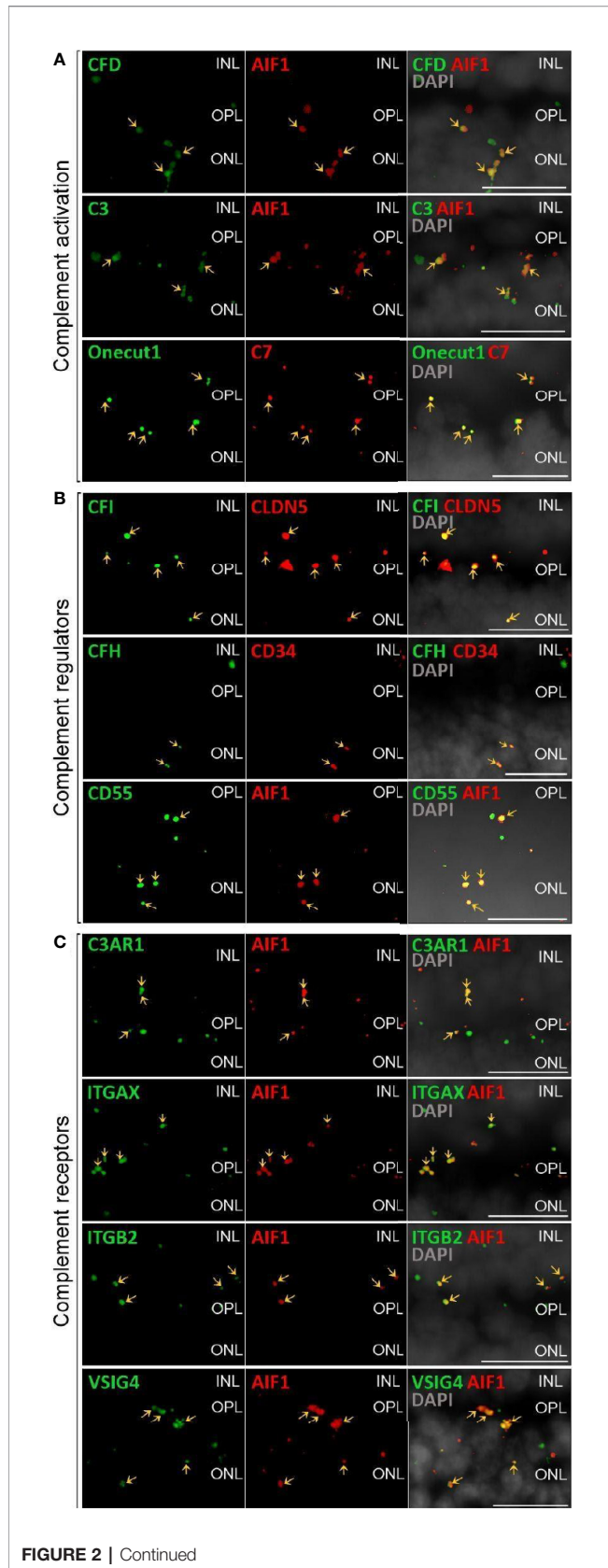
FIGURE 2 | Validation of scRNA-seq for retinal complement component expression by *in situ* hybridization. **(A)** Factors driving complement activation were chosen for detection by *in situ* hybridization. *CFD* expression from microglia was detected in the inner nuclear layer (INL), outer plexiform layer (OPL) and outer nuclear layer (ONL), but was mostly associated with microglia expressing *AIF1* (alias *IBA1*) in the OPL. *C3* expression was mostly limited to microglia located in OPL. *C7* transcripts were detected in the OPL with overlap of signal with the horizontal marker Onecut1 in the OPL. **(B)** Soluble (*CFH, CFI*) and membrane-bound (*CD55*) complement regulators primarily colocalized with vascular cells and microglia. Signals of *CFH* transcript were strongest from INL and OPL and overlapped with the endothelial marker *CD34*. *CFI* expression associated with the endothelial marker *CLDN5* was strongest in the INL and OPL. *CD55* was robustly expressed in microglia expressing *AIF*. **(C)** Complement receptor *C3AR1* transcripts were detected at low levels in the INL and OPL and co-localized with the microglia marker *AIF1*. *ITGAX* was robustly expressed in the OPL and co-localized with the microglia marker *AIF1* in the OPL. *ITGB2* transcripts were less abundant and co-localized with *AIF1* in the OPL. Also *VSIG4* was strongly expressed in OPL and ONL co-localizing with the microglia marker *AIF1*. **(A–C)** Arrows indicate co-localization of the gene of interest with respective cell marker. Scale bars, 20 µm.

Finally, we identified the cell types expressing complement receptors which would make these cells most responsive to changes in local complement homeostasis. The integrin family receptors, *ITGAM*, *ITGB2G* and *ITGAX*, bind iC3b facilitating immune clearance and phagocytosis (1). Retinal microglia expressed all three receptors (**Figures 1A**, **2C**). *VSIG4*, an immunoglobulin superfamily receptor, is also highly expressed in retinal microglia and is responsible for phagocytosis of C3b and iC3b (1). *CD93*, involved in clearance of apoptotic cells, is expressed in retinal endothelial cells. *C3AR* and *C5AR*, receptors for C3a and C5a, are modestly expressed in microglia cells. This microglia-specific expression pattern could also be confirmed by *in situ* hybridization for *C3AR*, *ITGAX*, *ITGB2* and *VSIG4* (**Figure 2C**). Interestingly, except for *C5AR1*, none of the complement receptors were detectable by scRNA-seq in the RPE. Choroidal macrophages demonstrated a similar expression profile to retinal microglia (**Figure 1**). In addition, choroidal T cells and leukocytes expressed *ITGB2*.

Differential Expression Between Normal Macula and Peripheral Retina and Choroid

Significant differences in complement expression were detected in healthy retinal cells from the macula and peripheral retina (**Data File S1**). We found transcript reduction in the macula for *CFI* in astrocytes, *CLU* in bipolar, horizontal and ganglion cells as well as *VTN* in rods. In contrast, *VTN* in cones, *CD46* in endothelial cells and *CD59* in pericytes were increased in the macula compared to the periphery.

Similarly, a number of choroidal genes showed significant expression differences between cells located in sub-macula and peripheral regions (**Data File S1**). These differences included decreased *CLU* in Schwann cells, *C3* in macrophages, *CFI* and *C1R* in endothelial cells, *CFH* in pericytes, *C1R*, *C1S*, *CLU*, *CFD*, *C3*, *CD55* and *SERPING* in fibroblasts, and *CFH* and *SERPING* in melanocytes. We found increased expression in the sub-macula region compared to the periphery in macrophages for *C1Q*, *C2* and *VSIG4*.

Complement Transcriptome of Human Retinal Cell Types, RPE and Choroid Partially Translated Into Protein Expression

It is known that transcript expression does not necessarily correlate with protein levels (52, 53). This has also been confirmed at the single cell level under very well-controlled conditions and underscores the necessity of measuring proteins as well as RNA (54). Accordingly, we validated select transcripts at the protein level (**Figures 3**–**6**). Purified retinal cells were obtained by sequential magnetic-activated cell sorting (MACS) of ITGAM-positive microglia, CD31-positive vascular cells (endothelium, pericytes), and CD29-positive Müller glia, while the remaining cell population consisted of photoreceptors and other neuronal types (**Figure S1**) (48). The cell populations with high yield in terms of cell numbers recovered after MACS (Müller glia, neurons, RPE/choroid) were subjected to LC-MS/MS mass spectrometry (**Figure 3**). The level of cell enrichment was determined by marker gene expression and marker protein abundance (**Figure S1**).

Remarkably, consistent with scRNA-seq, the soluble complement regulators CLU and C1QBP as well as the membrane bound regulator CD59 were detected at protein level (via LC-MS/MS mass spectrometry) in all cells of the inner and outer retina and in most cell types of the RPE/choroid, albeit at varying levels and rates (**Figure 3**). Western blot analysis of some selected candidates confirmed that their identified RNAs were translated (**Figures 4**–**6**). C1s is an esterase cleaving C2/C4, thereby facilitating the formation of the CP C3-convertase. C1s peptides were not detected by LC-MS/MS mass spectrometry possibly because this method is less sensitive to proteins of low abundance (**Figure 3**). Western blot did detect C1s heavy chain in the Müller cell population, which includes astrocytes, and also in the CD31-positive vascular cell population (**Figure 4B**). Thus, the findings of *C1S* transcripts in astrocytes, Müller cells, and pericytes (**Figure 1A**) by scRNA-seq were confirmed. To a lesser extent, C1s protein was also found in microglia, RPE/choroid and retinal neurons (**Figure 4A**).

C3, the central protein of the complement system, is under tight regulation to prevent inadvertent complement activation. *C3* transcript detection using scRNA-seq was mainly restricted to microglia and astrocytes in the retina and to fibroblasts in RPE/choroid (**Figure 1**). Its protein was also detected in or on purified retinal neurons *via* LC-MS/MS mass spectrometry (**Figure 3**) and western blot (**Figure 5**). Also, C3 cleavage product, C3d, was detected in or on all purified retinal cell types (**Figure 5A**).

Also, VTN and components of the terminal pathway (C5, C6, C8A, C8B, C8G, C9) proteins were detected in RPE/choroid samples (**Figure 3**). However, protein analysis sometimes provided contradictory results. This challenge of detecting secreted proteins is clearly reflected in our data. LC-MS/MS mass spectrometry is an unbiased screening method that can miss complement components already secreted and not tightly attached to cell surfaces. As a result, lower levels of intracellular proteins might be under the detection limit. The same is true for western blot analyses of enriched retinal cell populations,
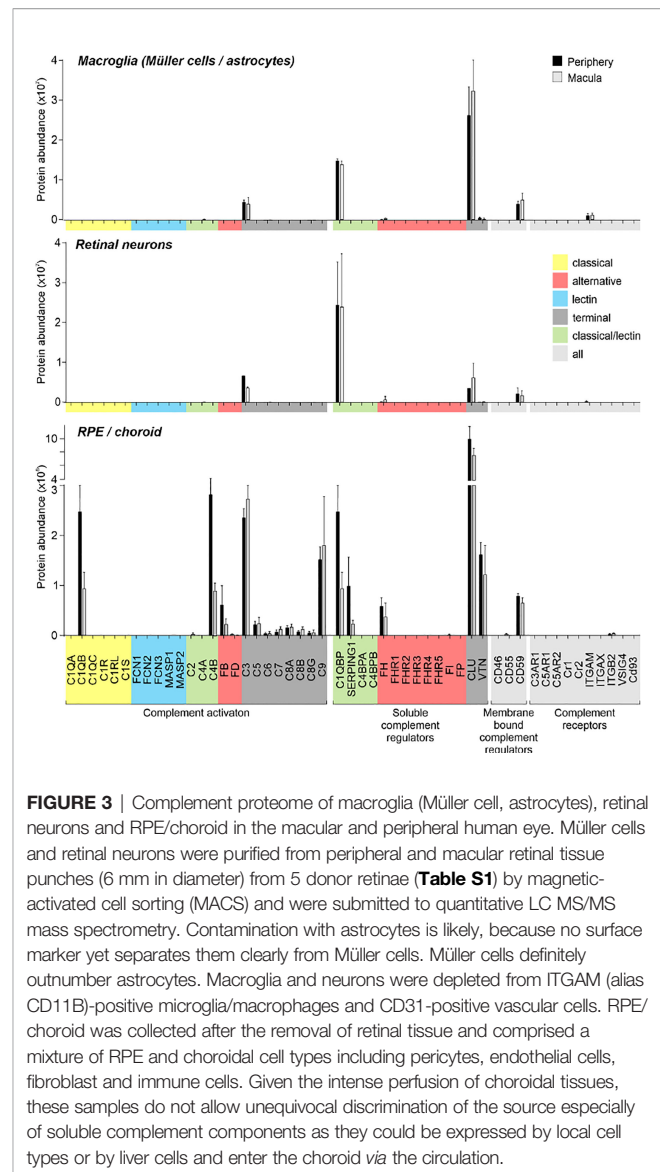

FIGURE 3 | Complement proteome of macroglia (Müller cell, astrocytes), retinal neurons and RPE/choroid in the macular and peripheral human eye. Müller cells and retinal neurons were purified from peripheral and macular retinal tissue punches (6 mm in diameter) from 5 donor retinae (**Table S1**) by magnetic-activated cell sorting (MACS) and were submitted to quantitative LC MS/MS mass spectrometry. Contamination with astrocytes is likely, because no surface marker yet separates them clearly from Müller cells. Müller cells definitely outnumber astrocytes. Macroglia and neurons were depleted from ITGAM (alias CD11B)-positive microglia/macrophages and CD31-positive vascular cells. RPE/choroid was collected after the removal of retinal tissue and comprised a mixture of RPE and choroidal cell types including pericytes, endothelial cells, fibroblast and immune cells. Given the intense perfusion of choroidal tissues, these samples do not allow unequivocal discrimination of the source especially of soluble complement components as they could be expressed by local cell types or by liver cells and enter the choroid *via* the circulation.

although they are more sensitive than LC-MS/MS mass spectrometry. To achieve the most complete picture of protein localization in the tissue, we added immunostaining to detect protein accumulation of select complement components at protein level, irrespective of the actual, expressing source in the tissue. C1s localized to the ganglion cell layer (GCL) and at spots all over the retina possibly reflecting its secretion into the interstitial space (**Figures 4C–E**). C3 was specifically detected on cones of the macular retina (**Figure 5E**), and also Müller cells (**Figure 5D**) – the latter being in line with transcript data.

Similarly, protein expression was determined for additional complement factors. C7 stood out from the list of terminal complement components, since scRNA-seq indicated a very specific expression by horizontal cells (**Figure 1**). However, LC-MS/MS mass spectrometry detected C7 in RPE/choroid samples only (**Figure 3**), while western blot detected whole C7 in neuroretina as well as RPE/choroid and C7 cleavage products

FIGURE 4 | C1s protein expression in the human retina. (A) Full C1s (~75 kDa) and the C1s heavy chain (~47 kDa) were reliably detected by Western blot using purified C1s protein and human serum (HS). C1s-depleted HS still contained remaining C1s heavy chain, while full length C1s was absent. (B) Western blot analysis of C1s on purified retinal cell types from peripheral human retina and RPE/choroid. The total protein extracted per cell population was loaded. PDHB (pyruvate dehydrogenase beta subunit) served as housekeeper that has been shown to be expressed at equal levels in all investigated cell types. In contrast to HS, primarily the heavy chain of C1s was detected in retinal samples. C1s levels were highest in Müller cells (MC) and vascular cells (VC). MG, microglia; NR, whole neuroretina. RPE, retinal pigment epithelium including choroid. (C) Representative micrographs of C1s-stainings from macular (left) and peripheral (right) retinae. Photoreceptors and cells of the ganglion cell layer (GCL) as well as punctate structures in the inner plexiform layer (IPL) displayed highest labeling intensities. Sections were co-stained for the Müller cell marker glutamine synthetase (GLUL). (D) Higher magnification of the outer nuclear layer (ONL) and Henle fiber layer (HL) in the macular retina showed a partial overlap of C1s and GLUL. (E) Co-staining of C1s with calretinin, a marker of inner retinal neurons such as ganglion and amacrine cells, yielded no considerable overlap. (C-E) INL, inner nuclear layer; OPL, outer plexiform layer; PRS, photoreceptor inner and outer segments. Scale bars, 20 µm.

FIGURE 5 | C3 protein expression in the human retina. (A) The C3 α-chain (~120 kDa) and its cleavage products were robustly detected by Western blot if purified C3 or human serum (HS) was loaded. No characteristic bands were detected in C3-depleted HS. (B) Western blot analysis of C3 on purified retinal cell types from peripheral human retina and RPE/choroid. The total protein extracted per cell population was loaded. PDHB served as housekeeper since not the exact same amount of protein could be loaded given the low protein yield from the microglial (MG) and vascular cell (VC) populations. The C3 α-chain and its cleavage product C3d were detected in every retinal cell population at comparable levels. MC, Müller cells; N, retinal neurons; NR, whole neuroretina; RPE, RPE/choroid mixed samples. (C) Representative micrographs of C3-stainings from macular (left) and peripheral (right) retinae. Photoreceptors, photoreceptor terminals and Müller cell processes were positively labeled. Co-staining for the Müller cell marker glutamine synthetase (GLUL) demonstrated an overlap primarily in cells from the peripheral retina. (D) Higher magnification of the inner nuclear layer (INL) highlighting the co-localization of C3 and GLUL (arrows). (E) Co-staining of C3 and GLUL did not result in an overlap in the outer retina. C3 stained cone photoreceptors (asterisk) which form a single row excluding rod photoreceptors from that layer in the central retina. (C–E) GCL, ganglion cell layer; IPL, inner plexiform layer; OPL, outer plexiform layer; ONL, outer nuclear layer; PRS, photoreceptor inner and outer segments. Scale bars, 20 µm.

in all retinal cell populations (**Figure 6B**). In support of this finding, C7 immunoreactivity was detected across the whole retinal section (**Figures 6C, D**).

Acting together with FH, FI inactivates C3b through sequential cleavage to iC3b, C3c, C3dg and finally C3d. Western blotting identified FI in/on microglia, Müller cells and CD31-positive vascular cells, but very little association with neurons or RPE/choroid (**Figure 6F**). The location of FI in microglia was confirmed by immunostaining (**Figure 6G**). FH, an additional regulator of complement activation, inactivates C3b in the presence of FI. LC-MS/MS mass spectrometry and western blots identified FH in RPE/choroid (**Figure 3**; **Figure 6J**). Since contamination of the RPE/choroid samples
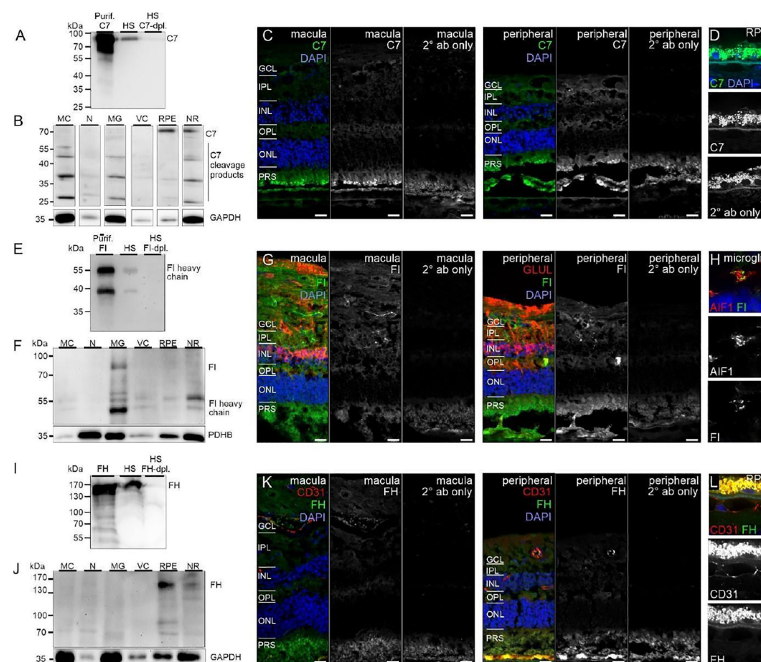
FIGURE 6 | CFI, CFH and C7 protein expression in the human retina. **(A)** Loading purified C7 or human serum (HS), full length C7 was detected as a single band (~90 kDa) and cleavage products <90 kDa. **(B)** Full-length C7 was detected at low levels in purified cell types, but robustly in RPE/choroid. Cleavage products were detected in all cell populations. C7 immunoreactivity was similar in macular and peripheral retinal sections. **(D)** Higher magnification of the C7 staining in RPE. **(E)** Loading purified CFI or HS, only the CFI heavy chain (~50 kDa) was unequivocally detected by Western blot. **(F)** CFI was present in Müller cells (MC), microglia (MG), vascular cells (VC) and RPE/choroid, but not in neurons. **(G)** Comparable CFI-labeling of structures of the macular and peripheral retina. CFI-immunoreactivity partially overlapped with that of the Müller cell marker glutamine synthetase (GLUL). **(H)** Higher magnification of the inner plexiform layer (IPL) demonstrating co-localization of CFI with IBA1-positive microglia. **(I)** Detection of CFH (~150 kDa) by Western blot using purified CFH and HS. **(J)** CFH was only detected in RPE/choroid. A contamination with CFH from the system circulation cannot be excluded. **(K)** CFH immunoreactivity was confined to vessel lumens. **(L)** Minor CFH immunoreactivity at the RPE – Bruch's membrane interface at higher magnification. **(B, F, J)** PDHB or GAPDH (Glyceraldehyde-3-phosphate dehydrogenase) served as housekeepers. N, neurons; NR, whole neuroretina. **(C, D, G, H, K, L)** GCL, ganglion cell layer; OPL, outer plexiform layer; ONL, outer nuclear layer; PRS, photoreceptor segments. Scale bars, 20 µm.

with systemic FH protein is likely, these results have to be interpreted with caution. Immunostaining located FH on the luminal side of retinal and choroidal vessels (**Figures 6K, L**), consistent with our scRNA-seq result of the endothelial cell's robust expression of *CFH* (**Figure 1**).

Human and Murine Retinal Cells Showed Species-Specific Complement Transcriptomes

Experimental approaches to investigate human diseases and underlying complement action involved studies in mouse models (48, 55–57). To facilitate the transfer of murine complement results to the human system, we compared the scRNA-seq expression of different complement components in the normal human peripheral (rod-dominated) retina and our own published study on rod-rich mouse retina (**Figure 7**) (48). Several differences in complement expression were observed between both species. For the CP, elevated expression levels were found in human compared to mouse retina: *C1Q*, the molecular recognition component for activation of the CP, is exclusively expressed by microglia in mice and humans, with

high expression of all three components of this complex (*C1QA*, *C1QB* and *C1QC*) in both human and mouse (**Figure 7**). The remaining components of the C1 complex, *C1R* and *C1S*, which activate C4 and C2 upon recognition of antigen-antibody complexes, show significant overlapping expression in pericytes. Human pericytes and astrocyte/Müller cell fractions express both *C1R* and *C1S* at similar levels. Mouse pericytes and endothelial cells also express these transcripts, whereby *C1S* is detected at higher levels than *C1R* in the mouse. LP proteins were almost not detectable in both mouse and human, suggesting this pathway has a negligible role in maintaining cellular homeostasis in the normal eye. With respect to the AP activators, *CFD* is expressed in human microglia and not detectable in scRNA-seq, but with qPCR, in the mouse retina. *C3*, involved in both CP and AP, is especially detected in human microglia (**Figure 7**). Murine microglia showed much lower expression levels (48).

The soluble regulators of the CP demonstrated differences between human and mouse (**Figure 7**). *C1QBP* expression was more robust across all human cell types compared to mouse. *SERPING1* also showed higher expression in human than in murine endothelial cells, microglia, Müller cells and pericytes.

The soluble regulators of the AP, *CFH* and *CFI*, showed very large differences. *CFH* was strongly expressed in human endothelial cells, while its expression in mouse was highest in microglia and pericytes. Interestingly, FI which acts in concert with FH, showed high expression in human endothelium and Müller glia but was almost undetectable in the mouse retina (**Figure 7**) (48). *VTN* and *CLU*, both soluble negative regulators of all complement pathways, are differentially expressed across all cell types, with expression of *CLU* higher in human than mouse in all cell types except cones. *VTN* is expressed at higher levels in mouse compared to human in all cell types except horizontal cells.

Overall, we found higher levels for the terminal soluble and membrane bound complement regulators in the human retina compared to the mouse retina (**Figure 7**). *CD46* was expressed in most human retinal cell types, but had no expression in mouse retina. Similarly, *CD55* was only expressed in human, specifically in microglia, endothelial and ganglion cells. Finally, *CD59* is expressed broadly, but differentially, across cell types, with expression generally being higher in human than in mouse in

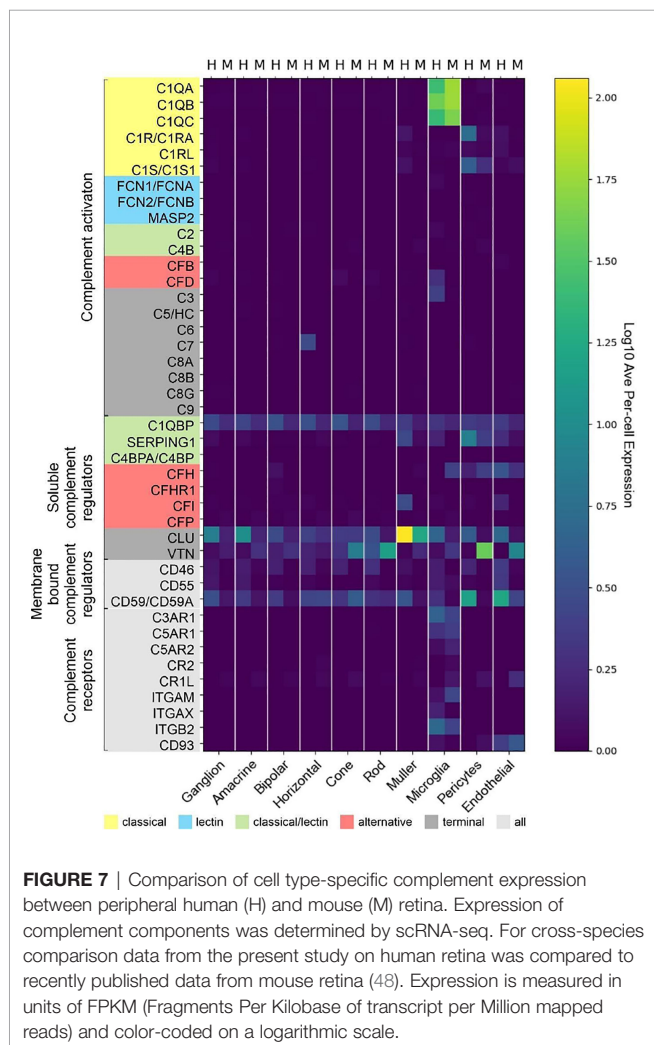all cell types except cones. *CD59* expression is absent in mouse microglia and pericytes.

Notably, we found more agreement of complement receptors for microglia in mouse and human. While mouse microglia express all three anaphylatoxin receptors, human microglia express only *C3AR1* and *C5AR1*. The expression of the integrins *ITGAM*, *ITGAX* and *ITGB2* are also exclusive to microglia. *ITGAX* and *ITGB2* show significant expression in human microglia, *ITGAM* and *ITGB2* in mouse microglia. The complexes of these integrins, ITGAM/ITGB2 and ITGAX/ITGB2, termed CR3 and CR4 respectively, recognize inactivated complement C3 (iC3b) on cell surfaces (58–60).
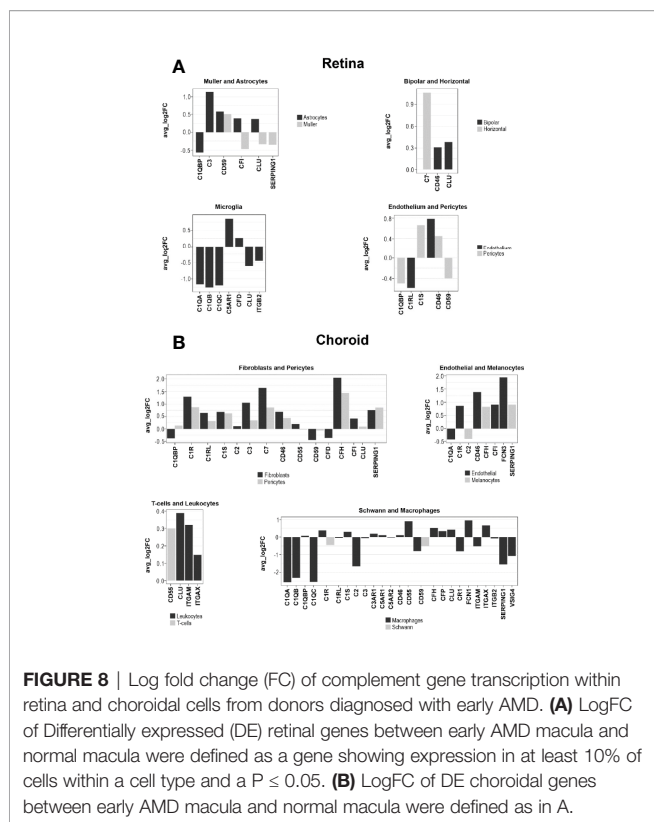
We also found interesting species-specific differences with respect to proteins. C3 protein was detected *via* western blot in all purified human retinal cell types (**Figure 4B**), while it could only be identified in samples from murine RPE and neurons (48). Moreover, the complement inhibitor FH was present in samples from all mouse retinal cell types except for vascular cells (48), but on the other hand FH protein was only detectable in human RPE (**Figure 6J**).

In summary, there are distinct complement expression differences between the mouse and human retina which should be considered when using the mouse as a model for developing therapeutics intended for humans.

AMD-Associated Changes of the Complement Transcriptome by Single-Cell RNA-seq in Human Retina and Choroid

The species-related differences in complement necessitate a focus on human donor tissue to fully understand the role of complement in AMD pathology. To achieve this, we applied scRNA-seq to samples from early AMD cases and healthy donors. We clustered human retinal cells collected from human retina from donor eyes (**Table S1**) and performed analyses of complement gene expression, comparing early AMD macula vs normal macula and macula vs periphery in early AMD samples. For the comparison of early AMD vs. normal macula retina we identified several complement genes with significant differential expression for the retina (p≤0.05); most fold changes are small in magnitude (**Figure 8A** and **Data File S1**). The largest fold changes (FC) were found for *C1Q* which is down-regulated in microglia, *C3* which is up-regulated in astrocytes, and *C7* which is upregulated in horizontal cells. In microglia the anaphylatoxin receptor *C5AR1* and *CFD* was up-regulated and *ITGB2* was down-regulated. Membrane-bound complement inactivator *CD46* was upregulated in endothelium, pericytes and in bipolar cells. *CFI* was up-regulated in astrocytes and potential gliotic Müller cells, but down-regulated in homeostatic Müller cells. The inhibitor of MAC formation *CD59* was up-regulated in astrocytes and Müller cells and down-regulated in pericytes. The complement regulator *CLU* was up-regulated in astrocytes and bipolar cells and down-regulated in microglia and in Müller cells. Complement regulator *C1QBP* was down-regulated in both astrocytes and pericytes. In pericytes, *C1S*, which is required for *C1* activation, was up-regulated 1.6-fold.

FIGURE 7 | Comparison of cell type-specific complement expression between peripheral human (H) and mouse (M) retina. Expression of complement components was determined by scRNA-seq. For cross-species comparison data from the present study on human retina was compared to recently published data from mouse retina (48). Expression is measured in units of FPKM (Fragments Per Kilobase of transcript per Million mapped reads) and color-coded on a logarithmic scale.

FIGURE 8 | Log fold change (FC) of complement gene transcription within retina and choroidal cells from donors diagnosed with early AMD. **(A)** LogFC of Differentially expressed (DE) retinal genes between early AMD macula and normal macula were defined as a gene showing expression in at least 10% of cells within a cell type and a P ≤ 0.05. **(B)** LogFC of DE choroidal genes between early AMD macula and normal macula were defined as in A.

To find regional expression differences for retina complement in AMD, we also compared early AMD macula vs. early AMD periphery (**Data File S1**). The largest differential expression between macula and periphery was found in astrocytes, where *C3* and *CFI* show about 2-fold lower expression in macula compared to periphery. *C3* showed higher expression in microglia in the macula. Other complement genes show fold change smaller than 1.5-fold.

Cells from the choroid were collected from the same donor eyes for single-cell complement analyses similar to retinal cells. In contrast to our results for retina, the choroid showed larger changes to 5-fold (**Figure 8B** and **Data File S1**). All the cell types in the choroid manifested transcriptional differences in one or more complement genes when comparing early AMD and normal macula sub-macular choroid (**Figure 8B** and **Data File S1**). Melanocytes had increased *SERPING1* and *CFH* expression. Macrophages showed a decline in *C1Q* (5-fold) and *SERPING1* (3.3-fold) and *CD59*. Increases in *CFH* expression were seen in early AMD sub-macular regions. In AMD donors, choroidal endothelial cells from the sub-macular region showed an increase in *CD46* and *FCN3* (3.8-fold). Pericytes showed increased expression of *C1R*, *C1S*, *CD46*, *CFH*, *C7*, *C3* and *SERPING1*. Choroidal fibroblasts from the sub-macular region had higher *C3*, *CFH*, *SERPING1* and *CFI* expression in early AMD. and a decrease of *CFD* (1.2-fold) in early AMD. Fibroblasts also expressed *C7* at higher levels than pericytes. Leukocytes, T and B cells had minimal differentially expressed (DE) complement transcripts.

Choroidal sub-macula and peripheral cells from early AMD donors were compared for potential clues to explain why the macula is the preferred site of AMD pathology. The largest differences between sub-macula and periphery (**Data File S1**) of the choroid in early AMD were present in Schwann cells, melanocytes, macrophages, endothelial, and fibroblasts. Schwann cells had less *CLU* and *CFD* expression in the sub-macular region. Macrophages from the sub-macula showed decreased *C1QB*, *CR1*, *C3* and increased *CFD*, *CD55*, and *FCN1*. Choroidal endothelial cells from the sub-macular region had a 2.8-fold increase of *FCN3*. Choroidal fibroblasts from the sub-macular region showed decreases in *CLU*, *SERPING1*, *C1R*, *C1S*, *C3*, *CD55* and increased *CFD* expression.

Early and Late AMD-Associated Changes of the Complement Transcriptome by Bulk RNA-seq in Human Retina and RPE/Choroid

We next determined the difference in complement expression using bulk RNA-seq data obtained from retina and RPE/choroid/sclera tissue samples from normal and patients diagnosed with AMD. Because this dataset includes results from early- and late-stage AMD cases, it also allowed us to answer the question of whether trends in complement changes in early AMD are confirmed or even amplified with disease progression. In macular retina (MR), the majority of complement genes are up-regulated in late AMD (**Data File S2** and **Figure 9**). The largest FC are for all components of the C1 complex (*C1QA, C1QB, C1QC, C1R, C1S*) that recognizes antibody-antigen interactions and initiates the CP of complement activation. FC (late AMD versus normal) for these genes range from 67-fold for *C1Q* to 32-fold for *C1R*. Activators of the AP, *CFB* (8-fold) and *CFD* (16-fold) were also strongly upregulated. *FCN1*, an activator of the LP, was 17-fold upregulated in the MR of late AMD. Interestingly, the gamma subunit of C8 is expressed in our samples at very low levels and with little variation with respect to location or disease state while C9 is completely absent in our data (**Figure 9**). The next-highest fold changes in MR are the soluble negative regulators of complement activation, *CFH* up-regulated 63-fold and *SERPING1* up-regulated 37-fold in late AMD. This trend was slightly visible already in early AMD retinae and is in line with *CFH* upregulation in pericytes determined by scRNA-seq as well. Of the membrane-bound inhibitors of complement activation, only *CD59* is significantly up-regulated (5-fold in late AMD). *CLU*, which inhibits formation of the terminal C5b-9 complex, is expressed at a high level irrespective of disease stage or location (**Figure 9**). *VTN*, another antagonist of C5b-9 complex formation, is expressed at low levels and is the only inhibitor down-regulated (3-fold) in MR of late AMD patients. Also, *CFP* is up-regulated 4-fold suggesting a more active amplification loop of C3 convertase formation in AMD. Other genes with significant up-regulation in MR in late AMD include the anaphylatoxin receptors, *C3AR1*, *C5AR1* and *C5AR2* (15-24-fold), the integrins *ITGAM*, *ITGAX*, *ITGB2* (3-20-fold), and the adhesion molecule *CD93* (20-fold). In peripheral retina (PR),
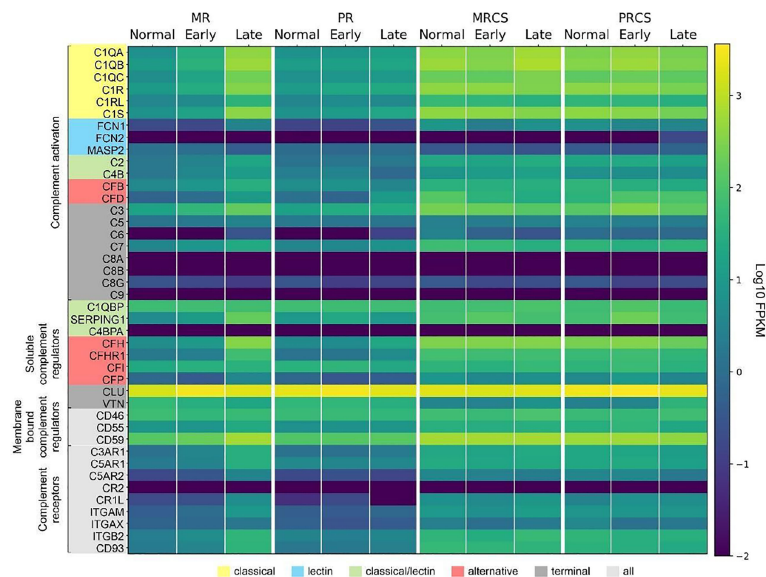
FIGURE 9 | Heat map of complement gene expression determined using bulk RNA-seq for macular retina (MR), peripheral retina (PR), macular RPE/choroid/sclera (MRCS) and peripheral RPE/choroid/sclera (PRCS) from normal, early AMD and advanced AMD donors. Expression is measured in units of FPKM and color-coded on a logarithmic scale.

some up-regulation is observed in late AMD, but with much smaller fold-changes (**Data File S2** and **Figure 9**).

In macular RPE/choroid/sclera (MRCS) and peripheral RPE/choroid/sclera (PRCS) bulk data, patterns of expression for most complement genes do not depend strongly on disease state. For some of the deviations the interpretation is not clear. For example, *CFD* shows modest down-regulation with AMD in MRCS and up-regulation in PRCS. Because these samples contain RPE cells and, most importantly, a large proportion of scleral cells in addition to choroidal cells, no cross-comparison was performed with the data from our scRNA-seq approach to avoid over- or misinterpretation of the data.

These observations thus partially confirm our findings from the scRNA-seq approach and, importantly, suggest a robust perturbation of complement homeostasis in the MR in advanced AMD which is not present in the retina periphery, choroid MRCS and PRCS.

DISCUSSION

Understanding how the local complement homeostasis in the retina and supporting tissues is changing in the course of diseases like AMD is key to identify appropriate targets and optimal timing for a successful therapeutic intervention. Anderson et al. published a comprehensive analysis of complement expression in human RPE, choroid and retina (17). Their analysis was done on tissue layer lysates as opposed to the current study which focused on single cells from these layers. They characterized the choroid as the predominant source of soluble regulators, SERPING1 and C4BP.

The membrane regulators, CD55 and CD46, were also higher expressed in the choroid than in RPE or retina. C3 and the terminal pathway genes, C5 and C7, expression was localized within the choroid as well. While the regulators CLU and VTN were expressed in all three layers. LP expression was very low in all three layers. Tissue lysates from several donors with AMD were also assayed by quantitative PCR but no significant differences were detected between normal and AMD eyes (17). Their overall results concluded that the choroid was the predominant source of CP and AP components, rather than the RPE or retina. Our study extends the Anderson et al. study to single cell expression of the complement genes in normal retina, RPE and choroid as well as early AMD retina and choroid (17).

A Refined Map of Complement Expression in Retina, RPE and Choroid

C1q is the recognition protein for the CP and it must complex with both C1r and C1s to activate the CP (1). The retina showed distributed transcription of *C1Q*, *C1R* and *C1S* with *C1Q* expressed in microglia and *C1R/ C1S* expressed in both astrocytes and pericytes (**Figure 1A**). Of note, *C1Q* was expressed by almost all sequenced microglia. Astrocytes and pericytes expressed also most of the soluble complement regulator *SERPING1*, a dissociator of the C1 complex (**Figure 1A**). Thus astrocytes/pericytes appear to have opposing roles as activators and inhibitors of the CP. Interestingly, *SERPING1* is significantly downregulated in astrocytes in macula vs periphery in early AMD (**Data File S1**).

In the normal choroid, *C1Q* is solely expressed in macrophages which is in line with findings for retinal

microglia (**Figures 1A, C**). Choroidal pericytes and fibroblasts express both *C1R* and *C1S* (**Figure 1C**). Multiple cell types in the choroid including fibroblasts, pericytes, Schwann cells and melanocytes show robust *SERPING1* expression. According to scRNA-seq results, the RPE has minimal transcription of CP activators (**Figure 1B**).

The initiators of the LP pathway, FCN1-3 and MASP1, showed no expression in the normal retina, choroid and RPE suggesting the LP pathway is inactive in all healthy layers.

The C3 convertase is short-lived with a half-life of about 90 seconds requiring stabilization to assure efficient host defense (1). Properdin (gene ID: CFP) stabilizes the alternative C3 convertase and is solely expressed in macrophages of the choroid but is not expressed in RPE and retina (**Figure 1**). While an antagonistic inactivator of C3, FI, was primarily contributed by Müller glia, an important macroglial cell type in the retina (**Figure 1A**).

The late-acting complement components of the terminal pathway, including C7, assemble into the terminal complement complex to form either a cell membrane pore that induces cell lysis or a soluble sC5b-9 complex with multiple functions. Except for C7, the other components of the terminal pathway were not detected in healthy cells. *C7* transcripts were expressed in both normal retina and choroid, albeit confined to the horizontal cells in the retina and fibroblasts in the choroid. *C7* transcripts translate into a 91 kDa protein that we demonstrated to be present in the healthy neuroretina and RPE by western blotting (**Figure 7B**). C7 has a prominent cathepsin D cleavage sites leading to lysosomal protein degradation fragments, which were additionally detected in all retinal cell types (61). The functional relevance of C7 cleavage products however is still unknown. Immunostaining showed a uniform distribution of C7 in the macular and peripheral human retina. This study, thus, provides new insights into the retinal localization of C7 as the only late complement protein expressed in the neuroretina (**Figure 2**). Additionally, *C7* is upregulated in both astrocytes and horizontal cells in early AMD.

Terminal complement components, namely the C5b-9 complex, have previously been detected only in the Bruch's membrane/choroid complex in aged healthy controls (17, 62). Pore formation is triggered *via* the conversion of C5 to C5b by surface-bound C5 convertases and subsequent local formation of C5b6. The next step, binding of C5b6 with C7 must occur rapidly to prevent release of C5b6 from the membrane surface. If C7 concentrations near the site of complement activation are limiting, the stable bimolecular C5b6 complex dissociates from the C5 activating complex and accumulates in solution (63). If this C5b6 complex subsequently encounters C7, fluid-phase C5b-7 is formed, and this complex can lyse normal cells at a different location from the initial site by 'reactive lysis' (64). Therefore, it is advantageous to have local retinal horizontal and choroidal fibroblasts expressing C7 so that its presence can prevent diffusion of C5b6 from the cell membrane.

The soluble inhibitors for the C5b-9 terminal complex, CLU and VTN, had different cellular expression patterns. In the retina, all cells expressed *CLU* but in the choroid its expression

was limited to mast, endothelial, melanocytes, Schwann, pericytes and fibroblasts. RPE also had robust *CLU* expression activity. *VTN* was expressed in rods, cones and horizontal cells. Very low *VTN* expression was detected in both choroid and RPE. The robust expression of *VTN* and *CLU* in healthy cells is important to decrease the deposition of C5b-9 onto their surface. Importantly, *CLU* was upregulated in both ganglion and horizontal cells in the macula of early AMD.

Implications of Cell Type-Specific Protein Signatures for Selected Complement Components

To infer functional implications of a particular complement component in retinal immune homeostasis, one must ask where the respective protein accumulates in the tissue, especially if, as it is the case with most complement components, the protein of interest is secreted. Our protein expression data of selected complement components in the healthy adult human retina showed for the first time (i) an intraretinal localization of C1s and C7, (ii) spatial differences for C3 detection in the macula and periphery, and (iii) a FI colocalization with microglial cells, indicating a physiological function of the complement system in the human retina.

C1s, is one of the first proteolytically active components of the CP. The assembly of the classical C3 convertase (C4bC2a) requires the activity of C1s. We detected the heavy chain of C1s mainly in Müller and vascular cells purified from healthy retinal tissue (**Figure 4B**). Human retinal immunostaining showed associated C1s deposition in the macular and peripheral areas in the inner plexiform, ganglion cell, and compartments of the photoreceptor layers (**Figures 4C, D**). The punctate C1s-positive structures did not overlap with the tested Müller cell, amacrine or ganglion cell markers or nuclei, but seemed to be allocated to cell surfaces or the intercellular space. According to the human cell atlas, C1s is mainly localized in the nucleoplasm and additionally in the cytoplasm (65). In line with present findings, we recently detected C1s heavy chain in the photoreceptor and ganglion cell layer of healthy, photodamaged and post-ischemic murine retinas (48, 66).

C3 is the central complement protein and all complement pathways converge at the level of C3 activation. It is expressed differently in the RPE, retina and choroid. *C3* mRNA was modestly expressed in retinal microglia and astrocytes, robustly expressed in choroidal fibroblasts and minimally expressed in RPE cells (**Figure 1**). We detected C3 protein deposition in healthy retinas (**Figures 6C–F**). In the retinal periphery, C3 protein colocalized with Müller cells, endothelium and with cells in the ganglion cell layer (**Figure 5D**). In the macular region, C3 protein was detected in the outer plexiform layer and on cone photoreceptors (**Figure 5C**). Previous work also reported C3 immunoreactivity for a subset of cone photoreceptors approximately 1.5 mm peripheral to geographic atrophy lesions but not in healthy retinas (67). The outer plexiform layer and photoreceptor-associated C3 deposition in healthy tissue was largely restricted to the macular region in our study (**Figure 5C**). Comparison of our results with other studies is

difficult as in most cases it is not clearly specified which retinal regions were used for staining in healthy controls and the ganglion cell layer was never imaged (17, 67, 68). Our C3 protein results for the healthy retina add to the current knowledge on C3 immunoreactivity in Bruch's membrane/choroid.

While the liver is the predominant source of circulating C3 (69), it has been shown to be synthesized by immune and nonimmune cells such as lymphocytes, neutrophils, epithelial, and endothelial cells (9, 70, 71). In some cases, the accumulation of intracellular C3 can aggravate tissue damage, while in others it can be protective against cytokine induced death (72–75). There is good evidence that intracellular complement provides tissue specific protection against distinct stimuli such as injury and in some cases functions in cell metabolism (76–78). Kulkarni et al. published elegant work on C3 biosynthesis in human airway epithelial cells that is augmented during times of stress and acts as a cytoprotectant (71). The same study found increased intracellular C3 in airway epithelial cells in end-stage lung disease due to cystic fibrosis or chronic obstructive pulmonary disease. In our study choroidal fibroblasts demonstrated an increase of C3 expression in early AMD, potentially for a protective effect. It is unknown how intracellular C3 stores in the choroid and retina are modulated and whether altering these stores is deleterious or protective.

Complement responses are tightly regulated. The damaging C3 cleavage product, C3b, is inhibited by FH and FI in the fluid phase and on membrane surfaces by the receptors CD55 and CD46. Retinal endothelial cells express *CFH* and *CFI*, while Müller glia express *CFI*. Also, the choroid had robust expression of *CFH* and *CFI* from endothelial cells and fibroblasts. Western blots associated FI mainly with the retinal microglial cell population (**Figure 6F**) and to a lesser extent to RPE/choroid. This corresponded with FI immunostaining in the plexiform layers in the adult healthy retina, and with overlapping microglial staining in the inner plexiform layer (**Figures 6G, H**) (79). In addition, partial overlap of FI staining with the Müller cell marker glutamine synthetase was observed, which is consistent with their single-cell mRNA profile (**Figures 2**, **6G**). In line with these findings, previous publications localized FI immunoreactivity mainly to the inner retina (17).

FH is the major complement inhibitor of the AP. Consistent with previous reports (17, 80), we detected FH protein in the RPE/choroid and at vessels in the healthy human retina. We could not identify spatial differences between macular and peripheral retinal tissue. This suggests a role in maintaining retinal immune privilege at the inner and outer retinal blood barrier rather than intraretinal activity.

Almost half the retinal cell types expressed *CD55* or *CD46* which inactivates C3b and C4b in the presence of FI. Not detectable expression of *CD55* and *CD46* in ganglion cells, astrocytes, microglia, rods, cones and Müller glia makes these cell types more susceptible to damage from C3b and C4b binding. In addition, every choroidal cell type expressed either *CD46* or *CD55*, providing broad protection from C3b and C4b. RPE expressed *CFH* and *CFI* and modestly expressed the receptors *CD46* and *CD55* that provide a reasonable barrier against complement damage. Our finding of less *CD46* and *CD55* expression on normal rods and cones might be the reason C3 is able to accumulate on photoreceptor surfaces in AMD.

ScRNA-seq Refines Our Understanding on the Cellular Contribution to Complement Changes in AMD

While only very moderate changes in complement expression were observed in early AMD for retinal cell types, our choroidal scRNA-seq findings demonstrated increased expression of the secreted complement components *CFI, C1R, FCN3, CFH, C3, C7* and *SERPING1*. *C3* was increased in fibroblasts (2-fold) and pericytes (1.3-fold) and *C7* was increased 3-fold in fibroblasts and 1.8-fold in pericytes. *FCN3* had minimal expression in normal endothelial cells but increased 3.8-fold in early AMD. Ficolins serve as recognition molecules for the LP and activate the MBL-associated serine protease family, MASPs. Importantly, *FCN3* is a primate specific gene and only exists as a pseudogene in mice (81). It has been reported to bind to apoptotic Jurkat cells promoting C3 and C4 activation (82). The membrane regulator CD46 was ubiquitously expressed in normal choroid and showed higher expression in most of the same cell types in early AMD (fold change ranging from 1.1-2.6). The rise in *CD46* expression could be a compensatory response to the enhanced secreted complement component expression. In early AMD, *CFH* also showed large increases in early AMD in macrophages, pericytes, and fibroblasts - most likely to offset increased C3b.

Our comparison of the sub-macula vs peripheral choroid in early AMD identified significant increases in *FCN3* expression in endothelial cells of the sub-macula (3-fold) than in peripheral choroid. Interestingly, FCN3 was reported to be elevated in the vitreous of eyes with proliferative diabetic retinopathy along with increased VEGF suggesting a collaboration between FCN3 and VEGF to stimulate inflammation and angiogenesis (83). Other differences in choroidal macular complement expression from early AMD eyes included a 3-fold decrease of *CFD* and 1.5-1.6-fold decrease of *CLU* in Schwann cells and fibroblasts as well as a 1.4-fold *FCN1* and 1.3-fold *CFD* increase in macrophages compared to their cellular counterparts from peripheral AMD choroid.

Currently, there are two competing theories of the tissue layer responsible for the initiation of AMD. One theory implicates RPE cell dysregulation as the starting location because drusen and RPE pigmentary changes often precede advanced AMD stages (84). Alternatively, more recent evidence cites the choriocapillaris as the initiating site due to capillary dropout, a hallmark of early AMD (85). In line with this, Lutty et al. reported attenuation of the vascular supply in the submacular region with overlying normal RPE in early AMD (86). The vascular diminution was confined to the macula and absent in the periphery providing strong evidence that the choroid, not the RPE, could be the initiation site of AMD (81). Our complement results in the macula of early AMD provide further evidence (i) that there are choroidal expression differences confined to the macula region and (ii) that the retinal cell complement

expression signature is not as dramatically changed as observed in the choroid which implies that (iii) the disruption of the local complement homeostasis in early AMD is driven by the choroid rather than retinal cell types. Since our analysis did not include RPE, we cannot determine its contribution to the pathology.

Bulk RNAseq Confirms Early Changes of Complement Expression That Are Accelerated With AMD Progression

While bulk RNA-seq data are relatively insensitive to gene expression changes limited to specific cell types (which might provide important clues to mechanisms of disease initiation), this approach does provide a global picture of large-scale changes in expression at the tissue level. In particular our data for macular and peripheral retina reveal that AMD progression is associated with increasing up-regulation of a number of complement genes associated with the CP and AP and therewith validate findings from our scRNA-seq approach, and that these changes are largely restricted to the macular retina (**Figure 8** and **Data File S2**).

In moving from normal through early and into late-stage AMD there is progressive up-regulation in the macula retina of complement genes associated with the CP, including all components *C1Q*, the *C1Q*-associated activators *C1R* and *C1S*, *C2* and *C3*, and the initial members of the membrane attack complex *C5*, *C6* and *C7*. The soluble complement inhibitors *CFH* and *SERPING1* are also up-regulated, as well as the membrane-bound regulator of the C5b-9, *CD59*, perhaps reflecting regulatory feedback accompanying complement activation. The up-regulation of anaphylatoxin receptors (*C3AR1*, *C5AR1*, *C5AR2*) is most pronounced in late AMD, as is the expression of *ITGAM* and *ITGB2*, implying the activation of phagocytosis related to complement-coated particles in late AMD. This pattern of progressive up-regulation of complement genes is only weakly observed in the peripheral retina.

In contrast, the expression levels of complement genes in the macular and peripheral RPE/choroid/sclera (RCS) are similar to the highest levels observed in the macular retina, and are relatively uniform with respect to disease stages, with a small number of differentially-expressed complement genes (**Data File S2**). Interestingly all the DE genes in macula RCS show down-regulation in late AMD, while genes in the periphery RCS are mainly up-regulated. In particular, expression of *CFD* is down-regulated in late AMD in MRCS, and up-regulated in PRCS. We note that the expression of the terminal C5b-9 components *C8* and *C9* are largely absent in all of our RNA-seq data, but are observed at the protein level which may reflect proteins transported from the choroid blood supply.

A recent study of nine complement genes in normal eyes and eyes with early, intermediate and advanced AMD partially recapitulates our results (87). Their results for macula retina showed a complex pattern of regulation for most of the nine complement genes examined when moving from early to intermediate AMD and partially agree with our results. However, their results are almost in complete accord with our findings for late-stage AMD, showing up-regulation of *C1QA*,

C3, *C4B*, *CFB*, *CFD*, *CFH* and *MASP1* in late AMD with respect to control. In contrast, we did not reproduce their finding of significant up-regulation of *CFI* and down-regulation of *CFP*. Our results for RCS similarly showed higher average expression for most complement genes compared to macula retina. Additionally, both studies showed down-regulation of *CFD* in the RPE/choroid. Both studies found no expression for terminal MAC component *C9*.

Our bulk data results suggest that even though the initiation of AMD may not depend strongly on changes in retinal cells, the macula retina is still the principal site of complement activation as the disease progresses.

Species Differences in Retinal Complement Expression Complicate the use of Animal Models in AMD Research

A thorough comparison of the cellular landscape of complement expression in the retina across species is important to assess the usability of animal and specifically mouse models to investigate pathological mechanisms of AMD for the development of human therapies. For that reason, we compared results from the present study on human retina with previous results collected from its mouse counterpart and, indeed, found considerable differences (48). These low levels in mouse retina (but significant detection in the human retina) should be considered when investigating the mouse AP. Finally, there is the striking difference regarding membrane bound complement regulator expression. Absence of CD46 and CD55 in mouse retina would suggest a different pathway for inactivating both C3b and C4b at the cell membrane surface. Of course, these expression differences exist under a normal physiological state and could change in the setting of disease.

Our results provide strong evidence of complement synthesis in the healthy retina, RPE and choroid. The body of evidence suggests that local complement expression impacts all cell types and that complement's functions in the tissue environment could go beyond its role in the innate system (88). Accordingly, there is an urgent need to further investigate alternative complement functions in the human eye. Multiple publications provide evidence for complement orchestrating normal cell and organ development even in the immune privileged central nervous system (89, 90). These include direct tissue repair and regulation of basic processes of the cell, particularly in metabolism (77). A receptor for C1q has been identified on mitochondria which in the presence of intracellular C1q mediates mitochondrial ROS production (91). A direct link between C3a and downregulation of proteasome activity was reported in human RPE cells from older individuals, suggesting a link with intracellular protein longevity (92). Our data identified multiple complement genes expressed under normal physiological conditions that must have biological functions that maintain integrity of the retina, RPE and choroid. Further studies are necessary to investigate complement function for its role in homeostasis to provide a foundation for AMD clinical trials evaluating treatment with complement inhibitors [reviewed in (36–38)].

Limitations of our study include a focus on European American donors and a limited number of disease donors for single cell analysis.

MATERIALS AND METHODS

Human Donor Eyes

Tissues were obtained from human eye donors at different institutions, as indicated below. The Institutional Review Boards of each institution approved the respective use of human tissues.

Study Subjects and scRNA-seq

Samples were taken from macular and peripheral regions of the retina from two normal donor eyes (**Table S1**, samples 18-1077-W, 18-1132-P) at UAB and used in scRNA-seq studies at UPenn as described in (93). Briefly, raw counts were converted to log-normalized expression values with a scale factor of 10,000 UMIs per cell, the 2,000 most variable genes across all cells were identified, and the cells were clustered using the DESC algorithm (94). Eleven major retinal cell types were identified using this data, providing cell-type-specific expression profiles for complement genes.

Additional samples were obtained from three donor eyes (**Table S1**, samples 20-1166-W, 20-1438-W, 20-1484-W) at UAB and used in scRNA studies at UPenn. All donor eyes were collected within 6 hours postmortem and characterized for presence of AMD and other pathology by author C.A.C. Following removal of the anterior chamber and vitreous, the eyecup was immersed in oxygenated Ames media. Relief cuts were made in the posterior eyecup to expose the tissue and 8mm punches were obtained from macular retina and temporal (peripheral) retina and carefully isolated from the retinal pigment epithelium. The choroidal layer was isolated similarly. The isolated tissue layers were dissociated with activated papain (Worthington Biochemical Corp.) as previously optimized to obtain a high percentage of viable cells. After dissociation, magnetic bead-based removal of dead cells (Miltenyi Biotec) was used to reach the optimum target for viability of 85-95% per sample. Viability was determined by FACS sort or by staining an aliquot of the dissociated cells with trypan blue, 0.4% (Sigma-Aldrich). Single cell transcriptome libraries were prepared by using 10xGenomics Single Cell 3' biased v2 kit according to the company's manual. The constructed single cell libraries were sequenced by HiSeq 2000 sequencer (Illumina, Inc., San Diego, CA, USA) with total reads per cell targeted for a minimum of 50,000. Raw base call (BCL) files were aligned to human genome reference GRCh38-2020-A and processed with 10x Genomics Cell Ranger 3.1.0 to produce gene count matrices for each sample. For each sample replicate, we performed initial quality control using Cell Ranger (Version 3.1.0). Then, we further filtered the data using Seurat (version 3.0). A cell was retained in downstream analyses if it meets the following criteria (1): More than 200 genes are detected (2); Total number of UMIs is between 1,000 and 25,000. Retina and choroid cells were

separated into two datasets and analyzed separately from each other. Each dataset was processed using Seurat 3.0, a statistical framework to combine cell gene expression profiles measured by scRNA-seq (95). Expression data was normalized by dividing the counts for each feature of a cell by the total counts for that cell and multiplying the result by a scale factor of 10,000; this was then transformed to a natural-log scale. Gene expression levels were normalized using the 2,000 most variable features in the datasets as identified by Seurat's *FindVariableFeatures* function. Cell clustering was completed using Seurat's shared nearest neighbor (SNN) modularity optimization-based clustering algorithm. This clustering was performed and evaluated using a range of resolution values, with a resolution of 1.5 being selected for the choroid cells and 0.2 for the retina cells. Differentially expressed genes for the generated clusters were compared to known choroid and retina cell type markers to identify and label cell-types, and cell-type-specific expression profiles for complement genes were determined. Eleven major retinal and ten major choroidal cell types were identified in this analysis. Since no RPE cells were recovered in this study, sc-RNA-seq data from Voigt et al. was reanalyzed and used to supplement our data with complement gene expression levels for that single cell type (51).

Bulk Tissue Processing and Data Generation

Eye Collection and AMD Assessment

This study utilized 14 pairs of eyes from non-diabetic Caucasian donors 69-95 yr of age (84.73 yr ± 5.53 yr; 7 males and 7 females) at a death-to-preservation interval of < 6 hr. Ocular health histories were not available. Eyes were opened by eye bank recovery personnel using an 18 mm diameter corneal trephine, followed by a snip to the iris to facilitate penetration of preservatives into the fundus. The left eye was preserved in RNAlater (Qiagen) at 4°C. Left eyes were shipped on wet ice *via* overnight courier to University of Pennsylvania where they were processed for bulk RNA sequencing upon arrival.The right eye was preserved in 2% glutaraldehyde and 1% paraformaldehyde in 0.1M phosphate buffer at 4°C. It was assessed for maculopathy at UAB by internal inspection using a dissecting scope (Nikon SMZ-U) with oblique trans- and epi-illumination in consultation with an MD medical retina specialist, ex vivo multimodal imaging of excised 8 mm diameter macular punches using digital color photography and spectral domain optical coherence tomography volume scans (SD-OCT; Spectralis, Heidelberg Engineering) with a custom tissue holder (co-author JDM), and high-resolution epoxy-resin histology, as described. The definition of AMD used in this study was the presence of one large druse (>125 μm in diameter) in the macula or severe RPE changes in the setting of at least one druse or continuous basal linear deposit, with or without the presence of neovascularization and its sequelae. Eyes with geographic atrophy had at least one region 250 μm in diameter lacking a continuous RPE layer (but possibly containing 'dissociated' RPE). Unremarkable eyes were those lacking characteristics of AMD or other chorioretinal disease as

discernible in either histology or ex vivo imaging; these served as comparison eyes.

Sequencing and Analysis of Bulk Data

RNA for the eye tissues was extracted using the AllPrep DNA/RNA Mini Kit (Qiagen). Extracted RNA samples underwent quality control assessment using R6K ScreenTape on a 2200 Tapestation (Agilent, Santa Clara, CA, USA) and were quantified using Qubit 2.0 Fluorometer from Life Technologies (Grand Island, NY). All RNA samples selected for sequencing had an RNA integrity number of ≥8. The Strand-specific RNA library was prepared from 100 ng total RNA using the Encore Complete RNA-seq library kit (Nugen Technologies, Inc., San Carlos, CA, USA) according to the manufacturer's protocol. RNA-sequencing was performed at the Center for Applied Genomics at the Children's Hospital of Philadelphia per standard protocols. The prepared libraries were clustered and then sequenced using HiSeq 2000 sequencer (Illumina, Inc., San Diego, CA, USA) with four RNA-seq libraries per lane (2×101-bp paired-end reads). The RNA-seq data were aligned to the hg38 reference genome using GSNAP (version 2016-06-30) with known splice sites (SNP file build 147) taken into account. In order to eliminate mapping errors and reduce potential mapping ambiguity owing to homologous sequences, several filtering steps were applied. Specifically, we required the mapping quality score of ≥30 for each read, reads from the same pair were mapped to the same chromosome with expected orientations and the mapping distance between members of the read pair was 200,000 bp. Quality control analysis of the aligned data was performed using program RNA-SeQC. All subsequent analyses were based on filtered alignment files. Per-gene counts were generated from the GSNAP alignments using the HTSeq-count program (version 0.6.0) using default 'union' mode and the HG38 reference genome.

In Situ Hybridization
Human Retina Tissue Preparation

Within 6 hours of death, posterior poles were fixed in freshly made 4% paraformaldehyde/0.1M phosphate-buffered (PB, pH 7.4, Thomas Scientific, LLC, Swedesboro, NJ, USA) overnight, then washed and stored in 1% paraformaldehyde/0.1 M PB at 4°C. Eyes were shipped on wet ice *via* overnight courier to University of Pennsylvania. This study conformed to Institutional Review Board regulations for use of human tissues at University of Alabama at Birmingham (UAB) and at University of Pennsylvania. Dissection of retina/choroid/sclera was performed as described (96). Retina tissues were cryoprotected in increasing concentration of sucrose as described (97) followed by embedding in OCT (Tissue Tek, Sakura Finetek USA, Torrance, CA, USA) and immediately snap-frozen in ice-cold 2-methylbutane. The frozen tissue was sliced at 10 μm in the cryostat and stored at -80°C.

RNA-FISH Protocol

Single molecule RNA *in situ* hybridization (RNA-FISH) was carried out with the RNAscope® Multiplex Fluorescent Reagent Kit v2 (Advanced Cell Diagnostics, INC, Newark, CA, USA). Probes were used for this study are: Hs-AIF1-C3 (#433121-C3),

Hs-ONECUT1 (#490081), Hs-CD34-C2 (#560821-C2), Hs-CFH (#428731), Hs-CFI (#421921), Hs-CLDN5-C2 (#517141-C2), Hs-RLBP1-C2 (#414221-C2), Hs-FOS (#319901), Hs-JUN (#470541), Hs-C3AR (#461101), Hs-ITGAX (#419151), Hs-ITGB2 (#480281), Hs-VSIG4 (#446361), Hs-C3 (#430701), Hs-C7-C3 (#534791-C3), Hs-CD46 (#430151), Hs-CD55 (#426551), Hs-CFD (#420831). Positive control RNAscope® 3-plex probe (#320861) and RNAscope® 3-plex negative control probe (#320871) were used (data not shown) for each experiment. In addition, probe diluent (#300041) was used for negative control.

Proteomic Profiling of MACS Enriched Retinal Cell Types
Tissue Collection

Samples for proteome profiling were isolated from a set of five donor eyes. The Institutional Review Board at University of Regensburg approved the use of human tissues for this purpose. One eye per donor from five non-diabetic Caucasian donors 59-89 yrs of age (4 males and 1 female) at a death-to-experimentation interval of < 30 hr were included in this analysis (**Table S1**). Ocular health histories were not available. Eyes were opened by eye bank recovery personnel using an 18 mm diameter corneal trephine and stored on ice for transfer to the laboratory for further processing.

Cell Purification From Human Donor Retina

Retinal cell types were enriched as described previously using magnetic-activated cell sorting (MACS) (98). Briefly, retinal punches (6 mm in diameter, centered over the fovea and for comparison, the peripheral punch was performed at 1 mm from the macular punch and inferiorly in relation to it) were treated with papain (0.2 mg/ml; Roche Molecular Biochemicals) for 30 minutes at 37 °C in the dark in Ca^{2+}- and Mg^{2+}-free extracellular solution (140 mM NaCl, 3 mM KCl, 10 mM HEPES, 11 mM glucose, pH 7.4). After several washes and 4 minutes of incubation with DNase I (200 U/ml), retinae were triturated in extracellular solution (now with 1 mM $MgCl_2$ and 2 mM $CaCl_2$). To purify microglial and vascular cells, the retinal cell suspension was subsequently incubated with anti-mouse/human ITGAM (alias CD11B) and anti-human CD31 microbeads according to the manufacturer's protocol (Miltenyi Biotec, Bergisch Gladbach, Germany). The respective binding cells were depleted from the retinal suspension using large cell (LS)-columns, prior to Müller cell enrichment. To purify Müller glia, the cell suspension was incubated in extracellular solution containing biotinylated anti-human CD29 (0.1 mg/ml, Miltenyi Biotec) for 15 minutes at 4°C. Cells were washed in an extracellular solution, spun down, resuspended in the presence of anti-biotin ultra-pure MicroBeads (1:5; Miltenyi Biotec,) and incubated for 10 minutes at 4°C. After washing, CD29+ Müller cells were separated using LS columns according to the manufacturer's instructions (Miltenyi Biotec). Cells in the flow through of the last sorting step - depleted of microglia, vascular cells and Müller glia - were considered as the neuronal population. RPE was obtained by scraping from the sclera of the punched-out piece of tissue after the retina had been removed, so those samples inevitably contained cells of the underlying choroid. Therefore,

those samples are referred to as RPE/choroid throughout the manuscript.

LC-MS/MS Mass Spectrometry Analysis

LC-MS/MS analysis was performed as described previously on a Q-Exactive HF mass spectrometer (Thermo Fisher Scientific Inc., Waltham, MA, U.S.A.) coupled to an Ultimate 3000 RSLC nano-HPLC (Dionex, Sunnyvale, CA) (99, 100). Briefly, 0.5 µg sample was automatically loaded onto a nano trap column (300 µm inner diameter × 5 mm, packed with Acclaim PepMap100 C18. 5 µm, 100 Å; LC Packings, Sunnyvale, CA) before separation by reversed phase chromatography (HSS-T3 M-class column, 25 cm, Waters) in an 80 minutes non-linear gradient from 3 to 40% acetonitrile (ACN) in 0.1% formic acid (FA) at a flow rate of 250 nl/min. Eluted peptides were analysed by the Q-Exactive HF mass spectrometer equipped with a nano-flex ionization source. Full scan MS spectra (from m/z 300 to 1500) and MS/MS fragment spectra were acquired in the Orbitrap with a resolution of 60,000 or 15000 respectively, with maximum injection times of 50 ms each. Up to ten most intense ions were selected for HCD fragmentation depending on signal intensity (TOP10 method). Target peptides already selected for MS/MS were dynamically excluded for 30 seconds. Spectra were analyzed using the Progenesis QI software for proteomics (Version 3.0, Nonlinear Dynamics, Waters, Newcastle upon Tyne, U.K.) for label-free quantification, as previously described (98). All features were exported as a Mascot generic file (mgf) and used for peptide identification with Mascot (version 2.4) in the UniProtKB/Swiss-Prot taxonomy mouse database (Release 2017.02, 16871 sequences). Search parameters used were: 10 ppm peptide mass tolerance, 20 mmu fragment mass tolerance, one missed cleavage allowed, carbamidomethylation set as fixed modification, and methionine oxidation, asparagine or glutamine deamidation were allowed as variable modifications. A Mascot-integrated decoy database search calculated an average false discovery rate (FDR) of < 1%.

Western Blot

Cell pellets of enriched cell populations from retinal punches were dissolved in reducing Laemmli sample buffer, denatured and sonicated. Neuronal protein extraction reagent (Thermo Fisher Scientific, Braunschweig, Germany) was added to the neuron populations. Samples were separated on a 12% SDS-PAGE. The immunoblot was performed as previously described (101). Detection was performed with primary and secondary antibodies diluted in blocking solution (**Table S2**). Blots were developed with WesternSure PREMIUM Chemiluminescent Substrate (LI-COR, Bad Homburg, Germany). To validate specificity of the antibodies, all of them were tested on human serum and purified proteins as positive control and human serum depleted for the respective complement factor as negative control (**Table S3**).

Immunofluorescence Labeling

To stain for complement components in the macular and peripheral retina, human eyes (postmortem time < 8 hours) were cryosectioned. The research complies with the human research act (HRA) stating that small quantities of bodily substances removed in the course of transplantation may be anonymized for research purposes without consent (HRA chapter 5, paragraph 38, Switzerland). Before sectioning, the eyes were immersion-fixated with 4% paraformaldehyde (PFA) for 48 hours. Thereafter, the central part of the eye cup containing the optic nerve head and the macula including the underlying RPE, choroid and sclera was dissected. The tissue was submitted to cryoprotection, embedded in OCT and cut into 20 µm thick sections. Retinal detachment from the RPE is an artifact commonly observed in cryosections

Retinal sections were permeabilized (0.3% Triton X-100 plus 1.0% DMSO in PBS) and blocked (5% normal donkey serum with 0.3% Triton X-100 and 1.0% DMSO in PBS) for 2 h at room temperature. Primary antibodies were incubated overnight at 4°C. Sections were washed (1% bovine serum albumin in PBS) and incubated with secondary antibodies (2 h at room temperature). Cell nuclei were labeled with DAPI (1:1000; Life Technologies). Control experiments without primary antibodies showed no nonspecific labeling. Images were taken with a custom-made VisiScope CSU-X1 confocal system (Visitron Systems, Puchheim, Germany) equipped with high-resolution sCMOS camera (PCO AG, Kehlheim, Germany).

Quantification and Statistical Analysis

Statistical analyses were performed using Prism (Graphpad Software, San Diego, CA, USA). In most of the experiments in the present study results from 4 to 5 biological replicates were collected. Since this low number of input values does not allow an appropriate estimation about a normal Gaussian distribution, significance levels were determined by the non-parametric Mann-Whitney U test unless stated otherwise. All data are expressed as mean ± standard error (SEM) unless stated otherwise. Detailed information about specific n-values, implemented statistical tests and coding of significance levels are provided in the respective Figure legends.

DATA AVAILABILITY STATEMENT

The datasets presented in this study can be found in online repositories. The names of the repository/repositories and accession number(s) can be found below: GEO, accession IDs: GSE188280, GSE155154, GSE155288.

AUTHOR CONTRIBUTIONS

Conceptualization: DP, AG, ML, DS. Methodology: RZ, JB, DS, YJ, MK, JH, LK, AP, NS, VE, US-S, TS, SH, PG, MM, JM, CS. Investigation: RZ, JB, YJ, DS, MK, LK, AP. Visualization: RZ, JB, YJ, MK, LK, AP. Supervision: DP, AG, ML, DS. Writing—original draft: RZ, JB, YJ, DP, AG, ML, DS. Writing—review & editing: RZ, JB, YJ, LK, SH, CC, DP, AG, ML, DS. All authors contributed to the article and approved the submitted version.

FUNDING

ACKNOWLEDGMENTS

SUPPLEMENTARY MATERIAL

The Supplementary Material for this article can be found online at: https://www.frontiersin.org/articles/10.3389/fimmu.2022.895519/full#supplementary-material

REFERENCES

1. Merle NS, Church SE, Fremeaux-Bacchi V, Roumenina LT. Complement System Part I - Molecular Mechanisms of Activation and Regulation. *Front Immunol* (2015) 6:262. doi: 10.3389/fimmu.2015.00262

2. Merle NS, Noe R, Halbwachs-Mecarelli L, Fremeaux-Bacchi V, Roumenina LT. Complement System Part II: Role in Immunity. *Front Immunol* (2015) 6:257. doi: 10.3389/fimmu.2015.00257

3. Stephan AH, Barres BA, Stevens B. The Complement System: An Unexpected Role in Synaptic Pruning During Development and Disease. *Annu Rev Neurosci* (2012) 35:369–89. doi: 10.1146/annurev-neuro-061010-113810

4. Presumey J, Bialas AR, Carroll MC. Complement System in Neural Synapse Elimination in Development and Disease. *Adv Immunol* (2017) 135:53–79. doi: 10.1016/bs.ai.2017.06.004

5. Schatz-Jakobsen JA, Pedersen DV, Andersen GR. Structural Insight Into Proteolytic Activation and Regulation of the Complement System. *Immunol Rev* (2016) 274:59–73. doi: 10.1111/imr.12465

6. Cserhalmi M, Papp A, Brandus B, Uzonyi B, Józsi M. Regulation of Regulators: Role of the Complement Factor H-Related Proteins. *Semin Immunol* (2019) 45:101341. doi: 10.1016/j.smim.2019.101341

7. Barnum SR. Complement: A Primer for the Coming Therapeutic Revolution. *Pharmacol Ther* (2017) 172:63–72. doi: 10.1016/j.pharmthera.2016.11.014

8. Barnum SR. Complement in Central Nervous System Inflammation. *Immunol Res* (2002) 26:7–13. doi: 10.1385/IR:26:1-3:007

9. Morgan BP, Gasque P. Extrahepatic Complement Biosynthesis: Where, When and Why? *Clin Exp Immunol* (1997) 107:1–7. doi: 10.1046/j.1365-2249.1997.d01-890.x

10. Nataf S, Stahel PF, Davoust N, Barnum SR. Complement Anaphylatoxin Receptors on Neurons: New Tricks for Old Receptors? *Trends Neurosci* (1999) 22:397–402. doi: 10.1016/S0166-2236(98)01390-3

11. Cunha-Vaz JG. The Blood-Retinal Barriers System. Basic Concepts and Clinical Evaluation. *Exp Eye Res* (2004) 78:715–21. doi: 10.1016/S0014-4835(03)00213-6

12. Cunha-Vaz J, Bernardes R, Lobo C. Blood-Retinal Barrier. *Eur J Ophthalmol* (2011) 21 Suppl 6:S3–9. doi: 10.5301/EJO.2010.6049

13. Kolb H. Simple Anatomy of the Retina. In: H Kolb, E Fernandez and R Nelson, editors. *Webvision: The Organization of the Retina and Visual System*. Salt Lake City UT: University of Utah Health Sciences Center (2005).

14. Strauss O. "The Retinal Pigment Epithelium". In: H Kolb, E Fernandez and R Nelson, editors. *Webvision: The Organization of the Retina and Visual System*. Salt Lake City, UT: University of Utah Health Sciences Center (2011).

15. Nickla DL, Wallman J. The Multifunctional Choroid. *Prog Retin Eye Res* (2010) 29:144–68. doi: 10.1016/j.preteyeres.2009.12.002

16. Bora NS, Gobleman CL, Atkinson JP, Pepose JS, Kaplan HJ. Differential Expression of the Complement Regulatory Proteins in the Human Eye. *Invest Ophthalmol Vis Sci* (1993) 34:3579–84.

17. Anderson DH, Radeke MJ, Gallo NB, Chapin EA, Johnson PT, Curletti CR, et al. The Pivotal Role of the Complement System in Aging and Age-Related Macular Degeneration: Hypothesis Re-Visited. *Prog Retin Eye Res* (2010) 29:95–112. doi: 10.1016/j.preteyeres.2009.11.003

18. Zhang J, Gerhardinger C, Lorenzi M. Early Complement Activation and Decreased Levels of Glycosylphosphatidylinositol-Anchored Complement Inhibitors in Human and Experimental Diabetic Retinopathy. *Diabetes* (2002) 51:3499–504. doi: 10.2337/diabetes.51.12.3499

19. Jha P, Sohn J-H, Xu Q, Nishihori H, Wang Y, Nishihori S, et al. The Complement System Plays a Critical Role in the Development of Experimental Autoimmune Anterior Uveitis. *Invest Ophthalmol Vis Sci* (2006) 47:1030–8. doi: 10.1167/iovs.05-1062

20. Mullins RF, Russell SR, Anderson DH, Hageman GS. Drusen Associated With Aging and Age-Related Macular Degeneration Contain Proteins Common to Extracellular Deposits Associated With Atherosclerosis, Elastosis, Amyloidosis, and Dense Deposit Disease. *FASEB J* (2000) 14:835–46. doi: 10.1096/fasebj.14.7.835

21. Zarbin MA. Age-Related Macular Degeneration: Review of Pathogenesis. *Eur J Ophthalmol* (1998) 8:199–206. doi: 10.1177/112067219800800401

22. Curcio CA. Soft Drusen in Age-Related Macular Degeneration: Biology and Targeting *Via* the Oil Spill Strategies. *Invest Ophthalmol Vis Sci* (2018) 59: AMD160–81. doi: 10.1167/iovs.18-24882

23. Johnson LV, Leitner WP, Staples MK, Anderson DH. Complement Activation and Inflammatory Processes in Drusen Formation and Age Related Macular Degeneration. *Exp Eye Res* (2001) 73:887–96. doi: 10.1006/exer.2001.1094

24. Anderson DH, Talaga KC, Rivest AJ, Barron E, Hageman GS, Johnson LV. Characterization of Beta Amyloid Assemblies in Drusen: The Deposits Associated With Aging and Age-Related Macular Degeneration. *Exp Eye Res* (2004) 78:243–56. doi: 10.1016/j.exer.2003.10.011

25. Crabb JW, Miyagi M, Gu X, Shadrach K, West KA, Sakaguchi H, et al. Drusen Proteome Analysis: An Approach to the Etiology of Age-Related Macular Degeneration. *Proc Natl Acad Sci USA* (2002) 99:14682–7. doi: 10.1073/pnas.222551899

26. Fritsche LG, Igl W, Bailey JNC, Grassmann F, Sengupta S, Bragg-Gresham JL, et al. A Large Genome-Wide Association Study of Age-Related Macular Degeneration Highlights Contributions of Rare and Common Variants. *Nat Genet* (2016) 48:134–43. doi: 10.1038/ng.3448

27. Ferris FL3rd. Senile Macular Degeneration: Review of Epidemiologic Features. *Am J Epidemiol* (1983) 118:132–51. doi: 10.1093/oxfordjournals.aje.a113624

28. Mitchell P, Liew G, Gopinath B, Wong TY. Age-Related Macular Degeneration. *Lancet* (2018) 392:1147–59. doi: 10.1016/S0140-6736(18)31550-2

29. Quinn N, Csincsik L, Flynn E, Curcio CA, Kiss S, Sadda SR, et al. The Clinical Relevance of Visualising the Peripheral Retina. *Prog Retin Eye Res* (2019) 68:83–109. doi: 10.1016/j.preteyeres.2018.10.001

30. Ambati J, Fowler BJ. Mechanisms of Age-Related Macular Degeneration. *Neuron* (2012) 75:26–39. doi: 10.1016/j.neuron.2012.06.018

31. Kuehlewein L, Dustin L, Sagong M, Hariri A, Mendes TS, Rofagha S, et al. Predictors of Macular Atrophy Detected by Fundus Autofluorescence in Patients With Neovascular Age-Related Macular Degeneration After Long-Term Ranibizumab Treatment. *Ophthalmic Surg Lasers Imaging Retina* (2016) 47:224–31. doi: 10.3928/23258160-20160229-04

32. Bhisitkul RB, Mendes TS, Rofagha S, Enanoria W, Boyer DS, Sadda SR, et al. Macular Atrophy Progression and 7-Year Vision Outcomes in Subjects From the ANCHOR, MARINA, and HORIZON Studies: The SEVEN-UP Study. *Am J Ophthalmol* (2015) 159:915–24.e2. doi: 10.1016/j.ajo.2015.01.032

33. Comparison of Age-related Macular Degeneration Treatments Trials (CATT) Research Group, Maguire MG, Martin DF, Ying G-S, Jaffe GJ, Daniel E, et al. Five-Year Outcomes With Anti-Vascular Endothelial Growth Factor Treatment of Neovascular Age-Related Macular Degeneration: The Comparison of Age-Related Macular Degeneration Treatments Trials. *Ophthalmology* (2016) 123:1751–61. doi: 10.1016/j.ophtha.2016.03.045

34. Holz FG, Strauss EC, Schmitz-Valckenberg S, van Lookeren Campagne M. Geographic Atrophy: Clinical Features and Potential Therapeutic Approaches. *Ophthalmology* (2014) 121:1079–91. doi: 10.1016/j.ophtha.2013.11.023

35. Fleckenstein M, Keenan TDL, Guymer RH, Chakravarthy U, Schmitz-Valckenberg S, Klaver CC, et al. Age-Related Macular Degeneration. *Nat Rev Dis Primers* (2021) 7:31. doi: 10.1038/s41572-021-00265-2

36. Desai D, Dugel PU. Complement Cascade Inhibition in Geographic Atrophy: A Review. *Eye* (2022) 36:294–302. doi: 10.1038/s41433-021-01765-x

37. Park YG, Park YS, Kim I-B. Complement System and Potential Therapeutics in Age-Related Macular Degeneration. *Int J Mol Sci* (2021) 22. doi: 10.3390/ijms22136851

38. Qin S, Dong N, Yang M, Wang J, Feng X, Wang Y. Complement Inhibitors in Age-Related Macular Degeneration: A Potential Therapeutic Option. *J Immunol Res* (2021) 2021:9945725. doi: 10.1155/2021/9945725

39. Chi Z-L, Yoshida T, Lambris JD, Iwata T. Suppression of Drusen Formation by Compstatin, a Peptide Inhibitor of Complement C3 Activation, on Cynomolgus Monkey With Early-Onset Macular Degeneration. *Adv Exp Med Biol* (2010) 703:127–35. doi: 10.1007/978-1-4419-5635-4_9

40. Park DH, Connor KM, Lambris JD. The Challenges and Promise of Complement Therapeutics for Ocular Diseases. *Front Immunol* (2019) 10:1007. doi: 10.3389/fimmu.2019.01007

41. Liao DS, Grossi FV, El Mehdi D, Gerber MR, Brown DM, Heier JS, et al. Complement C3 Inhibitor Pegcetacoplan for Geographic Atrophy Secondary to Age-Related Macular Degeneration: A Randomized Phase 2 Trial. *Ophthalmology* (2020) 127:186–95. doi: 10.1016/j.ophtha.2019.07.011

42. *Apellis Announces Detailed Results From Phase 3 DERBY and OAKS Studies Presented at Retina Society Annual Meeting*. Available at: https://investors.apellis.com/news-releases/news-release-details/apellis-announces-detailed-results-phase-3-derby-and-oaks (Accessed October 18, 2021).

43. Wu J, Sun X. Complement System and Age-Related Macular Degeneration: Drugs and Challenges. *Drug Des Devel Ther* (2019) 13:2413–25. doi: 10.2147/DDDT.S206355

44. Holz FG, Sadda SR, Busbee B, Chew EY, Mitchell P, Tufail A, et al. Efficacy and Safety of Lampalizumab for Geographic Atrophy Due to Age-Related Macular Degeneration: Chroma and Spectri Phase 3 Randomized Clinical Trials. *JAMA Ophthalmol* (2018) 136:666–77. doi: 10.1001/jamaophthalmol.2018.1544

45. Park J, Shrestha R, Qiu C, Kondo A, Huang S, Werth M, et al. Single-Cell Transcriptomics of the Mouse Kidney Reveals Potential Cellular Targets of Kidney Disease. *Science* (2018) 360:758–63. doi: 10.1126/science.aar2131

46. McKenna A, Gagnon JA. Recording Development With Single Cell Dynamic Lineage Tracing. *Development* (2019) 146. doi: 10.1242/dev.169730

47. Satija R, Farrell JA, Gennert D, Schier AF, Regev A. Spatial Reconstruction of Single-Cell Gene Expression Data. *Nat Biotechnol* (2015) 33:495–502. doi: 10.1038/nbt.3192

48. Pauly D, Agarwal D, Dana N, Schäfer N, Biber J, Wunderlich KA, et al. Cell-Type-Specific Complement Expression in the Healthy and Diseased Retina. *Cell Rep* (2019) 29:2835–48.e4. doi: 10.1016/j.celrep.2019.10.084

49. Macosko EZ, Basu A, Satija R, Nemesh J, Shekhar K, Goldman M, et al. Highly Parallel Genome-Wide Expression Profiling of Individual Cells Using Nanoliter Droplets. *Cell* (2015) 161:1202–14. doi: 10.1016/j.cell.2015.05.002

50. Shekhar K, Lapan SW, Whitney IE, Tran NM, Macosko EZ, Kowalczyk M, et al. Comprehensive Classification of Retinal Bipolar Neurons by Single-Cell Transcriptomics. *Cell* (2016) 166:1308–23.e30. doi: 10.1016/j.cell.2016.07.054

51. Voigt AP, Mulfaul K, Mullin NK, Flamme-Wiese MJ, Giacalone JC, Stone EM, et al. Single-Cell Transcriptomics of the Human Retinal Pigment Epithelium and Choroid in Health and Macular Degeneration. *Proc Natl Acad Sci USA* (2019) 116:24100–7. doi: 10.1073/pnas.1914143116

52. Liu Y, Beyer A, Aebersold R. On the Dependency of Cellular Protein Levels on mRNA Abundance. *Cell* (2016) 165:535–50. doi: 10.1016/j.cell.2016.03.014

53. Kjell J, Fischer-Sternjak J, Thompson AJ, Friess C, Sticco MJ, Salinas F, et al. Defining the Adult Neural Stem Cell Niche Proteome Identifies Key Regulators of Adult Neurogenesis. *Cell Stem Cell* (2020) 26:277–93.e8. doi: 10.1016/j.stem.2020.01.002

54. Brunner A-D, Thielert M, Vasilopoulou CG, Ammar C, Coscia F, Mund A, et al. Ultra-High Sensitivity Mass Spectrometry Quantifies Single-Cell Proteome Changes Upon Perturbation. *Mol Syst Biol* (2021) 18(3):e10798. doi: 10.1101/2020.12.22.423933

55. Radu RA, Hu J, Yuan Q, Welch DL, Makshanoff J, Lloyd M, et al. Complement System Dysregulation and Inflammation in the Retinal Pigment Epithelium of a Mouse Model for Stargardt Macular Degeneration. *J Biol Chem* (2011) 286:18593–601. doi: 10.1074/jbc.M110.191866

56. Lenis TL, Sarfare S, Jiang Z, Lloyd MB, Bok D, Radu RA. Complement Modulation in the Retinal Pigment Epithelium Rescues Photoreceptor Degeneration in a Mouse Model of Stargardt Disease. *Proc Natl Acad Sci USA* (2017) 114:3987–92. doi: 10.1073/pnas.1620299114

57. Jabri Y, Biber J, Diaz-Lezama N, Grosche A, Pauly D. Cell-Type-Specific Complement Profiling in the ABCA4 Mouse Model of Stargardt Disease. *Int J Mol Sci* (2020) 21. doi: 10.3390/ijms21228468

58. Bajic G, Yatime L, Sim RB, Vorup-Jensen T, Andersen GR. Structural Insight on the Recognition of Surface-Bound Opsonins by the Integrin I Domain of Complement Receptor 3. *Proc Natl Acad Sci USA* (2013) 110:16426–31. doi: 10.1073/pnas.1311261110

59. Xu S, Wang J, Wang J-H, Springer TA. Distinct Recognition of Complement Ic3b by Integrins αβ and αβ. *Proc Natl Acad Sci USA* (2017) 114:3403–8. doi: 10.1073/pnas.1620881114

60. Jensen RK, Bajic G, Sen M, Springer TA, Vorup-Jensen T, Andersen GR. Complement Receptor 3 Forms a Compact High Affinity Complex With Ic3b. *J Immunol* (2020) 206(12):3032–42. doi: 10.1101/2020.04.15.043133

61. Li F, Leier A, Liu Q, Wang Y, Xiang D, Akutsu T, et al. Procleave: Predicting Protease-Specific Substrate Cleavage Sites by Combining Sequence and Structural Information. *Genomics Proteomics Bioinf* (2020) 18:52–64. doi: 10.1016/j.gpb.2019.08.002

62. Mullins RF, Schoo DP, Sohn EH, Flamme-Wiese MJ, Workamelahu G, Johnston RM, et al. The Membrane Attack Complex in Aging Human Choriocapillaris: Relationship to Macular Degeneration and Choroidal Thinning. *Am J Pathol* (2014) 184:3142–53. doi: 10.1016/j.ajpath.2014.07.017

63. Doorduijn DJ, Bardoel BW, Heesterbeek DAC, Ruyken M, Benn G, Parsons ES, et al. Bacterial Killing by Complement Requires Direct Anchoring of Membrane Attack Complex Precursor C5b-7. *PLoS Pathog* (2020) 16:e1008606. doi: 10.1371/journal.ppat.1008606

64. Thompson RA, Lachmann PJ. Reactive Lysis: The Complement-Mediated Lysis of Unsensitized Cells. I. The Characterization of the Indicator Factor and its Identification as C7. *J Exp Med* (1970) 131:629–41. doi: 10.1084/jem.131.4.629

65. *Cell Atlas - C1S - The Human Protein Atlas*. Available at: https://www.proteinatlas.org/ENSG00000182326-C1S/cell (Accessed August 27, 2021).

66. Schäfer N, Grosche A, Schmitt SI, Braunger BM, Pauly D. Complement Components Showed a Time-Dependent Local Expression Pattern in Constant and Acute White Light-Induced Photoreceptor Damage. *Front Mol Neurosci* (2017) 10:197. doi: 10.3389/fnmol.2017.00197

67. Katschke KJJr, Xi H, Cox C, Truong T, Malato Y, Lee WP, et al. Classical and Alternative Complement Activation on Photoreceptor Outer Segments Drives Monocyte-Dependent Retinal Atrophy. *Sci Rep* (2018) 8:7348. doi: 10.1038/s41598-018-25557-8

68. Loyet KM, Deforge LE, Katschke KJJr, Diehl L, Graham RR, Pao L, et al. Activation of the Alternative Complement Pathway in Vitreous Is Controlled by Genetics in Age-Related Macular Degeneration. *Invest Ophthalmol Vis Sci* (2012) 53:6628–37. doi: 10.1167/iovs.12-9587

69. Circolo A, Garnier G, Fukuda W, Wang X, Hidvegi T, Szalai AJ, et al. Genetic Disruption of the Murine Complement C3 Promoter Region Generates Deficient Mice With Extrahepatic Expression of C3 mRNA. *Immunopharmacology* (1999) 42:135–49. doi: 10.1016/S0162-3109(99)00021-1

70. Vandermeer J, Sha Q, Lane AP, Schleimer RP. Innate Immunity of the Sinonasal Cavity: Expression of Messenger RNA for Complement Cascade Components and Toll-Like Receptors. *Arch Otolaryngol Head Neck Surg* (2004) 130:1374–80. doi: 10.1001/archotol.130.12.1374

71. Kulkarni HS, Elvington ML, Perng Y-C, Liszewski MK, Byers DE, Farkouh C, et al. Intracellular C3 Protects Human Airway Epithelial Cells From Stress-Associated Cell Death. *Am J Respir Cell Mol Biol* (2019) 60:144–57. doi: 10.1165/rcmb.2017-0405OC

72. Satyam A, Kannan L, Matsumoto N, Geha M, Lapchak PH, Bosse R, et al. Intracellular Activation of Complement 3 Is Responsible for Intestinal Tissue Damage During Mesenteric Ischemia. *J Immunol* (2017) 198:788–97. doi: 10.4049/jimmunol.1502287

73. Sünderhauf A, Skibbe K, Preisker S, Ebbert K, Verschoor A, Karsten CM, et al. Regulation of Epithelial Cell Expressed C3 in the Intestine - Relevance for the Pathophysiology of Inflammatory Bowel Disease? *Mol Immunol* (2017) 90:227–38. doi: 10.1016/j.molimm.2017.08.003

74. Atanes P, Ruz-Maldonado I, Pingitore A, Hawkes R, Liu B, Zhao M, et al. C3aR and C5aR1 Act as Key Regulators of Human and Mouse β-Cell Function. *Cell Mol Life Sci* (2018) 75:715–26. doi: 10.1007/s00018-017-2655-1

75. Dos Santos RS, Marroqui L, Grieco FA, Marselli L, Suleiman M, Henz SR, et al. Protective Role of Complement C3 Against Cytokine-Mediated β-Cell Apoptosis. *Endocrinology* (2017) 158:2503–21. doi: 10.1210/en.2017-00104

76. Arbore G, Kemper C, Kolev M. Intracellular Complement - the Complosome - In Immune Cell Regulation. *Mol Immunol* (2017) 89:2–9. doi: 10.1016/j.molimm.2017.05.012

77. Hess C, Kemper C. Complement-Mediated Regulation of Metabolism and Basic Cellular Processes. *Immunity* (2016) 45:240–54. doi: 10.1016/j.immuni.2016.08.003

78. Liszewski MK, Elvington M, Kulkarni HS, Atkinson JP. Complement's Hidden Arsenal: New Insights and Novel Functions Inside the Cell. *Mol Immunol* (2017) 84:2–9. doi: 10.1016/j.molimm.2017.01.004

79. Karlstetter M, Scholz R, Rutar M, Wong WT, Provis JM, Langmann T. Retinal Microglia: Just Bystander or Target for Therapy? *Prog Retin Eye Res* (2015) 45:30–57. doi: 10.1016/j.preteyeres.2014.11.004

80. Wyatt MK, Tsai J-Y, Mishra S, Campos M, Jaworski C, Fariss RN, et al. Interaction of Complement Factor H and Fibulin3 in Age-Related Macular Degeneration. *PloS One* (2013) 8:e68088. doi: 10.1371/journal.pone.0068088

81. Endo Y, Matsushita M, Fujita T. The Role of Ficolins in the Lectin Pathway of Innate Immunity. *Int J Biochem Cell Biol* (2011) 43:705–12. doi: 10.1016/j.biocel.2011.02.003

82. Kuraya M, Ming Z, Liu X, Matsushita M, Fujita T. Specific Binding of L-Ficolin and H-Ficolin to Apoptotic Cells Leads to Complement Activation. *Immunobiology* (2005) 209:689–97. doi: 10.1016/j.imbio.2004.11.001

83. Zheng B, Li T, Chen H, Xu X, Zheng Z. Correlation Between Ficolin-3 and Vascular Endothelial Growth Factor-To-Pigment Epithelium-Derived Factor Ratio in the Vitreous of Eyes With Proliferative Diabetic Retinopathy. *Am J Ophthalmol* (2011) 152:1039–43. doi: 10.1016/j.ajo.2011.05.022

84. Bhutto I, Lutty G. Understanding Age-Related Macular Degeneration (AMD): Relationships Between the Photoreceptor/Retinal Pigment Epithelium/Bruch's Membrane/Choriocapillaris Complex. *Mol Aspects Med* (2012) 33:295–317. doi: 10.1016/j.mam.2012.04.005

85. Whitmore SS, Sohn EH, Chirco KR, Drack AV, Stone EM, Tucker BA, et al. Complement Activation and Choriocapillaris Loss in Early AMD: Implications for Pathophysiology and Therapy. *Prog Retin Eye Res* (2015) 45:1–29. doi: 10.1016/j.preteyeres.2014.11.005

86. Lutty GA, McLeod DS, Bhutto IA, Edwards MM, Seddon JM. Choriocapillaris Dropout in Early Age-Related Macular Degeneration. *Exp Eye Res* (2020) 192:107939. doi: 10.1016/j.exer.2020.107939

87. Demirs JT, Yang J, Crowley MA, Twarog M, Delgado O, Qiu Y, et al. Differential and Altered Spatial Distribution of Complement Expression in Age-Related Macular Degeneration. *Invest Ophthalmol Vis Sci* (2021) 62:26. doi: 10.1167/iovs.62.7.26

88. Kolev M, Kemper C. Keeping It All Going-Complement Meets Metabolism. *Front Immunol* (2017) 8:1. doi: 10.3389/fimmu.2017.00001

89. Schafer DP, Lehrman EK, Kautzman AG, Koyama R, Mardinly AR, Yamasaki R, et al. Microglia Sculpt Postnatal Neural Circuits in an Activity and Complement-Dependent Manner. *Neuron* (2012) 74:691–705. doi: 10.1016/j.neuron.2012.03.026

90. Orsini F, De Blasio D, Zangari R, Zanier ER, De Simoni M-G. Versatility of the Complement System in Neuroinflammation, Neurodegeneration and Brain Homeostasis. *Front Cell Neurosci* (2014) 8:380. doi: 10.3389/fncel.2014.00380

91. Ten VS, Yao J, Ratner V, Sosunov S, Fraser DA, Botto M, et al. Complement Component C1q Mediates Mitochondria-Driven Oxidative Stress in Neonatal Hypoxic-Ischemic Brain Injury. *J Neurosci* (2010) 30:2077–87. doi: 10.1523/JNEUROSCI.5249-09.2010

92. Ramos de Carvalho JE, Klaassen I, Vogels IMC, Schipper-Krom S, van Noorden CJF, Reits E, et al. Complement Factor C3a Alters Proteasome Function in Human RPE Cells and in an Animal Model of Age-Related RPE Degeneration. *Invest Ophthalmol Vis Sci* (2013) 54:6489–501. doi: 10.1167/iovs.13-12374

93. Lyu Y, Zauhar R, Dana N, Strang CE, Hu J, Wang K, et al. Implication of Specific Retinal Cell-Type Involvement and Gene Expression Changes in AMD Progression Using Integrative Analysis of Single-Cell and Bulk RNA-Seq Profiling. *Sci Rep* (2021) 11:15612. doi: 10.1038/s41598-021-95122-3

94. Li X, Wang K, Lyu Y, Pan H, Zhang J, Stambolian D, et al. Deep Learning Enables Accurate Clustering With Batch Effect Removal in Single-Cell RNA-Seq Analysis. *Nat Commun* (2020) 11:2338. doi: 10.1038/s41467-020-15851-3

95. Stuart T, Butler A, Hoffman P, Hafemeister C, Papalexi E, Mauck WM3rd, et al. Comprehensive Integration of Single-Cell Data. *Cell* (2019) 177:1888–1902.e21. doi: 10.1016/j.cell.2019.05.031

96. Curcio CA, Sloan KR, Meyers D. Computer Methods for Sampling, Reconstruction, Display and Analysis of Retinal Whole Mounts. *Vision Res* (1989) 29:529–40. doi: 10.1016/0042-6989(89)90039-4

97. Guidry C, Medeiros NE, Curcio CA. Phenotypic Variation of Retinal Pigment Epithelium in Age-Related Macular Degeneration. *Invest Ophthalmol Vis Sci* (2002) 43:267–73.

98. Grosche A, Hauser A, Lepper MF, Mayo R, von Toerne C, Merl-Pham J, et al. The Proteome of Native Adult Müller Glial Cells From Murine Retina. *Mol Cell Proteomics* (2016) 15:462–80. doi: 10.1074/mcp.M115.052183

99. Frik J, Merl-Pham J, Plesnila N, Mattugini N, Kjell J, Kraska J, et al. Cross-Talk Between Monocyte Invasion and Astrocyte Proliferation Regulates Scarring in Brain Injury. *EMBO Rep* (2018) 19. doi: 10.15252/embr.201745294

100. Lepper MF, Ohmayer U, von Toerne C, Maison N, Ziegler A-G, Hauck SM. Proteomic Landscape of Patient-Derived CD4+ T Cells in Recent-Onset Type 1 Diabetes. *J Proteome Res* (2018) 17:618–34. doi: 10.1021/acs.jproteome.7b00712

101. Schäfer N, Grosche A, Reinders J, Hauck SM, Pouw RB, Kuijpers TW, et al. Complement Regulator FHR-3 Is Elevated Either Locally or Systemically in a Selection of Autoimmune Diseases. *Front Immunol* (2016) 7:542. doi: 10.3389/fimmu.2016.00542

Publication 2 - (Jabri, Biber et al., 2020)

Cell-Type-Specific Complement Profiling in the ABCA4$^{-/-}$ Mouse Model of Stargardt Disease

Yassin Jabri*, **Josef Biber***, Nundehui Diaz-Lezama, Antje Grosche and Diana Pauly

*: Shared first authorship

Conceptualization, Y.J., J.B., A.G. and D.P.; data curation, Y.J., J.B., N.D.-L., A.G. and D.P.; funding acquisition, A.G. and D.P.; investigation, Y.J., J.B., N.D.-L., A.G. and D.P.; methodology, Y.J., J.B., N.D.-L., A.G. and D.P.; project administration, A.G. and D.P.; supervision, A.G. and D.P.; visualization, Y.J., J.B., A.G. and D.P.; writing—original draft, Y.J., J.B., A.G. and D.P.; writing—review and editing, Y.J., J.B., N.D.-L., A.G. and D.P.All authors have read and agreed to the published version of the manuscript.

Article

Cell-Type-Specific Complement Profiling in the ABCA4−/− Mouse Model of Stargardt Disease

Yassin Jabri [1],[†], **Josef Biber** [2],[†], **Nundehui Diaz-Lezama** [2], **Antje Grosche** [2],[*]
and **Diana Pauly** [3],[4],[*]

[1] Department of Experimental Ophthalmology, Eye Clinic, University Hospital Regensburg,
D-93053 Regensburg, Germany; yassin.jabri@ukr.de

[2] Department of Physiological Genomics, Biomedical Center, Ludwig Maximilians University Munich,
D-82152 Planegg-Martinsried, Germany; Josef.biber@bmc.med.lmu.de (J.B.);
Nundehui.Diaz-Lezama@bmc.med.lmu.de (N.D.-L.)

[3] Experimental Ophthalmology, Philipps-University Marburg, D-35043 Marburg, Germany

[4] Department of Ophthalmology, University Hospital Regensburg, D-93053 Regensburg, Germany

[*] Correspondence: Antje.Grosche@bmc.med.lmu.de (A.G.); Diana.Pauly@uni-marburg.de (D.P.)

[†] These authors have equally contributed.

check for updates

Abstract: Stargardt macular degeneration is an inherited retinal disease caused by mutations in the ATP-binding cassette subfamily A member 4 (ABCA4) gene. Here, we characterized the complement expression profile in ABCA4−/− retinae and aligned these findings with morphological markers of retinal degeneration. We found an enhanced retinal pigment epithelium (RPE) autofluorescence, cell loss in the inner retina of ABCA4−/− mice and demonstrated age-related differences in complement expression in various retinal cell types irrespective of the genotype. However, 24-week-old ABCA4−/− mice expressed more *c3* in the RPE and fewer *cfi* transcripts in the microglia compared to controls. At the protein level, the decrease of complement inhibitors (complement factor I, CFI) in retinae, as well as an increased C3b/C3 ratio in the RPE/choroid and retinae of ABCA4−/−, mice was confirmed. We showed a corresponding increase of the C3d/C3 ratio in the serum of ABCA4−/− mice, while no changes were observed for CFI. Our findings suggest an overactive complement cascade in the ABCA4−/− retinae that possibly contributes to pathological alterations, including microglial activation and neurodegeneration. Overall, this underpins the importance of well-balanced complement homeostasis to maintain retinal integrity.

1. Introduction

Stargardt disease is an inherited macular dystrophy that affects children and young adults. It is characterized by autofluorescent lipofuscin deposition in the retinal pigment epithelium (RPE) and a progressive photoreceptor degeneration [1,2]. Stargardt macular degeneration is caused by mutations involving the ATP-binding cassette subfamily A member 4 (ABCA4) [3]. The ABCA4 transporter is involved in the visual cycle through the clearance of retinoid substrate, thereby avoiding the accumulation of lipofuscin in the RPE derived from phagocytosed photoreceptors [1].

The abnormal accumulation of lipofuscin in the RPE cells causes oxidative stress and complement system activation, leading to progressive macular degeneration and central vision loss [4–8]. The exact process of complement activation in this inherited retinal degenerative disease remains unclear. The complement system is part of the innate immune system and consists of more than 40 proteins that

act in a cascade-like manner, modulating the tissue immune homeostasis, e.g., via the opsonization and elimination of foreign microbes as well as damaged cells or by initiating inflammatory responses by the generation of anaphylatoxins [9,10]. Dysregulation of the complement system can lead to uncontrolled inflammation and retinal degeneration. Diseases such as age-related macular degeneration and diabetic retinopathy have shown evidence of altered complement homeostasis within the retina [11–14].

Previous studies have discovered disturbed complement homeostasis in albino and pigmented ABCA4$^{-/-}$ mice, which included the accumulation of C3 breakdown products together with a reduction of the complement inhibitor factor H at the level of the RPE (Figure 1A) [5,15]. Furthermore, an increase of oxidative stress markers has been described, which led to complement activation in early disease stages [5]. Such changes were followed by a loss of photoreceptors and, thus, a thinning of the outer nuclear layer. They were also accompanied by an enhanced autofluorescence of the RPE and a thickening of the Bruch's membrane (Figure 1A) [4–6,16–18].
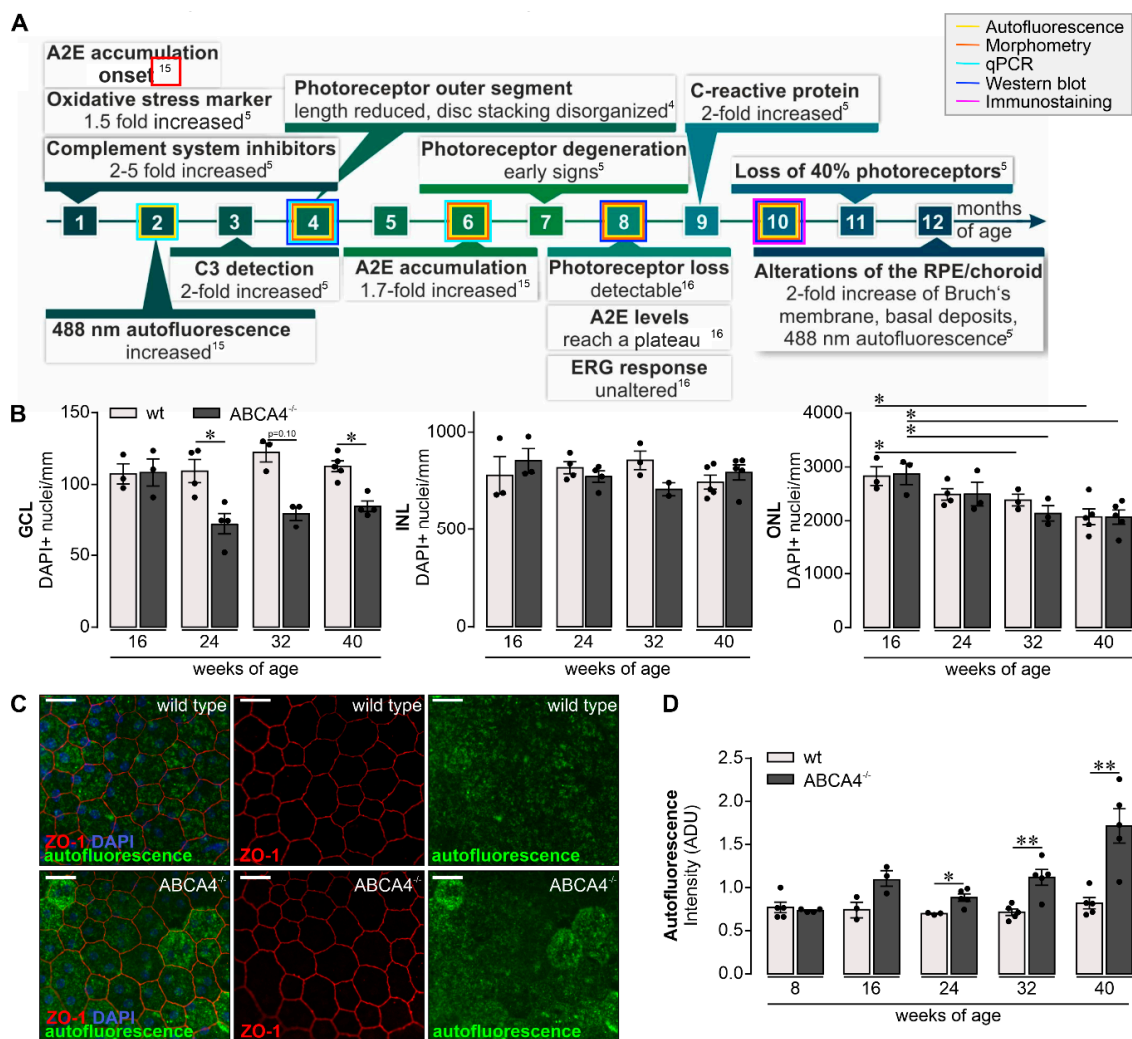

Figure 1. Retinal phenotype in the investigated albino ABCA4$^{-/-}$ strain. (**A**) Subsumed retinal phenotype of albino ABCA4$^{-/-}$ mice based on published studies [4,5,15,16]. ERG, electroretinogramm; ONL, outer nuclear layer; A2E, N-retinylidene-N-retinylethanolamine; C3, complement factor 3. Experiments performed in the course of the present study at different time points are highlighted by frames in respective colors. (**B**) A decrease in the number of DAPI+ cell nuclei in the ganglion cell layer

(GCL) is observed in ABCA4$^{-/-}$ mice aged 24, 32 and 40 weeks but not in the albino wild-type retina (data were obtained previously) [19]. Cell numbers in the retinal inner nuclear layer (INL) were stable in aging ABCA4$^{-/-}$ mice. Photoreceptor density, as determined by quantification of DAPI+ cell nuclei in the outer nuclear layer (ONL), was significantly decreased in ABCA4$^{-/-}$ and wild-type mice at 32 weeks of age and older [19]. (**C**) The integrity and autofluorescence of the retinal pigment epithelium (RPE) were investigated in fixed, flat-mounted eyecup preparations after careful removal of overlaying retinae. ZO-1 labeling delineates tight junctions formed by intact RPE cells. Autofluorescence was detected upon excitation with a 488 nm laser and revealed enhanced signals at 40 weeks of age from the RPE of ABCA4$^{-/-}$ mice as compared to the RPE from wild-type littermates. Scale bars, 20 μm. (**D**) Mean gray values for autofluorescence were measured over the whole scan field. (**B**,**D**). Bars represent mean values ± SEM from 2 to 5 animals. * $p < 0.05$, ** $p < 0.01$, Mann–Whitney U-test (two-tailed). ADU, arbitrary digital units.

Here, we describe early changes in C3 blood circulation levels and retinal deposition in the ABCA4$^{-/-}$ mice simultaneously with enhanced autofluorescence in the RPE. This was followed by later accumulation of C3 cleavage products in the RPE accompanied by lower levels of the complement inhibitor complement inhibitors (CFI) in the ABCA4$^{-/-}$ retina. Alterations of the complement homeostasis that appeared during aging seemed to be associated with an increase in numbers as well as signs of moderate activation of microglia and thinning of the ganglion cell layer (GCL). Based on our data, we suggest that rebalancing the complement activity could avoid microglial activation and part of the damage caused during aging and hereditary retinal degeneration.

2. Results

2.1. Retinal Phenotype is Changed in Albino ABCA4$^{-/-}$ Compared to Wild-Type Mice

To profile retinal changes in the albino mouse model for slow hereditary retinal degeneration lacking the functional ABCA4 transporter (ABCA4$^{-/-}$ mice; Figure 1A), we quantified DAPI-positive cell nuclei in the GCL, inner nuclear layer (INL) and outer nuclear layer (ONL) of mice aged 16-40 weeks (Figure 1B) and compared these numbers with previously obtained data from wild-type albino mice [19]. The ABCA4$^{-/-}$ mice showed a reduced number of cell nuclei in the GCL compared to wild-type controls starting at the age of 24 weeks. Of note, in addition to retinal ganglion cells, the GCL comprises displaced amacrine cells (about 50% of all GCL cells) and few microglia. The INL was not altered, while the number of the cell nuclei within the ONL was reduced in ABCA4$^{-/-}$ and wild-type mice at the ages of 32 and 40 weeks. This consecutive loss of photoreceptors was accompanied by a mild Müller cell gliosis detected in mice of both genotypes as early as eight weeks of age and onwards (Figure S1). A major consequence of the loss in *abca4* expression is the accumulation of lipofuscin deposits in the RPE and increased autofluorescence thereof (Figure 1C). To correlate retinal complement activation and lipofuscin accumulation, we determined changes in autofluorescence intensity in mice of increasing age (Figure 1D). Indeed, we found a significantly enhanced lipofuscin deposition in the RPE of ABCA4$^{-/-}$ mice older than 24 weeks compared to wild-type controls. However, the RPE monolayer was still intact in both genotypes, as indicated by continuous staining of tight junction protein ZO-1, the cell density and the ratio of cells carrying one, two or more nuclei (Figure 1C and Figure S2).

2.2. Complement Expression Changed in the Different Retinal Cell Types Over Time

Performing cell-type-specific analysis of the complement component expression shed light on the local complement homeostasis in the retina of 8-24-week-old ABCA4$^{-/-}$ mice. Müller cells, microglia, vascular cells and retinal neurons were purified by immunomagnetic separation, and RPE/choroid scratch samples were collected from respective mouse eyes. Successful cell enrichment was validated by the detection of marker genes of respective cell populations. Note that even though astrocytes were not positively selected, we could demonstrate that *gfap* (a marker for astrocytes and reactive

Müller cells) is highly enriched in the Müller cell fraction [20]). Given that the number of astrocytes (0.1% of the retinal cell population) per retina is very low compared to Müller cells (3% of the retinal cell population), we termed this macroglial fraction the Müller cell fraction. Moreover, we would like to mention that the neuronal fraction, though not positively selected for a specific neuronal marker, which is hard to do since there is no pan-neuronal marker suitable for immunomagnetic selection, can be considered a rather pure neuronal cell population since it is devoid of microglial (*itgam*, *aif1*), vascular (*icam*, *pecam1*) or macroglial markers (*glul*, *gfap*), as demonstrated in Figure S3. Importantly, marker gene expression was comparable across all tested ages and was independent from the genotype (Figure S3). Only *itgam*, a marker for microglia and macrophages, showed a slightly higher expression in microglia isolated from ABCA4$^{-/-}$ compared to wild-type controls at all investigated time points.

The complement expression (*c1s*, *c3*, *cfb*, *cfp*, *cfh* and *cfi*) of each cell type was measured by qRT-PCR and compared with the expression levels of wild-type albino mice measured in our previous study [19]. Significant age-dependent changes in complement expression were observed in wild-type albino and ABCA4$^{-/-}$ mice for most analyzed transcripts (Figure 2). Complement expression analysis of *c1s* showed a distinct age-dependent upregulation in Müller cells, vascular cells, neurons and the RPE irrespective of the genotype. In both mouse strains, mRNA for complement components *c3* and *cfb* was increased in the microglia, vascular cells and RPE. Similarly, *cfp* transcripts were elevated in these cell types and Müller cells during aging independent from the genotype. In Müller cells and neurons, the expression of the inhibitory factor *cfh* decreased, while this seemed to be counterbalanced by a strong upregulation in the RPE in ABCA4$^{-/-}$ mice, confirming our previous results in wild-type albino mice [19]. *Cfi*, a cofactor of CFH, was downregulated at the RNA level with aging in microglia, while it was expressed at increasing levels in the RPE.

Differences in cell-type-specific complement expression for ABCA4$^{-/-}$ mice compared to wild-type albino mice was found at the age of 24 weeks. ABCA4$^{-/-}$ mice upregulated transcripts of complement-activating *c3* in RPE cells compared to wild-type albino mice (Figure 2). Additionally, we detected a downregulation of the complement-inhibiting *cfi* mRNA in aged ABCA4$^{-/-}$ microglia (a trend that was also observed in Müller cells) compared to microglia from wild-type controls (Figure 2).

These changes in the local complement expression pattern toward proinflammation in ABCA4$^{-/-}$ mice at 24 weeks of age compared to wild-type mice were present at a time point where retinal cell loss was first detected in the GCL and, thus, occurred concomitantly (Figure 1B).

2.3. Increase of C3 Cleavage Products in ABCA4$^{-/-}$ Mice Compared to Wild-Type Mice

Based on the increased *c3* mRNA expression in ABCA4$^{-/-}$ mice, we investigated the protein level of complement component C3 in the retina, RPE/choroid and serum by Western blot analysis (Figure 3A–C, Supplementary Figure S4) and immunostaining (Figure 3D) using an anti-C3 α-chain antibody specific for the C3d region (His1002-Arg1303). We identified distinct C3 cleavage products, mainly C3α, C3b, iC3b, C3dg and C3d, under reduced conditions in the retina and RPE/choroid (Figure 3A, Figure 4B and Figure S4). In contrast, we detected only the full-length C3α chain and the C3d fragment in the serum (Figure 3C).
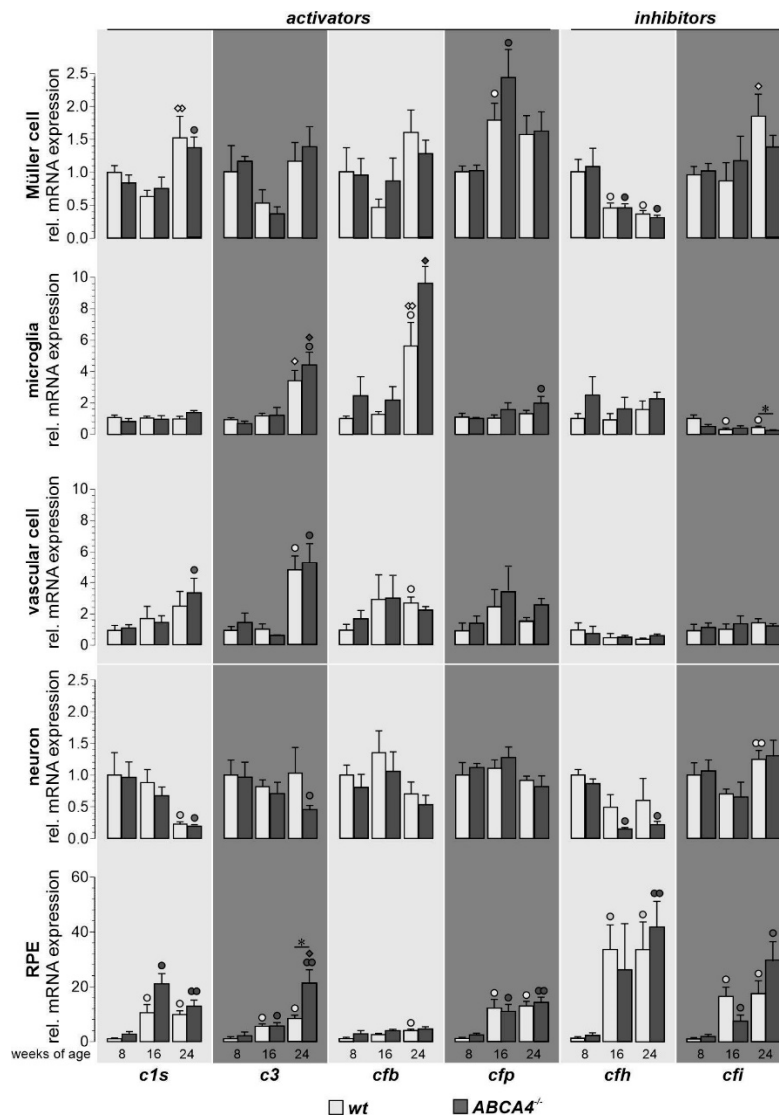
Figure 2. Comparison of complement component expression between retinal cell types of wild-type albino and ABCA4$^{-/-}$ mice. Complement expression analysis of *c1s*, *c3*, *cfb*, *cfp*, *cfh* and *cfi* by qRT-PCR was performed on Müller cells, microglia, vascular cells, neurons and RPE from 8-, 16- and 24-week-old ABCA4$^{-/-}$ mice and compared to previously published wild-type data [19]. We found a significantly enhanced expression of *c3* in RPE cells and decreased expression of *cfi* in microglia cells compared to wild-type controls. Most other age-dependent changes in complement expression were similar in both mouse strains [19]. Bars represent mean values ± SEM of cells purified from four to six animals. Mann–Whitney U-testing was performed on all data (*$p < 0.05$. White circle (○): significant difference compared to the expression level at eight weeks of age in wt; black circle (●): significant difference compared to the expression level at eight weeks of age in ABCA4$^{-/-}$ mice; white diamond (◊): significant difference compared to the expression level at 16 weeks of age in wt animals; black diamond (♦): significant difference compared to the expression level at 16 weeks of age in wt animals. ○/●/◊/♦: $p < 0.05$; ●●/◊◊: $p < 0.01$).
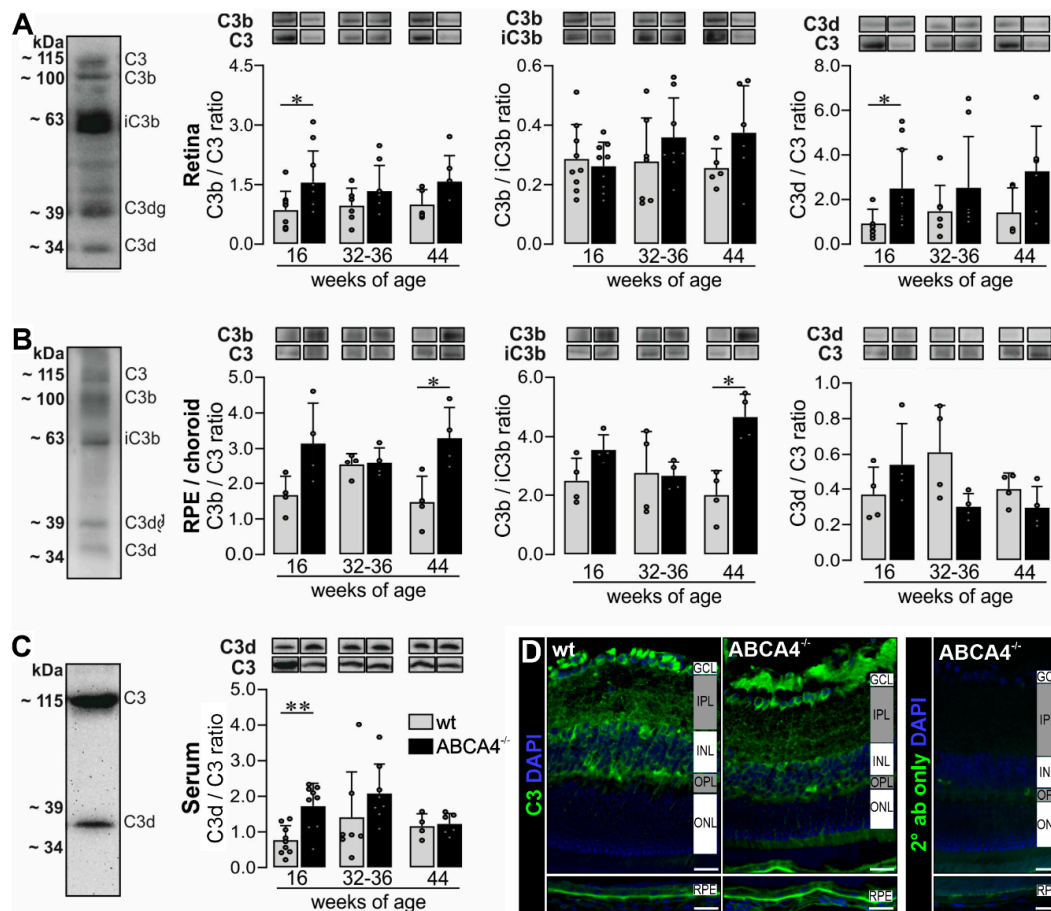
Figure 3. Western blot analysis and immunostaining of complement factor C3 in the RPE/choroid, retina and serum of wild-type albino and ABCA4$^{-/-}$ mice. (**A**,**B**) Western blot analysis under reduced condition using an anti-C3 α-chain antibody showed bands for C3, C3b, iC3b, C3dg and C3d fragments in the (**A**) retina and (**B**) RPE/choroid. (**A**) At 16 weeks of age, we detected a significant increase of C3b to C3 and C3d to C3 ratio in the retina of ABCA4$^{-/-}$ mice compared to wild-type mice. (**B**) The ratio of C3b to C3 and C3b to iC3b was significantly increased in the RPE/choroid of ABCA4$^{-/-}$ mice compared to wild-type mice at 44 weeks of age. (**C**) C3 and C3d fragments were detected in the serum using the C3d-fragment-specific antibody. The C3d to C3 ratio was increased at 16 weeks of age in ABCA4$^{-/-}$ mice. (**D**) Immunofluorescence staining using an anti-C3 (green/gray) antibody showed an increase of C3 fragments in the RPE in albino ABCA4$^{-/-}$ mice compared to wild-type mice. Cell nuclei were counterstained with DAPI (blue). Stainings were performed on sections from at least three mice per genotype and representative images were chosen. As a negative control, sections were incubated with the secondary antibody (2° ab) only. GCL, ganglion cell layer; IPL, inner plexiform layer; INL, inner nuclear layer; OPL, outer plexiform layer, ONL, outer nuclear layer. Scale bars, 20 µm. (**A**–**C**) Bars represent mean values ± SEM from 4 to 10 animals. * $p < 0.05$, ** $p < 0.01$, Mann–Whitney U-test.

The ratios C3b/C3 and C3d/C3 reflect complement activation and the ratio C3b/iC3b gives a better insight into the CFI-dependent conversion from the active C3b to the inactive iC3b. Measuring these ratios gives us a better understanding of complement activation/inactivation than only quantifying total C3.

We found that the C3b/C3 and C3d/C3 ratios were increased in retinae from 16-week-old albino ABCA4$^{-/-}$ mice compared to wild-type mice (Figure 3A). For the RPE/choroid, we detected an increase of the C3b/C3 ratio in ABCA4$^{-/-}$ mice at 44 weeks of age and a correlated increased C3b/iC3b ratio indicating an activated complement system, which was not counterbalanced by the degradation of C3b into inactive iC3b by CFI.

C3 cleavage products in the retina and RPE/choroid of ABCA4$^{-/-}$ mice compared to wild-type mice indicated an activated complement system on protein level in the albino ABCA4$^{-/-}$ mice.

2.4. Decrease of CFI Levels in the Retina of ABCA4$^{-/-}$ Mice

A decreased mRNA expression of *cfi* in the microglia cells of ABCA4$^{-/-}$ mice (Figure 2) and an enhanced C3b/iC3b ratio in the RPE/choroid (Figure 3B) suggested a lower activity of the complement regulator CFI. Accordingly, we next validated the CFI expression on protein levels via Western blot and immunostaining in the retinae and serum (Figures 4 and S5). A distinct signal for the full-length CFI (~88 kDa) was detected in the serum samples [21], but only a weak band could be found in the retinal tissue preparations (Figure 4A). We identified a double band for the CFI heavy chain in retinal and serum samples at ~55 kDa, but the corresponding putative double band for the light chain below 35 kDa was smaller than what was theoretically expected (Figure 4A). The intensity of the CFI heavy chain double band was slightly higher at 16 weeks and significantly reduced at 44 weeks of age in the retina of ABCA4$^{-/-}$ compared to wild-type mice (Figure 4B). Similar results were found for the putative CFI light chain (Figure S5).
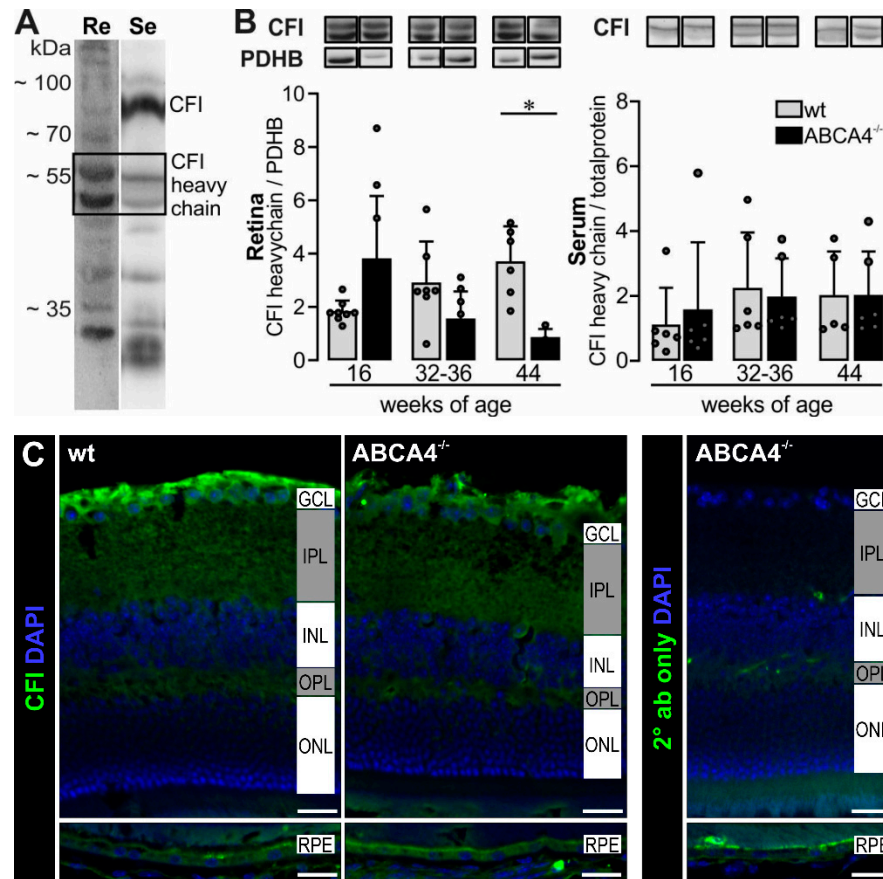

Figure 4: Complement inhibitors (CFI) heavy chain levels decreased in aging ABCA4$^{-/-}$ mice. (**A**) CFI heavy chain was detected in the retina (Re) and serum (Se) using Western blot under reduced condition. (**B**) Photometric quantification of CFI heavy chain showed a significant decrease in ABCA4$^{-/-}$ mice at 44 weeks of age compared to wild-type in the retina. Pyruvate dehydrogenase E1 subunit beta (PDHB, 30–35 kDa) was used to normalize the CFI levels in the retina. For the serum, no differences were found between respective genotypes. (**C**) Immunofluorescence detection of CFI in the cross-sections of mouse eyes. Nuclei were counterstained with DAPI. Stainings were performed on sections from at least three mice per genotype and representative images were chosen. As a negative control, sections were incubated with the secondary antibody (2° ab) only. GCL, ganglion cell layer; IPL, inner plexiform layer; INL, inner nuclear layer; OPL, outer plexiform layer, ONL, outer nuclear layer. Scale bars, 20 µm. (**A**,**B**) Bars represent mean values ± SEM from 4 to 10 animals. * $p < 0.05$, Mann–Whitney U-test.

2.4. Decrease of CFI Levels in the Retina of ABCA4$^{-/-}$ Mice

A decreased mRNA expression of *cfi* in the microglia cells of ABCA4$^{-/-}$ mice (Figure 2) and an enhanced C3b/iC3b ratio in the RPE/choroid (Figure 3B) suggested a lower activity of the complement regulator CFI. Accordingly, we next validated the CFI expression on protein levels via Western blot and immunostaining in the retinae and serum (Figure 4 and Figure S5). A distinct signal for the full-length

CFI (~88 kDa) was detected in the serum samples [21], but only a weak band could be found in the retinal tissue preparations (Figure 4A). We identified a double band for the CFI heavy chain in retinal and serum samples at ~55 kDa, but the corresponding putative double band for the light chain below 35 kDa was smaller than what was theoretically expected (Figure 4A). The intensity of the CFI heavy chain double band was slightly higher at 16 weeks and significantly reduced at 44 weeks of age in the retina of ABCA4$^{-/-}$ compared to wild-type mice (Figure 4B). Similar results were found for the putative CFI light chain (Figure S5).

Full-length CFI and the CFI heavy chain were also detected in the serum, but we did not find any differences in protein levels between ABCA4$^{-/-}$ and wild-type mice (Figure 4B). In line with the Western blot experiments, lower CFI levels could be determined by immunofluorescent staining in the 40-week-old wild-type and ABCA4$^{-/-}$ retinae, especially at the level of the ganglion cell/nerve fiber layer (Figure 4C).

2.5. Signs of Mild Microglial Activation in Aging ABCA4$^{-/-}$ Mice

Increased mRNA expression of complement activators (*c3*, *cfb*, *cfp*), altered protein cleavage products (C3) and decreased complement inhibitor activity (CFI) might be associated with modified immune homeostasis in ABCA4$^{-/-}$ that could be reflected by microglial activation, given that they are the retinal cell type with the highest expression of complement receptors [19,22,23]. Supporting this assumption, the number of detected microglia increased with aging in both mouse strains, which displayed signs of mild activation such as shorter processes as previously reported [19]. Therefore, they occupied a smaller retinal area in 32-40-week-old mice compared to 24-week-old mice (Figure 5). Interestingly, the number of microglia measured in the inner retinal layers of ABCA4$^{-/-}$ compared to wild-type mice at 32-40 weeks of age was significantly increased (Figure 5B), which is in line with an enhanced loss of cells in the ganglion cell layer compared to their wild-type counterparts (Figure 1B).
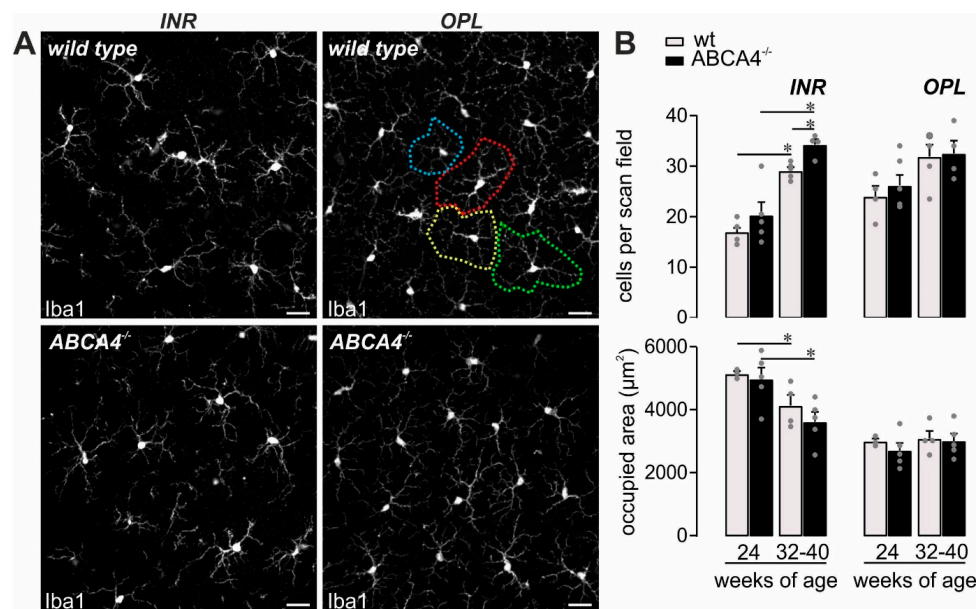

Figure 5. Mild microglia activation in ABCA4$^{-/-}$ mice. (**A**,**B**) Microglia were quantified in the inner retinal layers (INR), such as the ganglion cell layer and inner plexiform layer, and additionally in the outer plexiform layer (OPL) on the basis of Iba1 labeling in mice of the indicated age in ABCA4$^{-/-}$ mice and compared to previously published data of wild-type albino mice [19]. (**A**) The area occupied by the widely branched processes of a single microglia was measured as exemplarily depicted by the dashed circles of different colors for the OPL microglia in a retina from a wild-type animal. Scale bars, 20 μm. (**B**) Bars represent mean values ± SEM from 2-4 animals. * *p* < 0.05, Mann–Whitney U-test. ADU, arbitrary digital units.

3. Discussion

Contribution of an overactive complement system to retinal degeneration along with age-related macular degeneration or Stargardt's disease have been discussed in the literature [7,8,24–27]. Studying the albino ABCA4$^{-/-}$ mice as a model for the inherited retinal dystrophy Stargardt disease type [1,4,5,15,16], we described hallmarks of the disease, including cell loss in the GCL [28–30], accompanied by a significantly enhanced autofluorescence of the RPE (Figure 1), which was in line with previous reports using comparable ex vivo detection techniques for autofluorescence [4,6].

The observed retinal changes correlated with a distinct complement activation pattern (Figure 3, Table S1). Importantly, we set out to further validate putative changes in complement activity described by others [5,31]. In this study, we tried to identify the source of these changes in complement activation by defining the contribution of different retinal cell types to the local complement homeostasis and by investigating if systemic complement activity contributed to disease progression in albino ABCA4$^{-/-}$ mice.

Overall, we found mainly age-related retinal complement expression changes consistent in both genotypes. However, a lack of ABCA4 was associated with an increase of *c3* mRNA expression primarily in the RPE and a decrease of *cfi* mRNA in microglia (Figure 2). These data suggested a contribution of retinal cell transcripts to the local complement homeostasis in ABCA4$^{-/-}$ mice.

Based on our mRNA results, we compared changes in C3 protein level and its activation products in eye tissue and serum samples of ABCA4$^{-/-}$ and wild-type mice. The C3 alpha chain is a 115 kDa protein subunit cleaved by proteases into active (C3b) and inactive (C3d, C3dg) fragments. Interestingly, we identified two major C3 fragments in the mouse serum corresponding either to nonactive C3 or inactivated C3d (Figure 3C), suggesting a well-controlled, systemic complement environment. In contrast, C3 analysis in the retinal tissue uncovered a rather activated status in the retina and RPE/choroid detecting the larger C3 fragments, C3b and iC3b (Figure 3A–C) early in the disease progression. These large, activated C3 fragments were tissue-specific and not detected in the serum. However, a concomitantly increase of systemic inactive C3d fragments correlated with accumulated C3d fragments in the retina at 16 weeks of age in ABCA4$^{-/-}$ mice. This could indicate a relationship between systemic and local complement systems for these small, inactive C3d fragments, but not for the large active C3b fragments. According to our data of an early C3d accumulation in the serum and retina, one could speculate that a temporarily reduced integrity of the blood–retina–barrier (formed by endothelial cells of intraretinal vessels and by the RPE) enabled the influx of systemic C3d into the retina thereby causing increased C3d cleavage product deposition in the retina.

Indeed, it is well known that the C3 cleavage differs in tissue, cell lines and fluids, as well as in healthy and disease conditions [32–35]. Comparing C3 fragment levels in ABCA4$^{-/-}$ mice to wild-type mice, we identified the RPE as the cell population driving active C3b accumulation in the eye later in disease progression (Figure 3B,D), which did not correlate with systemic changes at 44 weeks of age. In line with our findings, others describe an enhanced deposition of C3 cleavage products at the level of the RPE in mice deficient for ABCA4 using Western blot and immunocytochemistry [5,31] but lacking any information regarding the systemic C3 status.

This tissue-specific differential pattern of C3 fragments in the murine retina compared to the blood points at a local, retinal regulation of complement activation that might be partially linked to changes of the complement activity in the systemic circulation. Therefore, we proposed that C3b deposition is related to a local tissue response, including loss of cells in the ganglion cell layer and increased microglia cell numbers indicative of neuroinflammatory processes.

Complement component C3 is cleaved in its inactive forms (C3d, C3dg, etc.) by the complement protease CFI and its cofactor CFH that act as complement inhibitors [36–38]. Along with the increased *c3* expression, *cfi* mRNA expression was decreased in 24-week-old ABCA4$^{-/-}$ mice. This suggested that dysregulated levels of a complement inhibitor could result in uncontrolled C3 activation and enhanced generation of activated C3b cleavage products in the retinal microenvironment [21,24]. The role of CFI has not yet been extensively studied in the ABCA4$^{-/-}$ model. Lower levels of distinct human

CFI variants in patients' serum were discussed to be associated with AMD [39]. We assumed that the dysregulation of *cfi* expression could be a reason for disease progression in the ABCA4$^{-/-}$ model. In support of this hypothesis, we confirmed lower CFI protein levels in the retina of 40-week-old ABCA4$^{-/-}$ compared to wild-type mice (Figure 4), as well as a constantly increased C3b fragment deposition in ABCA4$^{-/-}$ animals (Figure 3). In line with these results. Rose et al. showed that, in a CFI-deficient mouse, C3 circulates as active C3b with no evidence of other cleavage products (iC3b, C3dg, C3d) [21]. This finding may explain our detection of a higher C3b ratio in the ABCA4$^{-/-}$ mice during degeneration.

The expression of the second important complement inhibitor *cfh* has recently been shown to be decreased threefold in the eyecup (RPE/choroid/sclera) of four-week-old ABCA4$^{-/-}$ mice [5,31]. Those findings could not be confirmed in our study, which might be explained by differences regarding the age of mice investigated (in this study 8-24-week-old mice) and the sampling of tissues (in this study, RPE/choroid in contrast to whole eyecup preparations, including scleral tissue used by others). The sclera contains mainly collagen fibers and stroma cells, especially in the outer episcleral layer (including fibroblasts, endothelial cells, melanocytes and infiltrating immune cells) [40]. Krausgruber et al. recently described the three major structural cell types—endothelium, epithelium and fibroblasts—are key immune regulators and express complement genes in various tissues [41]. Voigt et al. have shown, via single-cell RNA sequencing, that *cfh* was exceptionally highly expressed in the fibroblasts in human RPE/choroid samples [42]. This may explain why we did not see an increase of *cfh* in our samples devoid of fibroblast-rich scleral tissue. RPE/choroid and sclera might respond differently to the pathology [42]. We found a low expression of *cfh* transcripts at eight weeks of age in both strains, followed by an upregulation starting from 16 weeks of age, especially in the RPE. On the other hand, there was a trend toward *cfh* downregulation in ABCA4-deficient neurons (Figure 2). This could imply an overall reduction of CFH protein levels in the retina during aging, given that neurons are the retinal cell population expressing the highest *cfh* mRNA levels [19]. Since we focused on significant genotype-related changes that could not be demonstrated for *cfh* mRNA levels, the latter were not further investigated.

In line with an enhanced complement activity in the course of aging, and even more so in the absence of ABCA4, an increase in the number of retinal microglia was found during aging in both mouse strains and was more prominent in ABCA4$^{-/-}$ retinae (Figure 5). Importantly, these changes regarding complement expression and microglial activation were detected in the ABCA4$^{-/-}$ animals before significant photoreceptor cell loss was observed (Figure 1) [43]. Our data correlate with those of others, describing an enhanced microglia activation and the detection of inflammation markers in the retina of ABCA4$^{-/-}$ mice [5,44]. We suggest that a close interplay of changes in the cell-type-specific retinal complement component expression, as well as complement activation product deposition during hereditary retinal degeneration in ABCA4$^{-/-}$ mice and activation of microglia cells, may possibly contribute to slow photoreceptor degeneration.

We conclude that the observed loss of cells in the inner retina, specifically in ABCA4$^{-/-}$ mice, could be due to the dysregulated complement activity in this microenvironment. It has recently been shown that thinning of the INL, the nerve fiber layer, as well as the inner retina, was prominent in different complement knockout mouse models [45]. Such observations suggest that thinning of the inner retina might be a key contributor to malfunction of a complement dysregulated retina or vice versa dysfunction of the complement might affect the integrity of the inner retina.

In sum, activation of the local complement cascade and an interplay with altered systemic complement homeostasis could be a response to an unbalanced, retinal microenvironment due to aging or pathological events in the course of retinal degeneration. Our results imply that rebalancing the local complement activity in inherited retinal diseases may help to prolong neuron survival and avoid potential secondary cell loss, as seen in the GCL of the ABCA4$^{-/-}$ mice. Moreover, this underlines the importance of anti-complement clinical trials in patients with Stargardt disease that in addition to photoreceptor degeneration also suffer from ganglion cell degeneration (such as, e.g., NCT03364153).

Furthermore, our cell-type-specific transcription analysis opens a new avenue to identify key genes in retinal degenerative diseases, including those related to aging.

4. Materials and Methods

4.1. Animals

Experiments were conducted with 8-, 16-, 24-, 32-, 36-, 40- and 44-week-old male and female mice. Albino ABCA4$^{-/-}$ mice on a BALB/c background were kindly provided by T. Krohne (University of Bonn, Bonn, Germany). To enable the use of littermates, these homozygous ABCA4$^{-/-}$ mice were crossbred with BALB/cJRj mice (Jackson Laboratories). For initial qRT-PCR data collection, 8-24-week-old BALB/cJRj wild-type mice were used. Data have already been partially published in a previous study addressing age-related complement expression changes [19]. To stick to the rules of the 3Rs, results are included here, such as wild-type controls for the qRT-PCR dataset. All other experiments were performed comparing littermates derived from the ABCA4$^{-/-}$; BALB/cJRj crossbreeding. Mice were housed in a 12 h light/dark cycle with 60-70 lux inside and 500 lux outside the cages. All experiments were done in accordance with the European Community Council Directive 2010/63/EU and the ARVO Statement for the Use of Animals in Ophthalmic and Vision Research. All animals enrolled in this study were reported to the local authorities (BY_UR_OE_PaulAuge_2016) according to local regulations. Genotyping of the mice was performed with the KAPA Mouse Genotyping Hot Start Kit (Merck, Darmstadt, Germany) using *abca4* primers (Table 1). To ensure that the observed findings of the present study are due to the lack of ABCA4 deficiency, we genotyped the mice for *rd1*, *rd8*, *rd10* and *rd12* (for primers, see Table 1) mutations and verified that no known mutations causing retinal degeneration were present in our mouse breeding.

Table 1. Primer sequences for mouse genotyping by PCR.

Gene ID	Primer Sequences: *Forward*	Primer Sequences: *Reverse*	Accession Number
abca4	5′ aggagaagcaatcaaatcagga 3′	5′ gaagatgctctggatatctctgc 3′ 5′ tgagtaggtgtcattctattctgg 3′	NM_007378.1
rd1	5′ tgacaattactccttttccctcagtctg 3′ 5′ tacccacccttcctaattttctcacgc 3′	5′ gtaaacagcaagaggctttattgggaac 3′	AH002075.2
rd8	5′ gtgaagacagctacagttctgatc 3′ 5′gccctgtttgcatggaggaaacttggaaga cagctacagttcttctg 3′	5′ gccccatttgcacactgatgac 3′	NM_133239.2
rd10	5′ acaaggaacaagggctctga 3′	5′ ccttccactcattgctaggac 3′	NM_008806.2
rd12	5′ tgacacctagttttaatattttgatcc 3′	5′cagagcttgaaccccatt 3′	NM_029987.2

4.2. Immunohistochemistry of Retina and RPE/Choroid Flat Mounts

Cell nuclei quantification in 10 μm sections of 4% paraformaldehyde (PFA)-fixated, paraffin-embedded eyes was performed with Hoechst33342 (1:1000; #H1399, Thermo Fisher Scientific, Braunschweig, Germany) as previously described [46].

Retinal microglia and RPE autofluorescence quantification were evaluated in PFA-fixated, permeabilized and blocked (1% BSA, 5% goat serum, 0.1 M NaPO4, pH 7) retinal or RPE/choroid flat mounts, respectively. RPE/choroid flat mounts were stained with anti-zonula occludens-1 (ZO-1) antibody (1:300, #61-7300, ThermoFisher, Braunschweig, Germany) and secondary anti-rabbit-Cy3 antibody (1:200, #A10520, ThermoFisher, Braunschweig, Germany). Retinal flat mounts were stained with anti-Iba1 antibody (1:400, #019-19741, Wako Chemicals, Neuss, Germany) and secondary anti-rabbit-Cy3 antibody.

To determine GFAP and complement expression in the retina and RPE, eyes were PFA-fixed, cryoprotected and embedded in Tissue-Tek O.C.T. compound (Cat. No. 4583, #SA62534-10 Sakura, Staufen, Germany). Twenty-micrometer slices were permeabilized, blocked (5% goat serum, 0.1%

Tween20, PBS) and incubated with primary antibodies specific for GFAP (1:500, G3893, Sigma, Saint-Louis, MO, USA), CFI (1:100, A313/6, Quidel, San Diego, CA, USA) or C3d (12 µg/mL, AF2655, R&D Systems, Minneapolis, MN, USA) diluted in a blocking buffer. Sections were labeled with Cy3-conjugated secondary antibodies (1:500, Cat. No. 705-165-147, Dianova, Hamburg, Germany) and DAPI nucleic acid stain (1:1000, Cat. No. 62248c, Invitrogen, Ltd., Paisley, UK). Slides were mounted with Aqua-Poly/Mount (Cat. No. 18606-20, Polysciences, Hirschberg, Germany). All images were taken with a confocal microscope (VisiScope, Visitron Systems, Puchheim, Germany).

4.3. Isolation of Retinal Cell Populations by Immunomagnetic Enrichment

Retinal cell types were enriched as described previously [46]. Briefly, retinae were treated with papain (0.2 mg/mL; Roche Molecular Biochemicals) in a Ca^{2+}- and Mg^{2+}-free extracellular solution (140 mM NaCl, 3 mM KCl, 10 mM HEPES, 11 mM glucose, pH 7.4). After DNase I (200 U/mL) incubation, retinae were triturated in an extracellular solution (1 mM $MgCl_2$ and 2 mM $CaCl_2$). To purify microglial and vascular cells, the retinal cell suspension was subsequently incubated with CD11b and CD31 microbeads according to the manufacturer's protocol (Miltenyi Biotec, Bergisch Gladbach, Germany). The respective binding cells were depleted from the retinal suspension using large cell (LS) columns (Miltenyi Biotec) prior to Müller cell enrichment. To purify Müller glia, the cell suspension was incubated in an extracellular solution containing biotinylated hamster anti-CD29 (clone Ha2/5, 0.1 mg/mL, BD Biosciences, Heidelberg, Germany). Cells were washed in the extracellular solution, spun down, resuspended in the presence of antibiotin MicroBeads (1:5; Miltenyi Biotec,) and incubated for 10 min at 4 °C. After washing, CD29+ Müller cells were separated using LS columns according to the manufacturer's instructions (Miltenyi Biotec). Cells in the flow through the last sorting step were considered a neuronal population as they were depleted from microglia, vascular cells and Müller glia. The retinal pigment epithelium was collected by scratching it out of the eyecup after the retina had carefully been removed and, thus, scratch samples also contained cells from the underlying choroid.

4.4. qRT-PCR

Total RNA was isolated from the enriched cell populations using the PureLink RNA Micro Scale Kit (Thermo Fisher Scientific, Schwerte, Germany). A DNase digestion step was included to remove genomic DNA (Roche). We performed RNA integrity validation and quantification using the Agilent RNA 6000 Pico chip analysis according to the manufacturer's instructions (Agilent Technologies, Waldbronn, Germany). First-strand cDNAs from the total RNA purified from each cell population were synthesized using the RevertAid H Minus First-Strand cDNA Synthesis Kit (Fermentas by Thermo Fisher Scientific, Schwerte, Germany). We designed primers using the Universal ProbeLibrary Assay Design Center (Roche) and measured transcript levels of candidate genes by qRT-PCR using the TaqMan hPSC Scorecard Panel (384-well, ViiA7, Life Technologies, Darmstadt, Germany) according to the company's guidelines [19]. Expression levels of respective complement genes (for primer sequences, see Table 2) were normalized to the expression of isocitrate dehydrogenase 3 (NAD+) beta (*idh3b*) that we validated in a recent studied to fulfill the criteria of a good housekeeping gene across retinal cell populations [19].

4.5. Western Blot

Retina and scratch RPE/choroid were pooled from two mouse eyes and homogenized in T-PER™ buffer (Pierce Biotechnology, Rockford, IL, USA) supplemented with protease and phosphatase inhibitors (Sigma-Aldrich, Taufkirchen, Germany). The homogenized retina, RPE/choroid or isolated serum were denatured in reducing a Laemmli sample buffer and separated on a 12% SDS-PAGE. The immunoblot was performed as previously described [47]. Detection was performed using a goat polyclonal C3 (1:1000, AF2655, R&D Systems, Minneapolis, MN, USA), a goat anti-CFI antibody (1:200, A313/6, Quidel, San Diego, CA, USA) or a rabbit anti-PDHB antibody (1:2000, Abcam, ab155996,

Cambridge, UK), followed by anti-goat (1:10,000, Dianova, Hamburg, Germany) or anti-rabbit (1:10,000, Dianova, Hamburg, Germany) secondary antibodies conjugated to horse-radish peroxidase. Respective primary and secondary antibodies were diluted in a blocking solution. Blots were developed with Western Sure PREMIUM Chemiluminescent Substrate (LI-COR, Bad Homburg, Germany).

Table 2. Primer and TaqMan probe combinations for the detection of complement components via qRT-PCR.

Gene ID	Primer Sequences: *Forward*	Primer Sequences: *Reverse*	TaqMan® Probe from Roche	Accession Number
idh3b	5′ gctgcggcatctcaatct 3′	5′ ccatgtctcgagtccgtacc 3′	# 67	NM_130884.4
c1s	5′ ggtggatacttctgctcctgtc 3′	5′ agggcagtgaacacatctcc 3′	# 69	NM_144938.2
c3	5′ accttacctcggcaagtttct 3′	5′ ttgtagagctgctggtcagg 3′	# 76	NM_009778.3
cfb	5′ ctcgaacctgcagatccac 3′	5′ tcaaagtcctgcggtcgt 3′	# 112	NM_008198.2
cfp	5′ tcttgagtggcagctacagg 3′	5′ cagaccagccacccatct 3′	# 56	NM_008823.4
cfh	5′ aaaaaccaaagtgccgagac 3′	5′ ggaggtgatgtctccattgtc 3′	# 25	NM_009888.3
cfi	5′ tttctcttggctctccacttg 3′	5′ tgcagtaagcatttctgatcg 3′	# 63	NM_007686.3

4.6. Statistics

Statistical analyses were performed using Prism (GraphPad Prism 7.04, San Diego, CA, USA). In most of the experiments in the present study, results from 4 biological replicates were collected to keep to the rules of the three Rs for the sake of animal welfare. Since this low number of input values does not allow an appropriate estimation of a normal Gaussian distribution, significance levels were determined by the nonparametric, two-tailed Mann–Whitney U-test, unless stated otherwise. All data are expressed as mean ± standard error (SEM) unless stated otherwise. Detailed information about specific n-values, implemented statistical tests and coding of significance levels are provided in the respective figure legends.

Supplementary Materials: Supplementary materials can be found at http://www.mdpi.com/1422-0067/21/22/8468/s1.

References

1. Molday, R.S. Insights into the Molecular Properties of ABCA4 and Its Role in the Visual Cycle and Stargardt Disease. *Prog. Mol. Biol. Transl. Sci.* **2015**, *134*, 415–431. [CrossRef] [PubMed]
2. Genead, M.A.; Fishman, G.A.; Stone, E.M.; Allikmets, R. The Natural History of Stargardt Disease with Specific Sequence Mutation in the ABCA4 Gene. *Investig. Opthalmol. Vis. Sci.* **2009**, *50*, 5867–5871. [CrossRef] [PubMed]
3. Allikmets, R.; Singh, N.; Sun, H.; Shroyer, N.F.; Hutchinson, A.; Chidambaram, A.; Gerrard, B.; Baird, L.; Stauffer, D.; Peiffer, A.; et al. A photoreceptor cell-specific ATP-binding transporter gene (ABCR) is mutated in recessive Starqardt macular dystrophy. *Nat. Genet.* **1997**, *15*, 236–246. [CrossRef] [PubMed]
4. Taubitz, T.; Tschulakow, A.V.; Tikhonovich, M.; Illing, B.; Fang, Y.; Biesemeier, A.; Julien-Schraermeyer, S.; Schraermeyer, U. Ultrastructural alterations in the retinal pigment epithelium and photoreceptors of a

Stargardt patient and three Stargardt mouse models: Indication for the central role of RPE melanin in oxidative stress. *PeerJ* **2018**, *6*, e5215. [CrossRef] [PubMed]

5.　Radu, R.A.; Hu, J.; Yuan, Q.; Welch, D.L.; Makshanoff, J.; Lloyd, M.; McMullen, S.; Travis, G.H.; Bok, D. Complement System Dysregulation and Inflammation in the Retinal Pigment Epithelium of a Mouse Model for Stargardt Macular Degeneration. *J. Biol. Chem.* **2011**, *286*, 18593–18601. [CrossRef]

6.　Lenis, T.L.; Sarfare, S.; Jiang, Z.; Lloyd, M.B.; Bok, D.; Radu, R.A. Complement modulation in the retinal pigment epithelium rescues photoreceptor degeneration in a mouse model of Stargardt disease. *Proc. Natl. Acad. Sci. USA* **2017**, *114*, 3987–3992. [CrossRef]

7.　Zhou, J.; Jang, Y.P.; Kim, S.R.; Sparrow, J.R. Complement activation by photooxidation products of A2E, a lipofuscin constituent of the retinal pigment epithelium. *Proc. Natl. Acad. Sci. USA* **2006**, *103*, 16182–16187. [CrossRef]

8.　Zhou, J.; Kim, S.R.; Westlund, B.S.; Sparrow, J.R. Complement Activation by Bisretinoid Constituents of RPE Lipofuscin. *Investig. Opthalmology Vis. Sci.* **2009**, *50*, 1392–1399. [CrossRef]

9.　Zipfel, P.F.; Skerka, C. Complement regulators and inhibitory proteins. *Nat. Rev. Immunol.* **2009**, *9*, 729–740. [CrossRef]

10.　Merle, N.S.; Church, S.E.; Fremeaux-Bacchi, V.; Roumenina, L.T. Complement System Part I—Molecular Mechanisms of Activation and Regulation. *Front. Immunol.* **2015**, *6*, 262. [CrossRef]

11.　Clark, S.J.; Bishop, P.N. The eye as a complement dysregulation hotspot. *Semin. Immunopathol.* **2018**, *40*, 65–74. [CrossRef]

12.　Shahulhameed, S.; Vishwakarma, S.; Chhablani, J.; Tyagi, M.; Pappuru, R.R.; Jakati, S.; Chakrabarti, S.; Kaur, I. A Systematic Investigation on Complement Pathway Activation in Diabetic Retinopathy. *Front. Immunol.* **2020**, *11*, 154. [CrossRef]

13.　Bradley, D.T.; Zipfel, P.F.; E Hughes, A. Complement in age-related macular degeneration: A focus on function. *Eye* **2011**, *25*, 683–693. [CrossRef] [PubMed]

14.　Heesterbeek, T.J.; Lechanteur, Y.T.E.; Lorés-Motta, L.; Schick, T.; Daha, M.R.; Altay, L.; Liakopoulos, S.; Smailhodzic, D.; Hollander, A.I.D.; Hoyng, C.B.; et al. Complement Activation Levels Are Related to Disease Stage in AMD. *Investig. Opthalmol. Vis. Sci.* **2020**, *61*, 18. [CrossRef]

15.　MacLaren, R.E.; Barnard, A.R.; Singh, M.S.; Carter, E.; Jiang, Z.; Radu, R.A.; Schraermeyer, U.; MacLaren, R.E. Fundus Autofluorescence in theAbca4−/−Mouse Model of Stargardt Disease—Correlation With Accumulation of A2E, Retinal Function, and Histology. *Investig. Opthalmol. Vis. Sci.* **2013**, *54*, 5602–5612. [CrossRef]

16.　Wu, L.; Nagasaki, T.; Sparrow, J.R. Photoreceptor Cell Degeneration in Abcr −/− Mice. *Retin. Degener. Dis.* **2010**, 533–539. [CrossRef]

17.　Issa, P.C.; Barnard, A.R.; Herrmann, P.; Washington, I.; MacLaren, R.E. Rescue of the Stargardt phenotype in Abca4 knockout mice through inhibition of vitamin A dimerization. *Proc. Natl. Acad. Sci. USA* **2015**, *112*, 8415–8420. [CrossRef]

18.　Sparrow, J.R.; Blonska, A.; Flynn, E.; Duncker, T.; Greenberg, J.P.; Secondi, R.; Ueda, K.; Delori, F.C. Quantitative Fundus Autofluorescence in Mice: Correlation with HPLC Quantitation of RPE Lipofuscin and Measurement of Retina Outer Nuclear Layer Thickness. *Investig. Opthalmol. Vis. Sci.* **2013**, *54*, 2812–2820. [CrossRef]

19.　Pauly, D.; Agarwal, D.; Dana, N.; Schäfer, N.; Biber, J.; Wunderlich, K.A.; Jabri, Y.; Straub, T.; Zhang, N.R.; Gautam, A.K.; et al. Cell-Type-Specific Complement Expression in the Healthy and Diseased Retina. *Cell Rep.* **2019**, *29*, 2835–2848.e4. [CrossRef]

20.　Grosche, A. GFAP expression across purified retinal cell populations after immunomagnetic separation. Unpublished work. 2020.

21.　Rose, K.L.; Paixao-Cavalcante, D.; Fish, J.; Manderson, A.P.; Malik, T.H.; Bygrave, A.E.; Lin, T.; Sacks, S.; Walport, M.J.; Cook, H.T.; et al. Factor I is required for the development of membranoproliferative glomerulonephritis in factor H–deficient mice. *J. Clin. Investig.* **2008**, *118*, 608–618. [CrossRef]

22.　Collier, R.J.; Wang, Y.; Smith, S.S.; Martin, E.; Ornberg, R.; Rhoades, K.; Romano, C. Complement Deposition and Microglial Activation in the Outer Retina in Light-Induced Retinopathy: Inhibition by a 5-HT1AAgonist. *Investig. Opthalmol. Vis. Sci.* **2011**, *52*, 8108–8116. [CrossRef] [PubMed]

23.　Kuehn, S.; Reinehr, S.; Stute, G.; Rodust, C.; Grotegut, P.; Hensel, A.-T.; Dick, H.B.; Joachim, S.C. Interaction of complement system and microglia activation in retina and optic nerve in a NMDA damage model. *Mol. Cell. Neurosci.* **2018**, *89*, 95–106. [CrossRef] [PubMed]

24. Geerlings, M.J.; De Jong, E.K.; Hollander, A.I.D. The complement system in age-related macular degeneration: A review of rare genetic variants and implications for personalized treatment. *Mol. Immunol.* **2017**, *84*, 65–76. [CrossRef] [PubMed]

25. Park, D.H.; Connor, K.M.; Lambris, J.D. The Challenges and Promise of Complement Therapeutics for Ocular Diseases. *Front. Immunol.* **2019**, *10*, 1007. [CrossRef] [PubMed]

26. McHarg, S.; Clark, S.J.; Day, A.J.; Bishop, P.N. Age-related macular degeneration and the role of the complement system. *Mol. Immunol.* **2015**, *67*, 43–50. [CrossRef] [PubMed]

27. Kassa, E.; Ciulla, T.A.; Hussain, R.M.; Dugel, P.U. Complement inhibition as a therapeutic strategy in retinal disorders. *Expert Opin. Biol. Ther.* **2019**, *19*, 335–342. [CrossRef]

28. Newman, N.M.; A Stevens, R.; Heckenlively, J.R. Nerve fibre layer loss in diseases of the outer retinal layer. *Br. J. Ophthalmol.* **1987**, *71*, 21–26. [CrossRef]

29. Ratra, D.; Jaishankar, D.; Sachidanandam, R.; Yusufali, H.; Ratra, V. Swept-source optical coherence tomography study of choroidal morphology in Stargardt disease. *Oman J. Ophthalmol.* **2018**, *11*, 150–157.

30. Lim, J.I.; Tan, O.; Fawzi, A.A.; Hopkins, J.J.; Gil-Flamer, J.H.; Huang, D. A Pilot Study of Fourier-Domain Optical Coherence Tomography of Retinal Dystrophy Patients. *Am. J. Ophthalmol.* **2008**, *146*, 417–426.e2. [CrossRef]

31. Racz, B.; Varadi, A.; Kong, J.; Allikmets, R.; Pearson, P.G.; Johnson, G.; Cioffi, C.L.; Petrukhin, K. A non-retinoid antagonist of retinol-binding protein 4 rescues phenotype in a model of Stargardt disease without inhibiting the visual cycle. *J. Biol. Chem.* **2018**, *293*, 11574–11588. [CrossRef]

32. Li, Q.; Li, Y.X.; Stahl, G.L.; Thurman, J.M.; He, Y.; Tong, H.H. Essential role of factor B of the alternative complement pathway in complement activation and opsonophagocytosis during acute pneumococcal otitis media in mice. *Infect Immun.* **2011**, *79*, 2578–2585. [CrossRef] [PubMed]

33. Kremlitzka, M.; Nowacka, A.A.; Mohlin, F.C.; Bompada, P.; De Marinis, Y.; Blom, A.M. Interaction of Serum-Derived and Internalized C3 With DNA in Human B Cells—A Potential Involvement in Regulation of Gene Transcription. *Front. Immunol.* **2019**, *10*, 493. [CrossRef] [PubMed]

34. Satyam, A.; Kannan, L.; Matsumoto, N.; Geha, M.; Lapchak, P.H.; Bosse, R.; Shi, G.-P.; Lucca, J.J.D.; Tsokos, M.G.; Tsokos, G.C. Intracellular Activation of Complement 3 Is Responsible for Intestinal Tissue Damage during Mesenteric Ischemia. *J. Immunol.* **2016**, *198*, 788–797. [CrossRef] [PubMed]

35. King, B.C.; Kulak, K.; Krus, U.; Rosberg, R.; Golec, E.; Wozniak, K.; Gomez, M.F.; Zhang, E.; O'Connell, D.J.; Renström, E.; et al. Complement Component C3 Is Highly Expressed in Human Pancreatic Islets and Prevents β Cell Death via ATG16L1 Interaction and Autophagy Regulation. *Cell Metab.* **2019**, *29*, 202–210.e6. [CrossRef] [PubMed]

36. Nilsson, S.C.; Sim, R.B.; Lea, S.M.; Fremeaux-Bacchi, V.; Blom, A.M. Complement factor I in health and disease. *Mol. Immunol.* **2011**, *48*, 1611–1620. [CrossRef]

37. Roversi, P.; Johnson, S.; Caesar, J.J.E.; McLean, F.; Leath, K.J.; Tsiftsoglou, S.A.; Morgan, B.P.; Harris, C.L.; Sim, R.B.; Lea, S.M. Structural basis for complement factor I control and its disease-associated sequence polymorphisms. *Proc. Natl. Acad. Sci. USA* **2011**, *108*, 12839–12844. [CrossRef]

38. Gallego, J.I.S.; Nita, I.M.; Nilsson, S.C.; Groeneveld, T.W.; Villoutreix, B.O.; Blom, A.M. Analysis of binding sites on complement Factor I that are required for its activity. *J Biol Chem.* **2010**, *285*, 6235–6245. [CrossRef]

39. Van De Ven, J.; Nilsson, S.; Tan, P.; Buitendijk, G.; Ristau, T.; Mohlin, F.; Nabuurs, S.; Schoenmaker-Koller, F.; Smailhodzic, D.; Campochiarro, P.; et al. A functional variant in the CFI gene confers a high risk of age-related macular degeneration. *Mol. Immunol.* **2013**, *56*, 247–248. [CrossRef]

40. Maggs, D.J. Cornea and Sclera. In *Slatter's Fundamentals of Veterinary Ophthalmology*; Elsevier Inc.: New York, NY, USA, 2008; pp. 175–202.

41. Krausgruber, T.; Fortelny, N.; Fife-Gernedl, V.; Senekowitsch, M.; Schuster, L.C.; Lercher, A.; Nemc, A.; Schmidl, C.; Rendeiro, A.F.; Bergthaler, A.; et al. Structural cells are key regulators of organ-specific immune responses. *Nat. Cell Biol.* **2020**, *583*, 296–302. [CrossRef]

42. Voigt, A.P.; Mulfaul, K.; Mullin, N.K.; Flamme-Wiese, M.J.; Giacalone, J.C.; Stone, E.M.; Tucker, B.A.; Scheetz, T.E.; Mullins, R.F. Single-cell transcriptomics of the human retinal pigment epithelium and choroid in health and macular degeneration. *Proc. Natl. Acad. Sci. USA* **2019**, *116*, 24100–24107. [CrossRef]

43. Radu, R.A.; Yuan, Q.; Hu, J.; Peng, J.H.; Lloyd, M.; Nusinowitz, S.; Bok, D.; Travis, G.H. Accelerated accumulation of lipofuscin pigments in the RPE of a mouse model for ABCA4-mediated retinal dystrophies following Vitamin A supplementation. *Investig. Opthalmol. Vis. Sci.* **2008**, *49*, 3821–3829. [CrossRef] [PubMed]

44. Kohno, H.; Chen, Y.; Kevany, B.M.; Pearlman, E.; Miyagi, M.; Maeda, T.; Palczewski, K.; Maeda, A. Photoreceptor Proteins Initiate Microglial Activation via Toll-like Receptor 4 in Retinal Degeneration Mediated by All-trans-retinal. *J. Biol. Chem.* **2013**, *288*, 15326–15341. [CrossRef] [PubMed]

45. Mukai, R.; Okunuki, Y.; Husain, D.; Kim, C.B.; Lambris, J.D.; Connor, K.M. The Complement System Is Critical in Maintaining Retinal Integrity during Aging. *Front. Aging Neurosci.* **2018**, *10*, 15. [CrossRef] [PubMed]

46. Mages, K.; Grassmann, F.; Jägle, H.; Rupprecht, R.; Weber, B.H.F.; Hauck, S.M.; Grosche, A. The agonistic TSPO ligand XBD173 attenuates the glial response thereby protecting inner retinal neurons in a murine model of retinal ischemia. *J. Neuroinflamm.* **2019**, *16*, 43. [CrossRef]

47. Schäfer, N.; Grosche, A.; Schmitt, S.I.; Braunger, B.M.; Pauly, D. Complement Components Showed a Time-Dependent Local Expression Pattern in Constant and Acute White Light-Induced Photoreceptor Damage. *Front. Mol. Neurosci.* **2017**, *10*, 197. [CrossRef]

Manuscript 1 – (Biber, Jabri, et al., 2023)

Gliosis Dependent Expression of Complement Factor H Variants attenuates Retinal Neurodegeneration Following Ischemic Injury

Josef Biber*, Yassin Jabri*, Sarah Glänzer, Oliver Bludau, Diana Pauly, Antje Grosche

*: Shared first authorship

Gliosis dependent expression of complement factor H truncated variants attenuates retinal neurodegeneration following ischemic injury

Josef Biber[1#], Yassin Jabri[2#], Sarah Glänzer[1], Aaron Dort[3], Oliver Bludau[1], Diana Pauly[3#*], Antje Grosche[1#]

[1]Department of Physiological Genomics, Ludwig-Maximilians-Universität München, Planegg-Martinsried, Germany

[2]Department of Ophthalmology, University Hospital Regensburg, Regensburg, Germany

[3]Experimental Ophthalmology, University of Marburg, Marburg, Germany

[#]contributed equally

*corresponding author: diana.pauly@uni-marburg.de

Abstract

Inherited, age-related, and acute retinal diseases are often exacerbated by an aberrant or excessive activity of the complement system. Cells not previously affected by an acute event or genetic variants may subsequently degenerate, resulting in visual impairment. The therapeutic potential of supplementation of complement factor H (FH), a key regulator of the complement cascade, is therefore particularly promising in the context retinal diseases caused by complement activation.

In this study, we engineered adeno-associated viruses (AAVs) containing sequences of two truncated human FH variants. These variants were regulated by the glial fibrillary acidic protein (GFAP) promoter, which is selectively active in gliotic Müller cells. Both CFH variants consisted of domains 19-20, which were connected to domains 1-4 and 1-7, respectively, by a poly-glycine linker. These AAVs were intravitreally injected following ischemic injury of C57BL/6J mouse retinas. We observed transgene expression exclusively in gliotic Müller cells and to some extent in astrocytes. The expression correlated directly with damage severity. Interventions resulted in decreased complement activation, accelerated normalization of microglia activity and morphological improvements. Reduced levels of *C3* transcripts and C3d protein in conjunction with higher transcript levels of inhibitory regulators like CFI and CFH, hinted attenuated complement activity.

This study demonstrates the generation of a promising complement regulatory gene addition therapy. With further *in vivo* testing it could be applied to treat a wide range of retinal diseases where no causative therapies are available.

Keywords:

Complement system, complement factor H (CFH), retinal degeneration, gene therapy

Introduction

Retinal diseases, such as age-related macular degeneration (AMD), diabetic retinopathy, glaucoma and uveitis, are leading causes of vision loss and blindness across all demographics and age groups (Aiello et al. 1998; Mitchell et al. 2018; Tsirouki et al. 2018). Despite their different pathological mechanism, these diseases share a common feature: the involvement of the complement system in their development and/or progression (Copland et al. 2010; Mondino et al. 1984; Mitchell et al. 2018; Muramatsu et al. 2013; Hu et al. 2020). However, effective treatments that address their underlying causes of these diseases are still limited. Therefore, targeting the complement system represents a promising approach for the treatment of these devastating conditions.

The complement system is an essential part of the innate immune response. It is responsible for recognizing and eliminating foreign particles such as bacteria and viruses, as well as apoptotic or modified host cells (Anderson et al. 2010). Complement components are continuously secreted into the circulation and are also locally expressed in immune-privileged tissues such as the retina (Zhou et al. 2016; Luo et al. 2013; Demirs et al. 2021; Pauly et al. 2019). In the retina, inflammation in early disease stages is primarily driven by local players (Anderson et al. 2010), including astrocytes, microglia and Müller cells. These cells contribute to the maintenance of complement homeostasis and are primary suppliers of key pro-inflammatory factors (Medzhitov 2008; Xu et al. 2009).

The complement cascade is initiated when complement recognition molecules bind to triggers such as antibody-antigen complexes or foreign particle surfaces (Anderson et al. 2010; Merle et al. 2015). This cascade involves a series of serine proteases that lead to cell lysis, the generation of anaphylatoxins and opsonization markers. The cleavage of C3 into C3a and C3b by C3 convertases is a pivotal part of this process (Anderson et al. 2010; Merle et al. 2015). This self-reinforcing response is negatively regulated by membrane-bound and soluble regulators, such as complement factor H (FH). FH is a soluble glycoprotein consisting of 20 complement control protein (CCP) domains that recognize self-structures in the form of glycosaminoglycans (GAG) as well as C3b (Barlow et al. 2008). FH regulates complement activation by acting as a cofactor for complement factor I (FI), destabilizing the C3bBb convertase, and competitively binding C3b, which cofactors FI for the hydrolysis of C3b to iC3b, and subsequently to C3dg and C3d (Zipfel et al. 1999; Pickering et al. 2008; Conrad et al.

1978). FH also undergoes conformational changes upon binding to C3b, which enhance its regulatory activity and promote its interaction with other complement regulators (Oppermann et al. 2006).

This complement cascade regulation by cleavage of C3b is limited to self but not to foreign surfaces (Kemper et al. 2003; Morgan et al. 2011). Structurally, the regulatory function on C3b in the fluid phase is mainly facilitated by FH CCP1-4, whereas the domains 19-20 are involved in GAG recognition and obstructing the thioester domain (TED) of C3d (Kajander et al. 2011; Wu et al. 2009; Morgan et al. 2011). Multiple mutations in the *CFH* gene have been associated with AMD (Fritsche et al. 2016; Yates et al. 2007). The pathology underlying *CFH* mutations such as the Y402H polymorphism in CCP 7 of *CFH*, where carriers have a 5.2-fold increased risk of developing AMD is still under investigation (Sofat et al. 2012; Klein et al. 2005).

Several studies aimed at replacing or substituting FH have been conducted with promising results (Biggs et al. 2022; Noris und Remuzzi 2008). Schmidt et al. previously reported the successful engineering of a size reduced FH in which domain sets 1-4 and 19-20 are linked by a poly-glycine linker, providing the flexibility to exert all regulatory functions and even enhancing the recognition of C3b degradation products by FH CCP 19-20 (Schmidt et al. 2013). This approach presented an upstream complement regulation that acts on cell surface and fluid phase C3 convertase and stops the amplification of the complement response while minimizing the potential negative effects of long-term inhibition of the complement system and the lack of its defensive functions (Schmidt et al. 2013).

In this study, we investigated the capabilities and limitations of two truncated versions of human FH in the murine ischemia/reperfusion model. During an ischemic event, inadequate vascular supply leads to nutrient and oxygen deprivation causing neurodegenerative damage in the retina. Ischemia and subsequent reperfusion result in inflammatory and oxidative stress, leading to microglial activation and degeneration of all retinal layers and the optic nerve (Razeghinejad et al. 2017; Renner et al. 2017; Wagner et al. 2017). This degenerative process is characterized by changes in the expression of cell-specific proteins, including complement components (Pauly et al. 2019).

The FH constructs were successfully delivered using adeno-associated viruses (AAV) and retain key functions necessary for host cell recognition and cofactor activity. We detected transgene activity primarily in gliotic Müller cells and to a lesser extent in astrocytes, with the level of expression correlating with the severity of the damage. The treatments resulted in reduced complement activation, faster stabilization of microglia, and structural improvements. Additionally, we observed lower levels of *C3* transcripts and C3d protein, along with increased expression of inhibitory regulators, indicated attenuated complement activity.

Results

Truncated FH Variants Retain Full Length FH Functions *in vitro*

We modified the miniFH regulator, originally developed by Schmidt et al., for expression in mice (Schmidt et al. 2013).This involved codon optimization and the addition of both a signal peptide and an epitope (myc) tag. MiniFH is derived from FH CCP1-4 and 19-20 domains of human FH. Replacement of the 14 middle domains with a poly-glycine linker provided structural advantages but eliminated some functions, notably the GAG recognition of CCP6-7 domains. The importance of the CCP7 domain, which contains the Y402 locus, was underscored by its recent identification as critical for the antiangiogenic functions of FH in a choroidal neovascularization model (Borras et al. 2020). Therefore, we introduced a second construct that combined the benefits of domain removal with the preservation of domains critical for tissue maintenance in AMD. Both truncated FH versions were within the loading capacity of an AAV. FH1-4^19-20 and FH1-7^19-20 were designed to exert important regulatory functions (Fig. 1A): CCP1-4 domains facilitated C3b binding and cofactor activity, whereas CCP5-7 and 19-20 domains ensured polyanion binding (Fig. 1A). The hypothesis was that these truncated FH variants mimic the regulatory functions of native FH by maintaining host cell recognition, competition for complement factor B (FB) binding sites on C3b (CCP1-4), and occlusion of the C3b TED (Fig. 1B).

Both variants were expressed using a mammalian expression system for the *in vitro* studies. FH1-4^19-20 and FH1-7^19-20 proteins were detected in cell lysates and supernatant of transfected HEK293 cells by Western blot and had the predicted sizes of 44 and 68 kDa, respectively (Fig. 1D). The control reporter protein, enhanced green fluorescent protein (EGFP) without signal peptide for secretion, was found mainly in cell lysates. This observation confirmed that the truncated FH proteins were actively secreted and not released by cell disruption (Fig. 1D). Evaluation both protein levels of the expressed truncated FH proteins compared with EGFP revealed that bicistronic mRNAs carrying the FH proteins and the EGFP reporter signal exhibited reduced expression under internal ribosome entry site (IRES) translational control than the single cistron in the EGFP control vector (Fig. 1D, Fig. S1).

Previously, miniFH variants were reported to effectively inhibit human C3b deposition on cell surfaces, suggesting that they modulate the complement pathway (Schmidt et al. 2013). Our matched FH1-4^19-20 and FH1-7^19-20 variants mirrored the dose-dependent abilities of the reference miniFH to prevent complement accumulation in mice, as evidenced by the reduction in C3b deposition from mouse serum on a lipopolysaccharide-coated surface (Fig. 1E).

CCP7, which has previously found to bind GAG (Clark et al. 2010), led to the expectation that FH1-7^19-20 would have an enhanced ability to recognize cell

surfaces through GAG binding. This assumption was confirmed by heparin-binding ELISA (Fig. 1F), in which FH1-7^19-20 showed the highest affinity for heparin among all FH variants. In contrast, FH1-4^19-20 did not showed any detectable interactions in this context (Fig. 1F). Because the structure of the peptide is identical to that of the reference miniFH, with the exception of an epitope tag at the C-terminus, this lack of interaction was likely due to an obstruction in the CCP20 GAG-binding domain.
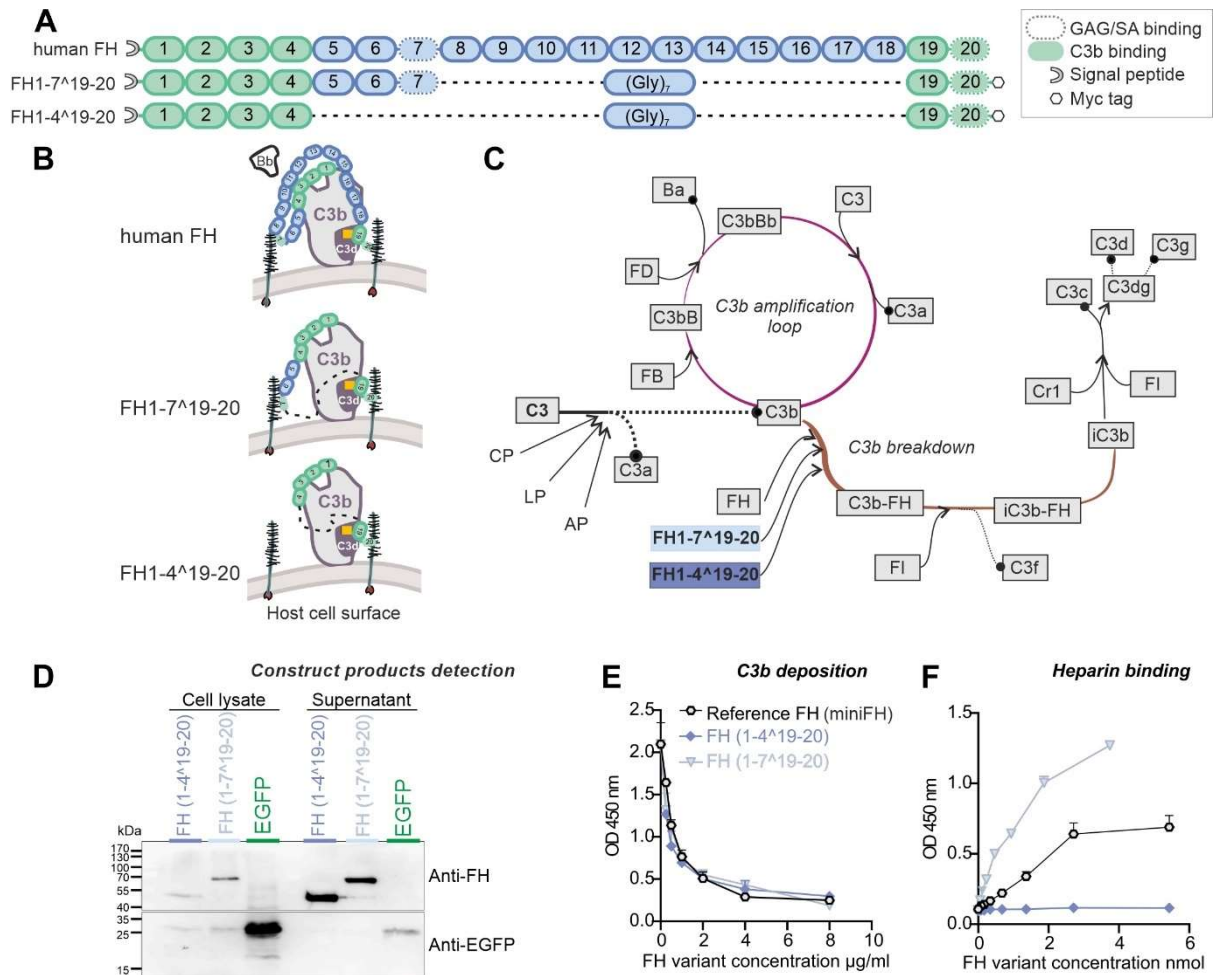

Figure 1: Illustration of FH variant structures, mechanisms of FH in the complement regulation and *in vitro* efficacy evaluation. GAG: Glycosaminoglycans, SA: Salicylic acid, FH: Factor H, FI: Factor I, FD: Factor D, Cr1: Complement C3b/C4b Receptor 1, CP: Classical Pathway, AP: Alternative Pathway, LP: Lectin Pathway

A Structural comparison between truncated FH proteins and native human FH. FH1-4^19-20 consisted of CCP1-4 and 19-20 domains, while FH1-7^19-20 contained additional CCP5-7 domains. Both variants are labeled with an epitope (myc) tag.

B Illustration of the theoretical mechanisms by which FH protects the host cell surface.

C Outline of the complement regulation by FH, modeled after (Dreismann et al. 2021). FH is involved in the degradation of C3b by accelerating the decay of the C3bBb convertase and acting as a cofactor for FI.

D FH1-4^19-20 and FH1-7^19-20 were expressed and secreted by HEK293 cells. Both truncated FH variants were found with their predicted size in Western Blot. EGFP was predominantly detected in cell lysates, corroborating that the FH1-4^19-20 and FH1-7^19-20 proteins were secreted and not released due to cell ruptures.

E Reduced deposition of C3b to lipopolysaccharide-coated microtiter plates was observed after addition of different truncated FH variants to mouse serum.

F GAG binding as assessment revealed that FH1-7^19-20 had the highest affinity for immobilized heparin. Compared to the FH1-7^19-20, reference miniFH of Schmidt et al. 2013 exhibited lower binding affinity. FH1-4^19-20 displayed no interactions, likely due to an epitope tag-induced blockade in the CCP20 GAG-binding domain.

Expression system is Müller cell specific and GFAP dependent

After demonstrating that the recombinant FH variants retained most of the full-length functions of FH, with the exception of GAG binding of FH1-4^19-20 (Fig. 1), we tested the influence of the constructs *in vivo* using the acute ischemia/reperfusion retinal mouse model (Pauly et al. 2019) (Fig. 2A).

To protect retinal neurons from transgene expression and focus the response on the risk of impending of retinal degeneration, we targeted the expression of the secreted factors to Müller cells. This was achieved by the AAVs enveloped by the Müller cell specific ShH10-AAV capsid, with expression linked to Müller cell gliosis via an optimized version of the human glial fibrillary acidic protein (GFAP) promoter (Klimczak et al. 2009). After ischemia induction, AAVs were injected intravitreally to access Müller cell end feed adjacent to the vitreous, which form the inner blood retinal barrier (Fig. 2A). Retinal samples were collected 3- and 14-days post ischemia (dpi), and retinal cell types were separated by magnetic-activated cell sorting (MACS).

The increased expression of GFAP in control eyes is likely due to transient gliotic response induced by intravitreal AAV injection (Seitz et al. 2013). Both Müller cells and microglia in mouse eyes respond throughout the retina after such injection (Seitz und Tamm 2014). Confirming the cell type specificity of our expression cassettes, we only observed cells with Müller cell morphology as positive for the EGFP reporter in immunostainings (Fig. 2B, C). In retinal flatmounts collected at 14 dpi, we mostly observed GFAP signal in astrocytes of the GCL and colocalization of EGFP signal only with the Müller cell marker glutamine synthetase (GLUL) (Fig. 2C). As exemplary in the ischemic FH1-4^19-20 flatmount pictures, but also occurring in some sagittal tissue sections, we observed only weak EGFP signals for some AAV injected animals, likely due to difficulties in the application experienced before (Fig. 2C) (REF!).

We analyzed the effects of AAVs carrying the truncated FH variants on ischemia/reperfusion hallmarks in purified Müller cells by qPCR. A previously reported decrease in *Glul* levels after ischemia/reperfusion was reproduced in the present study (data not shown). However, we observed no detectable treatment effect of AAVs on this Müller cell marker (Fig. 2D) (Nishiyama et al. 2000; Wagner et al. 2017).

As a marker of Müller cell gliosis, *Gfap* levels increased at 3 dpi and decreased significantly 14 days after injection of AAV_EGFP-control vector (P-value = 0.0218, fold change -2.5369) (Fig. 2D. After injection of AAV_FH1-4^19-20 or AAV_FH1-7^19-20, there were no significant shifts in *Gfap* expression between 3 and 14 dpi. However, a slight trend suggestive of reduced *Gfap*-upregulation at 3 dpi (P-value = 0.0536) was observed in Müller cells from ischemic retinas treated with FH variants compared to those treated with EGFP alone, an effect that diminished at 14 dpi (Fig. 2D).This could be a hint of reduced gliosis and might indicate that the treatment is effective in mitigating the cellular response to the injury.

Furthermore, analysis of *EGFP* and *Gfap* transcript levels at 14 dpi revealed a significant relationship between *Gfap* dCT and *EGFP* dCT values of AAV_EGFP (P-value = 0.0016), AAV_FH1-4^19-20 (P-value = 0.0085) and AAV_FH1-7^19-20 (P-value = 0.0034) (Fig. 2D). This suggests that expression of the transgenes is indeed coupled to that of *Gfap*. Finally, GFAP concentrations determined from immunostainings intensity scores did not differ significantly between treatments or time points (Fig. 2F).
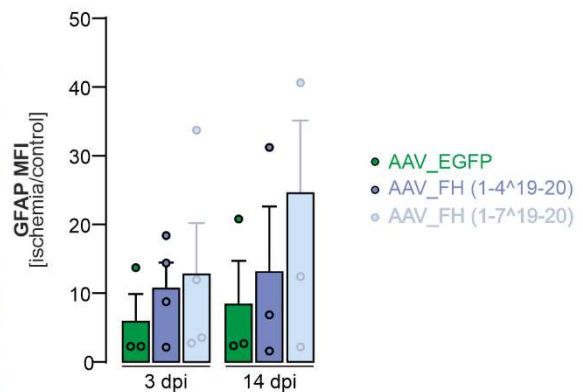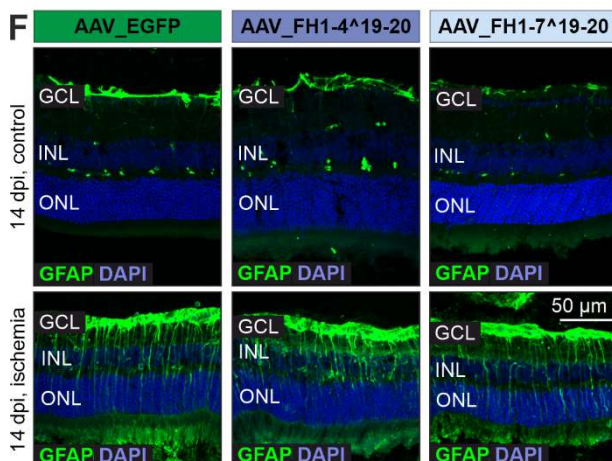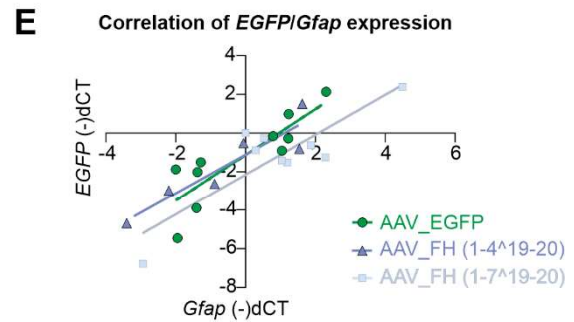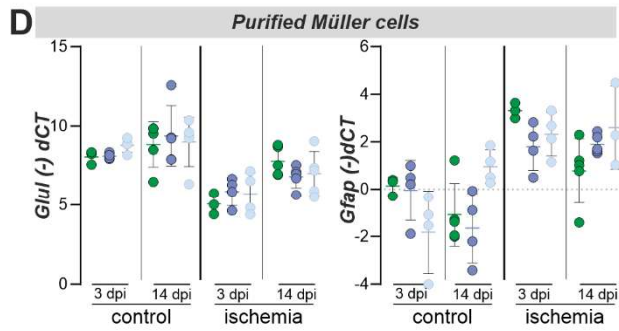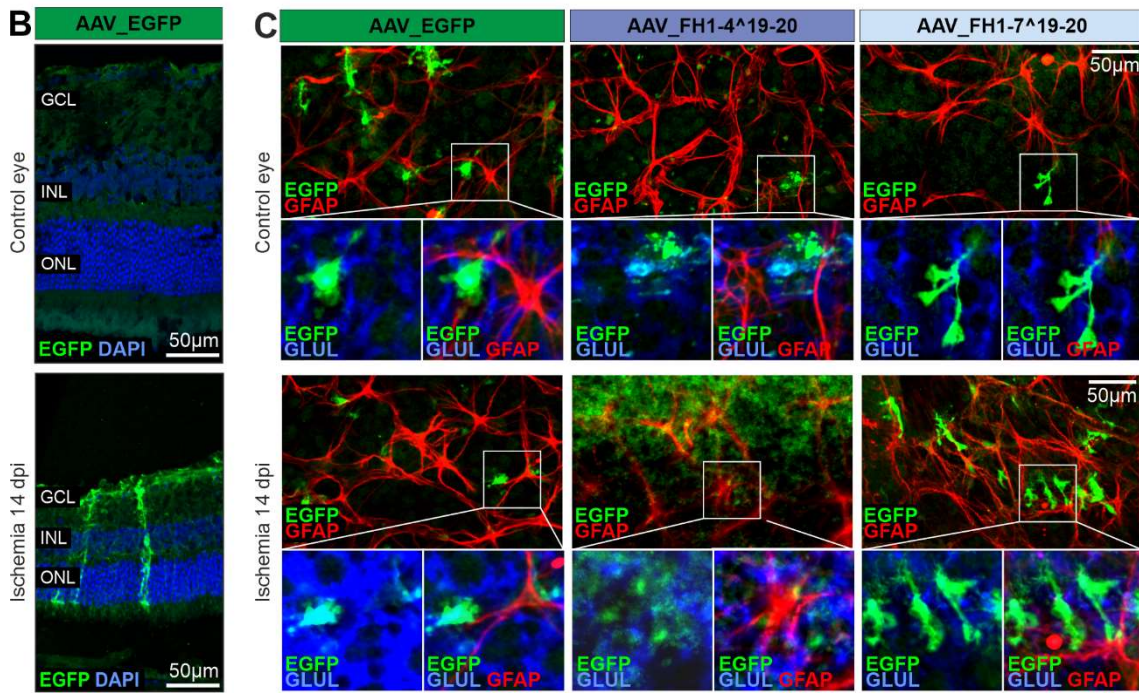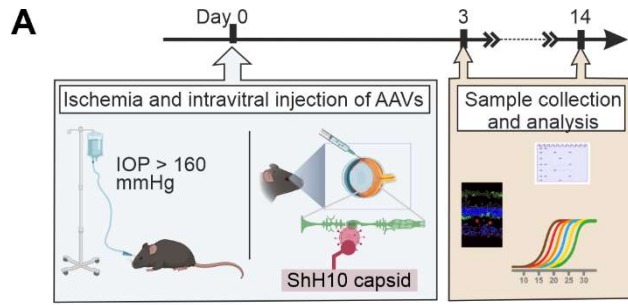
Figure 2: Effectiveness of the expression cassette with regard to coupling to GFAP transcription and Müller cell specificity in vivo.

A Experimental set up for *in vivo* studies: eyes of C57BL/6J wildtype mice were exposed to hypoxic conditions by elevated intraocular pressure (IOP), resulting in ischemic tissue responses. Subsequently, AAV vectors carrying expression cassettes for regulatory truncated FH variants and an EGFP-only control were injected. Tissue samples were collected for evaluation at intervals of 3 and 14 days post injections (dpi).

B Cryosections of the central retina showed that EGFP was exclusively present in Müller cells identifiable by their unique morphology spanning the whole tissue from the ganglion cell layer (GCL) to the outer border of the outer nuclear layer (ONL). This indicated a cell type-specific expression of the AAV construct confined to Müller cells.

C Immunohistochemistry (IHC) analysis of retinal flat mounts at 14 dpi at the level of the nerve fiber layer after ischemic injury and AAV application was performed to assess whether also astrocytes, that even in the healthy retina express high levels of GFAP, were transduced by the AAV. EGFP-positive cells co-expressed the Müller cell marker glutamine synthetase (Glul), but not high levels of GFAP. In contrast, highly GFAP-positive astrocytes were not highlighted by EGFP-labeling.

D Quantitative real-time PCR of isolated Müller cells showed a decrease in *Glul* expression in ischemic Müller cells at 3 dpi (left panel). This reduction attenuated by 14 dpi. In contrast, *Gfap* expression increased by 3 dpi and remained elevated until 14 dpi (right panel).

E *EGFP* expression levels showed correlation to Gfap expression in all three treatment groups as determined by qPCR (14 dpi). Pearson's correlation coefficients of *Gfap* (-)dCT vs *EGFP* (-)dCT were as follows: ρ(AAV_EGFP) = 0.8561, ρ(AAV_FH1-4^19-20) = 0.8561 and ρ(AAV_FH1-7^19-20)= 0.8534.

F Representative microscopic images showing GFAP immunostaining on sections at 14 dpi (left panel). Quantitative analysis of mean fluorescence intensity encompassing the retina from the outer limiting membrane to the inner plexiform layer (right panel). The ganglion and nerve fiber layers were excluded from the analysis to eliminate signals from astrocytic GFAP expression.

Microglia in ischemic retinas exhibited positive staining after treatment with AAV_FHs

In the early phase of the observation period, specifically at 3 dpi, FH variant transcripts were detectable only in trace amounts in the Müller cell fraction of both ischemic and control eyes (Fig. 3A). However, after 14 dpi, mRNA levels of FH variants were increased in Müller cells, indicating not only robust expression but also interanimal variability (Fig. 3A).

Following the ischemic injury, there was pronounced activation of microglia that spread through the whole retina (Fig. 3B). Interestingly, immunoreactivity with an antibody against FH was observed in retinas treated with AAV_FH1-4^19-20 and AAV_FH1-7^19-20 (Fig. 3B). It is important to note that although this antibody can also identify mouse FH, no microglia-specific staining was seen in eyes injected with the AAV_EGFP control. The microglia-specific FH signal was also evident at 14 dpi. Of note, blood vessels were also stained, likely due to nonspecific binding of secondary

antibody to endogenous mouse IgG, a phenomenon also observed in control staining with secondary antibody (Figure S3).
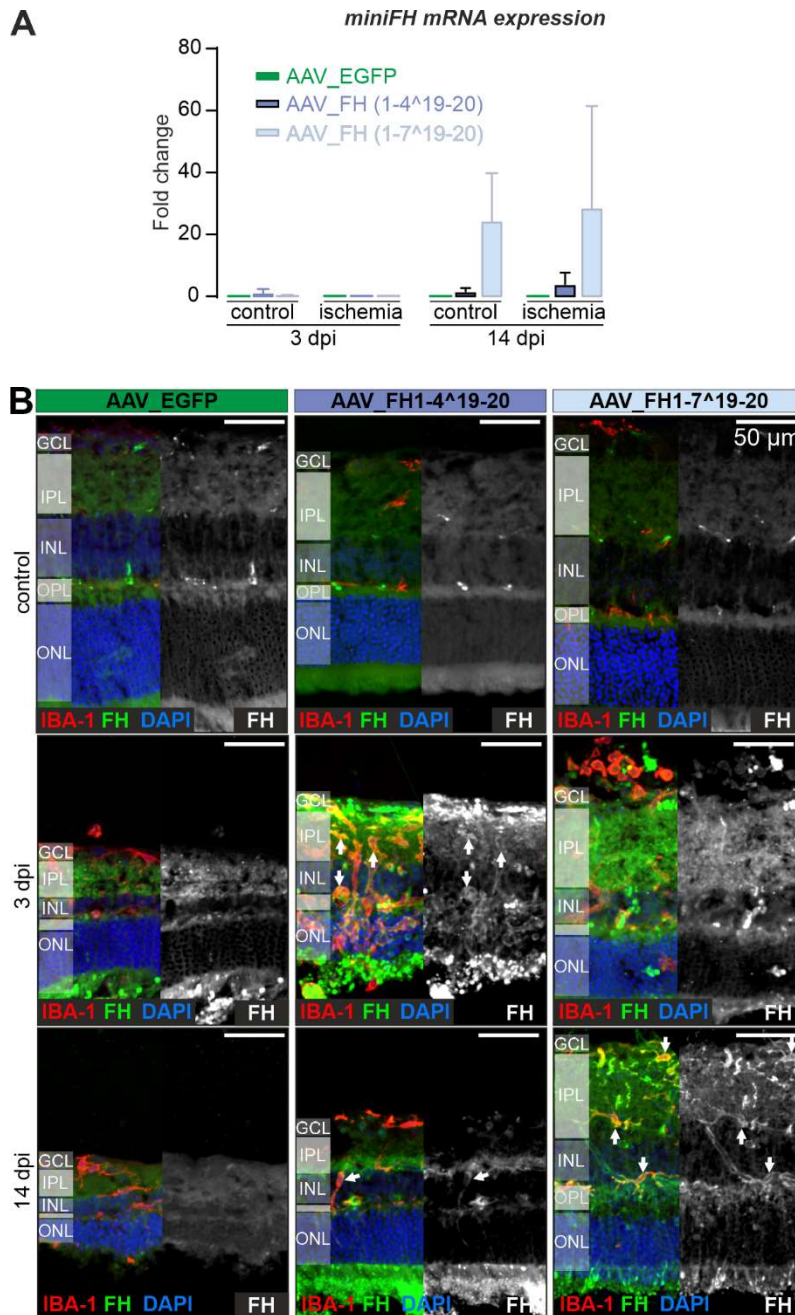
Figure 3: Expression of native and transgenic FH variants at transcript and protein levels.

A At 3 dpi, expression levels of regulatory FH variants were barely detectable in the Müller cell fraction. After 14 days, a strong expression of both FH1-4^19-20 and FH1-7^19-20 variants was observed. (n = 4 – 5)

B: IHC results from cryosections of control and postischemic retinae after AAV treatment delineating FH deposition and the localization of microglia/macrophages by a labeling for IBA-1, FH, factor H. Scale bar, 50 μm.

FH variants attenuate tissue damage in retinal ischemia/reperfusion model

Three days after the ischemic injury, TUNNEL staining showed apoptosis and/or necrosis in 10 to 25% of cells in the outer (ONL) and inner nuclear layer (INL), up to 60% in one case, and in approximately 18% of the cells of the ganglion cell layer (GCL) (Fig. 4A, B). After 14 dpi, these numbers decreased to less than 1% for ONL and INL and ranged from 2 to 4% for GCL cells. Despite notable differences, AAV_FH1-4^19-20 and AAV_FH1-7^19-20 treatments showed no statistically significant effect (Fig. 4B).

The ischemic episode resulted in severe disruption of retinal architecture and substantial decrease in cell nuclei in all cell layers: approximately 50% in the GCL and between 50 to 60% in the INL and ONL (Fig. 4A, B). This degeneration appeared to increase after the 3 dpi, as shown by greater losses at 14 dpi (Fig. 4D).

The increased apoptosis/necrosis rates at 3 dpi indicate a drastic loss of cells in determined samples up to 14 dpi. This loss was particularly pronounced in the ONL of the AAV_EGFP-injected group (P-value = 0.040, fold change 0.53) (Fig. 4D), with inner plexiform layer (IPL) thickness also showing a significant decrease (P-value = 0.0322, fold change 1,74) (Fig. 4C). The retinal structure of this group continued to deteriorate, with the thickness of the outer plexiform layer (OPL) decreasing to one-third of its value at 3 dpi by 14 dpi (P-value = 0.0311, fold change 0.31) (Fig. 4C). At the same time the INL showed a trend towards a reduction (P-value = 0.0708, fold change 0.58) (Fig. 4D).

Despite the emerging trends, the AAV_FH1-4^19-20 and AAV_FH1-4^19-20 treatments failed, on average, to significantly preserve the number of nuclei in GCL, INL, or ONL, or the thickness of IPL or OPL at 14 dpi compared to baseline labels at 3 dpi (Fig. 4D, C).

In contrast to the AAV_EGFP treated samples, the AAV_FH1-7^19-20 injected animals showed significant improvement in cell survival and retinal integrity (Fig. 4). After 14 dpi, the INL of the AAV_FH1-7^19-20 cohort contained 1.8 times more nuclei compared to the AAV_EGFP counterparts (P-value = 0.013, fold change 1.82) (Fig. 4D), which was also reflected in the improved INL thickness (P-value = 0.0299, fold change 1.72) (Fig. 4C). Animals treated with AAV_FH1-4^19-20 showed trends indicating similar improvements, although these differences were not statistically significant.

Amacrine and ganglion cells have previously been identified as particularly susceptible to retinal ischemia, with a 30% decrease in some rat models (Lee et al. 2011). in our study, we found a clear separation of three dendritic layers of calretinin-positive cells in the IPL, with calretinin-positive amacrine cell bodies in the INL and ganglion cells in the GCL (Fig. 4A, E). After 3 dpi, ischemia resulted in a loss of approximately 60% of ganglion and amacrine cells. Although some animals in the AAV_FH treatment groups had considerably higher cell survival, the treatments did not result in statistically significant improvement overall.
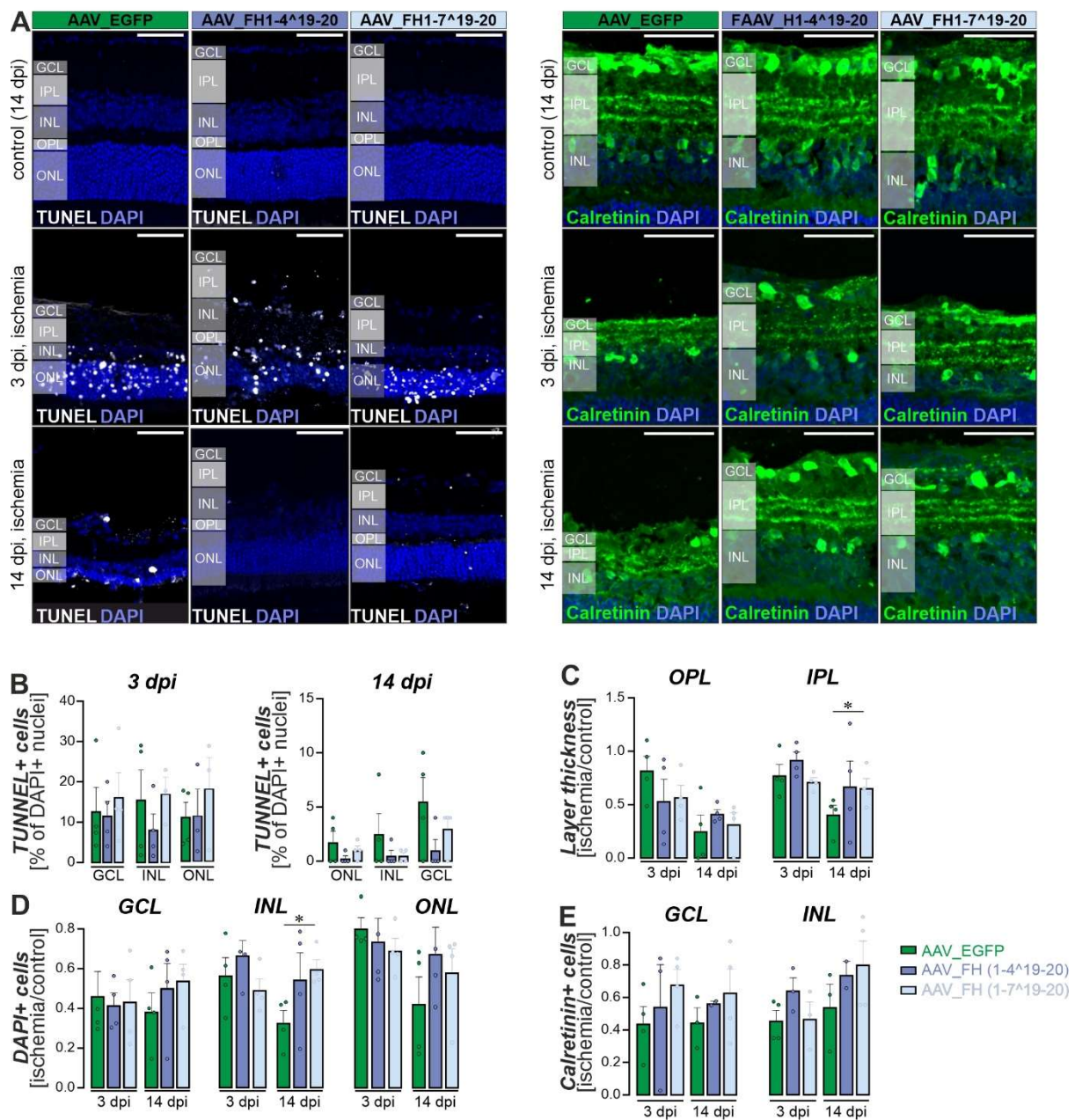
Figure 4: Characterization of neuronal survival in the ischemia/reperfusion model following treatment with AAV_EGFP, AAV_FH1-4^19-20 and AAV_FH1-7^19-20. (n = 3-6)

A Cryosections from the central retina revealed TUNEL-positive apoptotic/necrotic cells (left panel) and calretinin-positive amacrine and ganglion cells (right panel) in both non-ischemic control and ischemic eyes treated with AAVs.

B Quantification of nuclei within the ganglion cell layer (GCL), the inner nuclear layer (INL) and the outer nuclear layer (ONL) per scan field. Data were normalized to non-ischemic control eyes of the corresponding animals (Student's t-test).

C Evaluation of the inner plexiform layer (IPL) and the outer plexiform layer (OPL) thickness to assess the integrity of the synaptic connections representing neuronal processes. Values were normalized to non-ischemic control eyes of the corresponding animals (Student's t-test).

D Quantitative analysis of the percentage of TUNEL-positive cells in each retinal layer and treatment at 3 and 14 dpi.

E To examine cell-specific neuronal loss in more detail, particularly given the susceptibility of inner retinal neurons to ischemia/reperfusion, we quantified calretinin-positive cells. Calretinin labels ganglion cells and displaced amacrine cells in the GCL and amacrine cells in the INL (Student's t-test).

AAV_FH treatments modulate the pre- and postischemic complement transcriptome

Comparison of control eyes treated with AAV_EGFP, AAV_FH1-4^19-20 and AAV_FH1-7^19-20 with their ischemic counterparts revealed marked differences in complement expression. These differences reflect the distinct ischemia-associated immunological phenotype previously described (Pauly et al. 2019). Increased *C3* mRNA levels were observed in purified Müller cells of all ischemic treatment groups at 14 dpi and to some extent in the neuronal fraction at 3 dpi compared with their non-ischemic counterparts (Fig. 5, Table S3) The complement activating factors *Cfb* and *Cfd* showed increased expression in ischemic eyes in all treatment groups, although differences manifested in different cell fractions and time points (Fig. 5, Table S1&S2). Of note, innate murine *Cfh* was consistently downregulated after ischemia, regardless of whether the animals received AAV_FH-treatment. In contrast, its cofactor *Cfi* increased specifically in neurons at 3 dpi (Fig. 5, Table S3). Following ischemia, stabilizer of the alternative pathway C3 convertase *Cfp* was downregulated in Müller cells but upregulated in Microglia as observed before (Fig. 5, Table S3) (Pauly et al. 2019).

To identify the specific effects of AAV_FH gene addition therapy, we compared the expression levels of complement components in Müller cells, microglia and neurons from ischemic eyes with those receiving the AAV_EGFP control virus.

Interestingly, for the AAV_FH1-7^19-20 variant treatment, differences in complement expression compared to the AAV_EGFP control were already found between control eyes (Fig. 5). This effect leaned towards complement downregulation, with lower transcript levels of complement activators and higher levels of regulators (Fig. 5). For instance, activators *Cfb* and *Cfd* were less expressed in neurons (fold change -1,2 and -3,3 respectively) and more *Cfh* transcripts were found in microglia (Fig. 5). On the other hand, Müller cells of control eyes expressed higher levels of the central complement component *C3* (fold change 1,9) after treatment with AAV_FH1-7^19-20. This was interesting, since C3 was down regulated three days after ischemia in microglia (fold change -1,2) and neurons (fold change -2,8). Post-ischemic neurons treated with this construct showed less *Cfh* transcripts 3dpi (fold change -2,3), which flipped to an upregulation 14 dpi (fold change 1,4). Similar to *Cfh,* the C3b protease Cfi was also downregulated 3 days after ischemia when treated with AAV_FH1-7^19-20 (fold change -1,3).

For AAV_FH1-4^19-20 treatment only as slight upregulation of *Cfi* 14 days after ischemia was observed (fold change 1,3).

Transcript levels of the terminal pathway components *C9* and *C5* were also assessed. However, as demonstrated recently (Pauly et al. 2019) these transcripts were mostly out of assay range and no valid comparison could be made (data not shown).
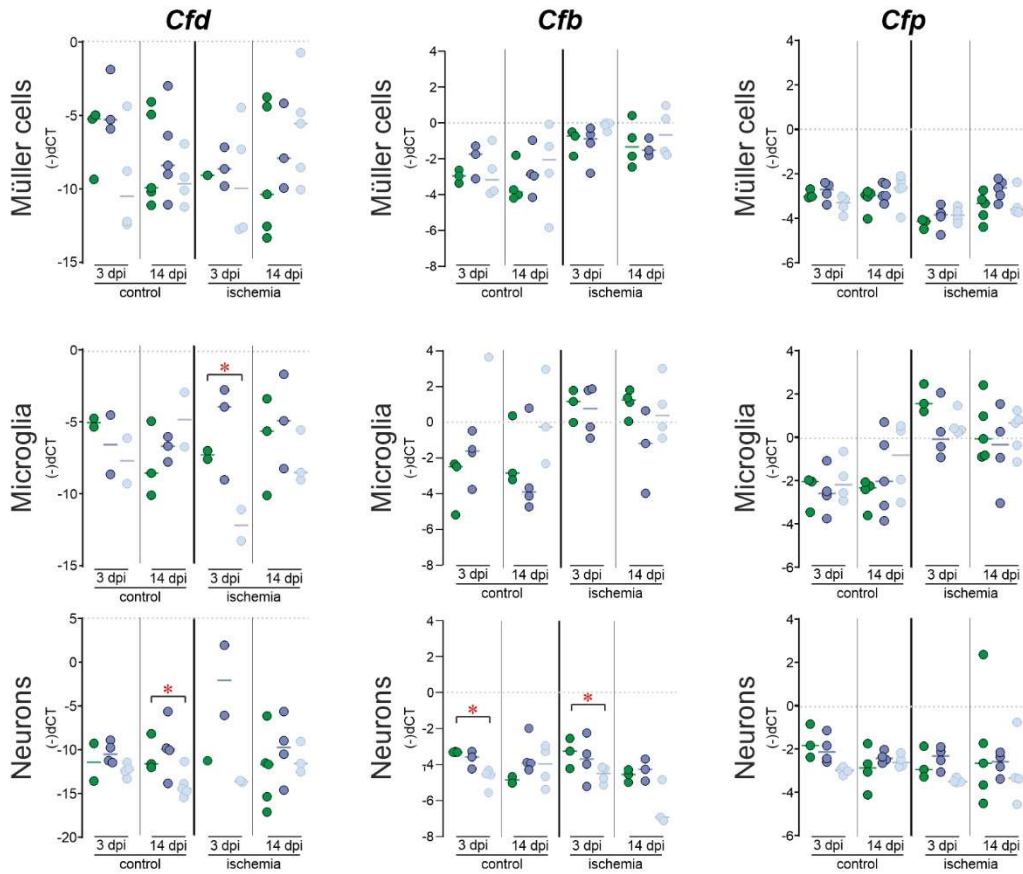
Post-ischemic retinae treated with AAV_FH constructs showed less C3 turnover and complement activation
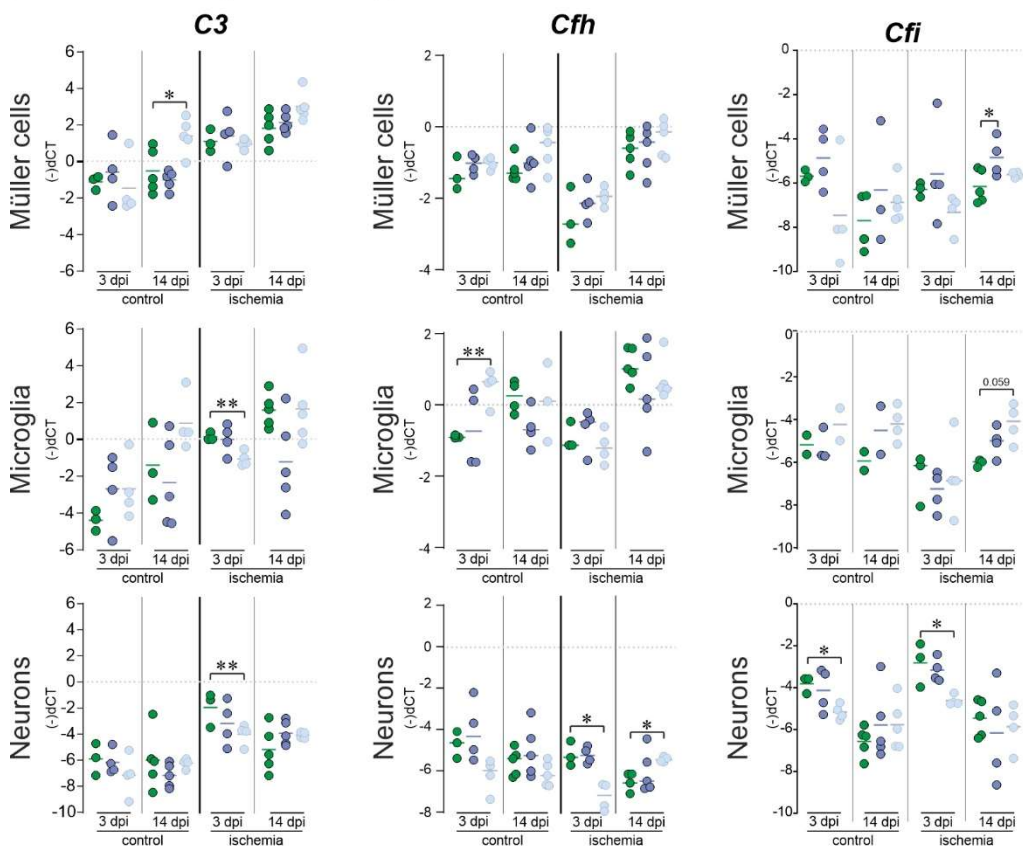
FH exerts a dual regulatory effect on the central complement factor C3, as shown in Figure 1 and 6A. First, it accelerates the decay of the C3-convertase, leading to the displacement of FB and arresting the cleavage of C3 cleavage into C3b. Second, FH serves as a cofactor for FI and facilitates the conversion of C3b into its inactive cleavage fragments: iC3b, C3dg, and C3d (Fig. 6A). After ischemia/reperfusion, a change in the C3 cleavage pattern was observed compared with control retinas. This pattern was modulated by gene addition therapy with the truncated FH variants AAV_FH1-4^19-20 and AAV_FH1-7^19-20 (Fig. 6B). Ischemic retinas had lower levels of intact, uncleaved C3 protein compared with control retinas (Fig. 6C), suggesting that consumption of full-length C3 is related to complement activation. Nevertheless, the level activated C3b remained the same in both retina models (Fig. 6D, E). A characteristic feature of the ischemic retinas was the increased ratio of C3b to C3 compared with untreated retinas (Fig. 6E) This was highlighted by a markedly increased amount of C3b/C3 fragments in AAV_EGFP-treated ischemic retinas compared with AAV_EGFP-treated control retinas, indicating complement activation in the ischemic retinas. In contrast, C3b/C3 levels in AAV_FH treated eyes of ischemic retinas were closer to those of control retinas (Fig. 6E). These observations suggest that complement activation in the ischemic retinas was attenuated by increased cofactor activity of the truncated FH variants AAV_FH1-4^19-20 and AAV_FH1-7^19-20, promoting the degradation and elimination of C3b fragments (Fig. 6F-H).

The peak concentration of iC3b, C3d and C3d was detected in the ischemic retinas treated with the AAV_EGFP control vector (Fig. 6F-H). In contrast, ischemic retinas treated with vectors expressing FH1-4^19-20 and FH1-7^19-20 had iC3b, C3dg, and C3d levels similar to those of non-ischemic retinas and lower than in the ischemic AAV_EGFP control vector treated retinas. These results emphasize that both the decay acceleration function and the cofactor activity of the truncated FH derivates were functional in this model of retinal degeneration.

Immunolabeling of C3 showed co-localization with the Müller cell marker glutamine synthetase within the GCL. Quantitative intensity assessments showed that ischemic eyes had up to 20-fold higher levels than in their non-ischemic counterparts.

Remarkable, treatment with AAV_FH1-4^19-20 showed the most marked reduction at 3 dpi, with intensity scores approximately four times lower than AAV_EGFP controls (Fig. 6I). Compared with intensity values at 3 dpi, the AAV_FH1-4^19-20 treatment showed an increase by day 14 dpi. Conversely, a decrease was observed in the AAV_FH1-7^19-20 treatment group during the same period.
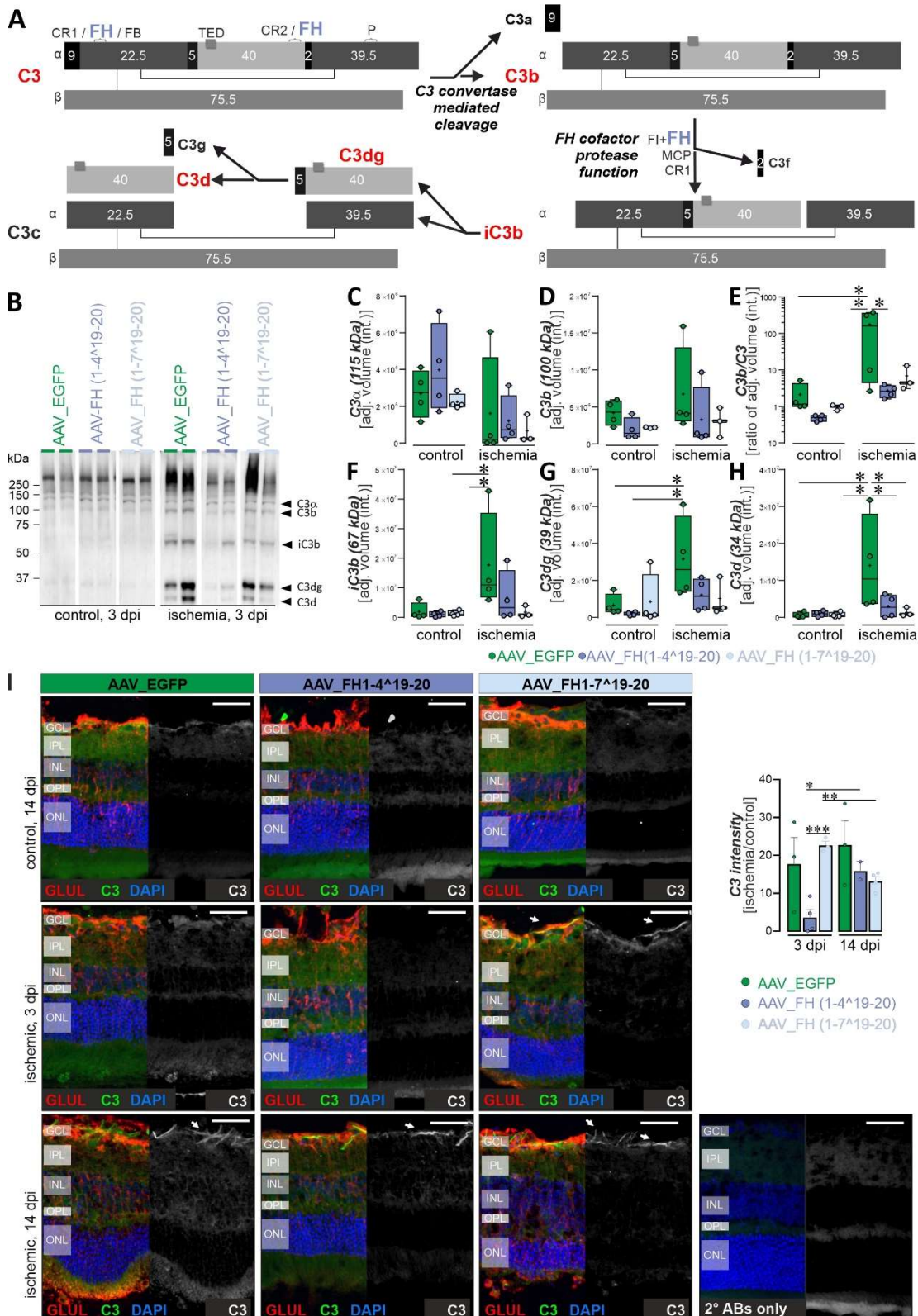
Figure 6: Quantitative analysis revealed that truncated FH variants modulate C3 fragmentation in the ischemic retina.

A Schematic representation of C3 cleavage. Numerical data indicate peptide sizes in kilodalton (kDa). The binding sites for complement receptors 1 and 2 (CR1 / CR2), FH, and factor B (FB) are highlighted. The alpha and beta chains of C3 are linked by the MG6 domains. C3 convertase cleaves C3 into C3b and C3a. With MCP, CR1 and FH as cofactors cleaves FI C3b into iC3b and C3f. Subsequent cleavage of iC3b by FI leads to C3c and C3dg, the latter being further converted to C3d. Modeled after (Łukawska et al. 2018)

B Representative Western blot of AAV treated retinas containing 70 µg total protein. Detection was performed by using a polyclonal antibody specific for C3d.

C-H Quantitative analysis of Western blot band intensities normalized to total protein loading. Boxplots represent median, quartiles and mean (indicated by a dot) without outliers. The mean of each data set was compared with the AAV_EGFP ischemia data using Dunnett's test for multiple comparisons. A significance level is indicated by $*p < 0.05$.

I Immunolabeling with an antibody against C3d (labelling C3, C3b, iC3b, C3dg and C3d) showed co-staining with the Müller cell marker glutamine synthetase (GLUL) in the GCL of the ischemic retina. Application of AAV_FH1-4^19-20 reduced C3 intensity at 3 dpi compared with AAV_EGFP, whereas treatment with AAV_FH1-7^19-20 resulted in a reduction after 14 dpi.

.

Microglial/macrophage reactivity decreased after AAV_FH supplementation

The expression of as ionized calcium-binding adapter molecule 1 (*Iba-1*) also known allograft inflammatory factor 1 (*Aif-1*) in immunoreactive microglia/macrophages in increased sharply and peaks approximately 3 days after ischemic injury before decreasing after 7 days (Ito et al. 2001). Our study showed that 14 dpi, the mRNA levels of *Iba-1* were significantly lower in AAV_FH1-4^19-20 treated animals compared with the AAV_EGFP control (Fig. 7A).

In the ischemic retina, we observed increased numbers of IBA1-positive cells in all retinal layers compared with the non-ischemic control. By 14 dpi, these numbers converged to the non-ischemic level. Interestingly, the number of IBA-1-positive cells in AAV_FH1-4^19-20 treated eyes was 1.5-fold higher in the GCL than in the corresponding AAV_EGFP control at 3 dpi (Fig. 7B).

CD68 serves as an additional marker for microglial/macrophage activity. The Intensity of this lysosomal protein was significantly increased in ischemic eyes, as shown by immunostainings (Fig. 7C). By 3 dpi, this intensity had decreased in both AAV_FH treatments compared with the AAV_EGFP control. In the AAV_FH1-4^19-20 group, intensity returned to the level of the non-ischemic control by day 14. However, CD68 intensity in the AAV_FH1-7^19-20 group remained elevated and was not significantly different from AAV_EGFP levels after 14 days (Fig. 7C).
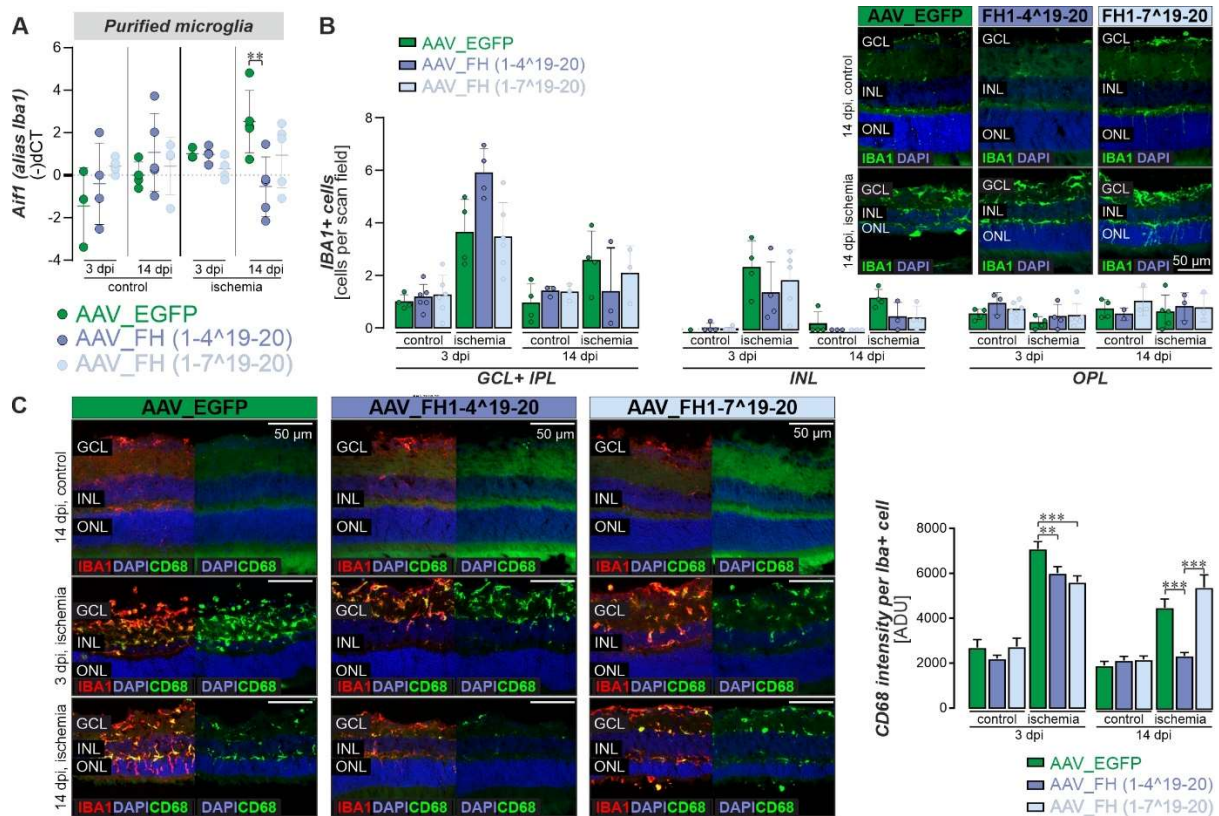
Figure 7: Microglia response to AAV_FH treatments following ischemia

A The expression of *Iba-1* mRNA in control and ischemic retinas after AAV treatment was determined by qPCR. At 14 dpi, *Iba-1* levels were lower in AAV_FH1-4^19-20 treated retinas compared with AAV_EGFP ischemic controls (Student's t-test).

B Quantification of IBA-1-positive microglia/macrophages was performed in the respective retinal layers to detect cellular migration in response to the tissue damage, mainly affecting the inner retina (left panels, analyzed with Student's t-test). Representative microscopic images of IBA-1 immunostaining on retinal sections at 14 dpi (right panel).

C Representative microscopic images of IBA-1 and CD68 co-immunostaining on retinal sections at 14 dpi (left panel). Mean fluorescence intensities of CD68, a lysosomal marker upregulated in activated microglia/macrophages, were measured in IBA+ cells (analyzed with Student's t-test).

Discussion

In this study, we elucidated the complement regulatory potential of truncated variants of human FH in an ischemic/reperfusion model in the murine retina. Mukay et. al highlighted the importance of the complement system also in maintaining retinal health during aging (Mukai et al. 2018). They pointed to detectable retinal thinning and reduced electroretinogram amplitudes in several complement knockout strains, including C3$^{-/-}$. Proper complement regulation by Cfh has also been investigated in several knockout studies, where *Cfh* was found to be central for retinal development and prevention of AMD-like pathologies (Sivapathasuntharam et al. 2019). Retinal

delayed retinal development was delayed, but, while the retina appeared ultimately morphologically normal, photoreceptor and RPE cells of *Cfh*^{-/-} retinas in mice showed mitochondrial dysfunction(Sivapathasuntharam et al. 2019). Importantly, Cfh^{-/-} mice developed an AMD-like phenotype with increasing age, which could be rescued by the addition of full-length human *CFH* (Ding et al. 2015).

Here, key functional domains of the human complement regulator FH, in particular either CCP1-4^19-20 or CCP1-7^19-20, have been synthesized to develop compact but efficient complement regulators that can be encapsulated into an AAV vector. By integrating a glia-specific promoter and using an AAV capsid with a preference for Müller cells (Klimczak et al. 2009), we were able to target the synthesis and subsequent release of these complement regulators predominantly to Müller glia.

Our results showed that several key properties of FH1-4^19-20, as described by Schmidt et al. (Schmidt et al. 2013), and the novel FH1-7^19-20 variant were conserved. This occurred despite the change in expression system from yeast to mammalian cells, despite codon optimization, and despite the incorporation of a signal peptide and an epitope tag. Importantly, both variants retained one of the major functions of FH, which is primarily determined by the CCP1-4 domains: inhibition of FB binding to C3b, resulting in accelerated C3 convertase-mediated decay. This observation is consistent with the results of other published miniFH variants (Schmidt et al. 2013). A pivotal deviation was observed in heparin binding after purification of FH1-4^19-20 from HEK293 cell supernatant. Because protein domains 19 and 20 of FH are central to GAG binding, the added c-terminal myc-tag may have potentially affected these domains. Interestingly, the FH1-7^19-20 variant exhibited a better heparin binding ability compared with FH1-4^19-20. The inclusion of the GAG-binding domain 7 in FH1-7^19-20 appeared to counteract the decreased performance of domains 19-20.

In addition, the AAV vector system was confirmed to be effective, with expression occurring exclusively in Müller cells. Intravitreal injections resulted in unambiguous EGFP detection in Müller cells, which was consistent with the observed GFAP levels. By using the truncated *Gfap* promoter, expression of the added, complement regulator could be strategically linked to Müller cell gliosis. Müller cells span the whole retina and their status as one of the most prolific secretors among all retinal cell types highlights the critical role they play. These cells not only support the neurons of the retina, but also strengthen the cells of the retinal pigment epithelium, and their secretions are even detectable in the vitreous. The linkage of the AAV transcript expression and the Müller cell gliosis associated *Gfap* promotor is likely to attenuate sustained inhibition of homeostatic complement functions. Morphometric analysis revealed a strong degeneration in the ischemic eye compared to the sham injected contralateral eye. All retinal layers suffered severe cell loss, retinal thickness was reduced, and microglia became active. Some treatment effects were also detected, despite high variability in the ischemia pathology within treatment groups. FH1-7^19-20 had a positive effect on the survival of INL cells that led to higher nuclei numbers and INL thickness. We also detected a clear microglia activation after ischemia,

compared to non-ischemic control with elevated CD68 levels. Microglia in FH1-4^19-20 mice had control levels of CD68 14 days after ischemia.

After establishing and validating our AAV_FH overexpression system, we investigated how this treatment approach affected the transcript levels of key endogenously expressed complement components. *C3* was less upregulated in microglia and neurons of the ischemic retina at 3 dpi when treated with the FH variants compared to EGFP controls, with FH1-7^19-20 showing the most significant effects. This could be due to a reduced demand for C3 as C3 convertases are inactivated by FH or by increased C3-fragment deposition, due to enhanced FH/FI mediated decay. This is supported by the higher C3b/C3 fragment detection in FH-treated retinas as detected via western blot. The increased expression of *Cfi* transcripts in Müller cells and microglia, combined with a less pronounced upregulation of *C3* in the injured retina after FH treatment, and the overall downregulation of endogenous *Cfh* transcripts support the concept of our treatment approach that exogenous FH could modulate the local complement expression.

Importantly, both truncated FH variants had a clear impact on the retinal complement homeostasis at functional level - their overexpression in Müller cells in the ischemic retina was sufficient to lower C3b/C3 protein ratios and the accumulation of C3d. Both findings suggest a reduced pro-inflammatiory complement activity as the turnover of C3b to iC3b and downstream short-lived C3 fragments including i3Cb and C3d (Heesterbeek et al. 2020; Dauchel et al. 1993) was enhanced. This also implies that overexpression of FH variants enhanced FI-mediated C3b degradation. Since we previously reported a downregulation of retinal *Cfh* mRNA after ischemia, our present results suggest that FH acts as a limiting factor for beneficial FI-mediated C3b degradation (Pauly et al. 2019).

We assessed the response pattern of different retinal cell types to ischemic retinal stress by examining the gliosis response of Müller cells. Although they expressed the therapeutic transgene, we did not observe a major difference between the control and the injured retina. Both *Gfap* transcripts and protein, as determined by immunolabeling, were upregulated with a similar time course in FH-treated eyes compared to EGFP controls. The same is true for glutamine synthetase transcripts, which followed the reported pattern of an initial down-regulation immediately after ischemia with a later return to baseline levels (Wagner et al. 2017). The microglia marker *Iba-1* is upregulated in this cell population with a peak around 3 days after retinal ischemia/reperfusion injury, and mRNA levels decline by day 7 after injury (Ito et al. 2001). Here we found that after 14 days, *Iba-1* mRNA levels from microglia or retinas treated with the FH1-4^19-20 variant were significantly lower than those of the corresponding AAV_EGFP-treated control. Interestingly, microglia from FH-treated retina also appeared to accumulate FH on their cell surface. Unfortunately, the myc-tag could not be detected by IHC staining, so it remains unclear whether these FH signals originate from the respective human miniFH variant or the endogenously expressed murine *Cfh*. However, binding of FH to microglial surfaces has been reported in an environment of complement activation (Enzbrenner et al. 2021). Calippe et. al. hypothesized that binding of FH to CR3A (CD11b) inhibits the leukocyte surface

antigen CD47, leading to retention of microglia in their activated state - an effect that is stronger with the Y402H variant of FH (Calippe et al. 2017). Another study showed increased APOE binding to monocytes with CR3A-mediated FH on their surface, which coincided with increased cholesterol efflux and decreased transcription of proinflammatory and proatherogenic factors (Nissilä et al. 2018). The conflicting nature of these studies highlights the need for further research into alternative FH-mediated mechanisms beyond complement cascade inhibition. We therefore thoroughly characterized the microglial response pattern in our model and did not observe enhanced microglial activation upon FH treatment. In contrast to EGFP controls, *Iba-1* transcript levels peaked at 3 dpi regardless of treatment group but normalized to near baseline levels in FH-treated ischemic microglia at 14 dpi suggesting a faster repolarization of microglia from pro-inflammatory towards homeostatic states. A similar trend was observed when microglia numbers were examined by IBA-1 labeling. Fewer microglia were present in the postischemic retinas of FH-treated eyes at 14 dpi. Therefore, future studies should focus on the specific mechanisms by which FH modulates the response of retinal microglia, which was beyond the scope of the present work.

Limitations of this study

Although our expression constructs and vectors worked well, potential options for optimization should be considered. First, the sequences were codon optimized to increase expression levels. While it has been reported that adaptation of rare and slowly translated codons to more common ones in the host organism can increase expression, it is also debated whether slower translation is critical for proper peptide folding (Hanson und Coller 2018). In a recent study of human CFI expression in mouse tissue, expression levels of codon-optimized sequences was significantly lower than the non-optimized sequence supporting the notion that codon-optimization could decrease instead of increase overall protein levels (Dreismann et al. 2021). Second, to further improve Müller cell-specificity of AAV-mediated transduction, the Y445F variant of the ShH10 capsid could be considered, as it has been shown to hit as much as 50% of all Müller cells (Zhong et al. 2008), whereas the original ShH10 fcapsid used here was only able to transduce 22% of Müller cells upon intravitreal injection (Klimczak et al. 2009). Alternatively, other AAV serotypes optimized for even higher transduction efficiency, such as recombinant AAV2 serotype AAV2.GL or AAV2.NN, could be considered since cell type-specific expression of the transgene is ensured by the GFAP promoter (Pavlou et al. 2021).

Because AAVs are not associated with any known diseases, do not integrate efficiently into the genome, and remain in an episomal state, they are considered safer than other viral vectors (Gross et al. 2022). However, as AAV vectors have recently been shown to induce immunological reactions to the virus and to contaminants in viral preparations such as DNA and peptides, this assumption has become increasingly controversial (Tobias et al. 2019; Bucher et al. 2021). AAVs were purified by polyethylene glycol precipitation and an iodixanol gradient. DNA carryover was

prevented by DNAse I treatment before purification and purity was checked by gel electrophoresis. Despite all the measures taken, contamination and immunogenicity of the AAV preparations used here cannot be completely excluded. In particular, as mentioned above, some analyses of FH1-7^19-20 like GFAP levels, transcript distribution and microglia activation were surprisingly pro-inflammatory at first glance and could be attributed to potential carryover of contaminants.

The I/R model was used to generate an environment of acute degeneration that allowed monitoring complement activity and its response to FH overexpression (Pauly et al., Cell Reports, 2019). While at the molecular level FH1-4^19-20 and FH1-7^19-20 clearly exerted their cofactor activity after ischemic injury, resulting in C3b degradation and downregulation, the effects at the cellular and expression levels were more difficult to interpret. Some benefits in cell survival and tissue integrity after ischemic injury were observed, but high variability and small sample sizes may have masked more subtle effects. Differences within treatment groups were partly due to variability in the severity of I/R injury due to individual prepositions and the difficulty of the procedure (Hartsock et al. 2016). While the I/R model served well for our proof-of-concept study to demonstrate the functionality and complement regulatory efficacy of our approach, potential treatment effects are expected to be more compelling in retinal degeneration models with slower disease progression, such as retinitis pigmentosa, AMD or even diabetic retinopathy.

Conclusion

We validated an approach to modulate local retinal complement homeostasis to improve cell survival in pathologically stressed tissue. Our gene addition approach could benefit a broad spectrum of patients with retinal pathologies not amendable to classical gene correction approaches, such as multifactorial retinal diseases like AMD, diabetic retinopathy, or glaucoma. By modulating only excessive complement responses to host tissue, it has a clear advantage over current complement regulatory drugs (e.g. eculizumab or pegcetacoplan) that completely and indiscriminatingly block complement activity. Further testing in disease specific models will be necessary, as well as optimization to the vector system to achieve optimal efficacy, as well as a better understanding of vector immunity.

Methods & Materials

Animals

Adult (3-8 months of age) C57BL/6 Mice were bred in a pathogen-free animal facility following federal guidelines and approved by local authorities. Animals were kept in an air-conditioned room with free access to water and food.

Vector generation

FH1-4^19-20 was adapted with permission from the miniFH developed by Schmidt et. al to express the gene in a murine system a signal peptide and a C-terminal myc tag were added to the sequence and codons were optimized using the software tool of the company that also synthesized the final DNA (genewiz, Regensburg). A synthesized sequence of FH domains 5-7 was subcloned into the FH1-4^19-20 vector to create the FH1-7^19-20 variant. For functional tests that required large amounts of protein, genes were cloned into a CMV promoter expression plasmid (Thermo Fisher, pcDNA3.1). For AAV production, the expression cassette containing the gfABC1D version of the GFAP promoter (developed by Lee et. al), the transgenes and an IRES sequence linked GFP reporter were cloned into a transfer plasmid.

AAV production

Recombinant AAV (rAAV) production was based on the protocol of (Zolotukhin et al. 1999). CaPO4 precipitation was used to transfect HEK 293T cells with equimolar levels of a helper plasmid, the ShH10 RepCap plasmid and the transfer plasmids containing the respective expression cassettes (Fig. S1). After 72h, cells and supernatant were collected separately. AAVs from the supernatant were precipitated by addition of 25ml of 40% PEG/NaCl solution (24g NaCl, 400g PEG 8000 in 1L (w/v) ddH2O) to 100ml of supernatant. The solution was stirred for 1h at 4°C, then kept at 4°C without stirring and finally precipitates were spun down at 2818G for 15 min. Collected cells were pelleted in the same manner and resuspended in lysis buffer. PEG precipitated virus and Bitnucleas (250 Units/u) were added, and the solution was incubated 2h at 37°C. Samples were frozen in liquid nitrogen and thawed. Cell debris was removed by centrifuging 8000 G 30 minutes. Virus containing supernatants were purified by iodixanol gradient ultracentrifugation (15, 25, 40, and 56% iodixanol 50,000G for 2h 17 min at 22°C in a Ti70 rotor (Beckman, Fullerton, CA, USA). AAV containing 40% iodixanol fraction was collected with a syringe and dialyzed using a Slide-A-Lyzer 10000 MWCO 5ml. Buffer change to PBS with 0.001% F68 and concentration of the virus was performed with Vivaspin 6. AAVs were quantified by Sybr Green qPCR with SV40 primers (D'Costaet al, 2016). 1e10 genomic copies of AAVs in 1µl of dilutant were injected into the vitreous of each eye if not stated otherwise.

Ischemia and AAV injection

The murine ischemia model is a well described procedure to introduce retinal degeneration (Grosche et al. 2016). In brief, to induce ischemia, animals were anesthetized with a ketamine/xylazine cocktail (100mg/kg body weight and 5mg/kg body weight respectively), and the anterior ocular chamber was punctured with a 30-gauge cannula connected to an isotonic saline drip. The reservoir of the drip was raised 2 meters above the animal to create a pressure (160 mmHg) higher than the systolic pressure of the mouse (<130 mm Hg), thus occluding retinal arteries. After 60 minutes, the drip was removed and 1µl of AAV solution was injected intravitreally into both eyes.

Purification of murine retinal cell types.

As previously reported in detail by (Grosche et al. 2016), retinal cell types were isolated from murine retinas and sorted into cell fractions with the Miltenyi Magnetic cells sorting system. Retinas were immediately removed from enucleated eyes and digested in 12 mM PBS glucose containing 0.2mg/ml papain (Roche). For 30 min 37°C Retinas were washed and treated with DNase I in PBS/Glucose (200U/ml 4 min RT). Supernatant was replaced with ECS, (136 mM NaCl, 3 mM KCl, 10 mM HEPES, 11 mM glucose, 1 mM $MgCl_2$ and 2 mM $CaCl_2$, pH 7.4) and the tissue dissociated. Cell types were subsequently subtracted from the cell suspension by incubating it with specific antibodies coupled to magnetic microbeads (CD11b (Milteny Biotec) for microglia, CD31 (Miltenyi, Biotec for perivascular cells and CD29 for Müller cells. In brief, for every purification step, the suspension was pipetted onto and Large Cell column (Milteny), clipped to a magnetic rack. Non-magnetically labeled cells were eluted by washing. The column was removed from the rack and labeled cells were eluted, spun down (10000g, 15 min, 4°C) and the pellet immediately frozen in dry ice. Finally, the neuron rich cell suspension depleted of microglia, vascular and Müller cells was collected in the same manner.

qPCR complement transcript analysis

PureLink RNAMicro Kit (Invitrogen (Massachusetts, USA, Cat# 2183-016) was used according to the manufacturers specifications to extract RNA from cell fractions. RNA was eluted in 10µl RNAse free water and transcribed into cDNA with the RevertAid First Strand cDNA Synthesis Kit (Thermo Fisher Scientific, Cat# K1621) using random hexamer primers. All cDNA was diluted 1:4 in nuclease free water. A 384 well plate was filled with 2.5µl of silicone oil in each well to prevent evaporation during qPCR cycles. 1µl of diluted cDNA as well as 1.5µl of TaqMan™ Fast Advanced Master Mix (Thermo Fisher Scientific , Cat# TF4444556) containing assay specific primers (Tab. 1, Metabion international, Planegg, Germany) and TaqMan probes (Roche Molecular Biochemicals, Basel, Switzerland) were added. For complement factor analysis, commercial qPCR by Thermo Fisher Scientific were multiplexed with a primer limited *pdhb* housekeeper assay (Mm00437859_g1, Mm00442739_m1, Mm01341415_m1, Mm01143935_g1, Mm00432470_m1, Mm01132441_g1, Mm00499323_m1). Final pipetting into the plate wells was done with the non-contact liquid handler i.dot (Dispendix, Stuttgart, Germany). qPCR assays were measured with a QuantStudio 6 machine (Thermo Fisher Scientific).

Table 1. Primers used for qPCR analysis.

Target Gene	Oligo	Probe
TM_EGFP_for	cgaccactaccagcagaaca	Nr. 74

TM_EGFP_rev	tctcgttggggtctttgc	
TaqMan_GFAP_for	tcgagatcgccacctacag	Nr. 67
TaqMan_GFAP_rev	gtctgtacaggaatggtgatgc	
TaqMan_Nrl_202_for	tgcctttctggttctgacagt	Nr. 53
TaqMan_Nrl_202_rev	gaaagccattctgggactga	
TaqMan_CD29_rev	cacaacagctgcttctaaaattg	Nr. 41
TaqMan_CD29_for	tccataaggtagtagagatcaataggg	
TaqMan_Nrl_202_for	tgcctttctggttctgacagt	Nr. 53
TaqMan_Nrl_202_rev	gaaagccattctgggactga	
TM_maus_Pecam1_for	gctggtgctctatgcaagc	Nr. 64
TM_maus_Pecam1_rev	atggatgctgttgatggtga	
humanFH_Variant_for	GCCAGCTCTGTGGAATACCA	Nr. 97
humanFH_Variant_rev	ACTGGCCGTTTCTACAGGTG	

Western Blot analysis

The retina and scratch RPE/choroid from mouse eyes were isolated and suspended in T-PER buffer supplemented with protease and phosphatase inhibitors. Protein isolation was achieved by sonicating the samples for ten minutes and incubating them for one hour on a checker at four degrees. Denatured proteins from the retina, RPE/choroid, or serum were separated on a 12.5 percent SDS-PAGE and transferred to PVDF membranes. Membranes were blocked for an hour in blocking buffer before being incubated with the appropriate primary antibody in blocking buffer overnight at 4 degrees. Following washing, membranes were incubated for 1 hour at room temperature in blocking buffer with appropriate HRP secondary antibodies. Following a final washing step, membranes were developed with lumi-light blotting substrate (Roche) or WesternSure PREMIUM Chemiluminescent Substrate (LI-COR Biosciences, Lincoln, NE, USA)

C3b Assay

For this ELISA based quantification of C3b, 96 well plates were coated with LPS and incubated overnight. Normal mouse serum was diluted 1:10 and incubated with activation buffer containing various concentrations of FHs variants. As positive controls, human FH was used. Human mAB properdin antibody was used as negative control. Following a one-hour incubation at 37 degrees, samples were washed and a secondary antibody C3-HRP was added for development.

Immunohistochemistry

Mouse eyes were fixed in 4% PFA for 1 h, incubated in sucrose (30% w/v in PBS) for cryoprotection, embedded in OCT compound and cut into sections of 20 µm thickness using a cryostat. Retinal slices were permeabilized (0.2% Triton X-100 in PBS) for ten minutes and then stained with primary antibodies (Tab. 2) diluted in blocking buffer (0.1% Tween and either 3% Normal Donkey Serum or 5% Normal Goat Serum in PBS, respective of the secondary antibody used) over night at 4°C. The slides were then incubated in a dilution of their respective secondary antibodies (Tab. 3) and 4,6-diamidino-2-phenylindole (DAPI, Sigma-Aldrich, 1:1000) in an identical blocking buffer for 45 minutes at room temperature, mounted using Aqua-Poly/Mount (Polysciences, Warrington, PA, USA) and dried overnight. Experiments missing primary antibody incubation served as negative controls. The samples were scanned using a confocal microscope (VisiScope, Visitron Systems).

Apoptotic and necrotic retinal cells were identified via terminal deoxynucleotidyl transferase dUTP Nick End Labeling (TUNEL) assay (In Situ Cell Death Detection Kit, TMR red by Roche Molecular Biochemicals, Mannheim, Germany) following the manufacturer`s instruction.

Table 2. Primary antibodies used in the present study.

Primary antibodies	Host	Dilution	Source	Catalogue number
GFAP	mouse	1:500	Sigma Aldrich/Merck (Darmstadt, Germany)	G3893
C3d	Goat	2 µg/ml	R&D Systems (Minneapolis, MN, USA)	AF2655
GFP	goat	1:200	Rockland Immunochemicals (Limerick, PA, USA)	600 101 215
IBA-1	rabbit	1:500	Wako Chemicals (Neuss, Germany)	019-19741
CFH	mouse	1:1200	Santa Cruz Biotechnology (Dallas, TX, USA)	sc-166613
Calretinin	Goat	1:500	Swant (Burgdorf, Switzerland)	CG1
Glutamine Synthetase	Mouse	1:500	Millipore	MAB302
CD68	Rat	1:500	AbDSerotec	MCA1957GA

Tab. 3. Secondary Antibodies implemented in the present study.

Secondary antibodies	Host	Dilution	Source	Catalog number

Alexa Fluor 647 anti-mouse	Donkey	1:500	Life Technologies/ Thermo Fisher Scientific (Waltham, MA, USA)	A31571
Alexa Fluor 647 anti-mouse-IgG1	Goat	1:500	Invitrogen (Massachusetts, USA)	A21240
Alexa Fluor 647 anti-goat	Donkey	1:500	Dianova (Hamburg, Germany)	705-605-003
Cy3 anti-goat	Donkey	1:500	Dianova (Hamburg, Germany)	705-165-147
Cy2 anti-goat	Donkey	1:500	Dianova (Hamburg, Germany)	705-225-147
Cy5 anti-rabbit	Donkey	1:500	Dianova (Hamburg, Germany)	711-175-152
Cy3 anti-rabbit	Goat	1:500	Dianova (Hamburg, Germany)	111-165-144
Alexa Fluor 488 anti-rat	Donkey	1:500	Life Technologies/ Thermo Fisher Scientific (Waltham, MA, USA)	A21208

Supplemental information

Gliosis dependent expression of complement factor H truncated variants attenuates retinal neurodegeneration following ischemic injury

Josef Biber[1#], Yassin Jabri[2#], Sarah Glänzer[1], Aaron Dort[3], Oliver Bludau[1], Diana Pauly[3#*], Antje Grosche[1#]

[1]Department of Physiological Genomics, Ludwig-Maximilians-Universität München, Planegg-Martinsried, Germany

[2]Department of Ophthalmology, University Hospital Regensburg, Regensburg, Germany

[3]Experimental Ophthalmology, University of Marburg, Marburg, Germany

[#]contributed equally

[*]corresponding author: diana.pauly@uni-marburg.de

Figure S1. Schematic representation of the AAV constructs for Müller cell-specific FH variant and/or EGFP overexpression. gfaABC1D: Truncated GFAP promoter; IRES: internal ribosome entry site, pA: Polyadenylation site; ITR: Inverted terminal repeat
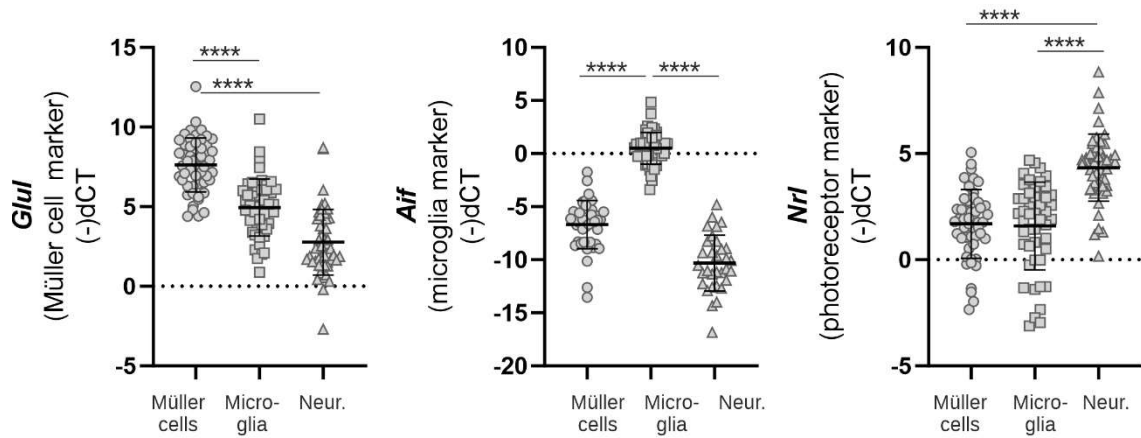
Figure S2. Validation of cell purification by magnetic activated cell sorting. mRNA levels of cell markers in the respective fractions were analyzed by qPCR. x axis = cell fractions. Analyzed with Student's t-test (n = 58-61 animals). Note that conditions (control, postischemic) and genotypes were combined for this analysis.
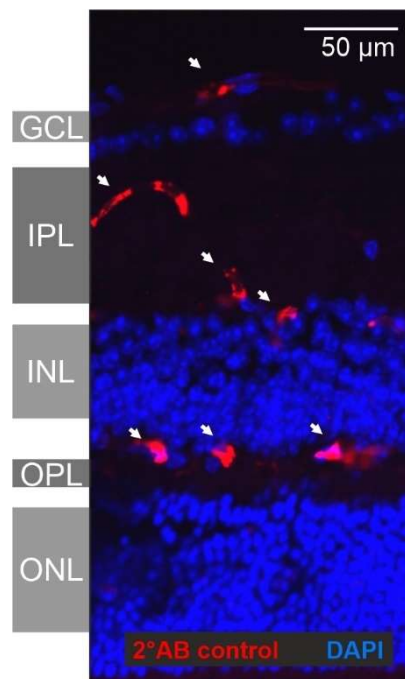
Figure S3: Secondary antibody control of immunostaining on mouse retinal tissue. Arrows point towards blood vessel that are likely stained due to binding of the secondary anti mouse antibody against endogenous antibodies. Stained with Alexa Fluor 647 anti-mouse-IgG1 A21240, Invitrogen 1:500.

Table S1. Summary of statistical analysis of the qPCR assay for differences of AAV EGFP injected vs FH1-4^19-20 injected samples. FC: Fold change, dct: delta CT, ddCt: delta delta CT

| Fraction	Target	dpi	Eye	GFP -dct	FH1-4^19-20 -dct	FC (ddCt)	P-value
Microglia	C3	3	Control	-4.3934	-2.6833	1.7101	0.2214
Microglia	C3	3	Ischemic	0.1402	0.0064	-0.1338	0.7965
Microglia	C3	14	Control	1.3203	-2.8053	-4.1256	0.1751
Microglia	C3	14	Ischemic	1.5964	-0.7537	-2.3501	0.0707
Microglia	CFB	3	Control	-3.3269	-1.8609	1.4659	0.2488
Microglia	CFB	3	Ischemic	0.9835	0.6351	-0.3485	0.7273
Microglia	CFB	14	Control	-1.9110	-2.9475	-1.0365	0.5833
Microglia	CFB	14	Ischemic	1.0962	-1.5012	-2.5974	0.0841
Microglia	CFD	3	Control	-5.1225	-6.6463	-1.5238	0.5386
Microglia	CFD	3	Ischemic	-7.3497	-5.3208	2.0289	0.4714
Microglia	CFD	14	Control	-7.9227	-6.8890	1.0336	0.5526
Microglia	CFD	14	Ischemic	-6.4427	-5.0212	1.4215	0.6285
Microglia	CFH	3	Control	-0.8964	-0.6603	0.2360	0.7305
Microglia	CFH	3	Ischemic	-0.8967	-0.6722	0.2245	0.5966
Microglia	CFH	14	Control	0.2234	-0.1398	-0.3632	0.5950
Microglia	CFH	14	Ischemic	1.1136	0.0302	-1.0834	0.0841
Microglia	CFI	3	Control	-5.1787	-5.2475	-0.0688	0.9240
Microglia	CFI	3	Ischemic	-6.6886	-7.3657	-0.6771	0.4356
Microglia	CFI	14	Control	-5.9388	-4.5005	1.4383	0.3577
Microglia	CFI	14	Ischemic	-5.0866	-5.0442	0.0424	0.9680
Microglia	CFP	3	Control	-2.4964	-2.5089	-0.0125	0.9874
Microglia	CFP	3	Ischemic	1.6709	0.1903	-1.4806	0.1313
Microglia	CFP	14	Control	-2.5868	-1.7547	0.8321	0.4304
Microglia	CFP	14	Ischemic	0.2704	-0.5801	-0.8505	0.4616
Müller Cells	C3	3	Control	-1.1192	-0.5795	0.5396	0.6008
Müller Cells	C3	3	Ischemic	1.1076	1.4058	0.2982	0.7229
Müller Cells	C3	14	Control	-0.5194	-1.0005	-0.4811	0.4357
Müller Cells	C3	14	Ischemic	1.8275	2.1329	0.3054	0.5329
Müller Cells	CFB	3	Control	-2.9973	-2.0468	0.9504	0.2986
Müller Cells	CFB	3	Ischemic	-1.0299	-1.2181	-0.1882	0.8110
Müller Cells	CFB	14	Control	-3.4479	-2.7466	0.7013	0.4456
Müller Cells	CFB	14	Ischemic	-1.1829	-1.3978	-0.2149	0.7947
Müller Cells	CFD	3	Control	-6.5176	-3.6390	2.8786	0.1698
Müller Cells	CFD	14	Ischemic	-9.0726	-8.5326	0.5400	--
Müller Cells	CFD	14	Control	-8.0431	-7.5611	0.4820	0.8161
Müller Cells	CFD	14	Ischemic	-8.8784	-7.3351	1.5433	0.6216
Müller Cells	CFH	3	Control	-1.3348	-1.0415	0.2933	0.3285
Müller Cells	CFH	3	Ischemic	-2.5357	-2.0900	0.4457	0.4079
Müller Cells	CFH	14	Control	-1.1971	-0.9613	0.2358	0.4683

Müller Cells	CFH	14	Ischemic	-0.6509	-0.6315	0.0193	0.9589
Müller Cells	CFI	3	Control	-5.6757	-4.8665	0.8092	0.4644
Müller Cells	CFI	3	Ischemic	-6.2857	-5.5857	0.7000	0.6297
Müller Cells	CFI	14	Control	-7.6991	-6.3111	1.3880	0.4125
Müller Cells	CFI	14	Ischemic	-6.1561	-4.8483	1.3079	**0.0449**
Müller Cells	CFP	3	Control	-2.9230	-2.7960	0.1271	0.6726
Müller Cells	CFP	3	Ischemic	-4.2322	-3.9520	0.2802	0.4695
Müller Cells	CFP	14	Control	-3.1376	-2.8357	0.3019	0.3260
Müller Cells	CFP	14	Ischemic	-3.4938	-2.7131	0.7807	0.0571
Neurons	C3	3	Control	-5.2992	-6.1707	-0.8715	0.3788
Neurons	C3	3	Ischemic	-1.1912	-3.1842	-1.9930	0.1940
Neurons	C3	14	Control	-5.9962	-7.1729	-1.1767	0.3045
Neurons	C3	14	Ischemic	-5.1828	-3.9320	1.2508	0.1959
Neurons	CFB	3	Control	-3.5318	-3.6999	-0.1681	0.6639
Neurons	CFB	3	Ischemic	-2.9066	-3.7141	-0.8076	0.4430
Neurons	CFB	14	Control	-4.8694	-3.5430	1.3264	0.1662
Neurons	CFB	14	Ischemic	-6.3055	-4.2957	2.0099	0.3687
Neurons	CFD	3	Control	-11.3754	-10.3437	1.0316	0.4512
Neurons	CFD	3	Ischemic		-2.0670	-2.0670	--
Neurons	CFD	14	Control	-10.6014	-9.8430	0.7584	0.7474
Neurons	CFD	14	Ischemic	-12.3602	-9.9296	2.4305	0.3973
Neurons	CFH	3	Control	-4.9610	-4.0908	0.8702	0.3266
Neurons	CFH	3	Ischemic	-4.9317	-5.2145	-0.2828	0.5013
Neurons	CFH	14	Control	-5.5778	-5.0376	0.5401	0.4169
Neurons	CFH	14	Ischemic	-6.8643	-6.0345	0.8298	0.2109
Neurons	CFI	3	Control	-3.3386	-4.1305	-0.7918	0.3144
Neurons	CFI	3	Ischemic	-3.2678	-3.1599	0.1078	0.8671
Neurons	CFI	14	Control	-6.5665	-5.7804	0.7860	0.3672
Neurons	CFI	14	Ischemic	-5.4552	-6.1631	-0.7079	0.5565
Neurons	CFP	3	Control	-1.9795	-1.9820	-0.0025	0.9965
Neurons	CFP	3	Ischemic	-2.5492	-2.3774	0.1718	0.7811
Neurons	CFP	14	Control	-2.8764	-2.3586	0.5178	0.3448
Neurons	CFP	14	Ischemic	-2.0179	-2.6538	-0.6358	0.6570

Table S2: Summary of statistical analysis of the qPCR testing for differences of AAV EGFP vs AAV FH1-7^19-20 injected samples. FC: Fold change, dct: delta CT, ddCt: delta delta CT

Fraction	Target	dpi	Eye	EGFP -dct	FH1-7^19-20 -dct	FC (ddCt)	P-value
Microglia	CFH	3	Control	-0.8964	0.5093	1.4057	**0.0046**
Microglia	C3	3	Ischemic	0.1402	-1.0620	-1.2022	**0.0054**
Microglia	CFD	3	Ischemic	-7.3497	-12.2035	-4.8539	**0.0494**
Microglia	CFP	3	Ischemic	1.6709	0.5607	-1.1103	0.0587

Microglia	CFI	14	Control	-5.9388	-4.2039	1.7348	0.0593
Microglia	CFP	14	Control	-2.5868	-1.0568	1.5300	0.1463
Microglia	C3	3	Control	-4.3934	-2.6834	1.7100	0.1596
Microglia	CFD	3	Control	-5.1225	-7.7605	-2.6380	0.2408
Microglia	CFH	14	Ischemic	1.1136	0.7067	-0.4069	0.2704
Microglia	CFD	14	Control	-7.9227	-4.9123	3.0104	0.2996
Microglia	CFB	14	Control	-1.9110	0.1170	2.0280	0.3490
Microglia	CFI	3	Control	-5.1787	-4.2258	0.9528	0.3952
Microglia	CFH	14	Control	0.2234	2.3168	2.0935	0.3963
Microglia	CFI	14	Ischemic	-5.0866	-4.1795	0.9071	0.4228
Microglia	CFH	3	Ischemic	-0.8967	-1.1682	-0.2715	0.4499
Microglia	CFP	3	Control	-2.4964	-1.9977	0.4987	0.5124
Microglia	CFD	14	Ischemic	-6.4427	-7.7490	-1.3063	0.5903
Microglia	CFB	14	Ischemic	1.0962	0.7287	-0.3675	0.7076
Microglia	C3	14	Control	1.3203	0.8819	-0.4384	0.8869
Microglia	CFP	14	Ischemic	0.2704	0.1984	-0.0720	0.9256
Microglia	C3	14	Ischemic	1.5964	1.6697	0.0733	0.9428
Microglia	CFI	3	Ischemic	-6.6886	-6.6432	0.0454	0.9728
Microglia	CFB	3	Control	-3.3269	3.6562	6.9830	--
Microglia	CFB	3	Ischemic	0.9835		-0.9835	--
Müller Cells	C3	14	Control	-0.5194	1.3927	1.9121	**0.0243**
Müller Cells	C3	14	Ischemic	1.8275	3.0144	1.1869	0.0589
Müller Cells	CFB	3	Ischemic	-1.0299	-0.1575	0.8725	0.0681
Müller Cells	CFH	14	Control	-1.1971	-0.5797	0.6174	0.0742
Müller Cells	CFI	3	Ischemic	-6.2857	-7.3177	-1.0320	0.1044
Müller Cells	CFP	3	Control	-2.9230	-3.3781	-0.4551	0.1391
Müller Cells	CFP	3	Ischemic	-4.2322	-3.8483	0.3839	0.1619
Müller Cells	CFI	14	Ischemic	-6.1561	-5.6158	0.5404	0.2015
Müller Cells	CFH	3	Ischemic	-2.5357	-1.9381	0.5976	0.2131
Müller Cells	CFH	3	Control	-1.3348	-1.0298	0.3050	0.2640
Müller Cells	CFD	14	Ischemic	-8.8784	-5.9296	2.9488	0.2882
Müller Cells	CFD	3	Control	-6.5176	-9.4391	-2.9216	0.3002

Müller Cells	CFI	14	Control	-7.6991	-6.8670	0.8321	0.3035
Müller Cells	CFH	14	Ischemic	-0.6509	-0.3095	0.3414	0.3035
Müller Cells	CFP	14	Control	-3.1376	-2.7324	0.4051	0.3344
Müller Cells	CFI	3	Control	-5.6757	-7.4607	-1.7849	0.3762
Müller Cells	CFD	14	Control	-8.0431	-9.3583	-1.3151	0.4989
Müller Cells	CFB	14	Ischemic	-1.1829	-0.5403	0.6427	0.5129
Müller Cells	CFB	14	Control	-3.4479	-2.5248	0.9231	0.5226
Müller Cells	C3	3	Ischemic	1.1076	0.9498	-0.1578	0.6577
Müller Cells	CFP	14	Ischemic	-3.4938	-3.3325	0.1613	0.7181
Müller Cells	C3	3	Control	-1.1192	-1.4517	-0.3325	0.7493
Müller Cells	CFB	3	Control	-2.9973	-2.8122	0.1851	0.8691
Müller Cells	CFD	14	Ischemic	-9.0726	-9.2717	-0.1991	--
Neurons	C3	3	Ischemic	-1.1912	-4.0055	-2.8142	**0.0100**
Neurons	CFI	3	Control	-3.3386	-5.1627	-1.8241	**0.0142**
Neurons	CFH	3	Ischemic	-4.9317	-7.2242	-2.2925	**0.0143**
Neurons	CFB	3	Ischemic	-2.9066	-4.5725	-1.6659	**0.0153**
Neurons	CFB	3	Control	-3.5318	-4.7471	-1.2153	**0.0153**
Neurons	CFH	14	Ischemic	-6.8643	-5.4502	1.4141	**0.0185**
Neurons	CFD	14	Control	-10.6014	-13.9682	-3.3668	**0.0402**
Neurons	CFI	3	Ischemic	-3.2678	-4.6208	-1.3531	**0.0455**
Neurons	CFH	3	Control	-4.9610	-6.2199	-1.2590	0.0615
Neurons	CFP	3	Control	-1.9795	-2.9706	-0.9911	0.0712
Neurons	CFP	3	Ischemic	-2.5492	-3.4375	-0.8883	0.1141
Neurons	C3	3	Control	-5.2992	-7.1523	-1.8532	0.1508
Neurons	CFH	14	Control	-5.5778	-6.1558	-0.5781	0.1758
Neurons	CFI	14	Control	-6.5665	-5.7731	0.7933	0.2299
Neurons	C3	14	Ischemic	-5.1828	-4.0796	1.1032	0.2576
Neurons	CFP	14	Control	-2.8764	-1.7539	1.1225	0.2957
Neurons	CFD	3	Control	-11.3754	-12.3526	-0.9772	0.4270
Neurons	CFP	14	Ischemic	-2.0179	-2.9763	-0.9584	0.5485
Neurons	CFI	14	Ischemic	-5.4552	-5.8647	-0.4095	0.5497
Neurons	C3	14	Control	-5.9962	-5.1694	0.8268	0.5872

Neurons	**CFD**	**14**	**Ischemic**	-12.3602	-11.0411	1.3191	0.6339
Neurons	**CFB**	**14**	**Control**	-4.8694	-5.4002	-0.5308	0.8284
Neurons	**CFB**	**14**	**Ischemic**	-6.3055	-6.2948	0.0107	0.9961
Neurons	**CFD**	**3**	**Ischemic**		-13.6300	-13.6300	--

Table S3: Summary of statistical analysis of the qPCR assay testing for differences of ischemic vs control samples. FC: Fold change, dct: delta CT, ddCt: delta delta CT

Fraktion	Target	dpi	Treatment	Control	Ischemic	FC (ddCt)	P-Value
Microglia	C3	3	GFP	-4.393379	0.14019489	4.533573786	**0.0001817**
Microglia	CFP	3	GFP	-2.496416	1.67094008	4.167356491	**0.0022874**
Microglia	CFH	3	FH1-7^19-20	0.5092943	-1.1681526	-1.677446842	**0.0024781**
Microglia	CFP	3	FH1-7^19-20	-1.997747	0.56067443	2.558421135	**0.0041341**
Microglia	CFP	14	GFP	-2.586801	0.27035732	2.857158613	**0.0070015**
Microglia	CFB	3	GFP	-3.326877	0.9835345	4.310411771	**0.0155624**
Microglia	CFP	3	FH1-4^19-20	-2.508896	0.19033241	2.699228048	**0.018183**
Microglia	CFI	3	FH1-4^19-20	-5.247459	-7.3656881	-2.11822931	**0.0244022**
Microglia	CFH	14	GFP	0.2233527	1.11360722	0.890254545	**0.0249858**
Microglia	CFD	3	GFP	-5.122509	-7.3496766	-2.227168083	**0.0336529**
Microglia	CFB	14	GFP	-1.910987	1.09615016	3.007136742	**0.03498**
Microglia	CFB	3	FH1-4^19-20	-1.860932	0.63507366	2.496005297	**0.0444759**
Microglia	C3	3	FH1-4^19-20	-2.683279	0.00635862	2.689637423	**0.0485033**
Microglia	C3	3	FH1-7^19-20	-2.683407	-1.0619891	1.621418238	0.1113434
Microglia	CFD	3	FH1-7^19-20	-7.760512	-12.203529	-4.443017006	0.1451675
Microglia	CFI	3	FH1-7^19-20	-4.225808	-6.6432056	-2.417397976	0.182445
Microglia	C3	14	FH1-4^19-20	-2.805287	-0.7536783	2.051609039	0.1877353
Microglia	CFP	14	FH1-7^19-20	-1.056808	0.1983736	1.255181122	0.2009603

Microglia	CFI	3	GFP	-5.178653	-6.6885796	1.509926796	-0.2113621
Microglia	CFD	14	FH1-7^19-20	-4.912296	-7.7489503	2.836654027	-0.2461405
Microglia	CFP	14	FH1-4^19-20	-1.754667	-0.5801342	1.174532747	0.3849348
Microglia	CFD	14	FH1-4^19-20	-6.88902	-5.0211989	1.867821376	0.3918623
Microglia	CFH	14	FH1-7^19-20	2.3168037	0.70673676	-1.610066938	0.4529793
Microglia	CFB	14	FH1-4^19-20	-2.947466	-1.5012318	1.446234306	0.4737238
Microglia	C3	14	FH1-7^19-20	0.88188	1.6696846	0.787804556	0.5398467
Microglia	CFI	14	FH1-4^19-20	-4.500495	-5.0441997	-0.543704748	0.5644757
Microglia	CFD	14	GFP	-7.922664	-6.4426502	1.480014165	0.5823542
Microglia	CFI	14	GFP	-5.938752	-5.0866201	0.852132082	0.5898703
Microglia	CFD	3	FH1-4^19-20	-6.64631	-5.3207661	1.325543722	0.6781631
Microglia	CFB	14	FH1-7^19-20	0.1170232	0.72866201	0.611638864	0.7243838
Microglia	CFH	14	FH1-4^19-20	-0.139835	0.03021932	0.170054674	0.8348011
Microglia	C3	14	GFP	1.3203053	1.59639359	0.276088238	0.9168176
Microglia	CFI	14	FH1-7^19-20	-4.20393	-4.1794834	0.024446726	0.9690711
Microglia	CFH	3	FH1-4^19-20	-0.660342	-0.6722326	-0.01189065	0.9853815
Microglia	CFH	3	GFP	-0.896371	-0.8966958	0.000324885	0.9989076
Microglia	CFB	3	FH1-7^19-20	3.6561508			--
Müller Cells	C3	14	FH1-4^19-20	-1.000463	2.13285694	3.133319473	**0.00001248**
Müller Cells	CFH	3	FH1-7^19-20	-1.029849	-1.9381187	-0.908269882	**0.001087**
Müller Cells	CFP	3	GFP	-2.923042	-4.2322474	-1.309205691	**0.0017758**
Müller Cells	C3	3	GFP	-1.119152	1.10759258	2.226744652	**0.0060876**
Müller Cells	C3	14	GFP	-0.519406	1.82745209	2.346857643	**0.0083029**
Müller Cells	CFB	3	FH1-7^19-20	-2.812194	-0.1574793	2.654714346	**0.0088197**

Müller Cells	CFH	3	FH1-4^19-20	-1.041517	-2.0900233	-1.048505783	**0.0108474**
Müller Cells	CFP	3	FH1-4^19-20	-2.795978	-3.9520264	-1.156048298	**0.0194332**
Müller Cells	C3	14	FH1-7^19-20	1.3926712	3.01436901	1.621697807	**0.0199047**
Müller Cells	CFD	3	FH1-4^19-20	-3.63897	-8.5325991	-4.893629233	**0.0220777**
Müller Cells	C3	3	FH1-7^19-20	-1.451675	0.9497664	2.401441336	**0.027245**
Müller Cells	CFB	14	GFP	-3.447865	-1.18293	2.264935017	**0.0353383**
Müller Cells	CFI	14	FH1-7^19-20	-6.867013	-5.6157546	1.251257992	**0.0362905**
Müller Cells	CFB	3	GFP	-2.997262	-1.0299365	1.967325052	**0.0474116**
Müller Cells	CFI	14	GFP	-7.699121	-6.1561333	1.542987728	0.0599627
Müller Cells	CFH	14	GFP	-1.19711	-0.6508684	0.546241379	0.0746838
Müller Cells	CFH	3	GFP	-1.3348	-2.5357161	-1.200915972	0.0883815
Müller Cells	C3	3	FH1-4^19-20	-0.579512	1.40583134	1.985342979	0.0983368
Müller Cells	CFP	3	FH1-7^19-20	-3.378099	-3.8483078	-0.470208645	0.1288684
Müller Cells	CFD	14	FH1-7^19-20	-9.35826	-5.9296276	3.428632545	0.1304888
Müller Cells	CFI	3	GFP	-5.675723	-6.285676	-0.609952927	0.1444251
Müller Cells	CFB	14	FH1-4^19-20	-2.746558	-1.397836	1.34872214	0.159095
Müller Cells	CFB	14	FH1-7^19-20	-2.524765	-0.5402699	1.984494686	0.2104307
Müller Cells	CFP	14	FH1-7^19-20	-2.732435	-3.3325222	-0.600087118	0.2362151
Müller Cells	CFB	3	FH1-4^19-20	-2.046833	-1.2180927	0.828740676	0.3492165
Müller Cells	CFP	14	GFP	-3.137567	-3.493811	-0.356243706	0.3552183
Müller Cells	CFI	14	FH1-4^19-20	-6.311105	-4.8482602	1.462844928	0.3564768
Müller Cells	CFH	14	FH1-4^19-20	-0.961334	-0.6315462	0.329787731	0.4289542
Müller Cells	CFH	14	FH1-7^19-20	-0.579697	-0.3094751	0.270222092	0.450025
Müller Cells	CFI	3	FH1-4^19-20	-4.866487	-5.5856843	-0.719197035	0.6058772

Müller Cells	CFP	14	FH1-4^19-20	-2.835665	-2.7131271	0.122537422	0.6664352
Müller Cells	CFD	14	GFP	-8.043131	-8.8784456	-0.83531456	0.7468406
Müller Cells	CFI	3	FH1-7^19-20	-7.460657	-7.3176799	0.142976761	0.9135902
Müller Cells	CFD	14	FH1-4^19-20	-7.561097	-7.3351065	0.225990423	0.9215847
Müller Cells	CFD	3	FH1-7^19-20	-9.439129	-9.2716627	0.167465925	0.9539786
Müller Cells	CFD	3	GFP	-6.517577	-9.0725784	-2.555001577	--
Neurons	C3	14	FH1-4^19-20	-7.172916	-3.9319841	3.240932274	**0.0005179**
Neurons	CFP	3	FH1-7^19-20	-2.970581	-3.4375339	-0.466953278	**0.0035721**
Neurons	C3	3	FH1-7^19-20	-7.152337	-4.0054641	3.146872997	**0.0129867**
Neurons	C3	3	FH1-4^19-20	-6.170654	-3.1841843	2.986469984	**0.0220291**
Neurons	C3	3	GFP	-5.299162	-1.1912236	4.107938766	**0.025373**
Neurons	CFH	14	GFP	-5.57776	-6.8642902	-1.286530113	**0.0326775**
Neurons	CFD	3	FH1-4^19-20	-10.34372	-2.0669732	8.276750088	**0.0343398**
Neurons	CFI	3	FH1-7^19-20	-5.162738	-4.6208413	0.541896343	**0.0465596**
Neurons	CFH	14	FH1-7^19-20	-6.155829	-5.4501579	0.705671358	0.0502096
Neurons	CFD	14	FH1-7^19-20	-13.96821	-11.041055	2.927159437	0.0512799
Neurons	CFI	14	GFP	-6.566451	-5.4551613	1.111289406	0.0559243
Neurons	CFD	3	FH1-7^19-20	-12.35257	-13.629989	-1.277421713	0.0908159
Neurons	CFH	3	FH1-7^19-20	-6.21995	-7.2242391	-1.00428915	0.1066519
Neurons	CFI	3	FH1-4^19-20	-4.130473	-3.1599054	0.970567465	0.1497691
Neurons	CFH	3	FH1-4^19-20	-4.090824	-5.2145193	-1.123695374	0.1880955
Neurons	CFB	3	GFP	-3.531822	-2.9065547	0.625267029	0.2015329
Neurons	CFH	14	FH1-4^19-20	-5.03763	-6.0344866	-0.996856117	0.204831
Neurons	CFP	14	FH1-7^19-20	-1.753875	-2.9763188	-1.222444248	0.3176823

Neurons	CFB	14	FH1-4^19-20	-3.542999	-4.2956937	0.752694448	-0.3187766
Neurons	CFP	14	FH1-4^19-20	-2.358586	-2.6537714	0.295185804	-0.3673317
Neurons	CFP	3	FH1-4^19-20	-1.981976	-2.3773749	0.395399332	-0.3789853
Neurons	C3	14	FH1-7^19-20	-5.169433	-4.0796206	1.089812803	0.4020806
Neurons	CFP	3	GFP	-1.979481	-2.5492039	0.569722652	-0.5133704
Neurons	CFD	14	GFP	-10.60137	-12.360177	1.758804957	-0.5345966
Neurons	C3	14	GFP	-5.996216	-5.1827965	0.813419914	0.5381086
Neurons	CFP	14	GFP	-2.876419	-2.0179483	0.858470726	0.5637061
Neurons	CFB	14	GFP	-4.869369	-6.3055489	1.436180353	-0.6040334
Neurons	CFB	3	FH1-7^19-20	-4.747126	-4.5724797	0.174646616	0.6467918
Neurons	CFB	14	FH1-7^19-20	-5.400183	-6.294823	0.894640287	-0.6585253
Neurons	CFI	14	FH1-4^19-20	-5.780433	-6.1630752	0.382642317	-0.7874792
Neurons	CFI	14	FH1-7^19-20	-5.773131	-5.8646848	0.091554022	-0.9081472
Neurons	CFI	3	GFP	-3.338631	-3.2677541	0.070876598	0.9390676
Neurons	CFH	3	GFP	-4.960989	-4.9317303	0.029258966	0.9630307
Neurons	CFD	14	FH1-4^19-20	-9.842963	-9.9296446	0.086681843	-0.97354
Neurons	CFB	3	FH1-4^19-20	-3.699947	-3.7141485	0.014201482	-0.9859596
Neurons	CFD	3	GFP	-11.37537			--

Literaturverzeichnis

Aiello, L. P.; Gardner, T. W.; King, G. L.; Blankenship, G.; Cavallerano, J. D.; Ferris, F. L.; Klein, R. (1998): Diabetic retinopathy. In: *Diabetes care* 21 (1), S. 143–156. DOI: 10.2337/diacare.21.1.143.

Anderson, Don H.; Radeke, Monte J.; Gallo, Natasha B.; Chapin, Ethan A.; Johnson, Patrick T.; Curletti, Christy R. et al. (2010): The pivotal role of the complement system in aging and age-related macular degeneration: hypothesis re-visited. In: *Progress in Retinal and Eye Research* 29 (2), S. 95–112. DOI: 10.1016/j.preteyeres.2009.11.003.

Barlow, Paul N.; Hageman, Gregory S.; Lea, Susan M. (2008): Complement factor H: using atomic resolution structure to illuminate disease mechanisms. In: *Advances in experimental medicine and biology* 632, S. 117–142.

Biggs, Robyn M.; Makou, Elisavet; Lauder, Scott; Herbert, Andrew P.; Barlow, Paul N.; Katti, Suresh K. (2022): A Novel Full-Length Recombinant Human Complement Factor H (CFH; GEM103) for the Treatment of Age-Related Macular Degeneration Shows Similar In Vitro Functional Activity to Native CFH. In: *Current eye research* 47 (7), S. 1087–1093. DOI: 10.1080/02713683.2022.2053725.

Borras, Céline; Delaunay, Kimberley; Slaoui, Yousri; Abache, Toufik; Jorieux, Sylvie; Naud, Marie-Christine et al. (2020): Mechanisms of FH Protection Against Neovascular AMD. In: *Frontiers in immunology* 11, S. 443. DOI: 10.3389/fimmu.2020.00443.

Bucher, Kirsten; Rodríguez-Bocanegra, Eduardo; Dauletbekov, Daniyar; Fischer, M. Dominik (2021): Immune responses to retinal gene therapy using adeno-associated viral vectors - Implications for treatment success and safety. In: *Progress in Retinal and Eye Research* 83, S. 100915. DOI: 10.1016/j.preteyeres.2020.100915.

Calippe, Bertrand; Augustin, Sebastien; Beguier, Fanny; Charles-Messance, Hugo; Poupel, Lucie; Conart, Jean-Baptiste et al. (2017): Complement Factor H Inhibits CD47-Mediated Resolution of Inflammation. In: *Immunity* 46 (2), S. 261–272. DOI: 10.1016/j.immuni.2017.01.006.

Clark, Simon J.; Bishop, Paul N.; Day, Anthony J. (2010): Complement factor H and age-related macular degeneration: the role of glycosaminoglycan recognition in disease pathology. In: *Biochem Soc Trans* 38 (5), S. 1342–1348. DOI: 10.1042/BST0381342.

Conrad, D. H.; Carlo, J. R.; Ruddy, S. (1978): Interaction of beta1H globulin with cell-bound C3b: quantitative analysis of binding and influence of alternative pathway components on binding. In: *The Journal of experimental medicine* 147 (6), S. 1792–1805. DOI: 10.1084/jem.147.6.1792.

Copland, D. A.; Hussain, K.; Baalasubramanian, S.; Hughes, T. R.; Morgan, B. P.; Xu, H. et al. (2010): Systemic and local anti-C5 therapy reduces the disease severity in experimental autoimmune uveoretinitis. In: *Clinical and Experimental Immunology* 159 (3), S. 303–314. DOI: 10.1111/j.1365-2249.2009.04070.x.

Dauchel, H.; Joly, P.; Delpech, A.; Thomine, E.; Sauger, F.; Le Loet, X. et al. (1993): Local and systemic activation of the whole complement cascade in human leukocytoclastic cutaneous vasculitis; C3d,g and terminal complement complex as sensitive markers. In: *Clinical and Experimental Immunology* 92 (2), S. 274–283. DOI: 10.1111/j.1365-2249.1993.tb03392.x.

Demirs, John T.; Yang, Junzheng; Crowley, Maura A.; Twarog, Michael; Delgado, Omar; Qiu, Yubin et al. (2021): Differential and Altered Spatial Distribution of Complement Expression in Age-Related Macular Degeneration. In: *Investigative ophthalmology & visual science* 62 (7), S. 26. DOI: 10.1167/iovs.62.7.26.

Ding, Jin-Dong; Kelly, Una; Landowski, Michael; Toomey, Christopher B.; Groelle, Marybeth; Miller, Chelsey et al. (2015): Expression of human complement factor H prevents age-related macular degeneration-like retina damage and kidney abnormalities in aged Cfh

knockout mice. In: *The American Journal of Pathology* 185 (1), S. 29–42. DOI: 10.1016/j.ajpath.2014.08.026.

Dreismann, Anna K.; McClements, Michelle E.; Barnard, Alun R.; Orhan, Elise; Hughes, Jane P.; Lachmann, Peter J.; MacLaren, Robert E. (2021): Functional expression of complement factor I following AAV-mediated gene delivery in the retina of mice and human cells. In: *Gene therapy* 28 (5), S. 265–276. DOI: 10.1038/s41434-021-00239-9.

Enzbrenner, Anne; Zulliger, Rahel; Biber, Josef; Pousa, Ana Maria Quintela; Schäfer, Nicole; Stucki, Corinne et al. (2021): Sodium Iodate-Induced Degeneration Results in Local Complement Changes and Inflammatory Processes in Murine Retina. In: *International journal of molecular sciences* 22 (17). DOI: 10.3390/ijms22179218.

Fritsche, Lars G.; Igl, Wilmar; Bailey, Jessica N. Cooke; Grassmann, Felix; Sengupta, Sebanti; Bragg-Gresham, Jennifer L. et al. (2016): A large genome-wide association study of age-related macular degeneration highlights contributions of rare and common variants. In: *Nature genetics* 48 (2), S. 134–143. DOI: 10.1038/ng.3448.

Grosche, Antje; Hauser, Alexandra; Lepper, Marlen Franziska; Mayo, Rebecca; Toerne, Christine von; Merl-Pham, Juliane; Hauck, Stefanie M. (2016): The Proteome of Native Adult Müller Glial Cells From Murine Retina. In: *Molecular & cellular proteomics : MCP* 15 (2), S. 462–480. DOI: 10.1074/mcp.M115.052183.

Gross, David-Alexandre; Tedesco, Novella; Leborgne, Christian; Ronzitti, Giuseppe (2022): Overcoming the Challenges Imposed by Humoral Immunity to AAV Vectors to Achieve Safe and Efficient Gene Transfer in Seropositive Patients. In: *Frontiers in immunology* 13, S. 857276. DOI: 10.3389/fimmu.2022.857276.

Hanson, Gavin; Coller, Jeff (2018): Codon optimality, bias and usage in translation and mRNA decay. In: *Nature reviews. Molecular cell biology* 19 (1), S. 20–30. DOI: 10.1038/nrm.2017.91.

Hartsock, Matthew J.; Cho, Hongkwan; Wu, Lijuan; Chen, Wan-Ju; Gong, Junsong; Duh, Elia J. (2016): A Mouse Model of Retinal Ischemia-Reperfusion Injury Through Elevation of Intraocular Pressure. In: *Journal of visualized experiments : JoVE* (113). DOI: 10.3791/54065.

Heesterbeek, Thomas J.; Lechanteur, Yara T. E.; Lorés-Motta, Laura; Schick, Tina; Daha, Mohamed R.; Altay, Lebriz et al. (2020): Complement Activation Levels Are Related to Disease Stage in AMD. In: *Investigative ophthalmology & visual science* 61 (3), S. 18. DOI: 10.1167/iovs.61.3.18.

Hu, Jane; Pauer, Gayle J.; Hagstrom, Stephanie A.; Bok, Dean; DeBenedictis, Meghan J.; Bonilha, Vera L. et al. (2020): Evidence of complement dysregulation in outer retina of Stargardt disease donor eyes. In: *Redox biology* 37, S. 101787. DOI: 10.1016/j.redox.2020.101787.

Ito, D.; Tanaka, K.; Suzuki, S.; Dembo, T.; Fukuuchi, Y. (2001): Enhanced expression of Iba1, ionized calcium-binding adapter molecule 1, after transient focal cerebral ischemia in rat brain. In: *Stroke* 32 (5), S. 1208–1215. DOI: 10.1161/01.str.32.5.1208.

Kajander, Tommi; Lehtinen, Markus J.; Hyvärinen, Satu; Bhattacharjee, Arnab; Leung, Elisa; Isenman, David E. et al. (2011): Dual interaction of factor H with C3d and glycosaminoglycans in host-nonhost discrimination by complement. In: *Proceedings of the*

National Academy of Sciences of the United States of America 108 (7), S. 2897–2902. DOI: 10.1073/pnas.1017087108.

Kemper, Claudia; Chan, Andrew C.; Green, Jonathan M.; Brett, Kelly A.; Murphy, Kenneth M.; Atkinson, John P. (2003): Activation of human CD4+ cells with CD3 and CD46 induces a T-regulatory cell 1 phenotype. In: *Nature* 421 (6921), S. 388–392. DOI: 10.1038/nature01315.

Klein, Robert J.; Zeiss, Caroline; Chew, Emily Y.; Tsai, Jen-Yue; Sackler, Richard S.; Haynes, Chad et al. (2005): Complement factor H polymorphism in age-related macular degeneration. In: *Science (New York, N.Y.)* 308 (5720), S. 385–389. DOI: 10.1126/science.1109557.

Klimczak, Ryan R.; Koerber, James T.; Dalkara, Deniz; Flannery, John G.; Schaffer, David V. (2009): A novel adeno-associated viral variant for efficient and selective intravitreal transduction of rat Müller cells. In: *PloS one* 4 (10), e7467. DOI: 10.1371/journal.pone.0007467.

Lee, Jong-Hyun; Shin, Ji Man; Shin, Yoo-Jin; Chun, Myung-Hoon; Oh, Su-Ja (2011): Immunochemical changes of calbindin, calretinin and SMI32 in ischemic retinas induced by increase of intraocular pressure and by middle cerebral artery occlusion. In: *Anatomy & Cell Biology* 44 (1), S. 25–34. DOI: 10.5115/acb.2011.44.1.25.

Łukawska, Emilia; Polcyn-Adamczak, Magdalena; Niemir, Zofia I. (2018): The role of the alternative pathway of complement activation in glomerular diseases. In: *Clinical and experimental medicine* 18 (3), S. 297–318. DOI: 10.1007/s10238-018-0491-8.

Luo, Chang; Zhao, Jiawu; Madden, Angelina; Chen, Mei; Xu, Heping (2013): Complement expression in retinal pigment epithelial cells is modulated by activated macrophages. In: *Experimental eye research* 112, S. 93–101. DOI: 10.1016/j.exer.2013.04.016.

Medzhitov, Ruslan (2008): Origin and physiological roles of inflammation. In: *Nature* 454 (7203), S. 428–435. DOI: 10.1038/nature07201.

Merle, Nicolas S.; Church, Sarah Elizabeth; Fremeaux-Bacchi, Veronique; Roumenina, Lubka T. (2015): Complement System Part I - Molecular Mechanisms of Activation and Regulation. In: *Frontiers in immunology* 6, S. 262. DOI: 10.3389/fimmu.2015.00262.

Mitchell, Paul; Liew, Gerald; Gopinath, Bamini; Wong, Tien Y. (2018): Age-related macular degeneration. In: *Lancet (London, England)* 392 (10153), S. 1147–1159. DOI: 10.1016/S0140-6736(18)31550-2.

Mondino, B. J.; Glovsky, M. M.; Ghekiere, L. (1984): Activated complement in inflamed aqueous humor. In: *Investigative ophthalmology & visual science* 25 (7), S. 871–873.

Morgan, Hugh P.; Schmidt, Christoph Q.; Guariento, Mara; Blaum, Bärbel S.; Gillespie, Dominic; Herbert, Andrew P. et al. (2011): Structural basis for engagement by complement factor H of C3b on a self surface. In: *Nature structural & molecular biology* 18 (4), S. 463–470. DOI: 10.1038/nsmb.2018.

Mukai, Ryo; Okunuki, Yoko; Husain, Deeba; Kim, Clifford B.; Lambris, John D.; Connor, Kip M. (2018): The Complement System Is Critical in Maintaining Retinal Integrity during Aging. In: *Frontiers in Aging Neuroscience* 10, S. 15. DOI: 10.3389/fnagi.2018.00015.

Muramatsu, Daisuke; Wakabayashi, Yoshihiro; Usui, Yoshihiko; Okunuki, Yoko; Kezuka, Takeshi; Goto, Hiroshi (2013): Correlation of complement fragment C5a with inflammatory cytokines in the vitreous of patients with proliferative diabetic retinopathy. In: *Graefe's archive for clinical and experimental ophthalmology = Albrecht von Graefes Archiv fur klinische und experimentelle Ophthalmologie* 251 (1), S. 15–17. DOI: 10.1007/s00417-012-2024-6.

Nishiyama, T.; Nishukawa, S.; Hiroshi; Tomita; Tamai, M. (2000): Müller cells in the preconditioned retinal ischemic injury rat. In: *The Tohoku journal of experimental medicine* 191 (4), S. 221–232. DOI: 10.1620/tjem.191.221.

Nissilä, Eija; Hakala, Pipsa; Leskinen, Katarzyna; Roig, Angela; Syed, Shahan; van Kessel, Kok P. M. et al. (2018): Complement Factor H and Apolipoprotein E Participate in Regulation of Inflammation in THP-1 Macrophages. In: *Frontiers in immunology* 9, S. 2701. DOI: 10.3389/fimmu.2018.02701.

Noris, M.; Remuzzi, G. (2008): Translational mini-review series on complement factor H: therapies of renal diseases associated with complement factor H abnormalities: atypical haemolytic uraemic syndrome and membranoproliferative glomerulonephritis. In: *Clinical and Experimental Immunology* 151 (2), S. 199–209. DOI: 10.1111/j.1365-2249.2007.03558.x.

Oppermann, M.; Manuelian, T.; Józsi, M.; Brandt, E.; Jokiranta, T. S.; Heinen, S. et al. (2006): The C-terminus of complement regulator Factor H mediates target recognition: evidence for a compact conformation of the native protein. In: *Clinical and Experimental Immunology* 144 (2), S. 342–352. DOI: 10.1111/j.1365-2249.2006.03071.x.

Pauly, Diana; Agarwal, Divyansh; Dana, Nicholas; Schäfer, Nicole; Biber, Josef; Wunderlich, Kirsten A. et al. (2019): Cell-Type-Specific Complement Expression in the Healthy and Diseased Retina. In: *Cell reports* 29 (9), 2835-2848.e4. DOI: 10.1016/j.celrep.2019.10.084.

Pavlou, Marina; Schön, Christian; Occelli, Laurence M.; Rossi, Axel; Meumann, Nadja; Boyd, Ryan F. et al. (2021): Novel AAV capsids for intravitreal gene therapy of photoreceptor disorders. In: *EMBO Molecular Medicine* 13 (4), e13392. DOI: 10.15252/emmm.202013392.

Pickering, G.; Estève, V.; Loriot, M-A; Eschalier, A.; Dubray, C. (2008): Acetaminophen reinforces descending inhibitory pain pathways. In: *Clinical pharmacology and therapeutics* 84 (1), S. 47–51. DOI: 10.1038/sj.clpt.6100403.

Razeghinejad, M. R.; Hamid, A.; Nowroozzadeh, M. H. (2017): Immediate IOP elevation after transscleral cyclophotocoagulation. In: *Eye (London, England)* 31 (8), S. 1249–1250. DOI: 10.1038/eye.2017.59.

Renner, Marina; Stute, Gesa; Alzureiqi, Mohammad; Reinhard, Jacqueline; Wiemann, Susanne; Schmid, Heiko et al. (2017): Optic Nerve Degeneration after Retinal Ischemia/Reperfusion in a Rodent Model. In: *Frontiers in cellular neuroscience* 11, S. 254. DOI: 10.3389/fncel.2017.00254.

Schmidt, Christoph Q.; Bai, Hongjun; Lin, Zhuoer; Risitano, Antonio M.; Barlow, Paul N.; Ricklin, Daniel; Lambris, John D. (2013): Rational engineering of a minimized immune inhibitor with unique triple-targeting properties. In: *Journal of immunology (Baltimore, Md. : 1950)* 190 (11), S. 5712–5721. DOI: 10.4049/jimmunol.1203548.

Seitz, Roswitha; Ohlmann, Andreas; Tamm, Ernst R. (2013): The role of Müller glia and microglia in glaucoma. In: *Cell and tissue research* 353 (2), S. 339–345. DOI: 10.1007/s00441-013-1666-y.

Seitz, Roswitha; Tamm, Ernst R. (2014): Müller cells and microglia of the mouse eye react throughout the entire retina in response to the procedure of an intravitreal injection. In: *Advances in experimental medicine and biology* 801, S. 347–353. DOI: 10.1007/978-1-4614-3209-8_44.

Sivapathasuntharam, Chrishne; Hayes, Matthew John; Shinhmar, Harpreet; Kam, Jaimie Hoh; Sivaprasad, Sobha; Jeffery, Glen (2019): Complement factor H regulates retinal development and its absence may establish a footprint for age related macular degeneration. In: *Scientific reports* 9 (1), S. 1082. DOI: 10.1038/s41598-018-37673-6.

Sofat, Reecha; Casas, Juan P.; Webster, Andrew R.; Bird, Alan C.; Mann, Samantha S.; Yates, John R. W. et al. (2012): Complement factor H genetic variant and age-related macular degeneration: effect size, modifiers and relationship to disease subtype. In: *Int J Epidemiol* 41 (1), S. 250–262. DOI: 10.1093/ije/dyr204.

Tobias, Peters; Philipp, Seitz Immanuel; Stylianos, Michalakis; Martin, Biel; Barbara, Wilhelm; Felix, Reichel et al. (2019): Safety and Toxicology of Ocular Gene Therapy with Recombinant AAV Vector rAAV.hCNGA3 in Nonhuman Primates. In: *Human gene therapy. Clinical development* 30 (2), S. 50–56. DOI: 10.1089/humc.2018.188.

Tsirouki, Theodora; Dastiridou, Anna; Symeonidis, Chrysanthos; Tounakaki, Ourania; Brazitikou, Irini; Kalogeropoulos, Christos; Androudi, Sofia (2018): A Focus on the Epidemiology of Uveitis. In: *Ocular immunology and inflammation* 26 (1), S. 2–16. DOI: 10.1080/09273948.2016.1196713.

Wagner, Lysann; Pannicke, Thomas; Rupprecht, Vanessa; Frommherz, Ina; Volz, Cornelia; Illes, Peter et al. (2017): Suppression of SNARE-dependent exocytosis in retinal glial cells and its effect on ischemia-induced neurodegeneration. In: *Glia* 65 (7), S. 1059–1071. DOI: 10.1002/glia.23144.

Wu, Jin; Wu, You-Qiang; Ricklin, Daniel; Janssen, Bert J. C.; Lambris, John D.; Gros, Piet (2009): Structure of complement fragment C3b-factor H and implications for host protection by complement regulators. In: *Nature immunology* 10 (7), S. 728–733. DOI: 10.1038/ni.1755.

Xu, Heping; Chen, Mei; Forrester, John V. (2009): Para-inflammation in the aging retina. In: *Progress in Retinal and Eye Research* 28 (5), S. 348–368. DOI: 10.1016/j.preteyeres.2009.06.001.

Yates, John R. W.; Sepp, Tiina; Matharu, Baljinder K.; Khan, Jane C.; Thurlby, Deborah A.; Shahid, Humma et al. (2007): Complement C3 variant and the risk of age-related macular degeneration. In: *The New England journal of medicine* 357 (6), S. 553–561. DOI: 10.1056/NEJMoa072618.

Zhong, Li; Li, Baozheng; Mah, Cathryn S.; Govindasamy, Lakshmanan; Agbandje-McKenna, Mavis; Cooper, Mario et al. (2008): Next generation of adeno-associated virus 2 vectors: point mutations in tyrosines lead to high-efficiency transduction at lower doses. In: *Proceedings of the National Academy of Sciences of the United States of America* 105 (22), S. 7827–7832. DOI: 10.1073/pnas.0802866105.

Zhou, Zhou; Xu, Ming-Jiang; Gao, Bin (2016): Hepatocytes: a key cell type for innate immunity. In: *Cellular & molecular immunology* 13 (3), S. 301–315. DOI: 10.1038/cmi.2015.97.

Zipfel, P. F.; Jokiranta, T. S.; Hellwage, J.; Koistinen, V.; Meri, S. (1999): The factor H protein family. In: *Immunopharmacology* 42 (1-3), S. 53–60. DOI: 10.1016/S0162-3109(99)00015-6.

Zolotukhin, S.; Byrne, B. J.; Mason, E.; Zolotukhin, I.; Potter, M.; Chesnut, K. et al. (1999): Recombinant adeno-associated virus purification using novel methods improves infectious titer and yield. In: *Gene therapy* 6 (6), S. 973–985. DOI: 10.1038/sj.gt.3300938.

Co-Author Publications

Publication 3 – (Enzbrenner, et al., 2021)

Sodium Iodate-Induced Degeneration Results in Local Complement Changes and Inflammatory Processes in Murine Retina

Anne Enzbrenner , Rahel Zulliger , **Josef Biber** , Ana Maria Quintela Pousa, Nicole Schäfer, Corinne Stucki, Nicolas Giroud, Marco Berrera, Elod Kortvely, Roland Schmucki, Laura Badi, Antje Grosche, Diana Pauly and Volker Enzmann

Conceptualisation, A.E., R.Z., D.P. and V.E.; Data curation, A.E., R.Z., J.B., A.M.Q.P., N.S., C.S., R.S., M.B., E.K., R.S., L.B., A.G., D.P. and V.E.; Funding acquisition, D.P. and V.E.; Investigation, A.E., R.Z., J.B., C.S., R.S., E.K., A.G., D.P. and V.E.; Methodology, A.E., R.Z., J.B., A.M.Q.P., N.S., C.S., N.G., E.K. and D.P.; Project administration, R.Z., D.P. and V.E.; Supervision, R.Z., A.G., D.P. and V.E.; Visualization, A.E., R.Z., J.B., M.B. and D.P.; Writing—original draft, A.E., R.Z., D.P. and V.E. and Writing—review and editing, A.E., R.Z., J.B., C.S., E.K., A.G., D.P. and V.E. All authors have read and agreed to the published version of the manuscript.

Article

Sodium Iodate-Induced Degeneration Results in Local Complement Changes and Inflammatory Processes in Murine Retina

Anne Enzbrenner [1], Rahel Zulliger [2], Josef Biber [3], Ana Maria Quintela Pousa [4,5], Nicole Schäfer [1], Corinne Stucki [2], Nicolas Giroud [2], Marco Berrera [2], Elod Kortvely [2], Roland Schmucki [2], Laura Badi [2], Antje Grosche [3], Diana Pauly [1,6,*,†] and Volker Enzmann [4,5,†]

[1] Department of Ophthalmology, University Hospital Regensburg, 93053 Regensburg, Germany; a.enzbrenner@googlemail.com (A.E.); Nicole.Schaefer@klinik.uni-regensburg.de (N.S.)
[2] Roche Pharma Research & Early Development, Roche Innovation Center Basel, F. Hoffmann-La Roche Ltd., 4070 Basel, Switzerland; rahel.zulliger@roche.com (R.Z.); corinne.stucki@roche.com (C.S.); nicolas.giroud@roche.com (N.G.); marco.berrera@roche.com (M.B.); elod.koertvely@roche.com (E.K.); roland.schmucki@roche.com (R.S.); laura.badi@roche.com (L.B.)
[3] Department of Physiological Genomics, Biomedical Center, Ludwig-Maximilians-University Munich, 82152 Planegg-Martinsried, Germany; Josef.Biber@bmc.med.lmu.de (J.B.); Antje.Grosche@bmc.med.lmu.de (A.G.)
[4] Department of Ophthalmology, University Hospital of Bern, 3010 Bern, Switzerland; quintelapousa@gmail.com (A.M.Q.P.); volker.enzmann@insel.ch (V.E.)
[5] Department of Biomedical Research, University of Bern, 3010 Bern, Switzerland
[6] Experimental Ophthalmology, University Marburg, 35043 Marburg, Germany
*   Correspondence: diana.pauly@uni-marburg.de
†   Contributed equally.

Abstract: Age-related macular degeneration (AMD), one of the leading causes of blindness worldwide, causes personal suffering and high socioeconomic costs. While there has been progress in the treatments for the neovascular form of AMD, no therapy is yet available for the more common dry form, also known as geographic atrophy. We analysed the retinal tissue in a mouse model of retinal degeneration caused by sodium iodate ($NaIO_3$)-induced retinal pigment epithelium (RPE) atrophy to understand the underlying pathology. RNA sequencing (RNA-seq), qRT-PCR, Western blot, immunohistochemistry of the retinas and multiplex ELISA of the mouse serum were applied to find the pathways involved in the degeneration. $NaIO_3$ caused patchy RPE loss and thinning of the photoreceptor layer. This was accompanied by the increased retinal expression of complement components *c1s*, *c3*, *c4*, *cfb* and *cfh*. C1s, C3, CFH and CFB were complement proteins, with enhanced deposition at day 3. C4 was upregulated in retinal degeneration at day 10. Consistently, the transcript levels of proinflammatory *ccl-2*, *-3*, *-5*, *il-1β*, *il-33* and *tgf-β* were increased in the retinas of $NaIO_3$ mice, but *vegf-a* mRNA was reduced. Macrophages, microglia and gliotic Müller cells could be a cellular source for local retinal inflammatory changes in the $NaIO_3$ retina. Systemic complement and cytokines/chemokines remained unaltered in this model of $NaIO_3$-dependent retinal degeneration. In conclusion, systemically administered $NaIO_3$ promotes degenerative and inflammatory processes in the retina, which can mimic the hallmarks of geographic atrophy.

Keywords: retinal degeneration; geographic atrophy; sodium iodate; local complement; inflammation; innate immunity; mouse

1. Introduction

Dysfunctional retinal pigment epithelium (RPE) and degenerated neurosensory retina play a central role in the pathobiology of age-related macular degeneration (AMD), the leading cause of blindness among the elderly in Western societies [1]. The oxidative events

and inflammation drive the pathological changes in the retina and RPE during degeneration [2,3]. This is seen in animal studies, which were performed to elucidate the molecular interplay of oxidative stress and tissue-specific complement activation in the eyes [4]. Furthermore, after the discovery of genetic risk variants in several complement pathway genes, the innate immunity was emphasised as an important mechanism in AMD [5]. Thereby, diverse components of the immune system, including resident microglia and recruited macrophages, inflammatory activators and pathways, especially from the complement cascade, as well as an activated inflammasome, are involved [6]. The sodium iodate ($NaIO_3$) model mimics the aspects of geographic atrophy [7]. Upon systemic administration, $NaIO_3$ specifically targets the RPE, resulting in its patchy loss via necrosis/necroptosis [8,9] and subsequent apoptosis of adjacent photoreceptors [7,10]. Oxidative stress and multiple caspase-dependent and -independent cell death pathways have been identified in retinal degeneration induced by $NaIO_3$ [11]. Furthermore, the increased expression of tissue modulators, including stromal cell-derived factor-1 (SDF-1), hepatocyte growth factor (HGF) and leukaemia inhibitory factor (LIF), have been found in $NaIO_3$-affected retinas [12]. A cellular response of the immune system, including the activation of macrophages, is involved as well [13]. Furthermore, the complement system as a pathway of the innate immune system has been observed to be upregulated after $NaIO_3$ treatment in vitro and in vivo [14,15].

In this study, a patchy RPE loss causing photoreceptor apoptosis was associated with the accumulation of classical (C1s and C4) and alternative (CFH and CFB) complement components in the retina, converging in the modulation of the complement pathway, as indicated by the accumulation of C3 in the retinal tissue. In addition, a local rise in chemokines was observed. Systemic inflammatory changes could not be detected. In sum, this suggested a retinal and not a blood-derived origin of the local rise in inflammatory mediators, even though $NaIO_3$ was administered systemically. Microglia, monocytes and gliotic Müller cells could be the main source of inflammatory proteins in the retina.

2. Results

2.1. $NaIO_3$-Induced Retinal Degeneration

To investigate the immunological consequences of damaged RPE in a mouse model of retinal degeneration, systemic $NaIO_3$ administration was used to disrupt the integrity of the RPE cell layer (Figure 1). Due to a high variability in previous studies using $NaIO_3$ and the varying oxidising potency of this agent, a confirmation of retinal degeneration for each $NaIO_3$ study cycle was needed. In the present study, the intravenous application of $NaIO_3$ resulted in the formation of RPE cell agglomerations (blebs) at day 3 and RPE disruption at day 10 (Figure 1A).

As a secondary effect, degeneration of the photoreceptor cells was observed (Figure 1), as they depend on an intact RPE to maintain their physiological metabolism. On day 3 following the treatment, the photoreceptor segments decreased in length, and at day 10, they were hardly detectable (Figure 1A). The number of photoreceptor nuclei significantly decreased in the $NaIO_3$-treated mice at day 3 and continued at day 10 in the central retina, while their number in the untreated control mice did not change (Figure 1B).

However, when evaluated longitudinally at the full length, the pattern of degeneration within a single retina was observed to be nonuniform (Supplementary Figure S1A): the zones of normal retinal morphology alternated with the areas of RPE and photoreceptor degeneration, a feature of $NaIO_3$ treatment commonly described as "patchy RPE loss" [16–18]. Further, the blood–retinal barrier was at least partly intact, as antibodies penetrating from the systemic bloodstream into the retinal tissue were not observed (Supplementary Figure S1B).
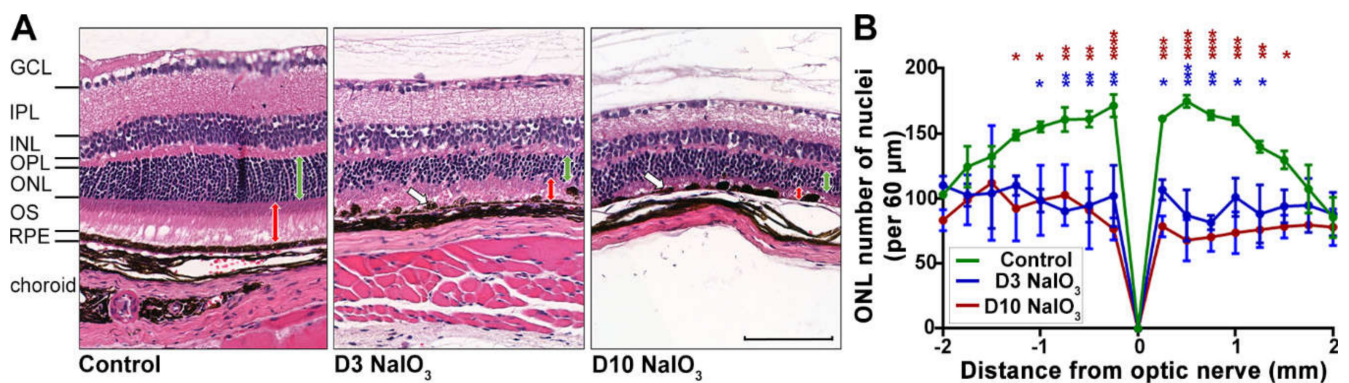
Figure 1. Time course of $NaIO_3$-induced retinal degeneration. (**A**) H&E staining of murine retinal cross-sections at three (D3) and ten (D10) days following the $NaIO_3$ treatment showed a disruption of the RPE layer, clustering of the RPE cells (white arrows) and photoreceptor degeneration. The photoreceptor segments (PS) were reduced at three days and nearly completely missing ten days after the treatment (red arrows), but also, the thickness of the outer nuclear layer (ONL) decreased substantially (green arrows). NFL, nerve fibre layer; GCL, ganglion cell layer; IPL, inner plexiform layer; INL, inner nuclear layer; OPL, outer plexiform layer. Scale bar: 50 μm. (**B**) The number of photoreceptor nuclei per 60-μm retinal section was counted to quantify the progress of degeneration. A two-way ANOVA with Bonferroni post-tests showed reduced photoreceptor numbers in treated versus untreated mice (* $p < 0.05$, ** $p < 0.01$, *** $p < 0.001$ and **** $p < 0.0001$).

2.2. NaIO_3 Treatment Increased Retinal Complement mRNA

Systemically applied $NaIO_3$ caused degeneration of the RPE and subsequent retinal degeneration. We then aimed to assess the associated inflammatory effects of the $NaIO_3$ treatment in the murine neurosensory retina. The RNA-seq analysis in the retinas revealed an upregulation of multiple complement component mRNAs in $NaIO_3$ retinas compared to those of the controls (Figure 2A and Supplementary Figure S2).

The influence of $NaIO_3$ on the expression of complement genes was confirmed in RT-qPCRs from isolated retinas, showing a consistent complement mRNA increase, including that of *c3*, *c3ar1*, *c1s* and *c4* in $NaIO_3$ mice compared to the controls on day 3 (Figure 2B). The *c1qb* and *cfp* transcripts were only significantly upregulated in the RNA-seq evaluation. In contrast, the *cfb* levels were significantly increased in the RT-qPCR experiments but were not detected in the RNA-seq analysis. To investigate the more long-term effects of $NaIO_3$; in addition to day 3, day 10 post-treatment was also evaluated by RT-qPCR (Figure 2B). Most components upregulated three days post-$NaIO_3$ were still expressed at significantly higher levels than in the control retinas, except for *c1s* mRNA, which returned to the control levels on day 10.
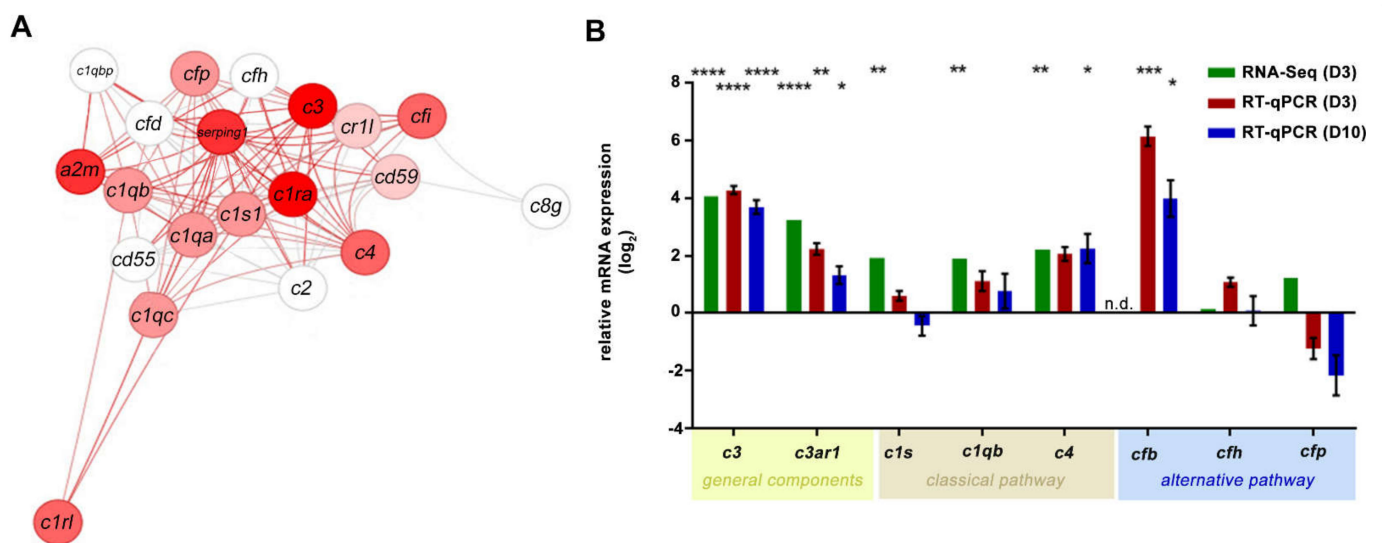
Figure 2. Increase in the mRNA expression of the complement components in the retina following NaIO$_3$ treatment. (**A**) The transcript quantity of the components of the complement pathway (GO: 0006956) was changed in the retinas after the NaIO$_3$ treatment at day 3. Nodes are the genes with their connections as defined in STRING database version 10, and the colour is given by the fold change (log2FC = 4) of the regulation (red = up, white = no regulation). (**B**) The fold change (log$_2$) mRNA expression levels of the general (*c3* and *c3ar1*), classical (*c1s* and *c4*) and alternative (*cfb*) pathway components were analysed in independent experiments using either RNA-seq or RT-qPCR. The retinal tissue was harvested at day 3 (RNA-seq analysis, n = 5) or day 3 and day 10 (RT-qPCR, n = 6) after NaIO$_3$ application. RNA-seq gene expression was normalised to the overall gene set. The RT-qPCR expression was normalised to the *idh3b* reference mRNA. Fold change in the expression (compared to the untreated control, line at y = 0) was calculated on the logarithm to base 2. The gene expressions of treated versus untreated retinas were evaluated using ordinary one-way ANOVA and Tukey's multiple comparisons test (* $0.01 < p < 0.05$, ** $0.001 < p < 0.01$, *** $0.0001 < p < 0.001$ and **** $p < 0.0001$).

2.3. NaIO$_3$ Treatment Promoted Retinal Complement Deposition

C3, the complement component that is central to all three complement pathways, was analysed at the protein level to confirm the RNA expression results (Figure 3). Comparative Western and Simple Western™ blots were performed on the retinal protein extracts in order to accommodate the different sample availability. Thereby, C3 was detected at ~115 kDa in all the neurosensory retina samples of both untreated and NaIO$_3$-treated mice. We confirmed increased C3 protein levels in NaIO$_3$-treated mouse retinas at day 3 (Figure 3A,B). However, and in contrast to the RNA data (Figure 2), the C3 protein signals returned to the baseline levels at day 10. The immunohistochemical staining (IHC) of C3 revealed an accumulation of proteins at the photoreceptor outer segment (POS) layer of NaIO$_3$-treated mouse retinas (Figure 3C). This distinct C3 accumulation was only present on day 3. Ten days post-treatment, a faint staining remained detectable in conjunction with almost completely degenerated POS (see Figure 1).
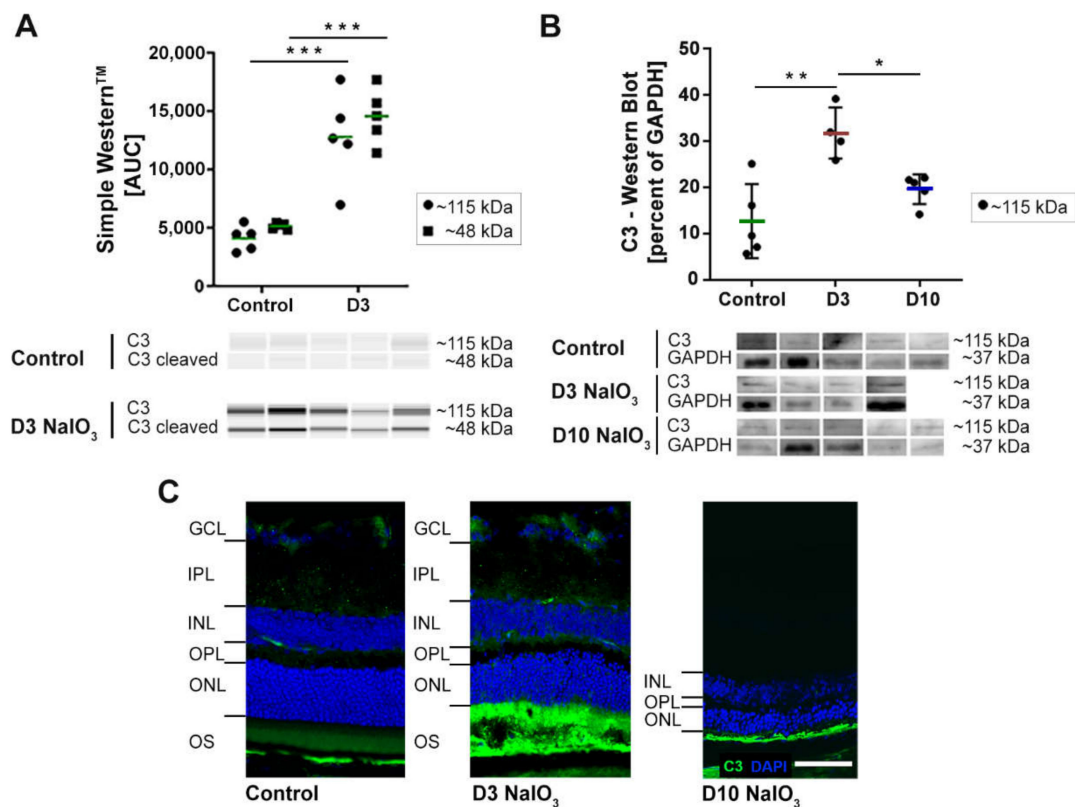
Figure 3. The C3 protein signals in murine neurosensory retina were increased after the NaIO₃ treatment. (**A**) The protein levels of the complement component C3 were significantly increased at day 3 after the NaIO₃ treatment in all the samples compared to the untreated control using Simple Western™ technology. Full blots are shown in Supplementary Figure S3A. (**B**) The Western blot signals of C3 in the retinal protein extracts of NaIO₃-treated mice under waning conditions were increased three days after treatment. The C3 protein levels were comparable to the untreated controls at day 10. GAPDH was used as a housekeeping protein. The intensity of the C3 signal in 3A and 3B was measured using ImageJ software. * $0.01 < p < 0.05$, ** $0.001 < p < 0.01$ and *** $0.0001 < p < 0.001$ (one-way ANOVA, Tukey's multiple comparisons test). The full blots are shown in Supplementary Figure S3B. (**C**) The immunohistochemical stainings of C3 and DAPI three days and ten days after the NaIO₃ treatment showed C3 accumulation in the POS at day 3, whereas the signal decreased after ten days. At this point in time, the ONL and PS thickness were reduced (see, also, Figure 1). Scale bar: 50 μm.

To determine whether NaIO₃ also enhances the systemic activation of the complement system, levels of the anaphylatoxin C3a were evaluated in mouse serum by ELISA (Supplementary Figure S4), but no changes of the systemic levels of C3a were detectable ten days following intravenous NaIO₃ injection compared to untreated mice (serum of day 3 was not available). Additionally, to the increased expression of complement component C3 post-NaIO₃ treatment; also, the mRNA of the classical/lectin pathway components *c1s* and *c4* were significantly increased (Figure 2). This corresponded to the respective protein levels in IHC stainings in the murine retina (Figure 4A,C).

Figure 4. Classical pathway proteins C1s and C4 accumulated in NaIO$_3$ damaged the retinas. (**A**) C1s immunoreactivity (green) was localised (white arrows) to the ONL at three days after the NaIO$_3$ treatment. At ten days, no specific C1s staining remained visible. DAPI staining (blue) delineated cell nuclei. (**B**) C1s protein levels were not changed in the Simple Western^{TM} three days after the NaIO$_3$ treatment. (**C**) C4 (green) was observed in the nerve fibre layer (NFL) ten days following the NaIO$_3$ treatment. In contrast, no distinct C4 staining was visible at day 3. Scale bar: 50 μm. (**D**) C4 cleavage products C4d (47 kDa) and iC4b (61 kDa) were increased at day 3 after the NaIO$_3$ treatment in all samples compared to the untreated control using Simple Western^{TM} technology. (**B**,**D**) Intensity of the signals was measured using ImageJ software. * $0.01 < p < 0.05$ (one-way ANOVA and Tukey's multiple comparisons test). The full blots are shown in Supplementary Figure S3C,D.

Three days after the treatment, the classical pathway initiator protein C1s were selectively upregulated in the ONL, apparently close to the photoreceptor nuclei (Figure 4A). Ten days post-NaIO$_3$, C1s staining disappeared, but C4 accumulated in the innermost part of the retina, the ganglion cell layer and nerve fibre layer, respectively (Figure 4C). Simple Western^{TM} studies confirmed C4d and iC4b accumulation in the retina three days after NaIO$_3$ (Figure 4B,D, respectively) but did not disclose the changes in the C1s levels shown with IHC.

Finally, changes in the mRNA levels of *cfb* (significant increase) but not for *cfh* (not a significant increase) were observed in NaIO$_3$-treated mice (Figure 2). Both are components of the alternative pathway. The protein analysis confirmed these findings for CFB but not for CFH (Figure 5), as both proteins were significantly increased in the retinas three days after the systemic NaIO$_3$ application.
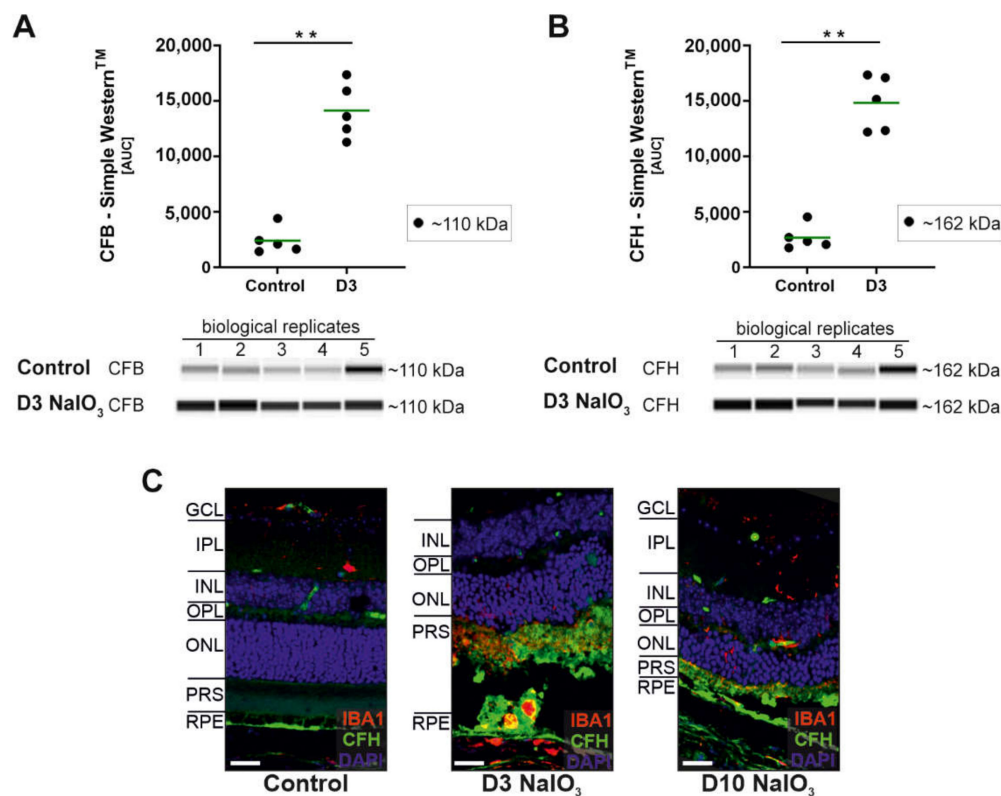
Figure 5. Alternative pathway component CFB and CFH protein levels were increased after the NaIO$_3$ treatment. (**A**) The CFB (~110 kDa) protein levels were increased at day 3 after the NaIO$_3$ treatment in all the samples compared to an untreated control using Simple Western^{TM} technology for detection. (**B**) Complement inhibitor CFH (~162 kDa) accumulated in the neurosensory retina of NaIO$_3$-treated mice compared to the control. (**C**) Retinal degeneration using NaIO$_3$ resulted in CFH deposition in the photoreceptor outer segment layer shown in immunohistochemical stainings. An overlapping with microglia marker IBA-1 was observed. (**A**,**B**) GAPDH was used as a housekeeping protein. The intensity of the protein signal was measured using ImageJ software. ** $0.001 < p < 0.01$ (unpaired, nonparametric Mann–Whitney *t*-test). The full blots are shown in Supplementary Figure S3E,F.

In addition to the complement component analysis, the systemic NaIO$_3$ treatment had a local effect on the retinal chemokine/cytokine status. Chemokines *ccl-2* and *ccl-3* were highly upregulated three and ten days after NaIO$_3$ in the RNA-seq and RT-qPCR analyses (Figure 6), and a similar trend was observed for *ccl-5*. The expression of proinflammatory cytokine *il-1β* increased compared to the control levels in one of the two transcription determining techniques, and for *il-33*, minimal changes were also determined. Consistently, the mRNA levels (as determined by RNA-Seq and RT-qPCR) of the multifunctional cytokine *tgf-β* showed an upward trend in response to NaIO$_3$, whereas *vegf-a*, a proangiogenic factor, was reduced three days after the NaIO$_3$ treatment and returned to the control levels on day 10.

To further evaluate to what extent intravenously applied NaIO$_3$ caused systemic inflammatory dysregulation, the serum cytokine protein levels were determined by multiplex ELISA (Supplementary Figure S5). For the tested chemokines (CCL-2, CCL-3 and CCL-5) and cytokines/growth factors (IL-1β and VEGF-A), no significant alteration of the serum concentrations ten days after NaIO$_3$ treatment were observed.
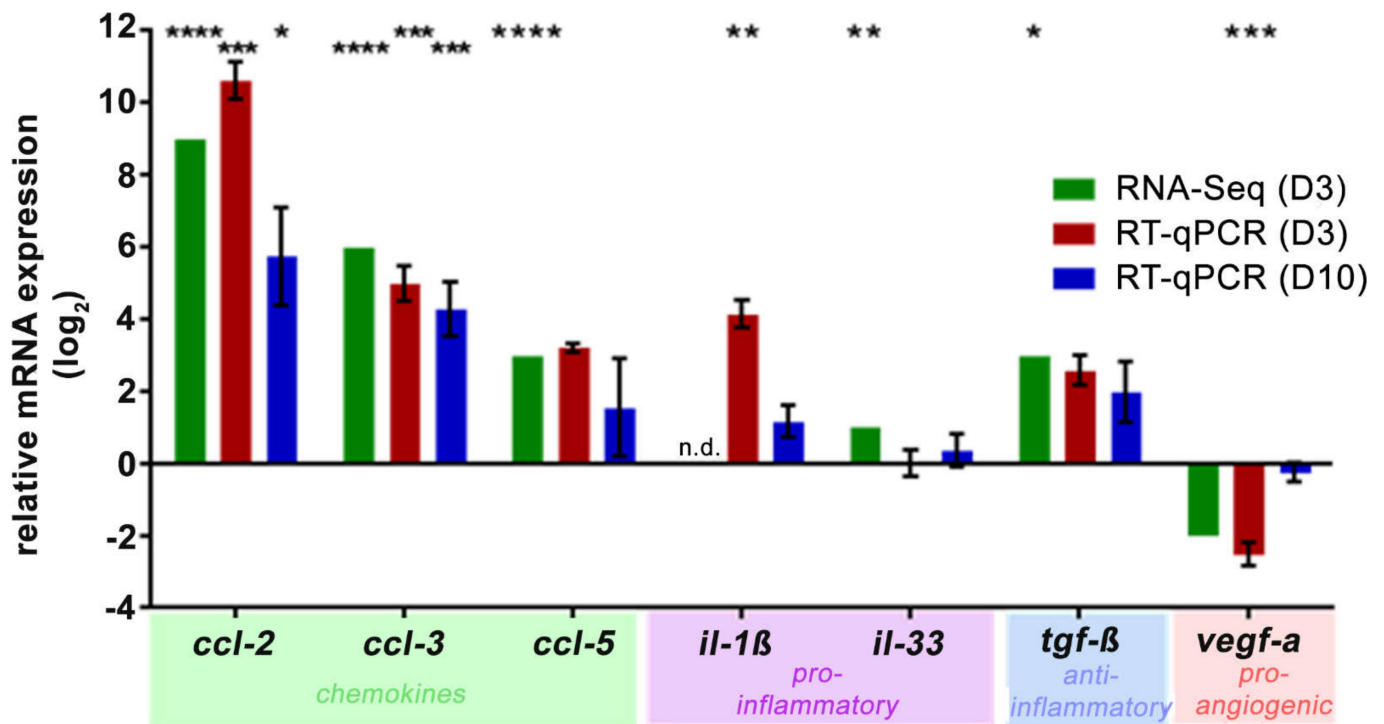
Figure 6. NaIO$_3$ increased the retinal transcription of the chemokines and cytokines. RNA-seq (day 3, green) and RT-qPCR analysis (day 3, red; day 10, blue) of the *ccl-2, 3, 5, il-1β and tgf-β* expression showed a significant upregulation after the NaIO$_3$ treatment. *Il-33* was not significantly upregulated, whereas *vegf-a* was decreased on the mRNA level at day 3 following the treatment. The expression was normalised to the overall gene set (RNA-seq) or *idh3b* reference mRNA (RT-qPCR), and the fold change in the expression (compared to the untreated control, line at y = 0) was calculated on the logarithm to base 2. * $0.01 < p < 0.05$, ** $0.001 < p < 0.01$, *** $0.0001 < p < 0.001$ and **** $p < 0.0001$ (ordinary one-way ANOVA and Tukey's multiple comparisons test).

Increased inflammatory signalling in the retina is often associated with microglia activation, monocyte invasion and Müller cell gliosis. Indeed, we found subretinal microglia/monocytes associated with the PR outer segments three days after treatment (Figure 7A). The outer segments seem to become opsonised by C3b (compared to Figure 4) and phagocytised. After ten days, the outer segments were almost completely degraded, and no IBA1-positive cells were present in this region anymore. Müller cell gliosis at day 10 was a consequence in the damaged retinas (Figure 7B).

In summary, systemic NaIO$_3$ application caused damage of the RPE and, subsequently, the neurosensory retina involving proinflammatory signalling via the local complement components and chemokines. Thereby, early complement proteins such as C3, C1s, CFH and CFB showed an increased deposition at day 3, whereas the late complement component C4 was involved in retinal degeneration at day 10.
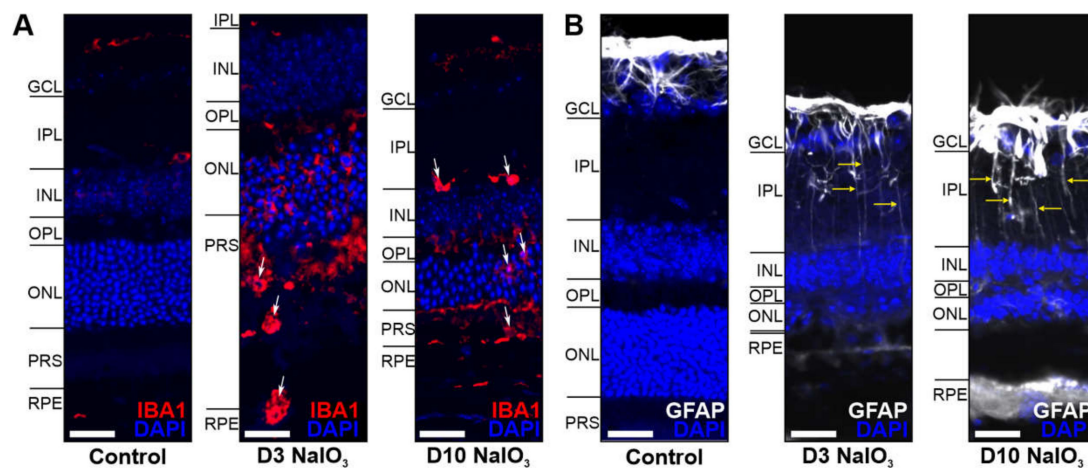
Figure 7. Glia cells were activated in the NaIO$_3$-damaged retina. (**A**) Microglia/monocytes (arrows) migrated into the photoreceptor outer segment layer at day 3 following the NaIO$_3$ treatment and were localised in the IPL at day 10. (**B**) GFAP (white), a marker for activated Müller cells, was enhanced in the GCL after NaIO$_3$ treatment during the investigated period. Scale bar: 20 μm.

3. Discussion

3.1. Validation of the NaIO$_3$-Induced Retinal Degeneration Model

Systemically applied NaIO$_3$ has been frequently used to investigate murine retinal degeneration. While the cause of morphological changes has been quite well-described over the past few decades [7], research defining the inflammatory consequences of NaIO$_3$ treatment has only come into focus recently [12,15].

The impact of different doses of NaIO$_3$ in mice has been extensively described in the literature [10,19]. The main conclusion was that a low dose only has a temporary effect on the function of the retina and does not lead to extensive changes in the morphology. An intermediate dose has been described to cause a "patchy" RPE cell loss with a subsequent degeneration of the photoreceptor cells, while a large dose inevitably leads to complete destruction of the retinal structure and function in a short amount of time. Variations between published studies are due to different application methods (intraperitoneal or intravenously) but also due to the unstable character of the chemical, NaIO$_3$, itself. Therefore, it is important that each study proves the potency of the NaIO$_3$ batch before any treatment studies are performed. We could confirm the patchy RPE cell loss, as well as the degeneration of the overlying photoreceptors in our model. A validated intermediate dose was then used for the analysis of the complement pathway and other inflammatory components.

3.2. The Complement System in the Eye and Its Involvement in NaIO$_3$-Induced Retinal Degeneration

As the complement system is an integral part of the innate immune system, it is also involved in inflammatory processes causing retinal degeneration in diseases like AMD, glaucoma and diabetic retinopathy. In the eye, as a partially immune-privileged compartment of the human body with a tight blood–retina barrier, the ocular tissue is required to produce a large number of innate immune system proteins itself, while other organs can rely on the supply from the liver [20]. This is especially true for the many components of the complement system, which, in fact, is a crucial pillar for innate immunity [21]. In line with this, our analyses of the retinal tissue in the acute phase of the NaIO$_3$ treatment induced retinal degeneration and showed a significant upregulation of complement components. We conclusively demonstrated that the central complement protein C3 was significantly upregulated at the transcript and protein levels upon the NaIO$_3$ treatment—a finding that served as a quality control for our model and was complementary to previous studies [12,13,15,22]. In addition, while C3 is the central connecting factor of the comple-

ment cascade, it does not lead to inflammatory processes by itself, and its interaction with additional complement proteins is always needed. We demonstrated recently that mainly complement components of the classical and the alternative pathways are expressed in healthy mouse retinal tissue [21], while the components of the lectin pathway (e.g., MASP1) were only expressed at very low levels or were not detectable at all. We could confirm these findings with our presented RNA-seq analysis. Interestingly, CFB was only detected by qPCR and not in RNA-seq, but as others described its presence in the mouse retina, the lack of detection in our analysis might be due to different technical preferences [23]. However, there is also evidence that the liver serves as the main source of ocular CFB, and very little if any expression is found in healthy eyes [24].

In the classical pathway, the initial components leading to an activation of the downstream cascade are C1q, C1s and C1r. In the RNA-seq analysis of the retinal tissue, these C1 complex components were, in fact, upregulated after the treatment with $NaIO_3$. For *c1s*, these results were also confirmed by qPCR, and via immunostaining, an accumulation at the ONL was demonstrated. Another crucial component of the classical pathway downstream of C1 is C4, whose expression in the retina was also significantly increased after $NaIO_3$ application. Katschke et al. (2018) also described a similar upregulation of various complement factors in the $NaIO_3$ model [25]. They found an accumulation of C1q/C3/C4 at the level of the photoreceptor outer segments. A comparable complement accumulation was observed in the retina of 26-month-old (aged) mice [26]. Luo et al. showed *c1s/c4* expression in the mouse retina, including RPE/choroid under physiologic conditions and a significant increase after treatments with inflammatory cytokines, including interferon (IFN)-γ or tumour necrosis factor (TNF)-α [27].

Activation of the alternative pathway is driven by CFB, which was upregulated on the RNA level, as well as with Simple Western on the protein level after $NaIO_3$ treatment. These results were comparable with published data from other groups regarding the detection of CFB under aged and inflammatory conditions [26,27]. The cell-type specific complement expression in healthy and diseased mouse retina was already shown by us in another retinal degeneration mouse model [21].

In the context of retinal complement activation, the complement inhibitor CFH has a pivotal role during pathological events. Single nucleotide polymorphisms in the CFH gene are associated with an increased risk for AMD, and studies with $cfh^{-/-}$ mice have shown a pathological accumulation of debris in CFH-deficient RPE cells [26,28]. Here, we found no significant changes in the *cfh* mRNA expression but detected a considerable drop in the protein level. As the CFH protein has been mainly associated with the basal side of RPE cells [29], there is the possibility that the protein originates from the bloodstream. As the levels of the complement components are very high in the serum, and it is known that $NaIO_3$ compromises the blood–retina barrier, we cannot exclude that at least some of the detected proteins stem from the blood circulation. However, as shown by us earlier, the Bruch's membrane is thickened but still intact after the $NaIO_3$ treatment [11]. This was also underscored by the fact that we could not detect any mouse IgG in the retina. Furthermore, the fact that the mRNA levels are upregulated in the ocular tissue itself—in some cases, to a very high level (16-fold increase for C3)—implies the presence of a tissue-specific activation cascade.

3.3. Inflammatory Processes Induced by $NaIO_3$

The $NaIO_3$-induced destruction of the retina is mediated by necrosis/necroptosis and, therefore, induces local inflammation [11]. Notably, the opsonisation of dying cells by complement components leads to clearance of the debris by the phagocytes. This can be associated with other inflammatory processes, e.g., immune cell activation and cytokine/chemokine increase, which can further aggravate the retinal degenerative processes. Importantly, the serum cytokine/chemokine levels were not significantly altered in this study. Similar observations were made by others [25,30]. However, we detected increased retinal cytokine/chemokine expression levels in the $NaIO_3$ model. Coincidently, aged mice

also showed an increased retinal CCL-2 secretion in a previous study [26]. In addition, to upregulated chemokines, the mRNA of *il-1β* was also increased. In accordance with the previous publications, IL-1β is the main downstream effector of the inflammasome and involved in NaIO$_3$ pathogenesis [13,30,31]. The inflammasome is also known to activate caspase 1, which has been found significantly upregulated in NaIO$_3$-mediated human RPE cell death [32]. The detected chemokines are directly involved in the recruitment of immune cells to the site of degeneration, as we have also shown with a staining for monocytes and microglia.

4. Materials and Methods

4.1. NaIO$_3$ Treatment

Experiments were conducted with 6 to 8-week-old male and female C57BL/6J mice (Charles River Laboratories, Sulzfeld, Germany). The mice were kept in individually ventilated cages (IVC; Tecniplast, Gams, Switzerland) at a temperature of 22 °C, humidity 50% and a 12-h/12-h light cycle with food and water ad libitum. A sterile 1% NaIO$_3$ solution (Sigma-Aldrich, Buchs SG, Switzerland) was injected once intravenously (i.v.) via the tail vein. The mice received either 35-mg/kg NaIO$_3$ for RNA sequencing or 50-mg/kg NaIO$_3$ for all the other experiments. The controls received i.v. the respective volume of 0.9% NaCl (B. Braun Melsungen AG, Melsungen, Germany; 100 µL). The eyes were enucleated three or ten days after treatment, whereas the serum was prepared after ten days only. The experiments were approved by the commission for involving animals in research of the Canton of Bern, Switzerland (BE8/18) and in accordance with the European Community Council Directive 2010/63/EU and the ARVO Statement for the Use of Animals in Ophthalmic and Vision Research.

4.2. Retinal Morphometric Analysis

A morphometric analysis was performed on H&E (a haematoxylin (Mayer's hemalum, Cat. # 09249.0500; Merck, Darmstadt, Germany) and eosin (Cat. # X883.2; Roth, Arlesheim, Switzerland) stained cross-section of murine eyeballs. To assess the number of photoreceptor cells, the nuclei per longitudinal stretches of 60 µm were counted manually at intervals of 250 µm using ImageJ software (Version 1.51n; National Institutes of Health, Bethesda, MD, USA).

4.3. RNA Sequencing

The sensory retina and RPE were harvested separately and immediately frozen in liquid nitrogen. The samples were kept at −80° C until RNA extraction with the RNAeasy Mini QIAcube kit (Cat. # 74116; Qiagen, Hilden, Germany) in the QIAcube (Cat. # 9001293; Qiagen). The samples were homogenised in the RLT buffer from the kit with the addition of 1% β-Mercaptoethanol (Cat. # 63689; Merck, Darmstadt, Germany) inside a TissueLyser II (Cat. # 1102664; Qiagen) with the addition of a stainless-steel bead, 5 mm in diameter (Cat. #69989; Qiagen). RNA quality control was performed on an Experion Automated Electrophoresis station (Cat. # 7007010; Bio-Rad Laboratories, Hercules, CA, USA), and the Experion RNA HighSens Analysis kit (Cat. # 7007105, Bio-Rad Laboratories, Munich, Germany) according to the manufacturer's protocols.

The samples were prepared with the HiSeq PE Rapid Cluster Kit v2 and HiSeq Rapid SBS Kit v2 with 50 cycles (Cat. PE-402-4002 and FC-402-4022, Illumina, San Diego, CA, USA) and sequenced with the HiSeq 2500 system (Cat. #SY-401-2501; Illumina) on rapid run mode. The sequencing reads were mapped on the mouse genome draft GRCm38 using the program STAR [33] and the Ensembl gene models (version 92). Genes with a low mean number of counts across the samples (<150) were removed, and about 14k genes passed this filtering step. A differential gene expression analysis was performed in R using the limma library [34–36]. The gene counts were converted into log2 CPM (log2 counts per million), and the dataset was assessed for inter- and intragroup variability and expression correlation profiles (pairwise Pearson correlation) in order to evaluate the data quality.

4.4. Quantitative Real-Time Polymerase Chain Reaction (qPCR)

After enucleation, the retinas of both mouse eyes were dissected, and the mRNA was isolated using a NucleoSpin RNA Kit (Macherey-Nagel, Düren, Germany). Eluted mRNA was reverse-transcribed to cDNA using the QuantiTect Reverse Transcription Kit (Qiagen, Hilden, Germany). To analyse the gene expression, qPCR was conducted using a Rotor-Gene Q Real-time PCR Cycler, Rotor Gene SYBR Green Kit (all Qiagen) and primers (Table 1; Metabion, Planegg, Germany). For amplification, 40 cycles consisting of an annealing temperature at 60 °C for 10 s was applied. The expression of *isocitrate dehydrogenase 3 subunit beta (idh3b)* was used for normalisation of the gene expression [21]. The fold change in the expression between the control and treatment groups was subsequently calculated employing the ΔΔCt method and transformed to the logarithm to base 2. The data are shown as log2(ΔΔCt).

Table 1. qPCR primer.

Gene	Sequence 5′–3′	Reference	T_m (°C)
c1qb	F: CTCTGGGCTCTGGGAATCCA	Primerblast	61
	R: CCTCAGGGGCTTCCTGTGTA		61
c1s	F: CCCTGTAGCCACTTCTGCAA	34	60
	R: GGGCAGTGAACACATCTCCA		60
c3	F: AGCCCAACACCAGCTACATC	34	60
	R: GAATGCCCCAAGTTCTTCGC		60
c3ar1	F: GTTTGCATGGAAGGCTGCTC	Primerblast	60
	R: AGGTTGCTTTTAGTGGGTGGC		61
c4	F: TCTGAAGCCTCCAACGTTCC	34	60
	R: TGGGATGGGGAAGGAAATGC		60
	R: TCCTGGTCAGGAGAGCAAGT		60
cfb	F: GGTGCCTCACCAACTTGATT	34	58
	R: CTTGGTGTTGGTCCCTGACT		60
cfh	F: AAAAACCAAAGTGCCGAGAC	20	57
	R: GGAGGTGATGTCTCCATTGTC		58
cfp	F: AGGTGCAAAGGCCTACTTGG	20	60
	R: TGACCATTGTGGAGACCTGC		60
idh3b	F: GCTGCGGCATCTCAATCT	20	58
	R: CCATGTCTCGAGTCCGTACC		60

4.5. Simple Western™ Protein Analysis

Frozen retinas were thawed on ice and transferred to Precellys tubes (soft tissue homogenising CK14, Cat. # KT03961-1-203.0.5; Bertin Technologies SAS, Montigny-le-Bretonneux, France) and 1x RIPA buffer (#20-188; Sigma, Burlington, VT, USA). Protease-inhibitor mix (1x cOmplete EDTA-free Mini, Cat. # 11836170001; Roche Diagnostics, Rotkreuz, Switzerland) was added for homogenisation in the Precellys 24 system (Bertin Technologies SAS) for 15 s with 5500 rpm twice, with intermittent cooling on ice. The homogenates were transferred into Protein Lo-Bind tubes (Cat. # 0030108434; Eppendorf, Hamburg, Germany) and centrifuged at $16,000\times g$ at 4 °C for 3 min. The supernatant was collected in fresh Protein Lo-Bind tubes and processed for the protein concentration analysis with BCA Protein Assay Kit Pierce™ (Cat. # 23225; Thermo Fisher Scientific, Waltham, MA, USA) and afterwards diluted to 1 mg/mL in aLISA buffer (AlphaLisa Immunoassay Buffer 10x, Cat. # AL000F; PerkinElmer, Waltham, MA, USA). A total volume of 35 μL was

prepared, and the samples were aliquoted into 6-µL aliquots into Simport strips (amplitude PCR reaction strips 8× 0.2 mL, attached domed cap #T320-3N Simport, Beloeil, QC, Canada) and frozen at −80 °C until use. As a positive control, normal mouse serum (Cat. # NMS, Complement-Technology, Tyler, TX, USA) was also prepared as a 1:50 dilution in aLISA buffer and frozen at −80 °C. Protein samples and primary and secondary antibodies were loaded into a 96-well plate and analysed by capillary electrophoresis using a 12–230-kDa separation matrix on a Peggy Sue device, as described by the provider (Cat. # 004-800, ProteinSimple, San Jose, CA, USA). The working solutions were diluted with Mastermix (according to the preparation datasheet of the provider) so that the final concentration for the lysates was 0.8 mg/mL.

The following commercially available antibodies were tested for specificity and optimised for the system: rabbit anti-C3 (Cat. #ab200999; Abcam, Cambridge, UK), goat anti-C1s (Cat. #A302; Quidel Corporation, San Diego, CA, USA), rat anti-C4 (Cat. #ab11863, Abcam), goat anti-CFB (Cat. #A311; Quidel Corporation), sheep anti-CFH (Cat. #AF4999; R&D Systems, Minneapolis, MN, USA), rabbit anti-GAPDH (Cat. #G9545; Sigma-Aldrich), anti-goat HRP (Cat. #043-522-2; ProteinSimple, San Jose, CA, USA), anti-sheep HRP (Cat. #HAF016; R&D Systems), anti-rabbit HRP (Cat. #040-0656; ProteinSimple) and anti-rat HRP (Cat. #HAF005; R&D Systems).

4.6. Western Blot

Protein extraction from the retinal tissue was carried out using T-PER buffer (Thermo Fisher Scientific) with the addition of 1% protease and 1% phosphatase inhibitor (Sigma-Aldrich). Protein samples were separated by SDS-PAGE using denatured, reducing conditions. The proteins were transferred onto a PVDF membrane. The membrane was blocked with blocking buffer (5% bovine serum albumin (BSA) and 0.1% Tween 20 in Tris-buffered saline) and primary antibodies (goat anti-C3d antibody (Cat. #AF2655; R&D Systems) or rabbit anti-GAPDH antibody (Cat. #CSB-PA00025A0Rb; Cusabio Technology LLC, Houston, TX, USA)) were added overnight. Detection was performed using secondary antibodies (anti-goat IgG-POD #SBA-6442-05, anti-rabbit-POD #711-546-152 (Dianova GmbH, Hamburg, Germany)) and the Lumi-Light Western Blotting Substrate (Cat. # 12015200001; Sigma-Aldrich) and imaged by the FluorChem FC2 Imaging System (AppliChem, Darmstadt, Germany). Western blot images were edited in Adobe Photoshop CS6 (San Jose, CA, USA) and analysed for signal intensity using ImageJ software (National Institutes of Health).

4.7. Immunohistochemistry Staining

Determination of the complement expression in the retina and RPE was performed as previously described [37,38]. Paraformaldehyde-fixed, cryoprotected and embedded eyes were cut into 20-µm slices, permeabilised, blocked with 5% goat or donkey serum/0.1% Tween20 in phosphate-buffered saline (PBS) and incubated with primary antibodies specific for C3d (Cat. #AF2655; R&D Systems), C1s (Cat. #14554–1–AP; Proteintech, Rosemont, IL, USA), C4 (Cat. #A205; Complement Technologies, Tyler, TX, USA), IBA (Cat. #019-19741; Wako Chemicals, Neuss, Germany) and glial fibrillary acidic protein (GFAP; G3893, Sigma-Aldrich) diluted in blocking buffer. The sections were labelled with fluorescence-conjugated secondary antibodies (anti-mouse Cy5 (Cat. #115-607-072; Dianova) & anti-goat Cy3 (Cat. #705-165-147; Dianova) and anti-rabbit AF-488 (Cat. #A-21206; Invitrogen)) and DAPI nucleic acid stain (Cat. # 62248c; Invitrogen). All images were taken with a confocal microscope (VisiScope; Visitron Systems, Puchheim, Germany).

4.8. C3a ELISA

Nunc-Immuno MaxiSorp 96-well plates were coated with anti-mouse C3a antibody (Cat. #558250; 3 µg/mL, BD Biosciences) in a phosphate buffer (pH 6.5) at 4 °C overnight. The plates were blocked using 1% BSA in PBS. Sera of the control and NaIO$_3$-treated mice (1:8000 and 1:16,000), as well as normal mouse serum (1:1000–1:64,000 for the standard

curve) were incubated in a sample buffer (0.1 mg/mL nafamostat mesylate in 1% BSA/PBS). Detection was performed with the anti-mouse C3a-biotin antibody (Cat. #558251, 2 µg/mL in PBS, BD Biosciences), streptavidin-HRP and 3,3′,5,5′-tetramethylbenzidine (TMB). The optical density (absorption) was measured photometrically at 450 nm using VarioScan Flash (Thermo Fisher).

4.9. Multiplex Cytokine ELISA

The customised ProcartaPlex was performed according to manufacturer's instructions (Invitrogen, Carlsbad, CA, USA). In brief, the magnetic beads for murine CCL3, CCL4, CCL5, IL-1β and VEGF-A were incubated with 1:2 diluted serum samples overnight. An antigen-specific biotinylated detection antibody mixture was applied following the streptavidin–phycoerythrin solution as a detection reagent. The assay was measured on Luminex™ MAGPIX™ (Austin, TX, USA) to determine the mean fluorescence intensity (MFI) for each chemokine or cytokine.

4.10. Statistical Analysis

Data were analysed statistically using GraphPad Prism 6 Software. To determine the statistical differences between the two groups unpaired, the nonparametric Mann–Whitney *t*-test was used. To compare three or more different treatment groups, ordinary one-way analysis of variance (ANOVA) with Tukey's multiple comparisons was performed. For a statistical analysis of the morphometrical data, a two-way ANOVA with Bonferroni post-tests was performed. p-values < 0.05 were considered statistically significant.

5. Conclusions

Retinal degeneration induced by $NaIO_3$ in mice can serve as a model mimicking retinal inflammatory sequence. The data could help to decipher possible mechanisms of retinal degenerative and inflammatory processes in human patients. We showed that soluble immune proteins, complement proteins and cytokines/chemokines are time-dependently altered locally in this mouse model. However, using a mouse model to understand the pathologies in a different species always has limitations. Therefore, our data, first of all, showed the situation in the murine environment. Nevertheless, as the induced retinal degeneration follows the main cell death pathways such as necrosis and apoptosis, a generalisation for mammalian retina might be appropriate. In sum, this body of evidence supports the hypothesis that a local immune response plays a pivotal role in retinal degeneration.

References

1. Wong, W.L.; Su, X.; Li, X.; Cheung, C.M.G.; Klein, R.; Cheng, C.-Y.; Wong, T.Y. Global Prevalence of Age-Related Macular Degeneration and Disease Burden Projection for 2020 and 2040: A Systematic Review and Meta-Analysis. *Lancet Glob. Health* **2014**, *2*, e106–e116. [CrossRef]

2. Chiras, D.; Kitsos, G.; Petersen, M.B.; Skalidakis, I.; Kroupis, C. Oxidative Stress in Dry Age-Related Macular Degeneration and Exfoliation Syndrome. *Crit. Rev. Clin. Lab. Sci.* **2015**, *52*, 12–27. [CrossRef]

3. Lashkari, K.; Teague, G.C.; Beattie, U.; Betts, J.; Kumar, S.; McLaughlin, M.M.; López, F.J. Plasma Biomarkers of the Amyloid Pathway Are Associated with Geographic Atrophy Secondary to Age-Related Macular Degeneration. *PLoS ONE* **2020**, *15*, e0236283. [CrossRef]

4. Pujol-Lereis, L.M.; Schäfer, N.; Kuhn, L.B.; Rohrer, B.; Pauly, D. Interrelation Between Oxidative Stress and Complement Activation in Models of Age-Related Macular Degeneration. *Adv. Exp. Med. Biol.* **2016**, *854*, 87–93.

5. Datta, S.; Cano, M.; Ebrahimi, K.; Wang, L.; Handa, J.T. The Impact of Oxidative Stress and Inflammation on RPE Degeneration in Non-Neovascular AMD. *Prog. Retin. Eye Res.* **2017**, *60*, 201–218. [CrossRef] [PubMed]

6. Ambati, J.; Atkinson, J.P.; Gelfand, B.D. Immunology of Age-Related Macular Degeneration. *Nat. Rev. Immunol.* **2013**, *13*, 438–451. [CrossRef]

7. Reisenhofer, M.H.; Balmer, J.M.; Enzmann, V. What Can Pharmacological Models of Retinal Degeneration Tell Us? *Curr. Mol. Med.* **2017**, *17*, 100–107. [CrossRef] [PubMed]

8. Kannan, R.; Hinton, D.R. Sodium Iodate Induced Retinal Degeneration: New Insights from an Old Model. *Neural Regen. Res.* **2014**, *9*, 2044–2045.

9. Hanus, J.; Anderson, C.; Sarraf, D.; Ma, J.; Wang, S. Retinal Pigment Epithelial Cell Necroptosis in Response to Sodium Iodate. *Cell Death Discov.* **2016**, *2*, 16054. [CrossRef] [PubMed]

10. Enzmann, V.; Row, B.W.; Yamauchi, Y.; Kheirandish, L.; Gozal, D.; Kaplan, H.J.; McCall, M.A. Behavioral and Anatomical Abnormalities in a Sodium Iodate-Induced Model of Retinal Pigment Epithelium Degeneration. *Exp. Eye Res.* **2006**, *82*, 441–448. [CrossRef] [PubMed]

11. Balmer, J.; Zulliger, R.; Roberti, S.; Enzmann, V. Retinal Cell Death Caused by Sodium Iodate Involves Multiple Caspase-Dependent and Caspase-Independent Cell-Death Pathways. *Int. J. Mol. Sci.* **2015**, *16*, 15086–15103. [CrossRef]

12. Li, Y.; Reca, R.G.; Atmaca-Sonmez, P.; Ratajczak, M.Z.; Ildstad, S.T.; Kaplan, H.J.; Enzmann, V. Retinal Pigment Epithelium Damage Enhances Expression of Chemoattractants and Migration of Bone Marrow-Derived Stem Cells. *Investig. Ophthalmol. Vis. Sci.* **2006**, *47*, 1646–1652. [CrossRef] [PubMed]

13. Moriguchi, M.; Nakamura, S.; Inoue, Y.; Nishinaka, A.; Nakamura, M.; Shimazawa, M.; Hara, H. Irreversible Photoreceptors and RPE Cells Damage by Intravenous Sodium Iodate in Mice Is Related to Macrophage Accumulation. *Investig. Ophthalmol. Vis. Sci.* **2018**, *59*, 3476–3487. [CrossRef] [PubMed]

14. Hwang, N.; Kwon, M.-Y.; Woo, J.M.; Chung, S.W. Oxidative Stress-Induced Pentraxin 3 Expression Human Retinal Pigment Epithelial Cells Is Involved in the Pathogenesis of Age-Related Macular Degeneration. *Int. J. Mol. Sci.* **2019**, *20*, 6028. [CrossRef]

15. Hadziahmetovic, M.; Pajic, M.; Grieco, S.; Song, Y.; Song, D.; Li, Y.; Cwanger, A.; Iacovelli, J.; Chu, S.; Ying, G.-S.; et al. The Oral Iron Chelator Deferiprone Protects Against Retinal Degeneration Induced through Diverse Mechanisms. *Transl. Vis. Sci. Technol.* **2012**, *1*, 2. [CrossRef] [PubMed]

16. Bhutto, I.A.; Ogura, S.; Baldeosingh, R.; McLeod, D.S.; Lutty, G.A.; Edwards, M.M. An Acute Injury Model for the Phenotypic Characteristics of Geographic Atrophy. *Investig. Ophthalmol. Vis. Sci.* **2018**, *59*, AMD143–AMD151. [CrossRef]

17. Yang, Y.; Ng, T.K.; Ye, C.; Yip, Y.W.Y.; Law, K.; Chan, S.-O.; Pang, C.P. Assessing Sodium Iodate-Induced Outer Retinal Changes in Rats Using Confocal Scanning Laser Ophthalmoscopy and Optical Coherence Tomography. *Investig. Ophthalmol. Vis. Sci.* **2014**, *55*, 1696–1705. [CrossRef]

18. Franco, L.M.; Zulliger, R.; Wolf-Schnurrbusch, U.E.K.; Katagiri, Y.; Kaplan, H.J.; Wolf, S.; Enzmann, V. Decreased Visual Function after Patchy Loss of Retinal Pigment Epithelium Induced by Low-Dose Sodium Iodate. *Investig. Ophthalmol. Vis. Sci.* **2009**, *50*, 4004–4010. [CrossRef]

19. Machalińska, A.; Lejkowska, R.; Duchnik, M.; Kawa, M.; Rogińska, D.; Wiszniewska, B.; Machaliński, B. Dose-Dependent Retinal Changes Following Sodium Iodate Administration: Application of Spectral-Domain Optical Coherence Tomography for Monitoring of Retinal Injury and Endogenous Regeneration. *Curr. Eye Res.* **2014**, *39*, 1033–1041. [CrossRef]

20. Anderson, D.H.; Radeke, M.J.; Gallo, N.B.; Chapin, E.A.; Johnson, P.T.; Curletti, C.R.; Hancox, L.S.; Hu, J.; Ebright, J.N.; Malek, G.; et al. The Pivotal Role of the Complement System in Aging and Age-Related Macular Degeneration: Hypothesis Re-Visited. *Prog. Retin. Eye Res.* **2010**, *29*, 95–112. [CrossRef] [PubMed]

21. Pauly, D.; Agarwal, D.; Dana, N.; Schäfer, N.; Biber, J.; Wunderlich, K.A.; Jabri, Y.; Straub, T.; Zhang, N.R.; Gautam, A.K.; et al. Cell-Type-Specific Complement Expression in the Healthy and Diseased Retina. *Cell Rep.* **2019**, *29*, 2835–2848.e4. [CrossRef] [PubMed]

22. Mulfaul, K.; Ozaki, E.; Fernando, N.; Brennan, K.; Chirco, K.R.; Connolly, E.; Greene, C.; Maminishkis, A.; Salomon, R.G.; Linetsky, M.; et al. Toll-like Receptor 2 Facilitates Oxidative Damage-Induced Retinal Degeneration. *Cell Rep.* **2020**, *30*, 2209–2224.e5. [CrossRef] [PubMed]

23. Chen, M.; Muckersie, E.; Robertson, M.; Forrester, J.V.; Xu, H. Up-Regulation of Complement Factor B in Retinal Pigment Epithelial Cells Is Accompanied by Complement Activation in the Aged Retina. *Exp. Eye Res.* **2008**, *87*, 543–550. [CrossRef] [PubMed]

24. Grossman, T.R.; Carrer, M.; Shen, L.; Johnson, R.B.; Hettrick, L.A.; Henry, S.P.; Monia, B.P.; McCaleb, M.L. Reduction in ocular complement factor B protein in mice and monkeys by systemic administration of factor B antisense oligonucleotide. *Mol. Vis.* **2017**, *23*, 561–571.

25. Katschke, K.J., Jr.; Xi, H.; Cox, C.; Truong, T.; Malato, Y.; Lee, W.P.; McKenzie, B.; Arceo, R.; Tao, J.; Rangell, L.; et al. Classical and Alternative Complement Activation on Photoreceptor Outer Segments Drives Monocyte-Dependent Retinal Atrophy. *Sci. Rep.* **2018**, *8*, 7348. [CrossRef] [PubMed]

26. Chen, H.; Liu, B.; Lukas, T.J.; Neufeld, A.H. The Aged Retinal Pigment Epithelium/choroid: A Potential Substratum for the Pathogenesis of Age-Related Macular Degeneration. *PLoS ONE* **2008**, *3*, e2339. [CrossRef]

27. Luo, C.; Chen, M.; Xu, H. Complement Gene Expression and Regulation in Mouse Retina and Retinal Pigment Epithelium/choroid. *Mol. Vis.* **2011**, *17*, 1588–1597. [PubMed]

28. Coffey, P.J.; Gias, C.; McDermott, C.J.; Lundh, P.; Pickering, M.C.; Sethi, C.; Bird, A.; Fitzke, F.W.; Maass, A.; Chen, L.L.; et al. Complement Factor H Deficiency in Aged Mice Causes Retinal Abnormalities and Visual Dysfunction. *Proc. Natl. Acad. Sci. USA* **2007**, *104*, 16651–16656. [CrossRef]

29. Fett, A.L.; Hermann, M.M.; Muether, P.S.; Kirchhof, B.; Fauser, S. Immunohistochemical Localization of Complement Regulatory Proteins in the Human Retina. *Histol. Histopathol.* **2012**, *27*, 357–364.

30. Ma, W.; Zhang, Y.; Gao, C.; Fariss, R.N.; Tam, J.; Wong, W.T. Monocyte Infiltration and Proliferation Re-establish Myeloid Cell Homeostasis in the Mouse Retina Following Retinal Pigment Epithelial Cell Injury. *Sci. Rep.* **2017**, *7*, 8433. [CrossRef]

31. Sachdeva, M.M.; Cano, M.; Handa, J.T. Nrf2 Signaling Is Impaired in the Aging RPE given an Oxidative Insult. *Exp. Eye Res.* **2014**, *119*, 111–114. [CrossRef] [PubMed]

32. Mao, X.; Pan, T.; Shen, H.; Xi, H.; Yuan, S.; Liu, Q. The Rescue Effect of Mesenchymal Stem Cell on Sodium Iodate-Induced Retinal Pigment Epithelial Cell Death through Deactivation of NF-κB-Mediated NLRP3 Inflammasome. *Biomed. Pharmacother.* **2018**, *103*, 517–523. [CrossRef]

33. Dobin, A.; Davis, C.A.; Schlesinger, F.; Drenkow, J.; Zaleski, C.; Jha, S.; Batut, P.; Chaisson, M.; Gingeras, T.R. STAR: Ultrafast Universal RNA-Seq Aligner. *Bioinformatics* **2013**, *29*, 15–21. [CrossRef]

34. Ritchie, M.E.; Phipson, B.; Wu, D.; Hu, Y.; Law, C.W.; Shi, W.; Smyth, G.K. Limma powers differential expression analyses for RNA-sequencing and microarray studies. *Nucleic Acids Res.* **2015**, *43*, e47. [CrossRef] [PubMed]

35. Law, C.W.; Chen, Y.; Shi, W.; Smyth, G.K. Voom: Precision weights unlock linear model analysis tools for RNA-seq read counts. *Genome Biol.* **2014**, *15*, R29.

36. Phipson, B.; Lee, S.; Majewski, I.J.; Alexander, W.S.; Smyth, G.K. Robust hyperparameter estimation protects against hypervariable gens and improves power to detect differential expression. *Ann. Appl. Stat.* **2016**, *10*, 946–963.

37. Jabri, Y.; Biber, J.; Diaz-Lezama, N.; Grosche, A.; Pauly, D. Cell-Type-Specific Complement Profiling in the ABCA4 Mouse Model of Stargardt Disease. *Int. J. Mol. Sci.* **2020**, *21*, 8468. [CrossRef]

38. Schäfer, N.; Grosche, A.; Schmitt, S.I.; Braunger, B.M.; Pauly, D. Complement Components Showed a Time-Dependent Local Expression Pattern in Constant and Acute White Light-Induced Photoreceptor Damage. *Front. Mol. Neurosci.* **2017**, *10*, 197. [CrossRef]

Publication 4 – (Pauly, et al., 2019)

Cell-Type-Specific Complement Expression in the Healthy and Diseased Retina

Diana Pauly, Divyansh Agarwal,, Nicholas Dana, Nicole Schäffer, Josef Biber, Kirsten A. Wunderlich, Yassin Jabri, Tobias Straub, Nancy R. Zhang, Avneesh K. Gautam, Bernhard H.F. Weber, Stefanie M. Hauck, Mijin Kim, Christine A. Curcio, Dwight Stambolian, Mingyao Li, 1 and Antje Grosche

Cell-Type-Specific Complement Expression in the Healthy and Diseased Retina

Graphical Abstract
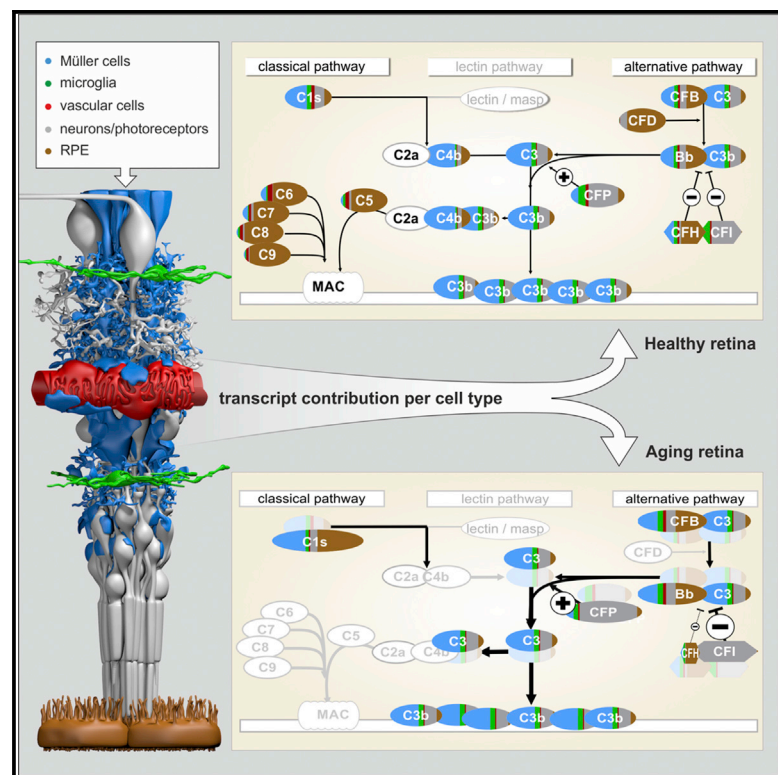
Authors

Diana Pauly, Divyansh Agarwal, Nicholas Dana, ..., Dwight Stambolian, Mingyao Li, Antje Grosche

Correspondence

diana.pauly@ukr.de (D.P.), antje.grosche@med.uni-muenchen.de (A.G.)

In Brief

Overshooting complement activity contributes to retinal degeneration. Pauly et al. demonstrate a distinct complement expression profile of retinal cell types that changes with aging and during retinal degeneration. This prompts the intriguing concept of a local retinal complement activation possibly independent of the systemic components typically produced by the liver.

Highlights

- Each retinal cell type expresses a specific signature of complement components

- Müller and RPE cells are the main source of retinal complement transcripts

- Components of the alternative and classical activating pathways were detected

- The cell-type-specific complement signature changes with aging and degeneration

CellPress

Cell-Type-Specific Complement Expression in the Healthy and Diseased Retina

Diana Pauly,[1,12,13,*] Divyansh Agarwal,[2,12] Nicholas Dana,[3] Nicole Schäfer,[1] Josef Biber,[4] Kirsten A. Wunderlich,[4] Yassin Jabri,[1] Tobias Straub,[5] Nancy R. Zhang,[6] Avneesh K. Gautam,[7] Bernhard H.F. Weber,[8] Stefanie M. Hauck,[9] Mijin Kim,[3] Christine A. Curcio,[10] Dwight Stambolian,[3] Mingyao Li,[11] and Antje Grosche[4,*]

[1]Experimental Ophthalmology, University Hospital Regensburg, Regensburg 93053, Germany
[2]Genomics and Computational Biology, Perelman School of Medicine, University of Pennsylvania, Philadelphia, PA 19104, USA
[3]Department of Ophthalmology, Perelman School of Medicine, University of Pennsylvania, Philadelphia, PA 19104, USA
[4]Department of Physiological Genomics, Biomedical Center, Ludwig Maximilians University Munich, Planegg-Martinsried 82152, Germany
[5]Core Facility Bioinformatics, Biomedical Center, Ludwig Maximilians University Munich, Planegg-Martinsried 82152, Germany
[6]Department of Statistics, The Wharton School, University of Pennsylvania, Philadelphia, PA 19104, USA
[7]Department of Medicine, Immunology and Allergy, Brigham and Women's Hospital, Harvard Medical School, Boston, MA 02115, USA
[8]Institute of Human Genetics, University of Regensburg, Regensburg 93053, Germany
[9]Research Unit Protein Science, Helmholtz Center Munich, Research Center for Environmental Health (GmbH), Munich 80939, Germany
[10]Department of Ophthalmology and Visual Sciences, University of Alabama at Birmingham, Birmingham, AL 35294-0019, USA
[11]Department of Biostatistics, Epidemiology and Informatics, University of Pennsylvania Perelman School of Medicine, Philadelphia, PA 19104, USA
[12]These authors contributed equally
[13]Lead Contact
*Correspondence: diana.pauly@ukr.de (D.P.), antje.grosche@med.uni-muenchen.de (A.G.)
https://doi.org/10.1016/j.celrep.2019.10.084

SUMMARY

Complement dysregulation is a feature of many retinal diseases, yet mechanistic understanding at the cellular level is limited. Given this knowledge gap about which retinal cells express complement, we performed single-cell RNA sequencing on ~92,000 mouse retinal cells and validated our results in five major purified retinal cell types. We found evidence for a distributed cell-type-specific complement expression across 11 cell types. Notably, Müller cells are the major contributor of complement activators *c1s*, *c3*, *c4*, and *cfb*. Retinal pigment epithelium (RPE) mainly expresses *cfh* and the terminal complement components, whereas *cfi* and *cfp* transcripts are most abundant in neurons. Aging enhances *c1s*, *cfb*, *cfp*, and *cfi* expression, while *cfh* expression decreases. Transient retinal ischemia increases complement expression in microglia, Müller cells, and RPE. In summary, we report a unique complement expression signature for murine retinal cell types suggesting a well-orchestrated regulation of local complement expression in the retinal microenvironment.

INTRODUCTION

Single-nucleotide polymorphisms in complement genes are associated with a number of retinal diseases, including glaucoma (Scheetz et al., 2013), age-related macular degeneration (AMD) (Weber et al., 2014), and diabetic retinopathy (Yang et al., 2016; Wang et al., 2013). The immune-privileged retina is among others under regular immune surveillance by proteins of the complement system. Although systemic complement is known to perform homeostatic functions that include opsonization for phagocytosis, formation of membrane attack complexes (MACs), and recruitment of immune cells (Merle et al., 2015), the local regulation of complement within the cellular architecture of the neurosensory retina is poorly understood. Current evidence suggests that complement components are locally expressed in the retinal pigment epithelium (RPE) (Schäfer et al., 2017; Luo et al., 2011; Anderson et al., 2010; Tian et al., 2015; Li et al., 2014; Rutar et al., 2012) as well as microglia (Rutar et al., 2012) and could be independent of the systemic complement, which is produced in hepatocytes and distributed via the bloodstream. A retinal complement system may help facilitate a rapid response to microbial invasion and disposal of damaged cells despite an intact blood-retina barrier.

Upregulation of complement expression, subsequent protein deposition, and MAC formation have been demonstrated in the normal aging (Chen et al., 2010; Ma et al., 2013; Chen et al., 2008) and diseased retina (Crabb, 2014; Sudharsan et al., 2017; Radu et al., 2011; Zhang et al., 2002; Kuehn et al., 2008). In fact, complement components present in extracellular deposits (termed "drusen") are the hallmark of AMD (Crabb, 2014). Consequently, it is tempting to speculate that a source of complement components during aging could be the retina/RPE itself, as animal studies have shown increased retinal expression of *c1q*, *c3*, *c4*, and *cfb* in older mice (Ma et al., 2013; Chen et al., 2010). Complement upregulation has also been observed in retinitis pigmentosa (Sudharsan et al., 2017), Stargardt disease (Radu et al., 2011), and conditions associated with transient ischemic tissue damage, viz. diabetic retinopathy (Zhang et al., 2002) and glaucoma (Andreeva et al., 2014; Kuehn

et al., 2008; Kim et al., 2013). Despite a clear indication for a fundamental role of the complement system in the retina, it remains unknown which retinal cell populations shape complement homeostasis in the healthy, aging, and diseased retina.

The retina consists of more than 40 different cell types, which cooperate to capture, process, and transmit visual signals to the brain (Macosko et al., 2015; Tian et al., 2015; Rheaume et al., 2018; Shekhar et al., 2016). Our understanding of the healthy and diseased retina and its supporting tissues like the RPE and choriocapillaris has grown recently (Tian et al., 2015; Pinelli et al., 2016). Transcriptomic studies have focused on the whole retina or RPE but miss information about cell-type-specific transcription (Pinelli et al., 2016; Tian et al., 2015). Droplet-based single-cell RNA sequencing (scRNA-seq) has identified the molecular differences among retinal ganglion cells (Rheaume et al., 2018), bipolar cells (Shekhar et al., 2016), and Müller cells (Roesch et al., 2008), but these studies provided little insight into complement expression of the major retinal cell types and changes occurring with aging and degeneration.

Here, we profile complement expression at the single-cell level in the major 11 retinal cell types of the mouse and further validate these results in enriched Müller cells, vascular cells, microglia, neurons, and RPE cells. We observed a characteristic contribution of complement transcripts from distinct retinal cell populations. Our data suggest that the classical and alternative complement pathway could be activated solely by local complement production and thereby could induce C3 cleavage. CFH is the major complement inhibitor in the mouse retina; retinal stress consistently downregulates *cfh* expression. Moreover, cell-type-specific changes in complement expression differed in aging and acute retinal degeneration induced by transient ischemia, implying a stress-dependent and cell-type-specific modulation of retinal complement homeostasis mediated by the tissue itself.

RESULTS

Single-Cell RNA Sequencing Reveals Complement Component Expression across Multiple Cell Types

Retinal cells, ~92,000 total, were isolated from six male healthy C57BL/6J mice and separated for scRNA-seq (Macosko et al., 2015; Shekhar et al., 2016; Cheng et al., 2013b; Kim et al., 2008). Following sequencing, the data were analyzed using 30 principal components as input to the t-Distributed Stochastic Neighbor Embedding (t-SNE) method for dimension reduction and data visualization (Figures 1A and S1). Cells were classified into eleven major types based on established markers (Tables S1 and S2). We then mapped the expression of complement genes across all 11 cell types and observed a distributed expression of complement components across various resident cells in the retina (Figure 1B; Table S3). We detected cell-type-specific complement expression mainly in the classical pathway via scRNA-seq. Moreover, we mapped the cell-type-dependent expression of both soluble and membrane-bound complement regulators (Figure 1C; Table S3) and found main soluble regulators *cfh*, *vtn*, and *clu*. Cell types expressing complement regulators at the highest levels were Müller cells, pericytes, and endothelial cells. Complement receptors, which detect complement activa-

tion (anaphylatoxins or opsonins), were only expressed in microglia cells (Figure 1B; Table S3).

The results from scRNA-seq regarding complement component transcription were exemplary validated using RNA fluorescence *in situ* hybridization (FISH) (Figure 2). Complement component *c4* expression colocalized with *gfap*-positive astrocytes/Müller cells in the retinal ganglion cell layer (GCL) (Figure 2A), which correlated with scRNA-seq data (Figure 1B). The scRNA-seq data were also confirmed for complement regulator *cfi*, which was specifically detected in bipolar cells both by transcription analyses (Figure 1C) and via RNA-FISH (Figure 2B). Complement receptor *c1qbp* was detected in all cell populations in RNA sequencing (RNA-seq) (Figure 1B). In line with that, we found a colocalization of *c1qpb* transcripts with markers of microglia/macrophages (hereafter termed microglia) (*tmem119*) in the GCL (Figure 2C), but rather evenly distributed signals were detected in all retinal layers except for the inner nuclear layer (INL).

qPCR-Based mRNA Analyses of Purified Neurons, Müller Cells, Microglia, Vascular Cells, and RPE Decipher the Differentially Transcriptional Relevance of Retinal Cells

Though our single-cell analysis uncovered complement expression in different cell types, some complement components remained undetectable or were found in relatively rare cell types at the single-cell level (Table S3). Therefore, we further validated our results on Müller cells, microglia, vascular cells, and retinal neurons purified by immunomagnetic cell separation using quantitative real-time PCR. RPE was purified through manual scratching of eyecups from male and female albino BALB/c and pigmented C57BL/6 mice (Figure 3A) (Grosche et al., 2016). All five cell populations were characterized by the expression of specific marker genes (Figures 3A–3F).

Commonly used housekeeping genes showed high transcriptional and translational variability across different cell types (Figures S2A–S2D) except pyruvate dehydrogenase E1 component subunit beta (*pdhb*) (Figures S2E and S2F) and isocitrate dehydrogenase 3 (NAD+) beta (*idh3b*) (Figures S2G and S2H), which had relatively homogeneous expression levels. We decided to use *idh3b* to determine how distinct cell populations proportionally contributed to the total retinal complement transcriptome, because it showed expression levels similar to those of the complement genes, while *gapdh*, for example, was expressed at much higher levels and thus appeared to be less appropriate (Figure S2C). Based on *idh3b*, we estimate that the neuronal fraction contributes 60% of the total retina transcriptome and Müller cells contribute 25% (Figure 4A). Vascular cells and microglia expressed lower levels of *idh3b*, indicating low cell numbers and/or low transcription activity of these cell types in the mouse retina. Quantifying total RNA by RNA picochip analysis, we found similar RNA quantities in Müller cells (33%), neurons (26%), and the RPE/choroid fraction (22%) per mouse (Figure 4B). In accordance with these results, PDHB protein levels were relatively similar across Müller cells, neurons, and RPE cells (Figure 4C), whereas microglia and vascular cells showed weaker PDHB signals. In agreement with previous reports of cell counts in the mouse, we found neurons make
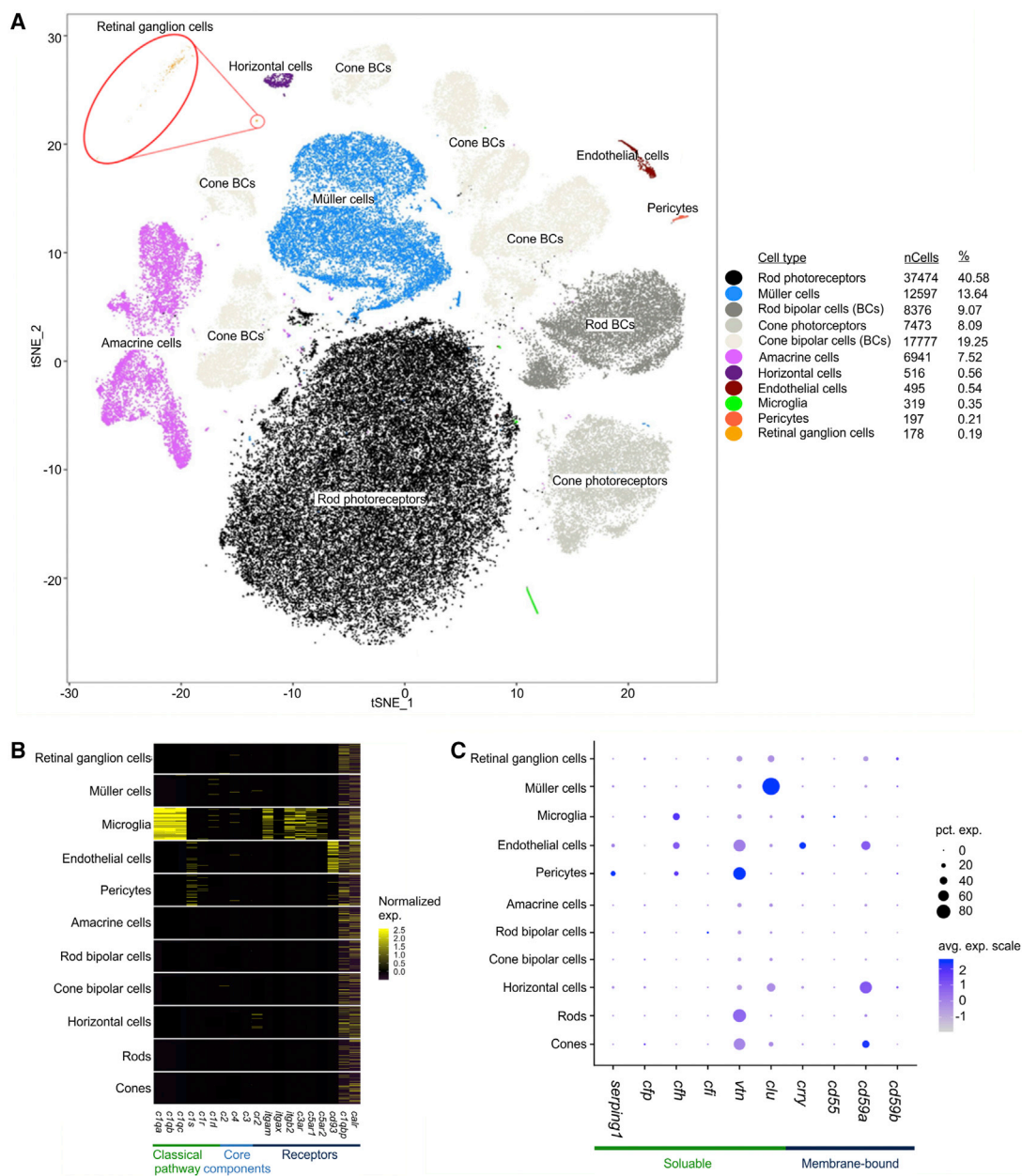
Figure 1. Single-Cell RNA-Seq of Murine Retina Reveals Complement Expression in Different Cell Types

Distribution of complement expression in normal mouse retina is delineated by single-cell transcriptomics.

(A) Using unsupervised clustering, we detect all 11 major cell classes in the mouse retina; the distinct cell types that passed quality control (described in STAR Methods) are shown in a t-SNE map (out of the 92,343 cells total, 91,798 cells passed the filter of having mitochondrial gene expression <50%, and 200 < unique gene counts <3,500). Percentages of assigned cell types are summarized in the right panel. BC, bipolar cell.

(B) Cell-type-specific expression of complement genes is shown in a heatmap. Mean expression values of the genes were calculated in each cluster by randomly subsampling a population of 100 cells for each cell type. Each row represents a retinal cell type, and each column corresponds to a gene.

(C) The expression of complement regulators among the various retinal cell types is shown by means of a dot plot. Cell types are arranged roughly by their location in the retina, from the inner layer (top) to the outer layer (bottom). The size of each circle (pct.exp) depicts the percentage of cells in which the gene was detected for a given cell type, and its color depicts the average transcript count in the expressing cells (avg.exp.scale).

See also Figure S1 and Tables S1–S3.

up 85%, RPE cells 13%, Müller cells 2%, and microglia and vascular cells are less than 1% of all retinal cell types (Figure 4D; Table S2) (Jeon et al., 1998). While Müller cells are a compara-

tively infrequent cell type (2%), they contribute up to one third of the total mRNA content in the retina (Figures 1A, 4A, 4B, and 4D; Table S2). Accordingly, our study provides important
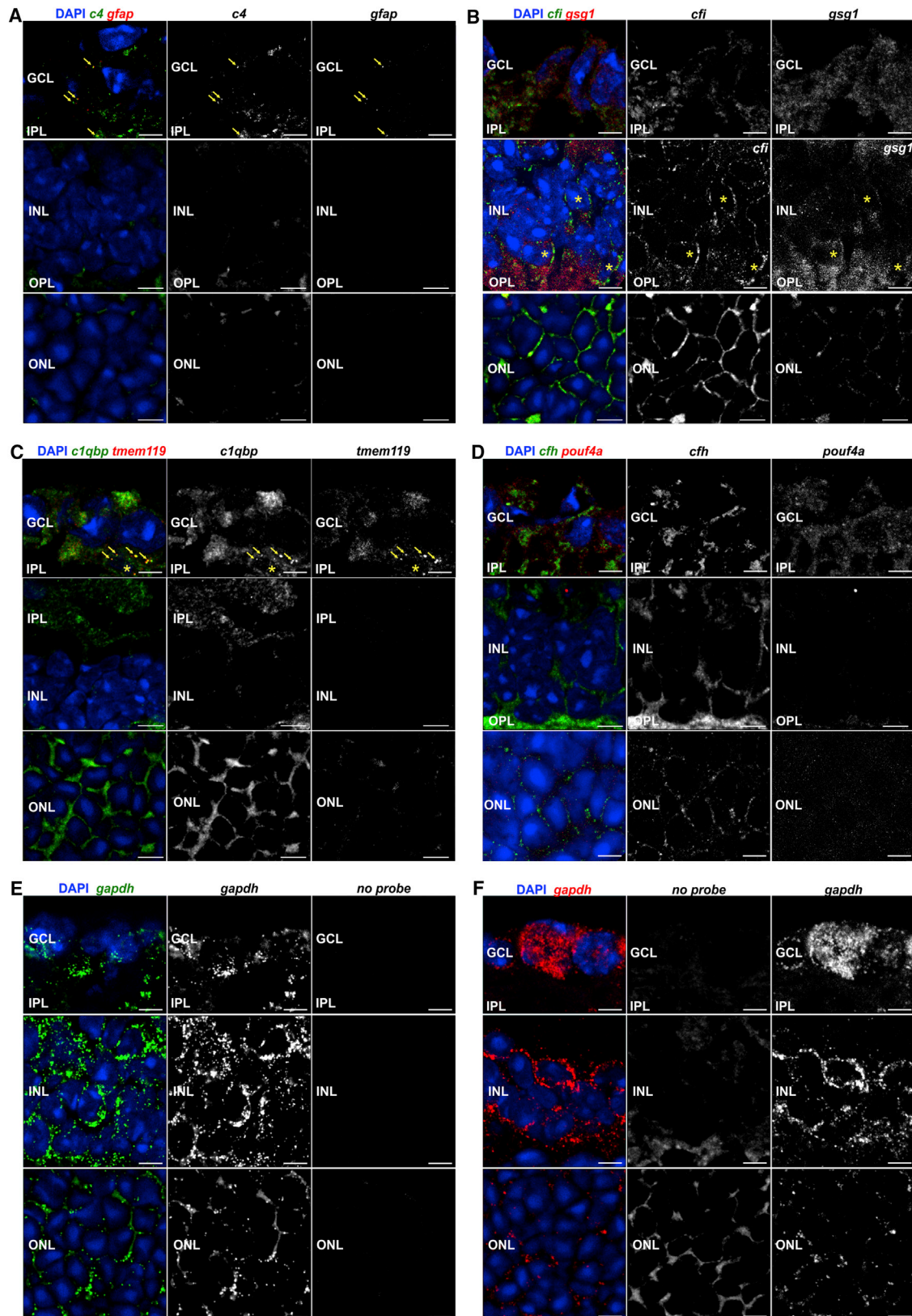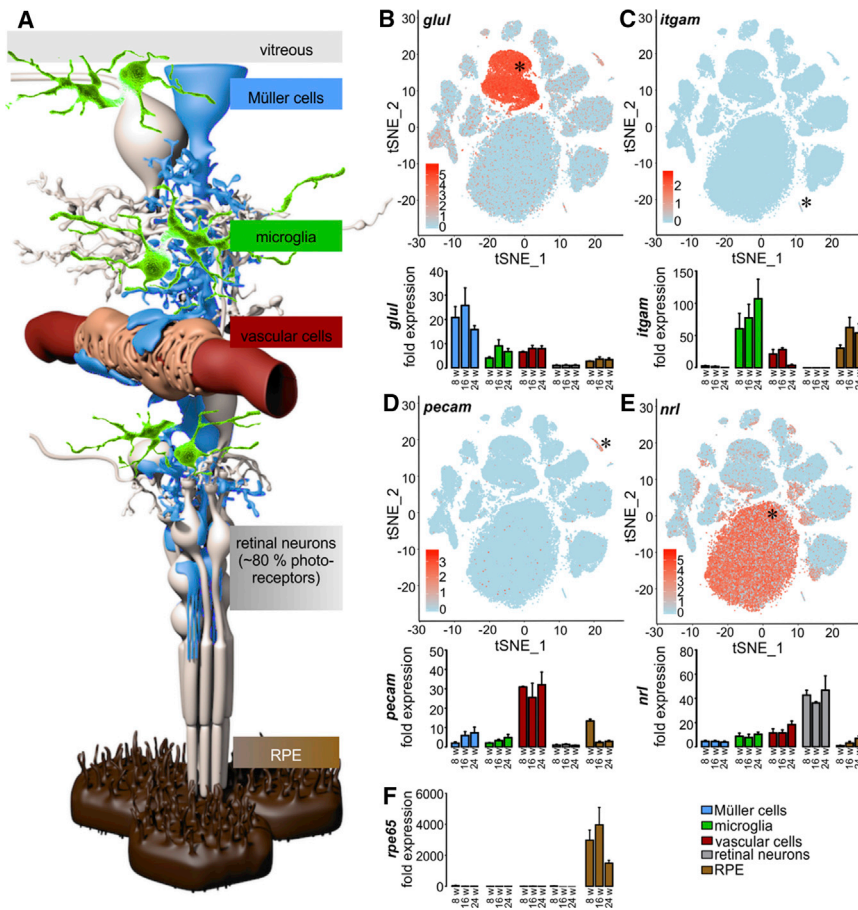
(legend on next page)

Figure 3. Validation of Enrichment of Different Retinal Cell Types

(A) Schematic view of distinct retinal cell types. Müller cells (blue), the central glia cells of the retina, are in direct contact with the vitreous and various retinal cell types: microglia (green), vascular cells (red), and neurons (gray). 80% of the retinal neurons are light-responsive photoreceptors that are supported by retinal pigment epithelial cells (RPE, brown).

(B) scRNA-seq data illustrating expression of glutamine synthetase (glul) across retinal cells (top panels). Murine retinal cell populations were enriched by immunomagnetic cell separation and characterized by quantitative real-time PCR using specific markers (bottom panels); Glul is a marker for the Müller cell fraction.

(C) Microglia (and putatively co-enriched macrophages) specifically express cd11b (itgam).

(D) Vascular cell enrichment was proven by strong expression of pecam.

(E) Retinal neurons were characterized by an enhanced detection of the photoreceptor-specific nrl mRNA compared to the other cell populations.

(F) Rpe65 was exclusively expressed in RPE/choroid. Exemplarily shown mean values ± SEM for cell preparations from BALB/c mice at 8, 16, and 24 weeks of age (n = 4–6 for each age).

See also Figure S2 and Table S7.

insight into the proportional transcriptional activities of these five major cell populations in the retina.

Retinal Cell Populations Express Unique Complement Signatures

Encouraged by the distributed complement expression pattern across 11 cell types (Figures 1B and 1C; Table S3), we hypothesized that specific retinal cell types shape the intraretinal complement homeostasis through expression of specific complement components. We selected six disease-associated genes (Schäfer et al., 2017; Weber et al., 2014) (c1s, c3, cfb, cfp, cfh, and cfi) and six supporting complement genes (c4, cfd, c5, c6, c7, c8, and c9) for further validation via quantitative real-time PCR and western blot (Figures 4E and 4F) and found that Müller cells contributed the most complement activator transcripts, expressing 47% of c1s, 67% of c4, and 54% of c3 retinal transcripts in 8-week-old mice (Figure 4E). Retinal neurons dominated the expression of the complement regulators cfi and cfp, while 59% of the cfh, 45% of the cfb,

Figure 2. Localization of Selected Complement Component Transcripts in the Healthy Retina ofPigmented 10-Week-Old Mice via Fluorescence In Situ Hybridization

(A) Spots indicative of c4 transcripts were detected in the GCL and clearly overlap with the very few particles positive for the astrocyte marker gfap (arrowheads). No transcripts of c4 or, as expected, the astrocyte marker gfap were detected in the INL or outer nuclear layer (ONL).

(B) Cfi expression was very weak in the GCL, with no clear association with cell somata, but was detected at a rather high level in the INL. There, signals partially overlapped with those of the bipolar marker gsg1 (asterisks). In the ONL, probes detecting cfi transcripts produced signals clearly above the autofluorescence background level. A clear distinction regarding whether cfi transcripts are localized in photoreceptors and/or in Müller glia that ensheathe photoreceptor somata in the ONL cannot be made.

(C) clqbp transcript was rather evenly distributed across the whole retina. A partial overlap with the microglia marker tmem119 in the GCL could be validated (arrowheads). Note that c1qbp transcripts were detected in the inner plexiform layer (IPL), but not in the INL.

(D) cfh transcripts were detected at low levels in the GCL and INL, and no clear overlap of signals with that of the ganglion cell marker pou4f1 was observed. It seemed to be more enriched in the outer plexiform layer (OPL). Similarly, cfh transcript levels are low in the ONL. The staining pattern could reflect an expression in Müller glia enwrapping photoreceptor somata.

(E and F) As positive control, probes conjugated either with (E) Quasar 670 (green) or (F) Quasar 570 (red) targeting transcripts of gapdh were used. Note the robust detection of the transcript especially in association with cell bodies, which confirms the high expression levels of gapdh detected via scRNA-seq. Autofluorescence background was detected in the recording channels if no appropriate probe was incubated with the tissue in the GCL, while some autofluorescence background was detected in the OPL and ONL if no appropriate probe was incubated with the tissue.
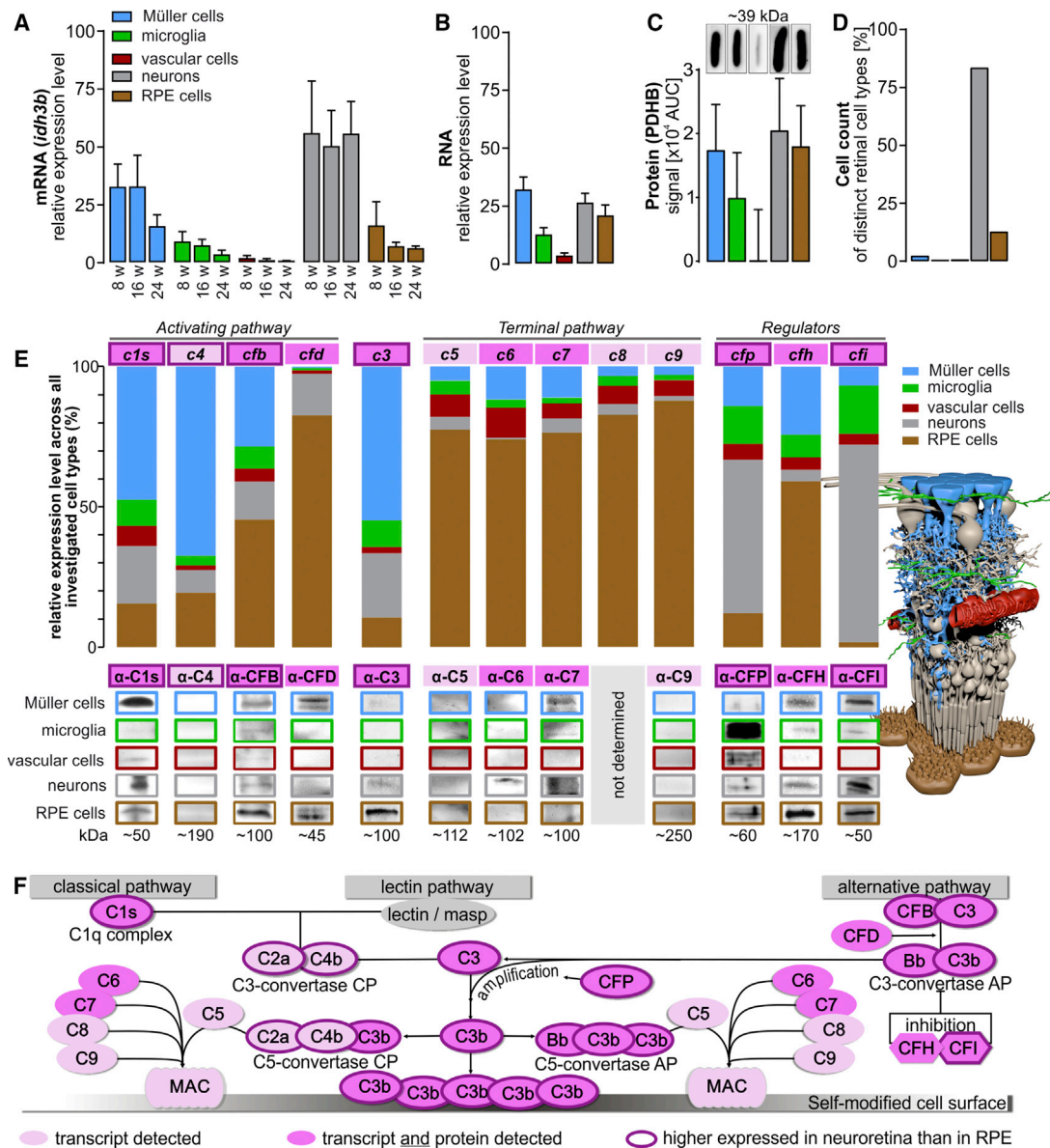
Scale bars, 5 μm.

Figure 4. Contribution of Retinal Cell Types to the Retinal Architecture, Expressome, and Complement Homeostasis

(A) mRNA expression of the housekeeping gene *idh3b* as determined in samples from retinal cell populations enriched from retinae of 8-, 16, and 24-week-old albino mice without adjusting the RNA input amount per cell type. This enables an estimate of the contribution of each cell type to the retinal transcriptome. Bars represent mean values ± SEM (n = 4–6).

(B) The total RNA amount isolated from retinal cell populations enriched from albino mice (8 to 16 weeks old) was investigated using picochip analysis. Bars represent mean values ± SEM (n = 5–8).

(C) Quantification of PDHB protein expression via western blots performed on five retinal cell types purified from 4–6 albino mice.

(D) Previously published (Jeon et al., 1998) and our own retinal cell counts in the healthy mouse retina.

(E) Expression levels of indicated complement components were determined from cells of albino mice at mRNA (bars, 8-week-old mice) and at protein level (western blot, 8- to 24-week -old mice). The overall contribution of each cell population to the local complement homeostasis was determined by analyzing the total yield of mRNA or protein derived from the respective cell population so that both are reflected by the data (expression level per cell type and the number of cells per cell type present in the retina).

(F) Scheme of the complement system that can be activated via three different mechanisms and is enhanced by an amplification loop. Note that complement components only detected at the transcript level are delineated in pink, and those that were also confirmed at the protein level are shown in dark pink. Complement components with higher expression in retinal cell types compared to the RPE/choroid fraction are pinpointed by a thick outline. CP, classical pathway; AP, alternative pathway.
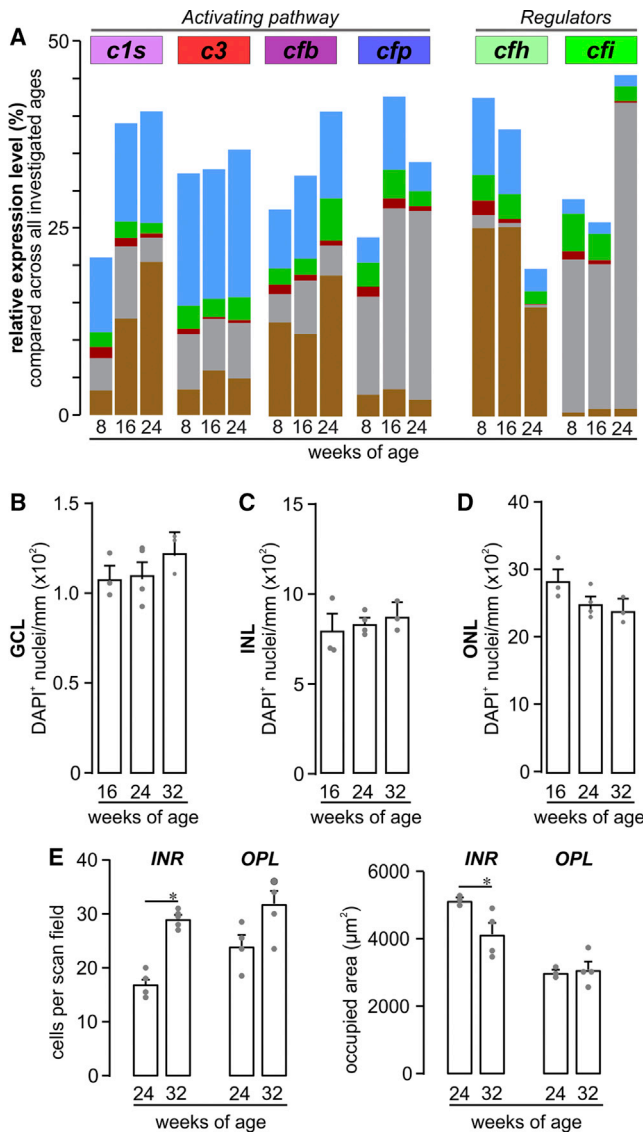
See also Figures S2 and S3 and Table S7.

Figure 5. Retinal Phenotype and Complement Homeostasis in Aging Albino Mice

(A) Expression levels of *c1s*, *c3*, *cfb*, *cfp*, *cfh*, and *cfi* were determined from cells of albino mice at the mRNA level (bars) at the indicated ages. The overall putative contribution of each cell population to the local complement homeostasis was determined by analyzing the total yield of mRNA derived from the respective cell population.

(B–D) The quantities of DAPI$^+$ cell nuclei in the (B) GCL, (C) INL, and (D) ONL were comparable in 16- to 32-week-old albino retinae.

(E) Left: microglia were quantified in the inner retinal layers (INR) such as ganglion cell and inner plexiform layer and additionally in the outer plexiform layer (OPL) on basis of Iba1 labeling in mice of the indicated age. Right: the area occupied by processes of a single microglia was measured as exemplarily depicted by the dashed circles of different color for OPL microglia in (D). Bars represent mean values ± SEM from 2–4 animals. *p < 0.05, **p < 0.01, Mann-Whitney *U* test. See also Figure S2 and Table S7.

and 82% of the *cfd* mRNA and *c5*–*c9* transcripts responsible for the terminal MAC were detected in RPE. Despite the relatively low number of microglia, the resident immune cells of the retina

contributed proportionally more *cfh* mRNA and a similar amount of *cfb* transcripts to the retinal complement population compared with retinal neurons.

We confirmed expression of complement activator C1s, CFB, and CFP proteins in all enriched murine cell populations (Figure 4E). Complement C3 protein was detected in RPE, Müller cells, and neurons, while the complement inhibitor CFH and CFI proteins were present in all cell types except the vascular cell population. Alternative pathway protease CFD was identified in the Müller cell and RPE fraction, while C6 was only found in neurons and C7 was detected in Müller cells and neurons. We could not detect C4, C5, and C9 proteins in any of the retinal cell populations (Figure 4E). For C8, no specific antibody was commercially available. There was an overlap in the complement transcript levels determined by quantitative real-time PCR and that of the complement proteins detected in various cell populations. For example, the strong *c1s* mRNA expression found in Müller cells matched the robust C1s protein levels, and *cfd* mRNA expression corresponded with CFD protein detection in RPE. Interestingly, neurons expressed ~40% of the total *cfp* mRNA, whereas CFP protein levels were highest in microglia (Figure 4E). This may imply a spatial separation of complement component transcription and complement component accumulation at the protein level within the retina.

Age-Dependent Changes in the Complement Expression of Different Retinal Cell Populations

We further investigated age-dependent changes in expression levels of known disease associated complement transcripts via quantitative real-time PCR among the different retinal cell populations in mice from 8 to 24 weeks of age. *C1s*, *cfb*, *cfp*, and *cfi* transcripts increased with age among all cell populations (Figure 5A). Upregulated *c1s* expression in RPE cells lead to doubling of the total retinal *c1s* mRNA between 8 and 24 weeks (Figure 5A). Transcripts of the alternative pathway activator *cfb*, primarily produced by Müller cells and RPE, increased at 16 and 24 weeks of age. The largest increase in *cfb* transcript levels (2.6-fold) was found in the microglial population between 8 and 24 weeks (Figure 5A). The highest proportional contribution of *cfp* retinal transcripts came from neurons (55%) at 8 weeks of age, and this contribution further increased to 73% at 16/24 weeks of age (Figure 5A). In contrast, *c3* expression remained relatively stable (Figure 4E), except for the vascular cell population, where the *c3* levels dropped by 50% between 8- and 24-week-old mice (Figure 5A).

CFH is the main negative regulator of the complement system. We found that *cfh* expression decreased by 50% in all cell populations in 24-week-old mice compared to 8-week-old mice. In 24-week-old mice, RPE cells produced the majority of the retinal *cfh* (Figure 5A), although the majority of the *cfi* transcripts (which act together with CFH) were produced by neurons, specifically rod bipolar cells (Figures 1C and 5A). Together with its functional counterpart, *cfp*, the expression of *cfi* also increased in neurons of 24-week-old mice compared to the 8- and 16-week-old mice (Figure 5A).

These divergent changes in the local complement expression in the retina of aging mice were not accompanied by any detectable retinal cell loss (Figures 5B–5D) but were accompanied by
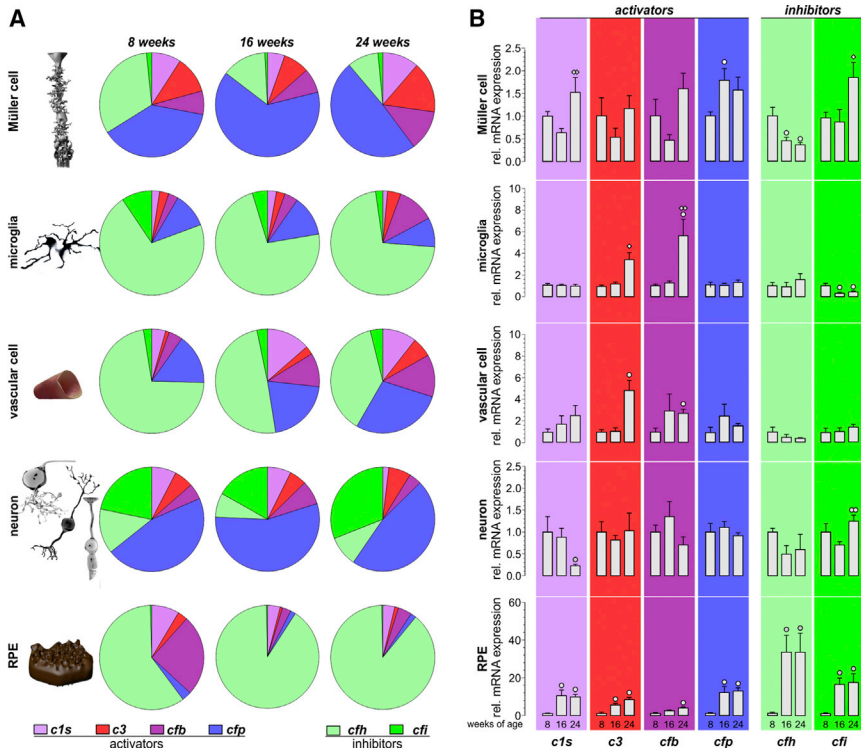
130

Figure 6. Comparison of Complement Component Expression between Retinal Cell Types of Aging Mice

(A) Expression of complement components was determined by quantitative real-time PCR. Diagrams represent the relative amount of transcripts per cell (normalized to the *idh3b* housekeeper expression) of the different complement components in the respective cell type enriched from mice at the indicated age. Note the high expression level of inhibitory complement factors in RPE/choroid samples as well as in microglial and vascular cells, while complement-activating genes appear to dominate in Müller cells and neurons. Data were collected from 4–6 wild-type albino mice (numbers are given in Table S4).

(B) Complement expression analysis by quantitative real-time PCR was performed on enriched retinal cell types from 8-, 16-, and 24-week-old mice. Bars represent mean values ± SEM of cells purified from 4–6 animals. Mann-Whitney *U* testing was performed on all data. A circle indicates a significant difference compared to the expression level at 8 weeks of age; whereas a diamond indicates a significant difference compared to the expression level at 16 weeks of age. °/◇ $p < 0.05$; °°/◇◇ $p < 0.01$.

See also Figure S2 and Table S7.

increased microglia numbers (Figure 5E) and enhanced microglial activation, as suggested by a decreased occupied area of microglial processes (Figure 5E).

A Characteristic Proportion of Activating and Inhibiting Complement Transcripts in Distinct Retinal Cell Types

Having noted a cell-type-specific complement expression in our data, we sought to understand the balance of complement activator and inhibitor expression in the different cell types by normalizing complement expression levels to the housekeeping gene to allow a comparison between cell populations independent of cell counts (Figure 6). Strikingly, we discovered that certain cell types like RPE and microglia mainly express inhibitory complement components (*cfh* and *cfi*), whereas other cell populations, such as neurons and Müller cells, mostly express complement activators (*c1s*, *c3*, *cfb*, and *cfp*) (Figure 6A). Interestingly, neurons expressed more *cfi* than *cfh* than the remaining cell types (Figure 6A).

Finally, we checked for age-dependent changes in the expression of the respective complement components—now, in contrast to results presented in Figure 5A, independent of putative changes in cell numbers. We could confirm a significant upregulation of complement activators such as *c1s*, *c3*, *cfb*, and *cfp* with increasing age (Figure 6B). Most of these changes were detected in RPE cells but at later stages (e.g., 24-week-old mice) also in microglia, vascular, and Müller cells. Expression changes of complement inhibitors were not consistent across cell types. While *cfh* was significantly downregulated in Müller glia in mice at 16 weeks of age, it was upregulated in RPE. More-

over, *cfi* was significantly downregulated in microglia but upregulated in Müller glia, retinal neurons, and RPE.

The spatial distribution of complement activators and regulators signifies a unique complement signature for each retinal cell type that was dynamically changing, even though relatively short intervals of aging were investigated.

Acute Ischemic Retinal Injury Triggers Robust Cell-Type-Specific Complement Expression

Retinal tissue injury is a common manifestation of retinal disease. To evaluate how tissue injury might change cell-type-specific complement expression, we used a retinal ischemia/reperfusion (I/R) injury model to induce acute retinal degeneration (Wagner et al., 2017). We found a significant increase in the expression of complement activators 24 h post-ischemia in the different isolated cell populations (Figure 7). Consistent with our previous results, *cfi* appeared to be the main complement inhibitor in neurons, whereas *cfh* was the major complement inhibitor expressed in the remaining cell populations. Compared to aging retina (Figures 5 and 6), the upregulation of *c1s*, *c3*, *cfb*, and *cfi* transcript expression of was more pronounced in post-ischemic retina at the mRNA level (Figures 7A–7C). Interestingly, this response in *c1s*, *c3*, and *cfb* expression was provoked by changes in the RPE. Moreover, *cfh* and *cfi* showed again a mutually opposite pattern of expression changes whereby *cfh* mRNA decreased and *cfi* increased in I/R retinae (Figure 7C). Detection of C3 (Figure 7D) and C1s (Figure 7E) at protein level via immunolabeling 3 days after the ischemic tissue injury was performed to enable detection of newly formed protein. C1s puncta were evenly distributed over all retinal layers, with a slight enrichment
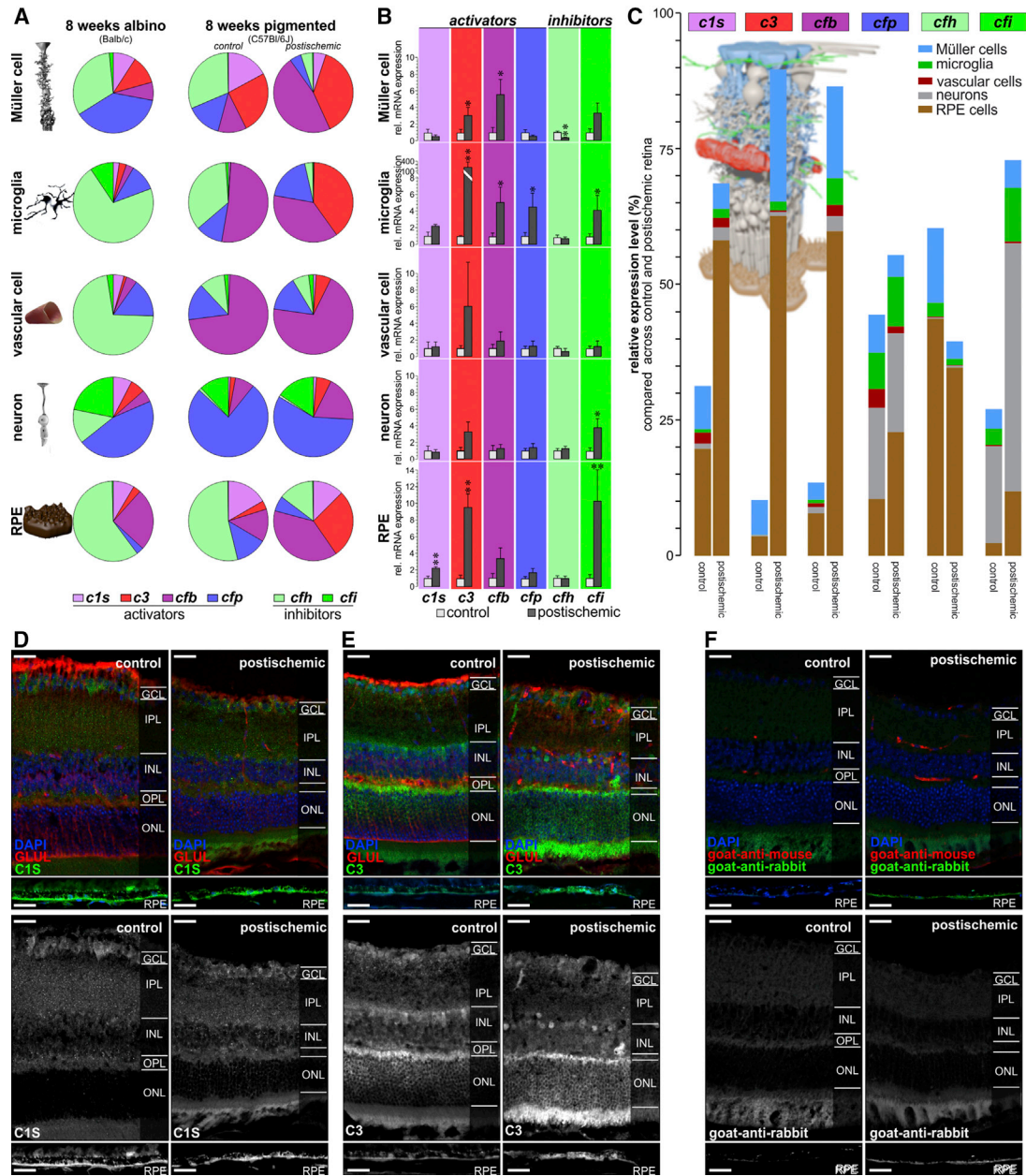
Figure 7. Transient Ischemic Stress Results in Cell-Type-Specific Upregulation of Transcripts from Activating Complement Components and Downregulation of *cfh*

(A) The relative amount of complement transcripts per retinal cell type indicated that complement-activating transcripts are more abundant in pigmented mice than in albino mice in which transcripts of complement inhibitors dominate at the same age. Note the strong relative upregulation and the resulting shift toward transcripts from complement activators 24 h after transient ischemic retinal stress in all retinal cell types of C57BL/6 mice (numbers are given in Table S5).

(B) Major changes of local complement expression (normalized to the housekeeper) were detected by quantitative real-time PCR 24 h after transient ischemia. The most pronounced upregulation of complement activators was found in Müller cells (*c3* and *cfb*), microglia (*c3*, *cfb*, and *cfp*) and RPE (*c1s* and *c3*). *Cfh* was downregulated in Müller cells, while *cfi* was upregulated in all investigated cell types. Significantly different expression as compared to that cells from healthy control eyes is indicated (*p < 0.05, **p < 0.01, Mann-Whitney *U* test).

(C) Complement transcript contribution of the different retinal cell populations (no normalization to the housekeeper and no adjustment of RNA input) indicated a pro-inflammatory milieu in the post-ischemic retina. Müller cells, microglia, and RPE cells mainly contributed to the changed complement homeostasis in post-ischemic retinae.

(legend continued on next page)

in the GCL and RPE (Figure 7D). Similarly, C3 labeling was observed in all retinal layers, and a moderate rise in labeling intensity could be observed 3 days after the ischemic tissue injury, especially in the outer retina affecting photoreceptors and RPE (Figure 7E). Complement components are typically secreted by the producing cells. In line with this fact, we did not find a perfect cell-type-specific match of protein distribution compared to the transcript signatures described above. It has to be considered that ischemic damage may lead to transient breakdown of the blood retinal barrier and that the complement components detected via this approach could also be derived from the systemic complement system, at least in post-ischemic tissue.

DISCUSSION

Since the retina is an immune-privileged tissue, understanding its local complement system is critical to our understanding of retinal inflammation. To identify the retinal cell types expressing complement, we isolated and sequenced ~92,000 cells from healthy mouse retinae. scRNA-seq was validated by RNA-FISH analysis for selected genes and 12 complement components by assays of RNA and protein in enriched cell populations of Müller cells, microglia, vascular cells, retinal neurons, and RPE. Collectively, our results show that complement components are locally expressed by different retinal cell populations, challenging the conventional belief that the complement source in the retina is confined to resident immune cells. We detected complement transcripts and proteins that were produced at higher levels in the neuroretina than in RPE that would be sufficient to activate the classical and/or alternative complement pathway. In consequence, cleavage of C3 into its anaphylatoxin C3a and opsonin C3b could be performed independently of blood-derived complement components (Figure 4F). Complement transcripts of the components that are key to MAC assembly were primarily detected in RPE and rarely found as proteins in the neuroretina. The RPE forms the outer retina-blood barrier, which is able to secrete substrates not only toward the subretinal space (apical) but also toward the choroidal side (basal). Considering its complement expression profile and the largely understudied idea of a context-specific apical or basal secretion pattern of complement by RPE sitting at the blood-retinal interface, it is tempting to speculate that by doing so, the RPE could actively shape the complement homeostasis of the retina, which needs to be addressed in future studies.

Given the cell-specific ratios of activating and inhibiting complement component expression levels, each cell type appears to have a specific role in maintaining retinal complement homeostasis. Moreover, cell populations present in the retina at relatively low numbers, such as microglia and Müller cells (Jeon et al., 1998), seem to have a major impact on retinal complement expression levels. We found that these cells contribute substantially to the total retinal transcriptome. This suggests that quan-

tification of cell numbers alone is insufficient to draw conclusions about the contribution of cellular activity to the global expression profile of the retina. Nonetheless, it has been shown that transcription is tightly regulated according to cell size, and cells with larger cell bodies, such as Müller cells, can provide more mRNA than the more abundant cells with a smaller volume (e.g., neurons and RPE) (Marguerat and Bähler, 2012; Kempe et al., 2015).

The complement system helps maintain normal ocular functions (Sohn et al., 2003, 2000), and its dysregulation significantly influences retinal disease (Sudharsan et al., 2017; Radu et al., 2011; Weber et al., 2014; Yang et al., 2016; Scheetz et al., 2013). Although earlier studies have found low background expression of complement in retinal microglia (Luo et al., 2011; Schäfer et al., 2017; Anderson et al., 2010; Rutar et al., 2012) and RPE/choroid (Schäfer et al., 2017; Luo et al., 2011, 2013), our results unequivocally show that other cell types are capable of local complement production. We did observe expression differences between the scRNA-seq and the MACS-enriched cell populations that can be explained by the lower sensitivity to detect gene expression compared to quantitative real-time PCR. For instance, compared to the single-cell analysis, quantitative real-time PCR allowed us to more readily detect the expression of *c1s* and *c3* in Müller cells, *cfp* in microglia and vascular cells, *cfb* in all major retinal cell types, and *cfd*, *c5–c9* mainly in RPE cells. Still, both approaches converged in their assessment of cell-type-specific expression for most complement components. Our results also add to previous work on retinal complement in humans (Tian et al., 2015; Li et al., 2014; Anderson et al., 2010), mice (Schäfer et al., 2017; Luo et al., 2011), and rats (Rutar et al., 2012) by also detecting protein expression for nine complement components that reflect their RNA expression.

The regulation of complement expression in whole-cell populations from the aging retina largely matched the changes we calculated for the normalized cellular expression rates in the distinct cell types. This implies that expression changes were driven by changes at the transcriptional level, not by changes in cell numbers, in accordance with the data from our morphometric analyses performed on aging BALB/c mice. Interestingly, the relative expression of all tested complement components increased in the whole-RPE-cell population with increasing age, except for *cfh*, whose expression decreased. We speculate that increased single-cell *cfh* expression alone is unable to counterbalance the overall age-associated RPE dysfunction and/or degeneration (as also indicated by a reduced *rpe65* expression). Accordingly, RPE-dependent *cfh* transcripts decrease at 24 weeks, the putative contribution of *cfh* in regulating the alternative complement pathway in the retinal microenvironment could be diminished, and the intraretinal milieu could be misbalanced.

We also discovered that healthy neurons produce the complement regulators *cfp* and *cfi*. The relevance of these complement

---

(D) Representative immunostaining of complement component C1S and C3 in the healthy and post-ischemic pigmented retina 3 days after injury. Sections were co-labeled for the Müller cell marker glutamine synthetase (GLUL), and nuclei were visualized by DAPI co-labeling.

(E) Representative micrographs of retinal sections incubated with the combination of secondary antibodies and DAPI only.

GCL, ganglion cell layer; IPL, inner plexiform layer; INL, inner nuclear layer; OPL, outer plexiform layer; ONL, outer nuclear layer; RPE, retinal pigment epithelium. Scale bars, 20 μm. In (A) and (B), data were collected from 3 – 5 animals. See also Figure S2 and Table S7.

components has already been shown for AMD (Fritsche et al., 2016; Weber et al., 2014; Micklisch et al., 2017). In murine models of retinal degeneration, *cfi* expression increases after polyethylene-glycol-induced insult, whereas *cfp* expression decreases in the light-damaged retina (Schäfer et al., 2017; Lyzogubov et al., 2014). Our single cell analysis demonstrated that *cfi* mRNA localizes specifically to rod bipolar cells and protein detection to neurons and Müller cells in mice. CFI inactivates the complement system, and the resulting cleavage products modulate the activity of phagocytes. Rods primarily govern scotopic vision, and mice have a rod-dominated retina similar to humans (except for the *fovea centralis*). This rod-bipolar-cell-specific *cfi* transcription in the mouse retina further suggests that the retinal complement system is influenced by functional and anatomical characteristics of the retina.

Age-related anatomical alterations in the retina have been demonstrated in histological analyses (Grossniklaus et al., 2013). Consistent with previous results (Damani et al., 2011; Friedman and Ts'o, 1968), we found increased microglial and decreased RPE marker gene expression with aging. In our study, the expression of complement transcripts *c1s*, *cfb*, *cfp*, and *cfi* increased while that of *cfh* decreased in retinal cells between 8 and 24 weeks of age. This indicates a role for complement in retinal adaptation during maturation and with processes of aging (Mukai et al., 2018). Although age-dependent upregulation of complement transcripts, including that of *c1q*, *c3*, *c4*, and *cfb*, in the retina has been described (Chen et al., 2010), our findings add a role for microglia in the expression of *c3* and *cfb*. Our results also show that Müller cells and neurons provide a substantial proportion of retinal complement transcripts and, thus, their impact on retinal complement homeostasis has likely been underestimated by past studies. Cell culture studies have suggested that Müller glia can produce C1q (Astafurov et al., 2014) and that complement activation products can regulate Müller cell activity via C5a-receptor and influence retinal disease (Cheng et al., 2013a). Our results show a direct involvement of Müller cells in the transcript expression of the retinal complement components, and it is likely that in the retina, similar to the brain, neurons and glia cells orchestrate complement-mediated maturation of nervous tissue via synaptic pruning, progenitor proliferation, and neuronal migration (Tenner et al., 2018). Aging and Alzheimer disease brains increase expression of *c1q*, *c3*, and *c4* (Walker and McGeer, 1992; Cribbs et al., 2012), which might point to a general mechanism of local complement function in the overall aging of the CNS.

Ischemia and subsequent reperfusion (e.g., upon treatment with anti-VEGF therapy) are associated with diabetic retinopathy (Silva et al., 2015; Traveset et al., 2016; Levin et al., 2017), and polymorphisms in CFB and CFH (Wang et al., 2013) have been implicated in modifying disease progression. We identified Müller cells as a major cell type involved in this process (by downregulating *cfh* transcripts and upregulating *cfb*) in the analysis of post-ischemic mouse retina. Gene profiling studies of whole mouse retinas also suggest an important role of the complement pathway in I/R-associated damage (Andreeva et al., 2014). Retinal *c1q*, *c1s*, *c1r*, *c2*, *c3*, *c4a*, and *cfh* expression has been reported after transient ischemia in mice (Kuehn et al., 2008; Kim et al., 2013; Andreeva et al., 2014). However,

it remains undetermined how individual retinal cell types modulate complement activity after retinal I/R injury. Here, we show that mainly Müller cells, microglia, and RPE increase *c3* and *cfb* expression following ischemia, while *cfp* is upregulated primarily in microglia. The complement inhibitor *cfi* also showed cell-type-specific enhanced mRNA levels in microglia, RPE, and retinal neurons, whereas expression of the complement inhibitor *cfh* was significantly reduced in Müller cells following ischemia. These expression changes suggest augmentation of local complement components following ischemia.

Genetic variation in several complement genes, such as CFH and CFI, are associated with AMD, glaucoma, and central serous retinopathy (Fritsche et al., 2016; Weber et al., 2014; Grassmann et al., 2016). CFI, along with cofactor CFH, regulates complement activity by degrading complement components C3b and C4b (Davis et al., 1984), thereby facilitating the cleavage of C3b into inactive fragments (Sim et al., 1993). We discovered a spatially distinct transcription pattern of *cfi* and its cofactor, *cfh*. *cfi* was mainly detected in retinal neurons (specifically rod bipolar cells), while *cfh* was detected primarily in vascular and RPE cells. Further, we found opposing transcriptional regulation of *cfi* and *cfh* during aging and ischemia. These findings hint at a CFH-independent function of CFI in the retina, perhaps in conjunction with other cofactors such as CR1 or CD46 (Sim et al., 1993). To date, there are no known AMD-associated polymorphisms in the *cd46* or *cr1* genes, but *cd46* knockout induces retinal degeneration (Lyzogubov et al., 2016), highlighting its relevant role in retinal physiology.

Given the cell-type-specific expression profile of complement genes in the retina, we propose that a balanced local complement expression is linked to normal retinal integrity. Moreover, our data show that changes in local, cell-type-specific complement expression during aging and acute stress can be induced by cell stress and retinal degeneration and, thus, could in the end also contribute to disease progression. For example, a reaction common to I/R damage and aging appears to be the decrease of intraretinal expression of the complement inhibitor *cfh*. This working hypothesis of course needs further validation at the functional level by future studies.

Taken together, our cell-type-specific analyses provide an alternative perspective on how expression of complement genes, such as those identified by a genome-wide association study (GWAS) for AMD and diabetic retinopathy, in various retinal cell types might be involved in the disease mechanisms in question. The tightly orchestrated reaction of all retinal cell types to distinct conditions of tissue stress suggests that cell-type-specific responses must be considered for successful development of therapeutic strategies targeting retinal complement activity in the future.

Finally, it needs to be pointed out that the analysis of complement activation and its putative role during retinal development, aging, and retinal degeneration was beyond the scope of the present study that was primarily set up to generate a detailed retinal complement expression atlas. However, complement function in the aforementioned processes (irrespective of its source) has been partially addressed and demonstrated by other research groups in the field (Sohn et al., 2003, 2000; Radu et al., 2011; Scheetz et al., 2013; Sudharsan et al., 2017; Weber et al.,

2014; Yang et al., 2016). We would like to point out that those local complement transcripts we were able to detect in distinct retinal cell types are sufficient to activate the classical and alternative complement pathways. Given the rather low expression of components of the terminal canonical complement pathway in cells from the neuroretina, it remains debatable whether it can be intraretinally active without input from the RPE that did produce moderate levels of respective transcripts and/or the systemic complement system. However, we also would like to stress the point that those complement components we demonstrated to be locally expressed are likely to have non-canonical functions in the retina (e.g., C3 in synapse pruning or CFH in phagocytosis or apoptosis) (Martin et al., 2016; Hawksworth et al., 2017). There is growing evidence for intracellular functions of early complement components, which could have an impact on normal cellular physiology (Liszewski et al., 2017). To follow up this intriguing line of thinking, future studies are needed to identify these intracellular functions in addition to their cell secretion and functional interactions.

STAR★METHODS

Detailed methods are provided in the online version of this paper and include the following:

- KEY RESOURCES TABLE
- LEAD CONTACT AND MATERIALS AVAILABILITY
- EXPERIMENTAL MODEL AND SUBJECT DETAILS
- METHOD DETAILS
  - Retinal ischemia/ reperfusion injury
  - Single Cell RNA Analysis of mouse retina
  - RNA-FISH
  - MACS enrichment of retinal cell types
  - qRT-PCR
  - LC-MS/MS mass spectrometry analysis
  - Western blot
  - Immunofluorescent labeling of retina and RPE
- QUANTIFICATION AND STATISTICAL ANALYSIS
- DATA AND CODE AVAILABILITY

SUPPLEMENTAL INFORMATION

Supplemental Information can be found online at https://doi.org/10.1016/j.celrep.2019.10.084.

SUPPORTING CITATIONS

The following references appear in the Supplemental Information: Cheng et al., 2013a

REFERENCES

Anderson, D.H., Radeke, M.J., Gallo, N.B., Chapin, E.A., Johnson, P.T., Curletti, C.R., Hancox, L.S., Hu, J., Ebright, J.N., Malek, G., et al. (2010). The pivotal role of the complement system in aging and age-related macular degeneration: hypothesis re-visited. Prog. Retin. Eye Res. 29, 95–112.

Andreeva, K., Zhang, M., Fan, W., Li, X., Chen, Y., Rebolledo-Mendez, J.D., and Cooper, N.G. (2014). Time-dependent gene profiling indicates the presence of different phases for ischemia/reperfusion injury in retina. Ophthalmol. Eye Dis. 6, 43–54.

Astafurov, K., Dong, C.Q., Panagis, L., Kamthan, G., Ren, L., Rozenboym, A., Perera, T.D., Coplan, J.D., and Danias, J. (2014). Complement expression in the retina is not influenced by short-term pressure elevation. Mol. Vis. 20, 140–152.

Chen, H., Liu, B., Lukas, T.J., and Neufeld, A.H. (2008). The aged retinal pigment epithelium/choroid: a potential substratum for the pathogenesis of age-related macular degeneration. PLoS ONE 3, e2339.

Chen, M., Muckersie, E., Forrester, J.V., and Xu, H. (2010). Immune activation in retinal aging: a gene expression study. Invest. Ophthalmol. Vis. Sci. 51, 5888–5896.

Cheng, L., Bu, H., Portillo, J.-A.C., Li, Y., Subauste, C.S., Huang, S.S., Kern, T.S., and Lin, F. (2013a). Modulation of retinal Müller cells by complement receptor C5aR. Invest. Ophthalmol. Vis. Sci. 54, 8191–8198.

Cheng, C.L., Djajadi, H., and Molday, R.S. (2013b). Cell-specific markers for the identification of retinal cells by immunofluorescence microscopy. Methods Mol. Biol. 935, 185–199.

Crabb, J.W. (2014). The proteomics of drusen. Cold Spring Harb. Perspect. Med. 4, a017194.

Cribbs, D.H., Berchtold, N.C., Perreau, V., Coleman, P.D., Rogers, J., Tenner, A.J., and Cotman, C.W. (2012). Extensive innate immune gene activation accompanies brain aging, increasing vulnerability to cognitive decline and neurodegeneration: a microarray study. J. Neuroinflammation 9, 179.

Damani, M.R., Zhao, L., Fontainhas, A.M., Amaral, J., Fariss, R.N., and Wong, W.T. (2011). Age-related alterations in the dynamic behavior of microglia. Aging Cell 10, 263–276.

Davis, A.E., 3rd, Harrison, R.A., and Lachmann, P.J. (1984). Physiologic inactivation of fluid phase C3b: isolation and structural analysis of C3c, C3d,g (alpha 2D), and C3g. J. Immunol. 132, 1960–1966.

Friedman, E., and Ts'o, M.O. (1968). The retinal pigment epithelium. II. Histologic changes associated with age. Arch. Ophthalmol. 79, 315–320.

Frik, J., Merl-Pham, J., Plesnila, N., Mattugini, N., Kjell, J., Kraska, J., Gómez, R.M., Hauck, S.M., Sirko, S., and Götz, M. (2018). Cross-talk between monocyte invasion and astrocyte proliferation regulates scarring in brain injury. EMBO Rep. 19, e45294.

Fritsche, L.G., Igl, W., Bailey, J.N.C., Grassmann, F., Sengupta, S., Bragg-Gresham, J.L., Burdon, K.P., Hebbring, S.J., Wen, C., Gorski, M., et al. (2016). A large genome-wide association study of age-related macular degeneration highlights contributions of rare and common variants. Nat. Genet. 48, 134–143.

Grassmann, F., Cantsilieris, S., Schulz-Kuhnt, A.-S., White, S.J., Richardson, A.J., Hewitt, A.W., Vote, B.J., Schmied, D., Guymer, R.H., Weber, B.H.F., and Baird, P.N. (2016). Multiallelic copy number variation in the complement component 4A (C4A) gene is associated with late-stage age-related macular degeneration (AMD). J. Neuroinflammation 13, 81.

Grosche, A., Hauser, A., Lepper, M.F., Mayo, R., von Toerne, C., Merl-Pham, J., and Hauck, S.M. (2016). The proteome of native adult Müller glial cells from murine retina. Mol. Cell. Proteomics 15, 462–480.

Grossniklaus, H.E., Nickerson, J.M., Edelhauser, H.F., Bergman, L.A.M.K., and Berglin, L. (2013). Anatomic alterations in aging and age-related diseases of the eye. Invest. Ophthalmol. Vis. Sci. 54, ORSF23-7.

Hawksworth, O.A., Coulthard, L.G., and Woodruff, T.M. (2017). Complement in the fundamental processes of the cell. Mol. Immunol. 84, 17–25.

Jeon, C.J., Strettoi, E., and Masland, R.H. (1998). The major cell populations of the mouse retina. J. Neurosci. 18, 8936–8946.

Kempe, H., Schwabe, A., Crémazy, F., Verschure, P.J., and Bruggeman, F.J. (2015). The volumes and transcript counts of single cells reveal concentration homeostasis and capture biological noise. Mol. Biol. Cell 26, 797–804.

Kim, D.S., Ross, S.E., Trimarchi, J.M., Aach, J., Greenberg, M.E., and Cepko, C.L. (2008). Identification of molecular markers of bipolar cells in the murine retina. J. Comp. Neurol. 507, 1795–1810.

Kim, B.-J., Braun, T.A., Wordinger, R.J., and Clark, A.F. (2013). Progressive morphological changes and impaired retinal function associated with temporal regulation of gene expression after retinal ischemia/reperfusion injury in mice. Mol. Neurodegener. 8, 21.

Kuehn, M.H., Kim, C.Y., Jiang, B., Dumitrescu, A.V., and Kwon, Y.H. (2008). Disruption of the complement cascade delays retinal ganglion cell death following retinal ischemia-reperfusion. Exp. Eye Res. 87, 89–95.

Lepper, M.F., Ohmayer, U., von Toerne, C., Maison, N., Ziegler, A.-G., and Hauck, S.M. (2018). Proteomic landscape of patient-derived CD4+ T cells in recent-onset type 1 diabetes. J. Proteome Res. 17, 618–634.

Levin, A.M., Rusu, I., Orlin, A., Gupta, M.P., Coombs, P., D'Amico, D.J., and Kiss, S. (2017). Retinal reperfusion in diabetic retinopathy following treatment with anti-VEGF intravitreal injections. Clin. Ophthalmol. 11, 193–200.

Li, M., Jia, C., Kazmierkiewicz, K.L., Bowman, A.S., Tian, L., Liu, Y., Gupta, N.A., Gudiseva, H.V., Yee, S.S., Kim, M., et al. (2014). Comprehensive analysis of gene expression in human retina and supporting tissues. Hum. Mol. Genet. 23, 4001–4014.

Liszewski, M.K., Elvington, M., Kulkarni, H.S., and Atkinson, J.P. (2017). Complement's hidden arsenal: New insights and novel functions inside the cell. Mol. Immunol. 84, 2–9.

Luo, C., Chen, M., and Xu, H. (2011). Complement gene expression and regulation in mouse retina and retinal pigment epithelium/choroid. Mol. Vis. 17, 1588–1597.

Luo, C., Zhao, J., Madden, A., Chen, M., and Xu, H. (2013). Complement expression in retinal pigment epithelial cells is modulated by activated macrophages. Exp. Eye Res. 112, 93–101.

Lyzogubov, V.V., Bora, N.S., Tytarenko, R.G., and Bora, P.S. (2014). Polyethylene glycol induced mouse model of retinal degeneration. Exp. Eye Res. 127, 143–152.

Lyzogubov, V.V., Bora, P.S., Wu, X., Horn, L.E., de Roque, R., Rudolf, X.V., Atkinson, J.P., and Bora, N.S. (2016). The complement regulatory protein CD46 deficient mouse spontaneously develops dry-type age-related macular degeneration-like phenotype. Am. J. Pathol. 186, 2088–2104.

Ma, W., Cojocaru, R., Gotoh, N., Gieser, L., Villasmil, R., Cogliati, T., Swaroop, A., and Wong, W.T. (2013). Gene expression changes in aging retinal microglia: relationship to microglial support functions and regulation of activation. Neurobiol. Aging 34, 2310–2321.

Macosko, E.Z., Basu, A., Satija, R., Nemesh, J., Shekhar, K., Goldman, M., Tirosh, I., Bialas, A.R., Kamitaki, N., Martersteck, E.M., et al. (2015). Highly parallel genome-wide expression profiling of individual cells using nanoliter droplets. Cell 161, 1202–1214.

Mages, K., Grassmann, F., Jägle, H., Rupprecht, R., Weber, B.H.F., Hauck, S.M., and Grosche, A. (2019). The agonistic TSPO ligand XBD173 attenuates the glial response thereby protecting inner retinal neurons in a murine model of retinal ischemia. J. Neuroinflammation 16, 43.

Marguerat, S., and Bähler, J. (2012). Coordinating genome expression with cell size. Trends Genet. 28, 560–565.

Martin, M., Leffler, J., Smoląg, K.I., Mytych, J., Björk, A., Chaves, L.D., Alexander, J.J., Quigg, R.J., and Blom, A.M. (2016). Factor H uptake regulates intracellular C3 activation during apoptosis and decreases the inflammatory potential of nucleosomes. Cell Death Differ. 23, 903–911.

Merle, N.S., Church, S.E., Fremeaux-Bacchi, V., and Roumenina, L.T. (2015). Complement system part I - molecular mechanisms of activation and regulation. Front. Immunol. 6, 262.

Micklisch, S., Lin, Y., Jacob, S., Karlstetter, M., Dannhausen, K., Dasari, P., von der Heide, M., Dahse, H.-M., Schmölz, L., Grassmann, F., et al. (2017). Age-related macular degeneration associated polymorphism rs10490924 in ARMS2 results in deficiency of a complement activator. J. Neuroinflammation 14, 4.

Mukai, R., Okunuki, Y., Husain, D., Kim, C.B., Lambris, J.D., and Connor, K.M. (2018). The complement system is critical in maintaining retinal integrity during aging. Front. Aging Neurosci. 10, 15.

Pannicke, T., Frommherz, I., Biedermann, B., Wagner, L., Sauer, K., Ulbricht, E., Härtig, W., Krügel, U., Ueberham, U., Arendt, T., et al. (2014). Differential effects of P2Y1 deletion on glial activation and survival of photoreceptors and amacrine cells in the ischemic mouse retina. Cell Death Dis. 5, e1353.

Pinelli, M., Carissimo, A., Cutillo, L., Lai, C.-H., Mutarelli, M., Moretti, M.N., Singh, M.V., Karali, M., Carrella, D., Pizzo, M., et al. (2016). An atlas of gene expression and gene co-regulation in the human retina. Nucleic Acids Res. 44, 5773–5784.

Radu, R.A., Hu, J., Yuan, Q., Welch, D.L., Makshanoff, J., Lloyd, M., McMullen, S., Travis, G.H., and Bok, D. (2011). Complement system dysregulation and inflammation in the retinal pigment epithelium of a mouse model for Stargardt macular degeneration. J. Biol. Chem. 286, 18593–18601.

Rheaume, B.A., Jereen, A., Bolisetty, M., Sajid, M.S., Yang, Y., Renna, K., Sun, L., Robson, P., and Trakhtenberg, E.F. (2018). Single cell transcriptome profiling of retinal ganglion cells identifies cellular subtypes. Nat. Commun. 9, 2759.

Roesch, K., Jadhav, A.P., Trimarchi, J.M., Stadler, M.B., Roska, B., Sun, B.B., and Cepko, C.L. (2008). The transcriptome of retinal Müller glial cells. J. Comp. Neurol. 509, 225–238.

Rose, K.L., Paixao-Cavalcante, D., Fish, J., Manderson, A.P., Malik, T.H., Bygrave, A.E., Lin, T., Sacks, S.H., Walport, M.J., Cook, H.T., et al. (2008). Factor I is required for the development of membranoproliferative glomerulonephritis in factor H-deficient mice. J. Clin. Invest. 118, 608–618.

Rutar, M., Natoli, R., Albarracin, R., Valter, K., and Provis, J. (2012). 670-nm light treatment reduces complement propagation following retinal degeneration. J. Neuroinflammation 9, 257.

Schäfer, N., Grosche, A., Reinders, J., Hauck, S.M., Pouw, R.B., Kuijpers, T.W., Wouters, D., Ehrenstein, B., Enzmann, V., Zipfel, P.F., et al. (2016). Complement regulator FHR-3 is elevated either locally or systemically in a selection of autoimmune diseases. Front. Immunol. 7, 542.

Schäfer, N., Grosche, A., Schmitt, S.I., Braunger, B.M., and Pauly, D. (2017). Complement components showed a time-dependent local expression pattern in constant and acute white light-induced photoreceptor damage. Front. Mol. Neurosci. 10, 197.

136

Scheetz, T.E., Fingert, J.H., Wang, K., Kuehn, M.H., Knudtson, K.L., Alward, W.L.M., Boldt, H.C., Russell, S.R., Folk, J.C., Casavant, T.L., et al. (2013). A genome-wide association study for primary open angle glaucoma and macular degeneration reveals novel loci. PLoS ONE 8, e58657.

Shekhar, K., Lapan, S.W., Whitney, I.E., Tran, N.M., Macosko, E.Z., Kowalczyk, M., Adiconis, X., Levin, J.Z., Nemesh, J., Goldman, M., et al. (2016). Comprehensive classification of retinal bipolar neurons by single-cell transcriptomics. Cell 166, 1308–1323.e30.

Silva, P.S., Dela Cruz, A.J., Ledesma, M.G., van Hemert, J., Radwan, A., Cavallerano, J.D., Aiello, L.M., Sun, J.K., and Aiello, L.P. (2015). Diabetic retinopathy severity and peripheral lesions are associated with nonperfusion on ultrawide field angiography. Ophthalmology 122, 2465–2472.

Sim, R.B., Day, A.J., Moffatt, B.E., and Fontaine, M. (1993). Complement factor I and cofactors in control of complement system convertase enzymes. Methods Enzymol. 223, 13–35.

Sohn, J.H., Kaplan, H.J., Suk, H.J., Bora, P.S., and Bora, N.S. (2000). Chronic low level complement activation within the eye is controlled by intraocular complement regulatory proteins. Invest. Ophthalmol. Vis. Sci. 41, 3492–3502.

Sohn, J.-H., Bora, P.S., Suk, H.-J., Molina, H., Kaplan, H.J., and Bora, N.S. (2003). Tolerance is dependent on complement C3 fragment iC3b binding to antigen-presenting cells. Nat. Med. 9, 206–212.

Stuart, T., Butler, A., Hoffman, P., Hafemeister, C., Papalexi, E., Mauck, W.M., 3rd, Hao, Y., Stoeckius, M., Smibert, P., and Satija, R. (2019). Comprehensive integration of single-cell data. Cell 177, 1888–1902.e21.

Sudharsan, R., Beiting, D.P., Aguirre, G.D., and Beltran, W.A. (2017). Involvement of innate immune system in late stages of inherited photoreceptor degeneration. Sci. Rep. 7, 17897.

Tenner, A.J., Stevens, B., and Woodruff, T.M. (2018). New tricks for an ancient system: Physiological and pathological roles of complement in the CNS. Mol. Immunol. 102, 3–13.

Tian, L., Kazmierkiewicz, K.L., Bowman, A.S., Li, M., Curcio, C.A., and Stambolian, D.E. (2015). Transcriptome of the human retina, retinal pigmented epithelium and choroid. Genomics 105, 253–264.

Traveset, A., Rubinat, E., Ortega, E., Alcubierre, N., Vazquez, B., Hernández, M., Jurjo, C., Espinet, R., Ezpeleta, J.A., and Mauricio, D. (2016). Lower hemoglobin concentration is associated with retinal ischemia and the severity of diabetic retinopathy in type 2 diabetes. J. Diabetes Res. 2016, 3674946.

Wagner, L., Pannicke, T., Frommherz, I., Sauer, K., Chen, J., and Grosche, A. (2016). Effects of IP3R2 receptor deletion in the ischemic mouse retina. Neurochem. Res. 41, 677–686.

Wagner, L., Pannicke, T., Rupprecht, V., Frommherz, I., Volz, C., Illes, P., Hirrlinger, J., Jägle, H., Egger, V., Haydon, P.G., et al. (2017). Suppression of SNARE-dependent exocytosis in retinal glial cells and its effect on ischemia-induced neurodegeneration. Glia 65, 1059–1071.

Walker, D.G., and McGeer, P.L. (1992). Complement gene expression in human brain: comparison between normal and Alzheimer disease cases. Brain Res. Mol. Brain Res. 14, 109–116.

Wang, J., Yang, M.M., Li, Y.B., Liu, G.D., Teng, Y., and Liu, X.M. (2013). Association of CFH and CFB gene polymorphisms with retinopathy in type 2 diabetic patients. Mediators Inflamm. 2013, 748435.

Weber, B.H.F., Charbel Issa, P., Pauly, D., Herrmann, P., Grassmann, F., and Holz, F.G. (2014). The role of the complement system in age-related macular degeneration. Dtsch. Arztebl. Int. 111, 133–138.

Yang, M.M., Wang, J., Ren, H., Sun, Y.D., Fan, J.J., Teng, Y., and Li, Y.B. (2016). genetic investigation of complement pathway genes in type 2 diabetic retinopathy: an inflammatory perspective. Mediators Inflamm. 2016, 1313027.

Zhang, J., Gerhardinger, C., and Lorenzi, M. (2002). Early complement activation and decreased levels of glycosylphosphatidylinositol-anchored complement inhibitors in human and experimental diabetic retinopathy. Diabetes 51, 3499–3504.

STAR★METHODS

KEY RESOURCES TABLE

REAGENT or RESOURCE	SOURCE	IDENTIFIER
Antibodies		
mouse anti-CD29-Biotin	Milteny Biotec (Bergisch-Gladbach, Germany)	130-101-943; RRID:AB_2660700
rabbit anti-PDHB	Abcam (Cambridge, UK)	ab155996; RRID:AB_2814826
rabbit anti-C1s	Proteintech (Rosemont, IL, USA)	#14554-1-AP / (Schäfer et al., 2017); RRID:AB_2814827
goat anti-C4	Complement Technologies (Tyler, TX, USA)	#A205; RRID:AB_2814828
goat anti-C3-HRP	MP Biomedicals (Santa Ana, CA, USA)	#55557 / (Schäfer et al., 2017)
rabbit anti-C3	Abcam (Cambridge, UK)	ab11887; RRID:AB_298669
goat anti-CFB	Merck (Darmstadt, Germany)	#341272 / (Schäfer et al., 2017); RRID:AB_2082392
sheep anti-CFD	R&D Systems (Minneapolis, MN, USA)	#AF5430; RRID:AB_1655868
mouse anti-C5	Quidel (San Diego, CA, USA)	#A217; RRID:AB_452484
goat anti-C6	Complement Technologies (Tyler, TX, USA)	#A223; RRID:AB_2814831
goat anti-C7	Tecomedical (Sissach, CH)	#A308; RRID:AB_2814832
rabbit anti-C9	Antibodies online (Aachen, Germany)	#ABIN1714714; RRID:AB_2814833
rat anti-CFP	in-house	(Schäfer et al., 2017)
goat anti-CFH	Merck (Darmstadt, Germany)	#341276; RRID:AB_2080303
goat anti-CFI	Quidel (San Diego, CA, USA)	A313 / (Rose et al., 2008): RRID:AB_452514
rabbit anti-IBA1	Wako Chemicals (Neuss, Germany)	#019-19741 / (Schäfer et al., 2016); RRID:AB_839504
mouse anti-glutamine sythetase	Merck (Darmstadt, Germany)	MAB302 /(Mages et al., 2019); RRID:AB_2110656
goat anti-rat Ig-HRP	Dianova (Hamburg, Germany)	#112-035-003; RRID:AB_2338128
goat anti-rabbit Ig-HRP	Dianova (Hamburg, Germany)	#111-035-003; RRID:AB2313567
rabbit anti-goat Ig-HRP	Dianova (Hamburg, Germany)	#305-035-003; RRID:AB2339400
goat anti-rabbit-IG-Cy3	ThermoFisher (Braunschweig, Germany)	#A10520; RRID:AB2534029
Chemicals, Peptides, and Recombinant Proteins		
CD11b (Microglia) MicroBeads, human and mouse	Milteny Biotec	130-093-634
CD31 MicroBeads, mouse	Milteny Biotec	130-097-418
Anti-Biotin MicroBeads UltraPure	Milteny Biotec	130-105-637
Critical Commercial Assays		
RevertAid H Minus First-Strand cDNA Synthesis Kit	Thermo Fisher Scientific	K1632
PureLink® RNA Micro Scale Kit	Thermo Fisher Scientific	12183016
Deposited Data		
scRNA sequencing data	Gene Expression Omnibus (GEO)	GSE116426
Experimental Models: Organisms/Strains		
BALB/cJRj mice	Janvier Labs	SC-BALBJ-M
C57BL/6J	Jackson Laboratories	000664
Oligonucleotides		
see Table S6	This paper	N/A
Software and Algorithms		
Progenesis QI software for proteomics (Version 3.0)	Nonlinear Dynamics, Waters, Newcastle upon Tyne, U.K.	N/A
R package Seurat	Stuart et al., 2019	N/A

(Continued on next page)

Continued

REAGENT or RESOURCE	SOURCE	IDENTIFIER
FIJI (ImageJ)	National Institutes of Health, Bethesda, MD, USA	N/A
R v 3.5.1	https://www.R-project.org	N/A

LEAD CONTACT AND MATERIALS AVAILABILITY

Further information and requests for resources and reagents should be directed to and will be fulfilled by the Lead Contact, Diana Pauly (diana.pauly@ukr.de). This study did not generate new unique reagents.

EXPERIMENTAL MODEL AND SUBJECT DETAILS

Single cell RNA-Seq and RNA-FISH was performed on wild-type (C57BL/6J) male mice (10 weeks old) purchased from Jackson Laboratory (Bar Harbor, ME, USA). All experimental procedures were approved by the University of Pennsylvania Animal Care and Use Committee. Mice were sacrificed with cervical dislocation under anesthesia. Experiments for immunomagnetic separation were done in accordance with the European Community Council Directive 2010/63/EU and the ARVO Statement for the Use of Animals in Ophthalmic and Vision Research and were approved by the local Bavarian authorities (55.2 DMS-2532-2-182, Germany). All mice were housed in a 12 hour light/ dark cycle with ~400 lux. Experiments on complement expression in aging mice were conducted with 8, 16 and 24 week old male and female on BALB/c mice. Retinal ischemia was induced in one eye of 8 week old male and female C57BL/6J mice. The untreated contralateral eye served as internal control and, accordingly, an additional control group was not needed thereby sticking to the rules of the three R's by keeping reducing the number of animals used in respective experiments.

METHOD DETAILS

Retinal ischemia/ reperfusion injury

The protocols for induction of transient retinal ischemia were approved by the local Bavarian authorities (55.2 DMS-2532-2-182, Germany). Ischemia was induced in one eye of 8 week old male and female C57BL/6J mice using the high intraocular pressure (HIOP) method (Pannicke et al., 2014; Wagner et al., 2016). The other eye remained untreated and served as an internal control. Anesthesia was induced with ketamine (100 mg/kg body weight, intraperitoneal (ip); Ratiopharm, Ulm, Germany), xylazine (5 mg/kg, ip; Bayer Vital, Leverkusen, Germany), and atropine sulfate (100 mg/kg, ip; Braun, Melsungen, Germany). The anterior chamber of the test eye was cannulated from the pars plana with a 30-gauge infusion needle, connected to a saline bottle. The intraocular pressure was increased to 160 mmHg for 90 minutes by elevating the bottle. After removing the needle, the animals survived for 24 hours and subsequently, they were sacrificed with carbon dioxide for tissue analyses.

Single Cell RNA Analysis of mouse retina

Mouse eyeballs were quickly removed and placed in cold phosphate buffered saline (PBS). The mouse retina was carefully removed under dissecting scope and tissue was dissociated immediately using the papain dissociation system (Worthington, Lakewood, NJ, USA) following the manufacturer's instructions. Briefly, the mouse retina was incubated at 37°C for 30 minutes in Eagle's Balanced Salt Solution (EBSS) with DNase followed by tissue trituration with a 10 mL pipette. Cell pellet was collected after centrifugation at 300 × g for 5 minutes and then resuspended in DNase albumin-inhibitor solution. The cell suspension was carefully layered on top of the albumin-inhibitor solution, then centrifuged at 70 × g for 6 minutes. The cell pellet was washed and resuspended in 1:1 DMEM/ F12 + 10% FBS. All centrifugation steps were performed at room temperature. The final cell suspension was filtered with 40 μm cell strainer (Falcon, Corning, NY, USA) to remove large debris. To assess cell viability, cells were stained with 0.4% trypan blue (Mediatech, Inc., Manassas, VA, USA) and counted using a hemocytometer. Viable cells (greater than 80%) were submitted to the Center for Applied Genomics at the Children's Hospital of Philadelphia (CHOP) for cell separation and lysis on the 10X Chromium Genomics instrument and sequencing on the Illumina Hi-Seq instrument.

All analyses were carried out in the statistical software *R* v 3.5.1. The R package Seurat was used for data analysis, dataset merging and cell clustering analysis. For clustering, we used 2000 or more genes that had detectable expression with high variability in the ~92,000 mouse retinal cells. Six genetically identical C57BL/6J mice were sequenced, our data were consistent across different batches (Figure S1). We filtered out low-quality cells in which < 90% of the reads did not map to the genome using the Cell Ranger pipeline from 10x genomics, and ultimately obtained 92,343 cells used in our subsequent analyses. Given the consistent number of genes (*nGene*), UMIs (*nUMI*), and the percentage of mitochondrial genes (*percent.mito*) detected in each batch, we merged the sequencing runs and used 30 principal components as an input to t-distributed stochastic neighbor embedding (t-SNE) method for dimension reduction and data visualization. We found 25 cell clusters within the retina using an unsupervised analysis that did

not rely on known markers of retinal cells. Marker genes were identified for all clusters with the function *markers.all* in the R package Seurat; all marker genes with power less than 0.4 were discarded. Moreover, only cells with mitochondrial gene percentages < 50%, and those with unique gene counts between 200 and 3,500 were used, leaving us with 91,798 retinal cells. After filtering, we sought to consolidate the 25 clusters into a total of 11 (for N = 91,798 cells), each of which represents a major, functionally important cell class in the retina. For this, we used the known, established marker genes for common retinal cell types summarized in Table S1. Although previous studies of scRNA-seq on the mouse retina have identified more than 30 different cell types, this difference is largely explained by their subdivision of bipolar cells (BCs) into numerous sub-categories. We decided to classify cell types based on general categories because we wanted to study complement expression in retinal cells more broadly. Using this approach, the cell type proportions in the retina proper are comparable between our study and past studies. Based on mean complement gene expression, we categorized positive expression for a gene within a cell type only if either $\geq$ 5% of cells or at least 50 cells within that class had non-zero expression for that gene.

RNA-FISH

Mouse protocol was approved by the University of Pennsylvania IACUC committee. A 10 week old C57BL/6J male was euthanized with 5 mg pentobarbital sodium. The eye was dissected free from the orbit, washed in PBS, embedded in OCT (Tissue Tek, Sakura Finetek USA, Torrance, CA, USA) and immediately snap-frozen in liquid nitrogen. The frozen tissue was sliced at 10 μm on a cryostat and stored at $-80°$C on glass slides.

Tissue fixation and RNA *in situ* hybridization (RNA-FISH) was carried out using Stellaris® RNA FISH (LGC Biosearch Technologies, Petaluma, CA, USA) following the manufacturer's instructions. Briefly, the tissue section was fixed in 3.7% formaldehyde in 1X PBS for 10 minutes at room temperature. After washing twice with 1X PBS, the tissue section was permeabilized in 70% ethanol for at least 1 hour at room temperature. Oligo probes were designed against mRNA coding sequence for each gene using the Stellaris Custom probe sets and labeled with Quasar® 570 dye or Quasar® 670 dye. For a positive control, mouse GAPDH probe (Stellaris ShipReady probe sets) was purchased. To secure tissues on the slide during hybridization, the HybriWell® sealing system (Grace Bio-Labs, Bend, OR, USA) was used. Each tissue section was incubated in hybridization buffer containing probe (final concertation was between 62.5 nM to 250 nM) overnight at 37°C and then washed in washing buffer A for 30 minutes at 37°C. Cell nuclei were stained with 4′,6-diamidino-2-phenylindole (DAPI, 0.1 μg/ml) followed by washing in Buffer B. All buffers were purchased from LGC Bioresearch Technologies. Finally, mounting medium (ProLong Gold antifade reagent, Invitrogen, Life Technologies, Eugene, OR, USA) was added and a coverglass was mounted on the slide. Confocal microscopy to image the RNA-FISH samples was performed at the Bioimaging Core Facility of the Biomedical Center of the LMU Munich. RNA FISH images were obtained with an inverted Leica SP8X WLL microscope with a 63x/1.3 Glyc objective. We sequentially recorded Quasar 670 (excitation 647 nm; emission 670 nm - 760 nm) and Quasar 570 (excitation 556 nm; emission 566 nm - 630 nm) with hybrid photo detectors (HyDs) and DAPI (excitation 405 nm; emission 415 nm - 450 nm) with a conventional photomultiplier tube. The same illumination and acquisition settings were used for all sections. Brightness and contrast of the images were adjusted with the open source software FIJI (ImageJ; National Institutes of Health, Bethesda, MD, USA).

MACS enrichment of retinal cell types

Retinal cell types were enriched as described previously using magnetic-activated cell sorting (MACS) (Grosche et al., 2016). Briefly, retinae were treated with papain (0.2 mg/ml; Roche Molecular Biochemicals) for 30 minutes at 37°C in the dark in Ca^{2+}- and Mg^{2+}-free extracellular solution (140 mM NaCl, 3 mM KCl, 10 mM HEPES, 11 mM glucose, pH 7.4). After several washes and 4 minutes of incubation with DNase I (200 U/ml), retinae were triturated in extracellular solution (now with 1 mM MgCl$_2$ and 2 mM CaCl$_2$). To purify microglial and vascular cells, the retinal cell suspension was subsequently incubated with CD11b- and CD31 microbeads according to the manufacturer's protocol (Miltenyi Biotec, Bergisch Gladbach, Germany). The respective binding cells were depleted from the retinal suspension using LS-columns, prior to Müller cell enrichment. To purify Müller glia, the cell suspension was incubated in extracellular solution containing biotinylated anti-CD29 (0.1 mg/ml, Miltenyi Biotec) for 15 minutes at 4°C. Cells were washed in an extracellular solution, spun down, resuspended in the presence of anti-biotin MicroBeads (1:5; Miltenyi Biotec,) and incubated for 10 minutes at 4°C. After washing, CD29+ Müller cells were separated using large cell (LS) columns according to the manufacturer's instructions (Miltenyi Biotec). Cells in the flow through of the last sorting step- depleted of microglia, vascular cells and Müller glia- were considered as the neuronal population. RPE was collected by scratching the eye cup after the retina had been removed and thus, scratch samples also contained cells from the underlying choroid. Samples were digested, and in subsequent steps, macrophages were depleted using anti-CD11b-microbeads and vascular cells using CD31-microbeads (Miltenyi Biotec).

qRT-PCR

Total RNA was isolated from the enriched cell populations using the PureLink® RNA Micro Scale Kit (Thermo Fisher Scientific, Schwerte, Germany). A DNase digestion step was included to remove genomic DNA (Roche). We performed RNA integrity validation and quantification using the Agilent RNA 6000 Pico chip analysis according to the manufactures instructions (Agilent Technologies, Waldbronn, Germany). First-strand cDNAs from the total RNA purified from each cell population were synthesized using the RevertAid H Minus First-Strand cDNA Synthesis Kit (Fermentas by Thermo Fisher Scientific, Schwerte, Germany). We designed primers using the Universal ProbeLibrary Assay Design Center (Roche, Table S6) and measured transcript levels of candidate genes

by qRT-PCR using the TaqMan hPSC Scorecard Panel (384 well, ViiA7, Life Technologies, Darmstadt, Germany) according to the company's guidelines.

LC-MS/MS mass spectrometry analysis

LC-MS/MS analysis was performed as described previously (Frik et al., 2018; Lepper et al., 2018) on a Q-Exactive HF mass spectrometer (Thermo Fisher Scientific Inc., Waltham, MA, U.S.A.) coupled to an Ultimate 3000 RSLC nano-HPLC (Dionex, Sunnyvale, CA). Briefly, 0.5 μg sample was automatically loaded onto a nano trap column (300 μm inner diameter × 5 mm, packed with Acclaim PepMap100 C18. 5 μm, 100 Å; LC Packings, Sunnyvale, CA) before separation by reversed phase chromatography (HSS-T3 M-class column, 25 cm, Waters) in an 80 minutes non-linear gradient from 3 to 40% acetonitrile (ACN) in 0.1% formic acid (FA) at a flow rate of 250 nl/min. Eluted peptides were analyzed by the Q-Exactive HF mass spectrometer equipped with a nano-flex ionization source. Full scan MS spectra (from m/z 300 to 1500) and MS/MS fragment spectra were acquired in the Orbitrap with a resolution of 60,000 or 15000 respectively, with maximum injection times of 50 ms each. Up to ten most intense ions were selected for HCD fragmentation depending on signal intensity (TOP10 method). Target peptides already selected for MS/MS were dynamically excluded for 30 s. Spectra were analyzed using the Progenesis QI software for proteomics (Version 3.0, Nonlinear Dynamics, Waters, Newcastle upon Tyne, UK) for label-free quantification, as previously described (Grosche et al., 2016). All features were exported as a Mascot generic file (mgf) and used for peptide identification with Mascot (version 2.4) in the UniProtKB/Swiss-Prot taxonomy mouse database (Release 2017.02, 16871 sequences). Search parameters used were: 10 ppm peptide mass tolerance, 20 mmu fragment mass tolerance, one missed cleavage allowed, carbamidomethylation set as fixed modification, and methionine oxidation, asparagine or glutamine deamidation were allowed as variable modifications. A Mascot-integrated decoy database search calculated an average false discovery rate (FDR) of < 1%.

Western blot

Cell pellets of enriched cell populations from pooled pair of mouse eyes were dissolved in reducing Laemmli sample buffer, denatured and sonicated. Neuronal protein extraction reagent (Thermo Fisher Scientific, Braunschweig, Germany) was added to the neuron populations. Samples were separated on a 12% SDS-PAGE. The immunoblot was performed as previously described (Schäfer et al., 2017). Detection was performed with primary and secondary antibodies diluted in blocking solution (Table S7). Blots were developed with WesternSure PREMIUM Chemiluminescent Substrate (LI-COR, Bad Homburg, Germany). To validate specificity of the antibodies, all of them were tested on mouse serum as positive control (Figure S3).

Immunofluorescent labeling of retina and RPE

To quantify cell nuclei and perform stainings for C1s, C3 and glutamine synthetase (GLUL) in retinal sections of 4% paraformaldehyde (PFA)-fixated and paraffin-embedded murine eyes, the sections were deparaffinised and incubated with Hoechst33342/DAPI (1:1000; #H1399, Thermo Fisher Scientific, Braunschweig, Germany) or detection antibodies as previously described (Schäfer et al., 2017) (Table S7). Images were acquired using confocal microscopy (VisiScope, Visitron Systems, Puchheim, Germany).

Retinal microglia quantification was performed in the retinal flat mounts. Anterior segments of mouse eyes were removed, and the retina carefully separated. Flat mounts were fixated in 4% PFA (retina 1 h room temperature), permeabilized (1% Triton X-100) and blocked (1% BSA, 5% goat serum, 0.1 M NaPO₄, pH 7). Retinal flat mounts were stained with anti-Iba1 antibody (3% Triton X-100, 1% DMSO, 5% normal goat serum, overnight at 4°C) and secondary antibody (1% BSA in PBS, overnight at 4°C) (Table S7). Retinal flat mounts were embedded with photoreceptors facing down, and the GCL facing up. Images were taken with a confocal microscope (VisiScope, Visitron Systems).

QUANTIFICATION AND STATISTICAL ANALYSIS

Statistical analyses were performed using Prism (Graphpad Software, San Diego, CA, USA). In most of the experiments in the present study results from 4 biological replicates were collected to keep to the rules of the three Rs for the sake of animal welfare. Since this low number of input values does not allow an appropriate estimation about a normal Gaussian distribution, significance levels were determined by the non-parametric Mann-Whitney U test unless stated otherwise. All data are expressed as mean ± standard error (SEM) unless stated otherwise. Detailed information about specific n-values, implemented statistical tests and coding of significance levels are provided in the respective figure legends.

DATA AND CODE AVAILABILITY

The accesssion number for the single cell RNA-Seq data reported in this paper is GSE116426 (Gene Expression Omnibus (GEO)). Other data supporting the findings of this study are available from the corresponding author upon request.

General Discussion

In my thesis work, I mapped which complement factor transcripts and proteins are present in different cell types of the retina and how the complement transcriptome and proteome change in disease states. This led to a more complete picture of which complement factors play a role in retinal functions and highlighted differences between human and mouse physiology. I then used this knowledge to modulate the complement system in the diseased retina to counteract the detrimental effects of inappropriate complement activation.

Local retinal complement expression

By analyzing the transcriptome from individual cells, I, together with collaborators, was able to generate a detailed cell type-specific expression atlas for complement factor expression in the human retina. Robust expression (i.e., over 10% of scRNA-seq analyzed cell population expressed the gene) for complement activators at mRNA level was found for *C1QA-C*, *C1R, C1RL, C1S, CFB, CFD, C3* and *C7*. On protein level, C1s, C7, C3 were detected via western blot in retinal cells.

Most proteins involved in complement activation do not bind, or if they do, get rapidly degraded on healthy host cells (Zewde et al. 2016).This may explain the detection of low amounts of C3 protein apparently attached to cells of all purified fractions, but also why multiple complement components were barely detectable via mass spectrometry or Western blot performed on MACS-purified cell populations.

Additionally, the proteome (determined by LC-MS/MS mass spectrometry) of the human RPE/choroid fraction containing RPE cells, endothelial cells, pericytes fibroblasts and immune cells included C1QB, C2, C4B, FB, C3, C5, C6, C7, C8a, C8B, C8G and C9. RPE cells, on the other hand, showed little to no complement transcripts of factors involved in complement activation in the scRNA-seq dataset by Voigt et al (Voigt et al. 2019). Since complement components secreted by choroidal cells or passing by via the blood circulation cannot enter the healthy retina with an intact BRB, it is of interest which factors are secreted by the RPE into the subretinal space. The RPE was surprisingly inactive from a transcriptional perspective with detectable but low (<15% of cells with average expression) transcript levels for *C1R, C1s* and *CFD*. At the protein level, distinct Western blot bands were detected for C1s, CFB, CFD, C5, CFP, CFH and CFI.

This local complement expression signature at first glance does not seem to enable the activation of the whole complement cascade through each of the three possible pathways. Several key components, especially lectins (FCN1-3 and MASP1) and

components of the terminal pathway (including C5, C6, C8, C9), were absent in our analysis. In contrast, proteins that initiate the classical pathway and contribute to the formation of the alternative pathway C3 convertase (CFB, CFD, CFP, C3) were detected. This suggests that the lectin pathway might not play a major role in the retina.

In the classical pathway, while recognition molecules of the C1 complex were among the most abundant transcript wise, proteins required for the classical pathway C3 convertase (C4bC2bC3b) formation were scarcely detected in the healthy retina. While a full cascade activation is also not expected in healthy tissue, the classical pathway has previously been shown to also act on tissue homeostasis, cell migration and tissue remodeling (Ricklin et al. 2010). The major targets of C1q are the Fc regions of IgG and IgM antibodies in immune complexes, but it has also been shown to be involved in clearance of debris and phagocytosis of apoptotic cells (Ricklin et al. 2010; Gaboriaud et al. 2011; Nauta et al. 2002). During the FH gene addition therapy study, I detected C1s deposits (which is part of the C1-complex) to be associated with terminal deoxynucleotidyl transferase-mediated dUTP nick end labeling (TUNEL)-positive cells in the ONL during degenerative events following ischemia. I also found C1s in immunostainings colocalizing with nuclear DNA after sodium iodate induced retinal degeneration. Phosphatidylserine and double-stranded DNA are thought to be the recognition patterns C1q, and their interaction may trigger apoptosis (Nauta et al. 2002; Gaboriaud et al. 2011). In line with this, it has been shown that C1q promotes clearance of apoptotic cells independent of complement activation, but the mechanisms are still under investigation (Bobak et al. 1987). Since we observed colocalization of C1s with apoptotic cells, it is likely that a fully formed C1 complex is capable of C1q-dependent enhancement of phagocytosis as well as initiation of the classical pathway because C1s would be proteolytically active toward its substrate C4 (Galvan et al. 2012).

Notably, a mechanism similar to C1q-facilitated apoptosis induction appears to underlie synaptic pruning (Györffy et al. 2018), as synaptic plasticity is maintained during development and in mature neuronal tissue by C1q-dependent removal of excess neurites. While C1q does not have a critical role in the development of neuronal circuits, such as the mouse visual cortex, it was recently found to be integral for proper horizontal cell neurite confinement in C1q knockout mice (Welsh et al. 2020; Burger et al. 2020). Welsh et al. did not observe differences in retinal development until postnatal day 13 (P13), after which horizontal cells extended neurites abnormally into the outer retina. They also found that this mechanism was microglia- but not C3aR- or CR3-dependent (Welsh et al. 2020). While postnatal C1q expression was not explored in our studies, C1q proteins were found in the retinae of all our human adult donors. Therefore, it seems very possible that C1q also plays a role in remodeling of retinal neuro plasticity in humans after birth, which could be scrutinized in future studies.

Whether synaptic elimination by C1q tagging is independent of the downstream complement cascade is still debated (Kovács et al. 2020). However, if the cascade is activated by any pathway, C3 plays the central role in its amplification and propagation to the terminal pathway. By mass spectrometry, we detected C3 in the macroglial and

neuronal fractions, whereas all other terminal pathway proteins were found only in RPE/choroid. Since the latter contains components of the circulatory system, these terminal pathway proteins could also originate from the liver and enter the choroid via the bloodstream (Zou et al. 2015). Intraretinally, C3 transcripts were detected in microglia in the OPL and in astrocytes in the NFL via scRNA-seq. Interestingly, besides C3, C7 was the only other terminal pathway for which mRNA was detectable, here in the OPL associated with horizontal cells. C7 binds the C5bC6 complex to form the MAC on cell surfaces, leading to pore formation in the cell membrane and ultimately inducing cell lysis. Since other MAC proteins do not appear to be present or expressed by the different retinal cell types, C7 may have non-canonical MAC-independent functions. On its own, C7 has recently be discussed to act as a tumor suppressor (Chen et al. 2020). Moreover, C7 variants have been implicated in pathogenesis of Alzheimer's disease, affecting brain morphology and memory in the early stages of the disease (Zhang et al. 2019).

Taken together, the low levels of some key complement components, but the abundance of others, provide a novel perspective on complement activity in the healthy retina, which appears to be homeostatic rather than pro-inflammatory and to be involved in maintenance and immune surveillance.

Complement inhibition in the retina

Because of complement's capacity to destroy cells, it is tightly regulated. Generally, complement is regulated by both fluid phase and surface bound molecules. Here, I identified clusterin and component 1q subcomponent binding protein (C1QBP) as complement inhibitors that are expressed by a large percentage of cells in all human retinal cell types. C1QBP regulates the activation of the classical pathway preventing the formation of the C1 complex by binding the globular heads of C1q molecules (Lynch et al. 1997; Lim et al. 1996). Clusterin is a disulfide-linked heterodimeric protein that binds to C7, C8 beta, and C9. Other targets include lipopolysaccharides, bacterial porins, CRP and pentraxin 3 (McGrath et al. 2006; Ricklin et al. 2010). The also secreted regulators CFH and CFI were detected on transcript level in our scRNA-seq approach in almost half of the endothelial cells, 25% of RPE cells and with the highest average expression in fibroblasts of the choroid. Finally, SERPING1, which binds C1r and C1s to dissociate the C1 complex was detected in astrocytes, pericytes and most choroid cells on transcript level. The main membrane bound complement inhibitor from a mRNA perspective was the MAC complex inhibitor CD59 with high expression across all retinal and choroidal cell types.

In mice, several inhibitory complement factors have been found to be expressed by RPE cells *in vitro* and *in vivo* including *C1r, Cfh, Daf1, Cd59, C1Inh, Crry* (Cr1-related protein Y)*, and C4bp* (Luo et al. 2013). With scRNA-seq and in situ hybridization, we took a

close look at the transcript levels and localization of complement regulators in retinal cells of mice. A predominant regulator was vitronectin, which was found to be expressed by several retinal cell types. Clusterin, which was ubiquitous among human cells was mainly expressed by Müller cells (>80%) of the murine retinas. Transcripts were also present in some ganglion and horizontal cells (<20%) but overall, the lesser expression in other cell types compared to human hinted differences in the complement regulation. A further example for these differences is the membrane bound complement regulator Crry that is considered the murine ortholog for Cr1 (Killick et al. 2013). Our scRNA-seq analysis detected *Crry* in ~32% of endothelial cells but only scarcely in other retinal cells. In a qPCR experiment, over half of all retinal *Cfh* transcripts in mice were found in RPE cells, while *Cfi* was predominantly expressed in neurons. Again, as in human, the most common membrane bound regulator was *Cd59*.

Overall, several fluid phase as well as membrane bound regulatory mechanisms are present in the human and murine retina. The direct comparison of human and mouse complement component expression (regulators activators and receptors) allowed the identification of cell type specific differences. These inter species discrepancies must be considered when designing and testing potential therapies in murine model organisms. Modeling for CFH based therapies appears viable since CFH and CFI seem to play a role in both organisms, albite at lower average per cell expression and in in different cell types.

The complosome in retinal cells

The complement system was previously thought to function solely in the extracellular space. Recent studies have discovered intracellular complement components as mediators for autophagy, metabolism and DNA repair (West and Kemper 2023). This discovery opened a whole new field of research, with implications for both basic and clinical science, including studies on retinal degeneration.

One of the best studied intracellular complement components is C1q. In addition to its binding to apoptotic cells, immune complexes, and certain pathogens, C1q has also been found to localize intracellularly in various cell types, such as neurons, endothelial cells and macrophages (Datta et al. 2020; Ten et al. 2010; Benoit et al. 2012). Intracellular C1q coordinates in multiple cellular functions. In murine neurons, intracellular C1q regulates oxidative stress after ischemic brain injury through its accumulation on mitochondria which led to increased ROS production (Ten et al. 2010). C1qA, one of the three sub chains of C1q, was found to act on the retinoic acid-inducible gene I (RIG-I) in the endothelial cell line 293T (Wang et al. 2012). C1qA overexpression caused RIG-I mediated IFN-stimulated responsive element (ISRE) activation and transcription of nuclear factor-kb and IFN-b which summed up to an enhanced anti-viral response

signaling (Wang et al. 2012). Macrophages were also shown to internalize and accumulate C1q after phagocytizing C1q-bound nuclei of apoptotic cells (Cai et al. 2015; Benoit et al. 2012). In consequence, the expression of genes associated with chemotaxis, immunoregulation, NLRP3 and JAK/STAT signaling was significantly changed (Benoit et al. 2012).

C3, the central component of the complement system, is another complement component that plays an important role for intracellular processes. In the extracellular space, C3 is cleaved upon activation into C3a and C3b. C3b can covalently bind to target surfaces, marking them for phagocytosis by immune cells. Intracellular C3 has been found in several cell types, including neurons, macrophages, B- and CD4 +T-cells (West and Kemper 2023). In these studies, intracellular C3 was found to contribute to the regulation of autophagy, lipid metabolism, and the activation of the NLRP3 inflammasome (West and Kemper 2023).

In my thesis, I detected C1q and C3 proteins in enriched mouse and human retinal cell fractions by Western blot and mass spectrometry. During the purification process of retinal cell populations, most unbound protein is washed away, while any remaining protein is likely firmly bound to the cell surface or located intracellularly. I detected significant amounts of C1q in the RPE/choroid fraction of healthy human samples, but not in any other retinal cell type. C3 on the other hand was additionally present in Müller cells, as well as the neuronal fraction. CFI, CFH, C7 and C1s were only detectable via Western blot in some cell types. The detectability of C3 and C1q could explain that they are indeed accumulating and acting intracellularly which would be well in line with recent reports (West and Kemper 2023).

Intracellular C3 is of particular interest in degenerative retinal diseases, as it has been shown to be integral for monocyte development and function (Kolev et al. 2020). Studies of monocytes from patients with primary C3 deficiency, caused by a missense mutation in the C3 gene, detected intracellular C3 in vesicular compartments of the Golgi apparatus, whereas in healthy donor monocytes it was uniformly distributed throughout the cytosol (Ghannam et al. 2008). Monocytes lacking C3 failed to differentiate into functional dendritic cells and memory T cells. B cells derived from these progenitors were unable to switch isotypes.

Finally, emerging evidence suggests that intrinsic C3 mediates IL1b production during infection, possibly through intracellular C3aR interaction (Asgari et al. 2013; Quell et al. 2017). While we detected C3aR in retinal microglia from human donors and mice, C3 was only distinctively expressed in human microglia. This means, that C3a/C3aR signaling could only happen thorough external sources of C3a, for example thorough endocytosis, for example after G-protein coupled receptor internalization (Settmacher et al. 1999).

Another intracellular complosome mechanism was detected in macrophages that produce C5 and a C5a/C5aR1 located on the macrophage mitochondrial membranes (Niyonzima et al. 2021). Autocrine C5/C5aR1 signaling could be activated by crystalline cholesterol that forms during atherogenesis, where cholesterol precipitates into crystals (Niyonzima et al. 2021). It was proposed that an intracellular conversion of C5 to C5a and C5b via C5 convertase leads to proinflammatory signaling and in turn to enhanced IL-1b expression (Niyonzima et al. 2021). Niyonzima et al. propose that via acting on the mitochondrial membrane, this intracellular complement activation could trigger a shift to aerobic glycolysis with enhanced ROS production through a reverse electron chain fluxion at the inner mitochondrial membrane. While a knockout of C5aR1 in a cardiovascular disease mouse model reduced symptoms, similar mechanisms have not been explored in the eye yet (Niyonzima et al. 2021). In our studies, I detected significantly higher (15-24-fold) expression of *C3AR1*, *C5AR1* and *C5AR2* in late stage AMD patients. Thus, all currently known players in intracellular complement functions are present in retinal microglia and appear to be gradually upregulated during AMD progression.

Another way of non-canonical complement activity might be executed by CFH itself. In the different studies subsumed in my thesis, I observed CFH as a complement factor acting/binding on microglia. During retinal degeneration, e.g., triggered by sodium iodate injections or ischemia, I found the microglia became CFH-positive as determined by immunolabeling. Although immunostainings showed CFH mostly on the microglial surface, transmembrane signaling could influence intracellular complement activity. Binding of CFH to CD11b is well known and was shown by Calippe and coworkers to obstruct CD47 which led to microglia remaining in their active state (Calippe et al. 2017; Losse et al. 2010). Since intrinsic C3 signaling has been proposed to be pro-inflammatory, it seems counterintuitive that CFH would also play a role in the same direction, whereas it is normally thought to counteract C3 activity. However, the relevant signaling molecule on the C3aR is C3a, a C3 cleavage product, and in the extracellular complement system CFH acts on C3b and its derivatives.

Nissilä et al. studied CFH binding to monocytes in the context of atherosclerosis. CFH domains 5-7 are capable of binding apolipoprotein E (APOE), which has antiatherogenic effects. When pre-incubated with CFH, immortalized THP1 monocytes (THP1 cell line) and primary monocytes had enhanced APOE binding and cholesterol efflux. Interestingly, these cells showed a shift from proinflammatory and proatherogenic transcripts towards an anti-inflammatory/anti-atherogenic expression profile. APOE deficiency and its antiatherogenic effects appear to be a possible cause of neovascular AMD, but no association with APOE variants has been found to date (DeAngelis et al. 2007). On the other hand, the Y402H mutation in the CFH 5-7 domain that binds APOE on activated microglia is a risk factor for wet AMD and could cause neovascularization due to reduced APOE binding to microglia (Goverdhan et al. 2008).

Complement regulatory therapy

My in-depth analysis of the complement system in the healthy and diseased immune-privileged retina led to an insight that allowed me to hypothesize about how to restore an aberrant complement homeostasis. CFH came into focus as potential treatment target since I found that it was downregulated in specific cell types of ischemic retinae in mice. Improper CFH function has also been established to be detrimental for AMD as mentioned above. I also found that CFH expression was significantly and sequentially upregulated with AMD progression.

Consequently, I developed a gene-addition therapy approach in which an AAV-delivered truncated version of CFH was introduced into Müller cells of the ischemic mouse retinas. Two different versions of these CFH-like regulators were used. Both contained the CCP-20 and 1-4 linked by a poly-glycine linker. One construct additionally contained the CFH domains 5-7 are essential for key CFH functions like microglia recruitment, host cell surface binding and C5b-9 formation reduction and also houses 402 allele (Borras et al. 2020).

A potential approach for CFH gene addition-therapy was already proposed in 2015 when Cashman et. al could show that expression of full length CFH counteracted AMD-like pathology in mice that was induced by adenoviral mediated overexpression of C3 (Cashman et al. 2011; Cashman et al. 2015). Compared to control virus injected animals, this model led to AMD hallmarks like RPE atrophy, loss of photoreceptor outer segments, reactive gliosis, retinal detachment, and reduced retinal function. subretinal injection of adenovirus that expressed C3 in C57Bl6/J mice (Cashman et al. 2015; Cashman et al. 2011). While the addition of a functional version of CFH into the retinal environment was therefore proven feasible and effective, it did not include a feedback mechanism to control expression according to needs of the tissue. The open reading frame of full length CFH also exceeds the loading capacity of the comparatively save AAVs and was therefore delivered with an adenoviral vector. Our approach to CFH-mediated complement regulation involved a fine-tuned mechanism that controlled the transgene expression according to retinal conditions, as its expression was controlled by the glial GFAP promotor, which is primarily active in diseased tissue. Removal of several CCPs in the CFH variants did not affect their functionality but improved some aspects like GAG binding and their C3 affinity. Moreover, the open reading frames of the truncated CFH variants fit into single AAV vectors. The treatment was effective in alleviating some morphological changes following ischemic injury in the retina and greatly affected the complement system by reducing levels of cleaved C3 and C3 itself.

These CFH constructs were successful in reducing markers of complement activation in ischemic retinae. C3 conversion seemed to be halted and C3d protein, which has a high half-life of more than 50 hours and is therefore long present at sites of active C3 degradation, was also found in significantly less amounts (Charlesworth et al. 1974; Asghar et al. 1989). Also, the expression of complement factor *C3* was lower than sham-

treated ischemic eyes and the expression of the complement regulator *Cfi* was increased. In addition to effects at the molecular level, I found slight morphological improvements in the retinal structure and an activation and migration of microglia.

In summary, the FH-variants tested here are viable candidates for therapies where reducing complement system activation is beneficial, e.g., to limit host responses to immunotherapies.

My approach of targeting the underlying complement dysregulation of a retinal degeneration is unique in the expression system and the regulators used, but several complement regulators have been the subject of studies and clinical trials on retinal diseases with mixed results. While it is unclear why some of the treatments did not meet expectations, the data set presented here on the complement system in the retina may have helped predict some outcomes. For instance, lampalizumab is a fragment of a human monoclonal antibody that binds and inhibits complement factor D and therefore the stabilization of the alternative pathway C3 convertase. In a clinical trial, the drug was administered to patients in 10 mg doses of purified antibody every 4 or 6 weeks by intravitreal injection. Lampalizumab was hypothesized to slow the formation of GA during the progression of dry AMD, but failed to prevent the macular RPE cell and photoreceptor loss in two phase 3 clinical trials (Dolgin 2017).

C3 is a popular target for complement-centered treatments since it is a pivotal part of the complement cascade, and its inhibition also blocks most of the downstream effector molecules like C5a and the MAC. One C3 inhibitor is pegcetacoplan (or APL-2, Brand name empaveli) which was approved for the treatment of paroxysmal nocturnal hemoglobinuria (PNH) in 2021 (Wong et al. 2023). In PNH, red blood cells lack the complement inhibitors DAF (CD55) and/or CD59 which normally block the formation of the C3 convertase on the cell surface (Hillmen et al. 2021). The erythrocytes are consequently marked for opsonization, and deposition of MAC proteins leads to cell lysis. Pegcetacoplan prevents persistent anemia resulting from the C3-mediated hemolysis and 85% of treated patients no longer require blood transfusions (Hillmen et al. 2021). This very effective C3 inhibitor was also approved for treatment of GA by the FDA in February of 2023. In a phase 2 clinical trial, pegcetacoplan reduced the spread of GA by 20% if administered intravitreally every other month and by ~29% if administered every month (Wykoff et al. 2021; Liao et al. 2020). In the second 6 months of treatment, this effect even improved to a reduction of 45% in the group that was treated monthly (Wykoff et al. 2021; Liao et al. 2020). Conversely, pegcetacoplan treatment also led to an increased incidence of wet AMD (~20% new cases in the monthly-treated group vs. 1.2% in sham- treated patients). In my thesis work, I found an increase in retinal C3 expression during the progression of AMD in patients. In this light, blocking C3 seems to be a viable strategy, especially since C3 transcript levels were particularly elevated in astrocytes at advanced stages. However, blocking C3 is a very broad approach to address complement dysregulation. In the absence of C3, the complement is essentially dysfunctional because no effector molecules beyond the

pattern recognition complexes are activated. It is also possible that the neovascularization stems from reduced CD55 levels, which could be downregulated given the lack of need for compensatory expression, highlighting the homeostatic importance of normal complement function (Ma et al. 2010).

In general, an effector-based approach to complement inhibition would be more desirable. Eculizumab is one of the most promising recent complement-based therapies that targets a downstream complement component. It is a humanized monoclonal antibody that binds the effector molecule C5 and inhibits its cleavage into C5a and C5b, thereby preventing the formation of the potent anaphylatoxin C5a and C5b, which is part of the MAC. Like pegcetacoplan , eculizumab was initially approved for the treatment of PNH and has been tested for ocular diseases such as neuromyelitis optica, atypical hemolytic uremic syndrome (aHUS) and C3 glomerulopathy-related choroidopathy (Hillmen et al. 2021; Pittock et al. 2019; Al-Ani et al. 2016). The efficacy of eculizmab in PNH treatment was lower than that of pegcatacoplan, with 15% of patients still requiring blood transfusions (Hillmen et al. 2021). A clinical trial in non-exudative macular degeneration in which 10 patients received intravenous injections of eculizumab did not show a reduction in GA progression 6 months after treatment (Yehoshua et al. 2014).
Tesisolumab, another C5 inhibitor, failed to improve GA in a clinical trial – this anti-complement C5 monotherapy was ineffective in reducing geographic atrophy lesion size (Abidi et al. 2022). In contrast, avacincaptad pegol, which like tesisolumab prevents C5 cleavage, effectively reduced the mean GA enlargement by 27.4% over the course of 12 months upon monthly intravitreal injections (Jaffe et al. 2021; Abidi et al. 2022). In my studies, C5 expression was undetectable in the healthy human retina and was also not detectable in AMD patients. This suggests that C5 does not play a major role in context of the local retinal complement homeostasis.

Several treatments for the prevention of MAC formation are currently in early-stage clinical trials (Cabral de Guimaraes et al. 2022). A soluble version of CD59 was shown to counteract neovascularization in a mouse model of CNV (Cashman et al. 2011) irrespective of the route of application. Both, intravitreal AAV-mediated transgene delivery as well as subretinal administration distal of the injury site resulted in significant treatment effects. In my thesis, I could not detect expression of key terminal pathway complement components in the retina such as C9, C8 and C6. Since the injury in the CNV model can lead to leakage of the BRB, systemic influx of the missing components is possible which could lead to the MAC formation.

Conclusion

The complement system is an important player in many diseases of the retina and other tissues. Its potent effectors make it a viable target for drugs that inhibit excessive or

unwanted effects that can damage sensitive tissues like the retina. Several drugs have been tested in this context with encouraging, but also at times with disappointing results. My studies show that with a profound understanding of how the complement system works in the retina at the local scale, it is possible to have a more rational approach to designing potential regulators. In addition to the drug itself, its dosage and patient predisposition, the adverse effects of drugs that inhibit parts of the complement system depend on the route of administration (e.g., intravenous, intravitreal, subretinal) and which the part of the complement system that is affected. Blocking C3, for example will reduce not only the effector molecules C3a and C3b, but also all downstream effectors like C5a and the MAC. Here I present the means to base a potential therapy on which elements of the complement cascade are active and which parts play a role in AMD. Based on my findings, I have developed truncated versions of CFH as complement regulators, which have shown promising results in first in vivo animal studies. With further testing and optimization, this approach will hopefully become an interesting treatment option for several diseases with underlying complement involvement and could also be used as immune modulator in the context of viral vector-based drug delivery.

List of references

Abdelsalam, A.; Del Priore, L.; Zarbin, M. A. (1999): Drusen in age-related macular degeneration: pathogenesis, natural course, and laser photocoagulation-induced regression. In: *Survey of ophthalmology* 44 (1), S. 1–29. DOI: 10.1016/s0039-6257(99)00072-7.

Abidi, Muhammad; Karrer, Erik; Csaky, Karl; Handa, James T. (2022): A Clinical and Preclinical Assessment of Clinical Trials for Dry Age-Related Macular Degeneration. In: *Ophthalmology science* 2 (4), S. 100213. DOI: 10.1016/j.xops.2022.100213.

Abu El-Asrar, A. M.; Desmet, S.; Meersschaert, A.; Dralands, L.; Missotten, L.; Geboes, K. (2001): Expression of the inducible isoform of nitric oxide synthase in the retinas of human subjects with diabetes mellitus. In: *American Journal of Ophthalmology* 132 (4), S. 551–556. DOI: 10.1016/s0002-9394(01)01127-8.

Agte, Silke; Junek, Stephan; Matthias, Sabrina; Ulbricht, Elke; Erdmann, Ines; Wurm, Antje et al. (2011): Müller glial cell-provided cellular light guidance through the vital guinea-pig retina. In: *Biophysical Journal* 101 (11), S. 2611–2619. DOI: 10.1016/j.bpj.2011.09.062.

Al-Ani, Fatimah; Chin-Yee, Ian; Lazo-Langner, Alejandro (2016): Eculizumab in the management of paroxysmal nocturnal hemoglobinuria: patient selection and special considerations. In: *Therapeutics and clinical risk management* 12, S. 1161–1170. DOI: 10.2147/TCRM.S96720.

Amadi-Obi, Ahjoku; Yu, Cheng-Rong; Dambuza, Ivy; Kim, Sung-Hye; Marrero, Bernadette; Egwuagu, Charles E. (2012): Interleukin 27 induces the expression of complement factor H (CFH) in the retina. In: *PloS one* 7 (9), e45801. DOI: 10.1371/journal.pone.0045801.

Anderson, Don H.; Radeke, Monte J.; Gallo, Natasha B.; Chapin, Ethan A.; Johnson, Patrick T.; Curletti, Christy R. et al. (2010): The pivotal role of the complement system in aging and age-related macular degeneration: hypothesis re-visited. In: *Progress in retinal and eye research* 29 (2), S. 95–112. DOI: 10.1016/j.preteyeres.2009.11.003.

Armento, Angela; Ueffing, Marius; Clark, Simon J. (2021): The complement system in age-related macular degeneration. In: *Cellular and molecular life sciences : CMLS* 78 (10), S. 4487–4505. DOI: 10.1007/s00018-021-03796-9.

Asgari, Elham; Le Friec, Gaelle; Yamamoto, Hidekazu; Perucha, Esperanza; Sacks, Steven S.; Köhl, Jörg et al. (2013): C3a modulates IL-1β secretion in human monocytes by regulating ATP efflux and subsequent NLRP3 inflammasome activation. In: *Blood* 122 (20), S. 3473–3481. DOI: 10.1182/blood-2013-05-502229.

Asghar, S. S.; Schraag, B.; Backhaus, A. H.; Zorn, I.; Venneker, G. T.; Hannema, A. J. (1989): A new method for the estimation of C3d. Affinity clearance of C-determinant-bearing C3 molecules and fragments followed by estimation of C3d by ELISA. In: *Journal of immunological methods* 120 (2), S. 207–214. DOI: 10.1016/0022-1759(89)90244-5.

Bajic, Goran; Yatime, Laure; Sim, Robert B.; Vorup-Jensen, Thomas; Andersen, Gregers R. (2013): Structural insight on the recognition of surface-bound opsonins by

the integrin I domain of complement receptor 3. In: *Proceedings of the National Academy of Sciences of the United States of America* 110 (41), S. 16426–16431. DOI: 10.1073/pnas.1311261110.

Benoit, Marie E.; Clarke, Elizabeth V.; Morgado, Pedro; Fraser, Deborah A.; Tenner, Andrea J. (2012): Complement protein C1q directs macrophage polarization and limits inflammasome activity during the uptake of apoptotic cells. In: *Journal of immunology (Baltimore, Md. : 1950)* 188 (11), S. 5682–5693. DOI: 10.4049/jimmunol.1103760.

Bexborn, Fredrik; Andersson, Per Ola; Chen, Hui; Nilsson, Bo; Ekdahl, Kristina N. (2008): The tick-over theory revisited: formation and regulation of the soluble alternative complement C3 convertase (C3(H2O)Bb). In: *Molecular immunology* 45 (8), S. 2370–2379. DOI: 10.1016/j.molimm.2007.11.003.

Bobak, D. A.; Gaither, T. A.; Frank, M. M.; Tenner, A. J. (1987): Modulation of FcR function by complement: subcomponent C1q enhances the phagocytosis of IgG-opsonized targets by human monocytes and culture-derived macrophages. In: *Journal of immunology (Baltimore, Md. : 1950)* 138 (4), S. 1150–1156.

Bora, N. S.; Gobleman, C. L.; Atkinson, J. P.; Pepose, J. S.; Kaplan, H. J. (1993): Differential expression of the complement regulatory proteins in the human eye. In: *Investigative Ophthalmology & Visual Science* 34 (13), S. 3579–3584.

Borras, Céline; Delaunay, Kimberley; Slaoui, Yousri; Abache, Toufik; Jorieux, Sylvie; Naud, Marie-Christine et al. (2020): Mechanisms of FH Protection Against Neovascular AMD. In: *Frontiers in Immunology* 11, S. 443. DOI: 10.3389/fimmu.2020.00443.

Bringmann, Andreas; Francke, Mike; Pannicke, Thomas; Biedermann, Bernd; Kodal, Hannes; Faude, Frank et al. (2000): Role of glial K+ channels in ontogeny and gliosis: A hypothesis based upon studies on Mller cells. In: *Glia* 29 (1), S. 35–44. DOI: 10.1002/(SICI)1098-1136(20000101)29:1<35::AID-GLIA4>3.0.CO;2-A.

Bringmann, Andreas; Pannicke, Thomas; Grosche, Jens; Francke, Mike; Wiedemann, Peter; Skatchkov, Serguei N. et al. (2006): Müller cells in the healthy and diseased retina. In: *Progress in retinal and eye research* 25 (4), S. 397–424. DOI: 10.1016/j.preteyeres.2006.05.003.

Burger, Courtney A.; Jiang, Danye; Li, Fenge; Samuel, Melanie A. (2020): C1q Regulates Horizontal Cell Neurite Confinement in the Outer Retina. In: *Frontiers in neural circuits* 14, S. 583391. DOI: 10.3389/fncir.2020.583391.

Cabral de Guimaraes, Thales Antonio; Daich Varela, Malena; Georgiou, Michalis; Michaelides, Michel (2022): Treatments for dry age-related macular degeneration: therapeutic avenues, clinical trials and future directions. In: *The British journal of ophthalmology* 106 (3), S. 297–304. DOI: 10.1136/bjophthalmol-2020-318452.

Cai, Yitian; Teo, Boon Heng Dennis; Yeo, Joo Guan; Lu, Jinhua (2015): C1q protein binds to the apoptotic nucleolus and causes C1 protease degradation of nucleolar proteins. In: *The Journal of biological chemistry* 290 (37), S. 22570–22580. DOI: 10.1074/jbc.M115.670661.

Calippe, Bertrand; Augustin, Sebastien; Beguier, Fanny; Charles-Messance, Hugo; Poupel, Lucie; Conart, Jean-Baptiste et al. (2017): Complement Factor H Inhibits CD47-Mediated Resolution of Inflammation. In: *Immunity* 46 (2), S. 261–272. DOI: 10.1016/j.immuni.2017.01.006.

Campbell, Matthew; Humphries, Peter (2012): The blood-retina barrier: tight junctions and barrier modulation. In: *Advances in experimental medicine and biology* 763, S. 70–84.

Cashman, Siobhan M.; Gracias, Jessica; Adhi, Mehreen; Kumar-Singh, Rajendra (2015): Adenovirus-mediated delivery of Factor H attenuates complement C3 induced pathology in the murine retina: a potential gene therapy for age-related macular degeneration. In: *The journal of gene medicine* 17 (10-12), S. 229–243. DOI: 10.1002/jgm.2865.

Cashman, Siobhan M.; Ramo, Kasmir; Kumar-Singh, Rajendra (2011): A non membrane-targeted human soluble CD59 attenuates choroidal neovascularization in a model of age related macular degeneration. In: *PLOS ONE* 6 (4), e19078. DOI: 10.1371/journal.pone.0019078.

Charlesworth, J. A.; Williams, D. G.; Naish, P.; Lachmann, P. J.; Peters, D. K. (1974): Metabolism of radio-labelled C3: effects of in vivo activation in rabbits. In: *Clinical and experimental immunology* 16 (3), S. 445–452. Online verfügbar unter https://pubmed.ncbi.nlm.nih.gov/4468849/.

Chen, Mei; Forrester, John V.; Xu, Heping (2007): Synthesis of complement factor H by retinal pigment epithelial cells is down-regulated by oxidized photoreceptor outer segments. In: *Experimental eye research* 84 (4), S. 635–645. DOI: 10.1016/j.exer.2006.11.015.

Chen, Mei; Xu, Heping (2015): Parainflammation, chronic inflammation, and age-related macular degeneration. In: *Journal of leukocyte biology* 98 (5), S. 713–725. DOI: 10.1189/jlb.3RI0615-239R.

Chen, Yingying; Xia, Qinghong; Zeng, Yue; Zhang, Yun; Zhang, Meixia (2022): Regulations of Retinal Inflammation: Focusing on Müller Glia. In: *Frontiers in cell and developmental biology* 10, S. 898652. DOI: 10.3389/fcell.2022.898652.

Chen, Zhao; Yan, Xin; Du, Guo-Wei; Tuoheti, Kurerban; Bai, Xiao-Jie; Wu, Hua-Hui et al. (2020): Complement C7 (C7), a Potential Tumor Suppressor, Is an Immune-Related Prognostic Biomarker in Prostate Cancer (PC). In: *Frontiers in oncology* 10, S. 1532. DOI: 10.3389/fonc.2020.01532.

Coffey, Peter J.; Gias, Carlos; McDermott, Caroline J.; Lundh, Peter; Pickering, Matthew C.; Sethi, Charanjit et al. (2007): Complement factor H deficiency in aged mice causes retinal abnormalities and visual dysfunction. In: *Proceedings of the National Academy of Sciences of the United States of America* 104 (42), S. 16651–16656. DOI: 10.1073/pnas.0705079104.

Colijn, Johanna M.; Buitendijk, Gabriëlle H. S.; Prokofyeva, Elena; Alves, Dalila; Cachulo, Maria L.; Khawaja, Anthony P. et al. (2017): Prevalence of Age-Related

Macular Degeneration in Europe: The Past and the Future. In: *Ophthalmology* 124 (12), S. 1753–1763. DOI: 10.1016/j.ophtha.2017.05.035.

Crabb, John W.; Miyagi, Masaru; Gu, Xiaorong; Shadrach, Karen; West, Karen A.; Sakaguchi, Hirokazu et al. (2002): Drusen proteome analysis: an approach to the etiology of age-related macular degeneration. In: *Proceedings of the National Academy of Sciences of the United States of America* 99 (23), S. 14682–14687. DOI: 10.1073/pnas.222551899.

Cullen, D. Kacy; Simon, Crystal M.; LaPlaca, Michelle C. (2007): Strain rate-dependent induction of reactive astrogliosis and cell death in three-dimensional neuronal-astrocytic co-cultures. In: *Brain research* 1158, S. 103–115. DOI: 10.1016/j.brainres.2007.04.070.

Dale Purves; George J Augustine; David Fitzpatrick; Lawrence C Katz; Anthony-Samuel LaMantia; James O McNamara; S Mark Williams (2001): Phototransduction. In: Dale Purves, George J. Augustine, David Fitzpatrick, Lawrence C. Katz, Anthony-Samuel LaMantia, James O. McNamara und S. Mark Williams (Hg.): Neuroscience. 2nd edition: Sinauer Associates. Online verfügbar unter https://www.ncbi.nlm.nih.gov/books/NBK10806/.

Dartt, Darlene A.; Besharse, Joseph (Hg.) (2010): Encyclopedia of the eye. Amsterdam: Elsevier (Encyclopedia of the eye, v. 1). Online verfügbar unter http://www.sciencedirect.com/science/referenceworks/9780123742032.

Datta, Dibyadeep; Leslie, Shannon N.; Morozov, Yury M.; Duque, Alvaro; Rakic, Pasko; van Dyck, Christopher H. et al. (2020): Classical complement cascade initiating C1q protein within neurons in the aged rhesus macaque dorsolateral prefrontal cortex. In: *J Neuroinflammation* 17 (1), S. 8. DOI: 10.1186/s12974-019-1683-1.

DeAngelis, Margaret M.; Ji, Fei; Kim, Ivana K.; Adams, Scott; Capone, Antonio; Ott, Jurg et al. (2007): Cigarette smoking, CFH, APOE, ELOVL4, and risk of neovascular age-related macular degeneration. In: *Archives of ophthalmology (Chicago, Ill. : 1960)* 125 (1), S. 49–54. DOI: 10.1001/archopht.125.1.49.

Dolgin, Elie (2017): Age-related macular degeneration foils drugmakers. In: *Nature biotechnology* 35 (11), S. 1000–1001. DOI: 10.1038/nbt1117-1000.

Eastlake, K.; Banerjee, P. J.; Angbohang, A.; Charteris, D. G.; Khaw, P. T.; Limb, G. A. (2016): Müller glia as an important source of cytokines and inflammatory factors present in the gliotic retina during proliferative vitreoretinopathy. In: *Glia* 64 (4), S. 495–506. DOI: 10.1002/glia.22942.

Fagerness, Jesen A.; Maller, Julian B.; Neale, Benjamin M.; Reynolds, Robyn C.; Daly, Mark J.; Seddon, Johanna M. (2009): Variation near complement factor I is associated with risk of advanced AMD. In: *European Journal of Human Genetics* 17 (1), S. 100–104. DOI: 10.1038/ejhg.2008.140.

Fearon, D. T.; Austen, K. F.; Ruddy, S. (1973): Formation of a hemolytically active cellular intermediate by the interaction between properdin factors B and D and the activated third component of complement. In: *The Journal of experimental medicine* 138 (6), S. 1305–1313. DOI: 10.1084/jem.138.6.1305.

Fernández-Sánchez, Laura; Lax, Pedro; Campello, Laura; Pinilla, Isabel; Cuenca, Nicolás (2015): Astrocytes and Müller Cell Alterations During Retinal Degeneration in a Transgenic Rat Model of Retinitis Pigmentosa. In: *Frontiers in cellular neuroscience* 9, S. 484. DOI: 10.3389/fncel.2015.00484.

Fett, Anna L.; Hermann, Manuel M.; Muether, Philipp S.; Kirchhof, Bernd; Fauser, Sascha (2012): Immunohistochemical localization of complement regulatory proteins in the human retina. In: *Histology and histopathology* 27 (3), S. 357–364. DOI: 10.14670/HH-27.357.

Franze, Kristian; Grosche, Jens; Skatchkov, Serguei N.; Schinkinger, Stefan; Foja, Christian; Schild, Detlev et al. (2007): Müller cells are living optical fibers in the vertebrate retina. In: *Proceedings of the National Academy of Sciences of the United States of America* 104 (20), S. 8287–8292. DOI: 10.1073/pnas.0611180104.

Fritsche, Lars G.; Igl, Wilmar; Bailey, Jessica N. Cooke; Grassmann, Felix; Sengupta, Sebanti; Bragg-Gresham, Jennifer L. et al. (2016): A large genome-wide association study of age-related macular degeneration highlights contributions of rare and common variants. In: *Nature genetics* 48 (2), S. 134–143. DOI: 10.1038/ng.3448.

Fromell, Karin; Adler, Anna; Åman, Amanda; Manivel, Vivek Anand; Huang, Shan; Dührkop, Claudia et al. (2020): Assessment of the Role of C3(H2O) in the Alternative Pathway. In: *Frontiers in Immunology* 11, S. 530. DOI: 10.3389/fimmu.2020.00530.

Gaboriaud, Christine; Frachet, Philippe; Thielens, Nicole M.; Arlaud, Gérard J. (2011): The human c1q globular domain: structure and recognition of non-immune self ligands. In: *Frontiers in Immunology* 2, S. 92. DOI: 10.3389/fimmu.2011.00092.

Galvan, Manuel D.; Greenlee-Wacker, Mallary C.; Bohlson, Suzanne S. (2012): C1q and phagocytosis: the perfect complement to a good meal. In: *Journal of leukocyte biology* 92 (3), S. 489–497. DOI: 10.1189/jlb.0212099.

Gehrs, Karen M.; Anderson, Don H.; Johnson, Lincoln V.; Hageman, Gregory S. (2006): Age-related macular degeneration--emerging pathogenetic and therapeutic concepts. In: *Annals of medicine* 38 (7), S. 450–471. DOI: 10.1080/07853890600946724.

Geoffrey P. Lewis; Steven K. Fisher (2000): Müller Cell Outgrowth after Retinal Detachment: Association with Cone Photoreceptors. In: *Invest. Ophthalmol. Vis. Sci.* 41 (6), S. 1542–1545. Online verfügbar unter https://iovs.arvojournals.org/article.aspx?articleid=2123411.

Ghannam, Arije; Pernollet, Martine; Fauquert, Jean-Luc; Monnier, Nicole; Ponard, Denise; Villiers, Marie-Bernadette et al. (2008): Human C3 deficiency associated with impairments in dendritic cell differentiation, memory B cells, and regulatory T cells. In: *Journal of immunology (Baltimore, Md. : 1950)* 181 (7), S. 5158–5166. DOI: 10.4049/jimmunol.181.7.5158.

Giannakis, Eleni; Jokiranta, T. Sakari; Male, Dean A.; Ranganathan, Shoba; Ormsby, Rebecca J.; Fischetti, Vince A. et al. (2003): A common site within factor H SCR 7 responsible for binding heparin, C-reactive protein and streptococcal M protein. In: *European journal of immunology* 33 (4), S. 962–969. DOI: 10.1002/eji.200323541.

Goverdhan, S. V.; Hannan, S.; Newsom, R. B.; Luff, A. J.; Griffiths, H.; Lotery, A. J. (2008): An analysis of the CFH Y402H genotype in AMD patients and controls from the UK, and response to PDT treatment. In: *Eye (London, England)* 22 (6), S. 849–854. DOI: 10.1038/sj.eye.6702830.

Györffy, Balázs A.; Kun, Judit; Török, György; Bulyáki, Éva; Borhegyi, Zsolt; Gulyássy, Péter et al. (2018): Local apoptotic-like mechanisms underlie complement-mediated synaptic pruning. In: *Proceedings of the National Academy of Sciences of the United States of America* 115 (24), S. 6303–6308. DOI: 10.1073/pnas.1722613115.

Hageman, Gregory S.; Anderson, Don H.; Johnson, Lincoln V.; Hancox, Lisa S.; Taiber, Andrew J.; Hardisty, Lisa I. et al. (2005): A common haplotype in the complement regulatory gene factor H (HF1/CFH) predisposes individuals to age-related macular degeneration. In: *Proceedings of the National Academy of Sciences of the United States of America* 102 (20), S. 7227–7232. DOI: 10.1073/pnas.0501536102.

Haines, Jonathan L.; Hauser, Michael A.; Schmidt, Silke; Scott, William K.; Olson, Lana M.; Gallins, Paul et al. (2005): Complement factor H variant increases the risk of age-related macular degeneration. In: *Science (New York, N.Y.)* 308 (5720), S. 419–421. DOI: 10.1126/science.1110359.

Hannan, Jonathan P.; Laskowski, Jennifer; Thurman, Joshua M.; Hageman, Gregory S.; Holers, V. Michael (2016): Mapping the Complement Factor H-Related Protein 1 (CFHR1):C3b/C3d Interactions. In: *PloS one* 11 (11), e0166200. DOI: 10.1371/journal.pone.0166200.

Harada, T.; Harada, C.; Nakayama, N.; Okuyama, S.; Yoshida, K.; Kohsaka, S. et al. (2000): Modification of glial-neuronal cell interactions prevents photoreceptor apoptosis during light-induced retinal degeneration. In: *Neuron* 26 (2), S. 533–541. DOI: 10.1016/S0896-6273(00)81185-X.

Harada, Takayuki; Harada, Chikako; Kohsaka, Shinichi; Wada, Etsuko; Yoshida, Kazuhiko; Ohno, Shigeaki et al. (2002): Microglia-Müller glia cell interactions control neurotrophic factor production during light-induced retinal degeneration. In: *J. Neurosci.* 22 (21), S. 9228–9236. DOI: 10.1523/JNEUROSCI.22-21-09228.2002.

Harboe, Morten; Johnson, Christina; Nymo, Stig; Ekholt, Karin; Schjalm, Camilla; Lindstad, Julie K. et al. (2017): Properdin binding to complement activating surfaces depends on initial C3b deposition. In: *Proceedings of the National Academy of Sciences of the United States of America* 114 (4), E534-E539. DOI: 10.1073/pnas.1612385114.

Haynes, Tracy; Luz-Madrigal, Agustin; Reis, Edimara S.; Echeverri Ruiz, Nancy P.; Grajales-Esquivel, Erika; Tzekou, Apostolia et al. (2013): Complement anaphylatoxin C3a is a potent inducer of embryonic chick retina regeneration. In: *Nature communications* 4, S. 2312. DOI: 10.1038/ncomms3312.

Hillmen, Peter; Szer, Jeff; Weitz, Ilene; Röth, Alexander; Höchsmann, Britta; Panse, Jens et al. (2021): pegcetacoplan versus Eculizumab in Paroxysmal Nocturnal Hemoglobinuria. In: *The New England journal of medicine* 384 (11), S. 1028–1037. DOI: 10.1056/NEJMoa2029073.

Hoon, Mrinalini; Okawa, Haruhisa; Della Santina, Luca; Wong, Rachel O. L. (2014): Functional architecture of the retina: development and disease. In: *Progress in retinal and eye research* 42, S. 44–84. DOI: 10.1016/j.preteyeres.2014.06.003.

Inafuku, Saori; Klokman, Garrett; Connor, Kip M. (2018): The Alternative Complement System Mediates Cell Death in Retinal Ischemia Reperfusion Injury. In: *Frontiers in molecular neuroscience* 11, S. 278. DOI: 10.3389/fnmol.2018.00278.

Jaffe, Glenn J.; Westby, Keith; Csaky, Karl G.; Monés, Jordi; Pearlman, Joel A.; Patel, Sunil S. et al. (2021): C5 Inhibitor Avacincaptad Pegol for Geographic Atrophy Due to Age-Related Macular Degeneration: A Randomized Pivotal Phase 2/3 Trial. In: *Ophthalmology* 128 (4), S. 576–586. DOI: 10.1016/j.ophtha.2020.08.027.

Jager, Rama D.; Mieler, William F.; Miller, Joan W. (2008): Age-related macular degeneration. In: *The New England journal of medicine* 358 (24), S. 2606–2617. DOI: 10.1056/NEJMra0801537.

Kang, Seoyoung; Larbi, Daniel; Andrade, Monica; Reardon, Sara; Reh, Thomas A.; Wohl, Stefanie G. (2020): A Comparative Analysis of Reactive Müller Glia Gene Expression After Light Damage and microRNA-Depleted Müller Glia-Focus on microRNAs. In: *Frontiers in cell and developmental biology* 8, S. 620459. DOI: 10.3389/fcell.2020.620459.

Kaur, Geetika; Singh, Nikhlesh K. (2021): The Role of Inflammation in Retinal Neurodegeneration and Degenerative Diseases. In: *International Journal of Molecular Sciences* 23 (1). DOI: 10.3390/ijms23010386.

Killick, R.; Hughes, T. R.; Morgan, B. P.; Lovestone, S. (2013): Deletion of Crry, the murine ortholog of the sporadic Alzheimer's disease risk gene CR1, impacts tau phosphorylation and brain CFH. In: *Neuroscience Letters* 533, S. 96–99. DOI: 10.1016/j.neulet.2012.11.008.

Koeberle, P. D.; Ball, A. K. (1999): Nitric oxide synthase inhibition delays axonal degeneration and promotes the survival of axotomized retinal ganglion cells. In: *Experimental Neurology* 158 (2), S. 366–381. DOI: 10.1006/exnr.1999.7113.

Kolb, Helga (1995): Webvision: The Organization of the Retina and Visual System. Simple Anatomy of the Retina. Hg. v. Helga Kolb, Eduardo Fernandez und Ralph Nelson. Salt Lake City (UT).

Kolev, Martin; West, Erin E.; Kunz, Natalia; Chauss, Daniel; Moseman, E. Ashley; Rahman, Jubayer et al. (2020): Diapedesis-Induced Integrin Signaling via LFA-1 Facilitates Tissue Immunity by Inducing Intrinsic Complement C3 Expression in Immune Cells. In: *Immunity* 52 (3), 513-527.e8. DOI: 10.1016/j.immuni.2020.02.006.

Kovács, Réka Á.; Vadászi, Henrietta; Bulyáki, Éva; Török, György; Tóth, Vilmos; Mátyás, Dominik et al. (2020): Identification of Neuronal Pentraxins as Synaptic Binding Partners of C1q and the Involvement of NP1 in Synaptic Pruning in Adult Mice. In: *Frontiers in Immunology* 11, S. 599771. DOI: 10.3389/fimmu.2020.599771.

Labin, A. M.; Ribak, E. N. (2010): Retinal glial cells enhance human vision acuity. In: *Physical review letters* 104 (15), S. 158102. DOI: 10.1103/physrevlett.104.158102.

Lachmann, Peter J. (2009): The amplification loop of the complement pathways. In: *Advances in immunology* 104, S. 115–149. DOI: 10.1016/S0065-2776(08)04004-2.

Liao, David S.; Grossi, Federico V.; El Mehdi, Delphine; Gerber, Monica R.; Brown, David M.; Heier, Jeffrey S. et al. (2020): Complement C3 Inhibitor pegcetacoplan for Geographic Atrophy Secondary to Age-Related Macular Degeneration: A Randomized Phase 2 Trial. In: *Ophthalmology* 127 (2), S. 186–195. DOI: 10.1016/j.ophtha.2019.07.011.

Liepe, B. A.; Stone, C.; Koistinaho, J.; Copenhagen, D. R. (1994): Nitric oxide synthase in Müller cells and neurons of salamander and fish retina. In: *The Journal of neuroscience : the official journal of the Society for Neuroscience* 14 (12), S. 7641–7654. DOI: 10.1523/JNEUROSCI.14-12-07641.1994.

Lim, B. L.; Reid, K. B.; Ghebrehiwet, B.; Peerschke, E. I.; Leigh, L. A.; Preissner, K. T. (1996): The binding protein for globular heads of complement C1q, gC1qR. Functional expression and characterization as a novel vitronectin binding factor. In: *The Journal of biological chemistry* 271 (43), S. 26739–26744. DOI: 10.1074/jbc.271.43.26739.

Losse, Josephine; Zipfel, Peter F.; Józsi, Mihály (2010): Factor H and factor H-related protein 1 bind to human neutrophils via complement receptor 3, mediate attachment to Candida albicans, and enhance neutrophil antimicrobial activity. In: *Journal of immunology (Baltimore, Md. : 1950)* 184 (2), S. 912–921. DOI: 10.4049/jimmunol.0901702.

Luo, Chang; Chen, Mei; Xu, Heping (2011): Complement gene expression and regulation in mouse retina and retinal pigment epithelium/choroid. In: *Molecular Vision* 17, S. 1588–1597.

Luo, Chang; Zhao, Jiawu; Madden, Angelina; Chen, Mei; Xu, Heping (2013): Complement expression in retinal pigment epithelial cells is modulated by activated macrophages. In: *Experimental eye research* 112, S. 93–101. DOI: 10.1016/j.exer.2013.04.016.

Lynch, N. J.; Reid, K. B.; van den Berg, R. H.; Daha, M. R.; Leigh, L. A.; Ghebrehiwet, B. et al. (1997): Characterisation of the rat and mouse homologues of gC1qBP, a 33 kDa glycoprotein that binds to the globular 'heads' of C1q. In: *FEBS letters* 418 (1-2), S. 111–114. DOI: 10.1016/S0014-5793(97)01348-3.

Ma, Kelly N.; Cashman, Siobhan M.; Sweigard, J. Harry; Kumar-Singh, Rajendra (2010): Decay Accelerating Factor (CD55)–Mediated Attenuation of Complement: Therapeutic Implications for Age-Related Macular Degeneration. In: *Invest. Ophthalmol. Vis. Sci.* 51 (12), S. 6776. DOI: 10.1167/iovs.10-5887.

Maddox, D. A.; Brenner, B. M. (1977): Glomerular filtration of fluid and macromolecules: the renal response to injury. In: *Annual review of medicine* 28, S. 91–102. DOI: 10.1146/annurev.me.28.020177.000515.

Maller, Julian B.; Fagerness, Jesen A.; Reynolds, Robyn C.; Neale, Benjamin M.; Daly, Mark J.; Seddon, Johanna M. (2007): Variation in complement factor 3 is

associated with risk of age-related macular degeneration. In: *Nature genetics* 39 (10), S. 1200–1201. DOI: 10.1038/ng2131.

Maria Frasson; Serge Picaud; Thierry Léveillard; Manuel Simonutti; Saddek Mohand–Said; Henri Dreyfus et al. (1999): Glial Cell Line–Derived Neurotrophic Factor Induces Histologic and Functional Protection of Rod Photoreceptors in the rd/rd Mouse. In: *Invest. Ophthalmol. Vis. Sci.* 40 (11), S. 2724–2734. Online verfügbar unter https://arvojournals.org/article.aspx?articleid=2199753.

Markiewski, Maciej M.; Lambris, John D. (2007): The role of complement in inflammatory diseases from behind the scenes into the spotlight. In: *The American journal of pathology* 171 (3), S. 715–727. DOI: 10.2353/ajpath.2007.070166.

Masland, R. H. (2001): The fundamental plan of the retina. In: *Nature neuroscience* 4 (9), S. 877–886. DOI: 10.1038/nn0901-877.

Masland, Richard H. (2012): The neuronal organization of the retina. In: *Neuron* 76 (2), S. 266–280. DOI: 10.1016/j.neuron.2012.10.002.

McGrath, Fabian D. G.; Brouwer, Mieke C.; Arlaud, Gérard J.; Daha, Mohamed R.; Hack, C. Erik; Roos, Anja (2006): Evidence that complement protein C1q interacts with C-reactive protein through its globular head region. In: *J Immunol* 176 (5), S. 2950–2957. DOI: 10.4049/jimmunol.176.5.2950.

Merle, Nicolas S.; Church, Sarah Elizabeth; Fremeaux-Bacchi, Veronique; Roumenina, Lubka T. (2015a): Complement System Part I - Molecular Mechanisms of Activation and Regulation. In: *Frontiers in Immunology* 6, S. 262. DOI: 10.3389/fimmu.2015.00262.

Merle, Nicolas S.; Noe, Remi; Halbwachs-Mecarelli, Lise; Fremeaux-Bacchi, Veronique; Roumenina, Lubka T. (2015b): Complement System Part II: Role in Immunity. In: *Frontiers in Immunology* 6, S. 257. DOI: 10.3389/fimmu.2015.00257.

Mihlan, M.; Stippa, S.; Józsi, M.; Zipfel, P. F. (2009): Monomeric CRP contributes to complement control in fluid phase and on cellular surfaces and increases phagocytosis by recruiting factor H. In: *Cell death and differentiation* 16 (12), S. 1630–1640. DOI: 10.1038/cdd.2009.103.

Molins, Blanca; Fuentes-Prior, Pablo; Adán, Alfredo; Antón, Rosa; Arostegui, Juan I.; Yagüe, Jordi; Dick, Andrew D. (2016): Complement factor H binding of monomeric C-reactive protein downregulates proinflammatory activity and is impaired with at risk polymorphic CFH variants. In: *Scientific reports* 6, S. 22889. DOI: 10.1038/srep22889.

Mukai, Ryo; Okunuki, Yoko; Husain, Deeba; Kim, Clifford B.; Lambris, John D.; Connor, Kip M. (2018): The Complement System Is Critical in Maintaining Retinal Integrity during Aging. In: *Frontiers in Aging Neuroscience* 10, S. 15. DOI: 10.3389/fnagi.2018.00015.

Nauta, Alma J.; Trouw, Leendert A.; Daha, Mohamed R.; Tijsma, Odette; Nieuwland, Rienk; Schwaeble, Wilhelm J. et al. (2002): Direct binding of C1q to apoptotic cells and cell blebs induces complement activation. In: *Eur. J. Immunol.* 32 (6), S. 1726. DOI: 10.1002/1521-4141(200206)32:6<1726::AID-IMMU1726>3.0.CO;2-R.

Neuroscience (2001). Unter Mitarbeit von Dale Purves. 2nd ed. Sunderland, Mass.: Sinauer Associates.

Newman, E.; Reichenbach, A. (1996): The Müller cell: a functional element of the retina. In: *Trends in Neurosciences* 19 (8), S. 307–312. DOI: 10.1016/0166-2236(96)10040-0.

Niyonzima, Nathalie; Rahman, Jubayer; Kunz, Natalia; West, Erin E.; Freiwald, Tilo; Desai, Jigar V. et al. (2021): Mitochondrial C5aR1 activity in macrophages controls IL-1β production underlying sterile inflammation. In: *Science immunology* 6 (66), eabf2489. DOI: 10.1126/sciimmunol.abf2489.

Oku, Hidehiro; Ikeda, Tsunehiko; Honma, Youichi; Sotozono, Chie; Nishida, Kohji; Nakamura, Yo et al. (2002): Gene expression of neurotrophins and their high-affinity Trk receptors in cultured human Müller cells. In: *Ophthalmic Res* 34 (1), S. 38–42. DOI: 10.1159/000048323.

Paulson, O. B.; Newman, E. A. (1987): Does the release of potassium from astrocyte endfeet regulate cerebral blood flow? In: *Science (New York, N.Y.)* 237 (4817), S. 896–898. DOI: 10.1126/science.3616619.

Pauly, Diana; Nagel, Benedikt M.; Reinders, Jörg; Killian, Tobias; Wulf, Matthias; Ackermann, Susanne et al. (2014): A novel antibody against human properdin inhibits the alternative complement system and specifically detects properdin from blood samples. In: *PloS one* 9 (5), e96371. DOI: 10.1371/journal.pone.0096371.

Perkins, Stephen J.; Fung, Ka Wai; Khan, Sanaullah (2014): Molecular Interactions between Complement Factor H and Its Heparin and Heparan Sulfate Ligands. In: *Frontiers in Immunology* 5, S. 126. DOI: 10.3389/fimmu.2014.00126.

Pittock, Sean J.; Berthele, Achim; Fujihara, Kazuo; Kim, Ho Jin; Levy, Michael; Palace, Jacqueline et al. (2019): Eculizumab in Aquaporin-4-Positive Neuromyelitis Optica Spectrum Disorder. In: *The New England journal of medicine* 381 (7), S. 614–625. DOI: 10.1056/NEJMoa1900866.

PubMed (2023): complement retina - Search Results - PubMed. Online verfügbar unter https://pubmed.ncbi.nlm.nih.gov/?term=complement+retina, zuletzt aktualisiert am 22.08.2023, zuletzt geprüft am 22.08.2023.

Purves, Dale; Augustine, George J.; Fitzpatrick, David; Katz, Lawrence C.; LaMantia, Anthony-Samuel; McNamara, James O.; Williams, S. Mark (Hg.) (2001): Neuroscience. 2nd edition: Sinauer Associates.

Quell, Katharina M.; Karsten, Christian M.; Kordowski, Anna; Almeida, Larissa Nogueira; Briukhovetska, Daria; Wiese, Anna V. et al. (2017): Monitoring C3aR Expression Using a Floxed tdTomato-C3aR Reporter Knock-in Mouse. In: *Journal of immunology (Baltimore, Md. : 1950)* 199 (2), S. 688–706. DOI: 10.4049/jimmunol.1700318.

Rashid, Khalid; Akhtar-Schaefer, Isha; Langmann, Thomas (2019): Microglia in Retinal Degeneration. In: *Frontiers in Immunology* 10, S. 1975. DOI: 10.3389/fimmu.2019.01975.

Rawal, Nenoo; Rajagopalan, Rema; Salvi, Veena P. (2008): Activation of complement component C5: comparison of C5 convertases of the lectin pathway and the classical pathway of complement. In: *The Journal of biological chemistry* 283 (12), S. 7853–7863. DOI: 10.1074/jbc.M707591200.

Reichenbach, A.; Schneider, H.; Leibnitz, L.; Reichelt, W.; Schaaf, P.; Schümann, R. (1989): The structure of rabbit retinal Müller (glial) cells is adapted to the surrounding retinal layers. In: *Anat Embryol* 180 (1), S. 71–79. DOI: 10.1007/BF00321902.

Reichenbach, Andreas; Bringmann, Andreas (2013): New functions of Müller cells. In: *Glia* 61 (5), S. 651–678. DOI: 10.1002/glia.22477.

Reid, Kenneth B. M. (2018): Complement Component C1q: Historical Perspective of a Functionally Versatile, and Structurally Unusual, Serum Protein. In: *Frontiers in Immunology* 9, S. 764. DOI: 10.3389/fimmu.2018.00764.

Ricklin, Daniel; Hajishengallis, George; Yang, Kun; Lambris, John D. (2010): Complement: a key system for immune surveillance and homeostasis. In: *Nature immunology* 11 (9), S. 785–797. DOI: 10.1038/ni.1923.

Schäfer, Nicole; Grosche, Antje; Schmitt, Sabrina I.; Braunger, Barbara M.; Pauly, Diana (2017): Complement Components Showed a Time-Dependent Local Expression Pattern in Constant and Acute White Light-Induced Photoreceptor Damage. In: *Frontiers in molecular neuroscience* 10, S. 197. DOI: 10.3389/fnmol.2017.00197.

Schmalen, Adrian; Lorenz, Lea; Grosche, Antje; Pauly, Diana; Deeg, Cornelia A.; Hauck, Stefanie M. (2021): Proteomic Phenotyping of Stimulated Müller Cells Uncovers Profound Pro-Inflammatory Signaling and Antigen-Presenting Capacity. In: *Frontiers in pharmacology* 12, S. 771571. DOI: 10.3389/fphar.2021.771571.

Scholl, Hendrik P. N.; Charbel Issa, Peter; Walier, Maja; Janzer, Stefanie; Pollok-Kopp, Beatrix; Börncke, Florian et al. (2008): Systemic complement activation in age-related macular degeneration. In: *PLOS ONE* 3 (7), e2593. DOI: 10.1371/journal.pone.0002593.

Schütte, M.; Werner, P. (1998): Redistribution of glutathione in the ischemic rat retina. In: *Neuroscience Letters* 246 (1), S. 53–56. DOI: 10.1016/s0304-3940(98)00229-8.

Settmacher, B.; Bock, D.; Saad, H.; Gärtner, S.; Rheinheimer, C.; Köhl, J. et al. (1999): Modulation of C3a activity: internalization of the human C3a receptor and its inhibition by C5a. In: *J Immunol* 162 (12), S. 7409–7416.

Shahulhameed, Shahna; Vishwakarma, Sushma; Chhablani, Jay; Tyagi, Mudit; Pappuru, Rajeev R.; Jakati, Saumya et al. (2020): A Systematic Investigation on Complement Pathway Activation in Diabetic Retinopathy. In: *Frontiers in Immunology* 11, S. 154. DOI: 10.3389/fimmu.2020.00154.

Skerka, Christine; Chen, Qian; Fremeaux-Bacchi, Veronique; Roumenina, Lubka T. (2013): Complement factor H related proteins (CFHRs). In: *Molecular immunology* 56 (3), S. 170–180. DOI: 10.1016/j.molimm.2013.06.001.

Stenkamp, Deborah L. (2015): Development of the Vertebrate Eye and Retina. In: *Progress in molecular biology and translational science* 134, S. 397–414. DOI: 10.1016/bs.pmbts.2015.06.006.

Sunness, J. S.; Rubin, G. S.; Applegate, C. A.; Bressler, N. M.; Marsh, M. J.; Hawkins, B. S.; Haselwood, D. (1997): Visual function abnormalities and prognosis in eyes with age-related geographic atrophy of the macula and good visual acuity. In: *Ophthalmology* 104 (10), S. 1677–1691. DOI: 10.1016/s0161-6420(97)30079-7.

Sweigard, J. Harry; Yanai, Ryoji; Gaissert, Philipp; Saint-Geniez, Magali; Kataoka, Keiko; Thanos, Aristomenis et al. (2014): The alternative complement pathway regulates pathological angiogenesis in the retina. In: *FASEB journal : official publication of the Federation of American Societies for Experimental Biology* 28 (7), S. 3171–3182. DOI: 10.1096/fj.14-251041.

Taylor, P. R.; Carugati, A.; Fadok, V. A.; Cook, H. T.; Andrews, M.; Carroll, M. C. et al. (2000): A hierarchical role for classical pathway complement proteins in the clearance of apoptotic cells in vivo. In: *The Journal of experimental medicine* 192 (3), S. 359–366. DOI: 10.1084/jem.192.3.359.

Ten, Vadim S.; Yao, Jun; Ratner, Veniamin; Sosunov, Sergey; Fraser, Deborah A.; Botto, Marina et al. (2010): Complement component c1q mediates mitochondria-driven oxidative stress in neonatal hypoxic-ischemic brain injury. In: *J. Neurosci.* 30 (6), S. 2077–2087. DOI: 10.1523/JNEUROSCI.5249-09.2010.

Tezel, Gülgün; Yang, Xiangjun; Luo, Cheng; Kain, Angela D.; Powell, David W.; Kuehn, Markus H.; Kaplan, Henry J. (2010): Oxidative stress and the regulation of complement activation in human glaucoma. In: *Investigative Ophthalmology & Visual Science* 51 (10), S. 5071–5082. DOI: 10.1167/iovs.10-5289.

Tout, S.; Chan-Ling, T.; Holländer, H.; Stone, J. (1993): The role of Müller cells in the formation of the blood-retinal barrier. In: *Neuroscience* 55 (1), S. 291–301. DOI: 10.1016/0306-4522(93)90473-s.

Uga, Shigekazu; Smelser, George (1973): Comparative Study of the Fine Structure of Retinal MÜller Cells in Various Vertebrates. In: *Invest. Ophthalmol. Vis. Sci.* 12 (6), S. 434–448. Online verfügbar unter https://iovs.arvojournals.org/article.aspx?articleid=2158334.

van der Laan, L. J.; Ruuls, S. R.; Weber, K. S.; Lodder, I. J.; Döpp, E. A.; Dijkstra, C. D. (1996): Macrophage phagocytosis of myelin in vitro determined by flow cytometry: phagocytosis is mediated by CR3 and induces production of tumor necrosis factor-alpha and nitric oxide. In: *Journal of neuroimmunology* 70 (2), S. 145–152. DOI: 10.1016/s0165-5728(96)00110-5.

Vinores, S. A. (2010): Breakdown of the Blood–Retinal Barrier. In: Darlene A. Dartt und Joseph Besharse (Hg.): Encyclopedia of the eye. Amsterdam: Elsevier (Encyclopedia of the eye, v. 1), S. 216–222.

Vizi, E. S.; Fekete, A.; Karoly, R.; Mike, A. (2010): Non-synaptic receptors and transporters involved in brain functions and targets of drug treatment. In: *British journal of pharmacology* 160 (4), S. 785–809. DOI: 10.1111/j.1476-5381.2009.00624.x.

Vogt, Susan D.; Barnum, Scott R.; Curcio, Christine A.; Read, Russell W. (2006): Distribution of complement anaphylatoxin receptors and membrane-bound regulators

in normal human retina. In: *Experimental eye research* 83 (4), S. 834–840. DOI: 10.1016/j.exer.2006.04.002.

Voigt, A. P.; Whitmore, S. S.; Flamme-Wiese, M. J.; Riker, M. J.; Wiley, L. A.; Tucker, B. A. et al. (2019): Molecular characterization of foveal versus peripheral human retina by single-cell RNA sequencing. In: *Experimental eye research* 184, S. 234–242. DOI: 10.1016/j.exer.2019.05.001.

Vyawahare, Hrishikesh; Shinde, Pranaykumar (2022): Age-Related Macular Degeneration: Epidemiology, Pathophysiology, Diagnosis, and Treatment. In: *Cureus* 14 (9), e29583. DOI: 10.7759/cureus.29583.

Wakselman, Shirley; Béchade, Catherine; Roumier, Anne; Bernard, Delphine; Triller, Antoine; Bessis, Alain (2008): Developmental neuronal death in hippocampus requires the microglial CD11b integrin and DAP12 immunoreceptor. In: *The Journal of neuroscience : the official journal of the Society for Neuroscience* 28 (32), S. 8138–8143. DOI: 10.1523/JNEUROSCI.1006-08.2008.

Wang, Haijun; Song, Guobin; Chuang, Haoyu; Chiu, Chengdi; Abdelmaksoud, Ahmed; Ye, Youfan; Zhao, Lei (2018): Portrait of glial scar in neurological diseases. In: *International journal of immunopathology and pharmacology* 31, 2058738418801406. DOI: 10.1177/2058738418801406.

Wang, Lan; Clark, Mark E.; Crossman, David K.; Kojima, Kyoko; Messinger, Jeffrey D.; Mobley, James A.; Curcio, Christine A. (2010): Abundant lipid and protein components of drusen. In: *PLOS ONE* 5 (4), e10329. DOI: 10.1371/journal.pone.0010329.

Wang, Minhua; Ma, Wenxin; Zhao, Lian; Fariss, Robert N.; Wong, Wai T. (2011a): Adaptive Müller cell responses to microglial activation mediate neuroprotection and coordinate inflammation in the retina. In: *J Neuroinflammation* 8, S. 173. DOI: 10.1186/1742-2094-8-173.

Wang, Minhua; Wang, Xu; Zhao, Lian; Ma, Wenxin; Rodriguez, Ignacio R.; Fariss, Robert N.; Wong, Wai T. (2014): Macroglia-microglia interactions via TSPO signaling regulates microglial activation in the mouse retina. In: *J. Neurosci.* 34 (10), S. 3793–3806. DOI: 10.1523/JNEUROSCI.3153-13.2014.

Wang, Y.; Wang, V. M.; Chan, C-C (2011b): The role of anti-inflammatory agents in age-related macular degeneration (AMD) treatment. In: *Eye (London, England)* 25 (2), S. 127–139. DOI: 10.1038/eye.2010.196.

Wang, Yetao; Tong, Xiaomei; Zhang, Junjie; Ye, Xin (2012): The complement C1qA enhances retinoic acid-inducible gene-I-mediated immune signalling. In: *Immunology* 136 (1), S. 78–85. DOI: 10.1111/j.1365-2567.2012.03561.x.

Welsh, Christina A.; Stephany, Céleste-Élise; Sapp, Richard W.; Stevens, Beth (2020): Ocular Dominance Plasticity in Binocular Primary Visual Cortex Does Not Require C1q. In: *J. Neurosci.* 40 (4), S. 769–783. DOI: 10.1523/JNEUROSCI.1011-19.2019.

West, Erin E.; Kemper, Claudia (2023): Complosome - the intracellular complement system. In: *Nature reviews. Nephrology*, S. 1–14. DOI: 10.1038/s41581-023-00704-1.

Wong, Raymond Siu Ming; Navarro-Cabrera, Juan Ramon; Comia, Narcisa Sonia; Goh, Yeow Tee; Idrobo, Henry; Kongkabpan, Daolada et al. (2023): pegcetacoplan controls hemolysis in complement inhibitor-naive patients with paroxysmal nocturnal hemoglobinuria. In: *Blood advances* 7 (11), S. 2468–2478. DOI: 10.1182/bloodadvances.2022009129.

Wong, Wan Ling; Su, Xinyi; Li, Xiang; Cheung, Chui Ming G.; Klein, Ronald; Cheng, Ching-Yu; Wong, Tien Yin (2014): Global prevalence of age-related macular degeneration and disease burden projection for 2020 and 2040: a systematic review and meta-analysis. In: *The Lancet. Global health* 2 (2), e106-16. DOI: 10.1016/S2214-109X(13)70145-1.

Wykoff, Charles C.; Rosenfeld, Philip J.; Waheed, Nadia K.; Singh, Rishi P.; Ronca, Nick; Slakter, Jason S. et al. (2021): Characterizing New-Onset Exudation in the Randomized Phase 2 FILLY Trial of Complement Inhibitor pegcetacoplan for Geographic Atrophy. In: *Ophthalmology* 128 (9), S. 1325–1336. DOI: 10.1016/j.ophtha.2021.02.025.

Xu, Heping; Chen, Mei (2016): Targeting the complement system for the management of retinal inflammatory and degenerative diseases. In: *European journal of pharmacology* 787, S. 94–104. DOI: 10.1016/j.ejphar.2016.03.001.

Yang, Ming Ming; Wang, Jun; Dong, Li; Kong, De Ju; Teng, Yan; Liu, Ping et al. (2017): Lack of association of C3 gene with uveitis: additional insights into the genetic profile of uveitis regarding complement pathway genes. In: *Scientific reports* 7 (1), S. 879. DOI: 10.1038/s41598-017-00833-1.

Yang, Ping; Tyrrell, Jillian; Han, Ian; Jaffe, Glenn J. (2009): Expression and modulation of RPE cell membrane complement regulatory proteins. In: *Investigative Ophthalmology & Visual Science* 50 (7), S. 3473–3481. DOI: 10.1167/iovs.08-3202.

Yasuhara, Takao; Shingo, Tetsuro; Date, Isao (2004): The potential role of vascular endothelial growth factor in the central nervous system. In: *Reviews in the Neurosciences* 15 (4), S. 293–307. DOI: 10.1515/revneuro.2004.15.4.293.

Yehoshua, Zohar; Amorim Garcia Filho, Carlos Alexandre de; Nunes, Renata Portella; Gregori, Giovanni; Penha, Fernando M.; Moshfeghi, Andrew A. et al. (2014): Systemic complement inhibition with eculizumab for geographic atrophy in age-related macular degeneration: the COMPLETE study. In: *Ophthalmology* 121 (3), S. 693–701. DOI: 10.1016/j.ophtha.2013.09.044.

Yu, Haining; Muñoz, Eva M.; Edens, R. Erik; Linhardt, Robert J. (2005): Kinetic studies on the interactions of heparin and complement proteins using surface plasmon resonance. In: *Biochimica et biophysica acta* 1726 (2), S. 168–176. DOI: 10.1016/j.bbagen.2005.08.003.

Zewde, Nehemiah; Gorham, Ronald D.; Dorado, Angel; Morikis, Dimitrios (2016): Quantitative Modeling of the Alternative Pathway of the Complement System. In: *PloS one* 11 (3), e0152337. DOI: 10.1371/journal.pone.0152337.

Zhang, Dao-Qi; Zhou, Tongrong; Ruan, Guo-Xiang; McMahon, Douglas G. (2005): Circadian rhythm of Period1 clock gene expression in NOS amacrine cells of the

mouse retina. In: *Brain research* 1050 (1-2), S. 101–109. DOI: 10.1016/j.brainres.2005.05.042.

Zhang, Deng-Feng; Fan, Yu; Xu, Min; Wang, Guihong; Wang, Dong; Li, Jin et al. (2019): Complement C7 is a novel risk gene for Alzheimer's disease in Han Chinese. In: *National science review* 6 (2), S. 257–274. DOI: 10.1093/nsr/nwy127.

Zipfel, Peter F.; Skerka, Christine (2009): Complement regulators and inhibitory proteins. In: *Nature reviews. Immunology* 9 (10), S. 729–740. DOI: 10.1038/nri2620.

Zou, Qing-Mei; Li, Xiao-Hui; Song, Rui-Xia; Xu, Nan-Ping; Zhang, Ting; Zhang, Ming-Ming et al. (2015): Early decreased plasma levels of factor B and C5a are important biomarkers in children with Kawasaki disease. In: *Pediatr Res* 78 (2), S. 205–211. DOI: 10.1038/pr.2015.81.

Acknowledgements

Completing this PhD has been a transformative experience, and I am humbled to have had the privilege to work alongside such exceptional individuals. Each person mentioned here has played an integral role in shaping my academic and personal growth, and for that, I am eternally grateful.

List of Publications

- Randy Zauhar, **Josef Biber**, Yassin Jabri, Mijin Kim, Jian Hu, Lew Kaplan, Anna M Pfaller, Nicole Schäfer, Volker Enzmann, Ursula Schlötzer-Schrehardt, Tobias Straub, Stefanie Hauck, Paul D Gamlin, Michael Mcferrin, Jeffrey Messinger, Christianne E Strang, Christine A. Curcio, Nicholas Dana, Diana Pauly, Antje Grosche, Mingyao Li and Dwight Stambolian, **As in Real Estate, Location Matters: Cellular Expression of Complement Varies between Macular and Peripheral Regions of the Retina and Supporting Tissues**, Original Research, Front. Immunol. - Molecular Innate Immunity 2022 doi: 10.3389/fimmu.2022.895519

- Yassin Jabri, Josef Biber, Nundehui Diaz-Lezama, Antje Grosche, and Diana Pauly. 2020. "**Cell-Type-Specific Complement Profiling in the ABCA4$^{-/-}$ Mouse Model of Stargardt Disease**" *International Journal of Molecular Sciences* 21, no. 22: 8468. https://doi.org/10.3390/ijms21228468

- Diana Pauly, Divyansh Agarwal, Nicholas Dana, Nicole Schäfer, **Josef Biber**, Kirsten A. Wunderlich, Yassin Jabri, Tobias Straub, Nancy R. Zhang, Avneesh K. Gautam, Bernhard H.F. Weber, Stefanie M. Hauck, Mijin Kim, Christine A. Curcio, Dwight Stambolian, Mingyao Li, Antje Grosche, **Cell-Type-Specific Complement Expression in the Healthy and Diseased Retina**. Cell Reports, https://doi.org/10.1016/j.celrep.2019.10.084.

- Enzbrenner, Anne, Rahel Zulliger, **Josef Biber**, Ana M.Q. Pousa, Nicole Schäfer, Corinne Stucki, Nicolas Giroud, Marco Berrera, Elod Kortvely, Roland Schmucki, Laura Badi, Antje Grosche, Diana Pauly, and Volker Enzmann. 2021. "**Sodium Iodate-Induced Degeneration Results in Local Complement Changes and Inflammatory Processes in Murine Retina**" *International Journal of Molecular Sciences* 22, no. 17: 9218. https://doi.org/10.3390/ijms22179218.

- Díaz-Lezama N, Wolf A, Koch S, Pfaller AM, **Biber J**, Guillonneau X, Langmann T, Grosche A. PDGF Receptor Alpha Signaling Is Key for Müller Cell Homeostasis Functions. Int J Mol Sci. 2021 Jan 25;22(3):1174. doi: 10.3390/ijms22031174. PMID: 33503976 PMCID: PMC7865899.